International
Progress Report

IPR-99-02

Äspö Hard Rock Laboratory

Äspö Task Force on Modelling of Groundwater Flow and Transport of Solutes

Proceedings from the 11th task force meeting at Äspö, Sweden, September 1-3, 1998

Mansueto Morosini

Svensk Kärnbränslehantering AB

February 1999

Svensk Kärnbränslehantering AB
Swedish Nuclear Fuel
and Waste Management Co
Box 5864
SE-102 40 Stockholm Sweden
Tel 08-459 84 00
+46 8 459 84 00
Fax 08-661 57 19
+46 8 661 57 19

Äspö Hard Rock Laboratory

Äspö Hard Rock Laboratory

Äspö Task Force on Modelling of Groundwater Flow and Transport of Solutes

Proceedings from the 11th task force meeting at Äspö, Sweden, September 1–3, 1998

Mansueto Morosini

Svensk Kärnbränslehantering AB

February 1999

Keywords: Groundwater flow, solute transport, tracer test, fractured rock, underground laboratory, stochastic modelling, deterministic modelling.

Contents

Appendix A – Experimental results from STT-1b

Appendix B – Task 4E modelling results

B.1 Comparisons of modelling results

B.2 Contributions of modelling results of Task 4E

- Modelling of reactive-radioactive and sorbing tracer tests in Feature A at Äspö HRL. Lutz Liedtke & Hua Shao (BMBF/BGR)
- Tracer tests with sorbing tracers. Task 4E-II: Analysis of STT-1 blind predictions and Task 4EIII: Predictions of STT-1b. T.T. Cladouhos, William S. Dershowitz, Ian Miller (Golder) and Masahiro Uchida (PNC)
- Modelling of the sorbing tracer tests by using the Channel Network model. B. Khademi &Luis Moreno (SKB/KTH-KAT)
- Numerical analysis with FEGM/FERM for TRUE-1 sorbing tracer tests. Yasuharu Tanaka, Toshifumu Igarashi, Motoi Kawanishi (CRIEPI)
- Predictions of the sorbing tracer test STT1b of the TRUE. Antii Poteri (POSIVA)
- Evaluation of STT-1 and prediction of STT-1b. Vladimir Cvetkovic, (SKB/TRUE)
- Modelling and blind predictions for STT-1b tracer test. Andreas Jakob (NAGRA/PSI)
- The interaction of sorbing and non-sorbing tracers with different Äspö rock types. Sorption and diffusion experiments in the laboratory scale. Johan Byegård, Henrik

Appendix C – Task 5 Preliminary modelling

- The origin and composition of groundwater leaking into the Äspö tunnel. Urban Svenson (SKB/CFE)
- DFN modelling of Task 5. William Dershowitz (Golder) & Masahiro Uchida (PNC)
- Modelling of the hydraulic regime in and around the Äspö HRL considering the results of hydrochamical measurements. Lutz Liedtke, Hua Shao (BMBF/BGR)
- Preliminary groundwater flow modelling results of Task 5. Eero Kattilakoski (POSIVA)
- Preliminary application of smeared fracture model to Task No 5. Takuma Hasegawa (CRIEPI)

List of Figures

List of Tables

1 Introduction

The Äspö Task Force on Modelling of Groundwater Flow and Transport of Solutes is a forum for the organizations supporting the Äspö HRL Project to interact in the area of conceptual and numerical modelling of groundwater flow and solute transport in fractured rock. In particular, the Task Force proposes, reviews, evaluates and contributes to such work in the Project.

The work within the Äspö Task Force constitutes an important part of the international co-operation within the Äspö Hard Rock Laboratory. The group was initiated by SKB in 1992 and is a forum for the organisations to interact in the area of conceptual and numerical modelling of groundwater flow and transport. The work within the Task Force is being performed on well-defined and focused Modelling Tasks and the following have been defined so far:

- **Task No 1**: The LPT-2 pumping and tracer experiments. Site scale.
- **Task No 2:** Scoping calculations for a number of planned experiments at the Äspö site. Detailed scale.
- **Task No 3:** The hydraulic impact of the Äspö tunnel excavation. Site scale.
- **Task No 4:** TRUE - The Tracer Retention and Understanding Experiment, 1st stage. Non-reactive and reactive tracer tests. Detailed scale.
- **Task No 5:** Integration of hydrogeology and hydrochemistry at site scale.

As of October 1998 ten foreign organizations in addition to SKB are participating in the Äspö HRL. These organizations are: Atomic Energy of Canada Limited (AECL); Power Reactor & Nuclear Fuel Development Corporation (PNC), Japan; Central Research Institute of Electric Power Industry (CRIEPI), Japan; Agence National Pour la Gestion des Déchets Radioactifs (ANDRA), France; Posiva Oy, Finland; Nirex, United Kingdom; Nationale Genossenschaft für die Lagerung von radioaktiver Abfälle (Nagra), Switzerland; Bundesministerium für Bildung, Wissenschaft, Forschung und Technologie (BMBF), Germany , Empresa Nacional de Residuos Radiactivas (ENRESA), Spain and US DOE/Sandia National Laboratories.

This report summarises the main findings of the modelling work done in the Task Force since the previous meeting and presented at the 11th Task Force meeting held at Äspö in Sweden September 1-3, 1998. It also constitutes a status report of the Task Force work. Task 1-3 have been completed and the subject of this report is only Task 4 and Task 5. Specifically, these proceedings include the modelling results of Task 4E:II from the different modelling groups compiled into common tables and graphs for purposes of comparing. For Task 5 some preliminary modelling results are presented in interim reports and copies of slides from the oral presentation.

Contributions for Tasks No 4E and No 5 were received during the meeting from the modelling groups according to Table 1-1.

Table 1-1. Modelling contributions.

Modelling Group	Task #4E	Task #5
SKB/CFE	n/a	submitted
PNC/Golder	submitted	submitted
BMBF/BGR	submitted	submitted
POSIVA/VTT	submitted	submitted
CRIEPI	submitted	submitted
ENRESA	n/a	submitted
SKB/KAT	submitted	n/a
SKB/TRUE	submitted	n/a
NAGRA/PSI	submitted	n/a

n/a : not applicable

Reports produced within the framework of the Äspö Task Force published since the previous 10th Task Force meeting are listed in the the References.

2 Task 4 – Tracer retention and understanding experiments, 1st stage.

2.1 Background

Within the Äspö HRL project a programme called Tracer Retention Understanding Experiments (TRUE) has been defined for tracer tests at different experimental scales. The overall objective of the TRUE experiments is to increase the understanding of the processes which govern retention of radionuclides transported in crystalline rock, and to increase the credibility in the computer models for radionuclide transport which will be used in the licensing of a repository.

The first tracer test cycle (TRUE-1) constitutes a training and testing exercise for tracer testing technology on a detailed scale using non-reactive and reactive tracers in a simple test geometry. In addition, supporting technology development is performed in order to understand tracer transport through detailed aperture distributions obtained from resin injection. The TRUE-1 test cycle is expected to contribute data and experience which will constitute the necessary platform for subsequent, more elaborate experiments within TRUE.

2.1.1 Introduction to the TRUE-1 sorbing tracer tests

The objectives of the sorbing tracer tests part of TRUE-1 /Andersson et al, 1997B/ are:

- Test equipment and methodology for performing tracer tests with weakly sorbing radioactive tracers
- Increase understanding of transport of tracers subject to sorption in the studied feature
- Obtain parameters which describe retention of tracer transport
- Test different weakly and moderately sorbing radioactive tracers

The initial experimental scope includes:

- One main geometrical configuration KXTT4:R3-->KXTT3:R2
- 2-3 pump rates
- Weakly (Na, Ca, Sr) and moderately (Rb, Cs, Ba) sorbing tracers as well as the two non-sorbing tracers tritiated water and uranine.

- STT-1 (q=400 ml/min): highest flow rate, diffusion into the matrix (dead end pores are minimised)
- STT-2 (q=200 ml/min): intermediate flow rate, surface sorption, however there are questions regarding the effect of diffusion into the rock matrix
- STT-3 (q=100 ml/min): PDT-1 indicates that this experiment is not feasible!

However, the scope changed such that STT-2 will not be performed as part of TRUE-1. Instead, another injection of tracers using the STT-1 flow field was performed:

- STT-1b: complementary injection of sorbing tracers in KXTT1:R2

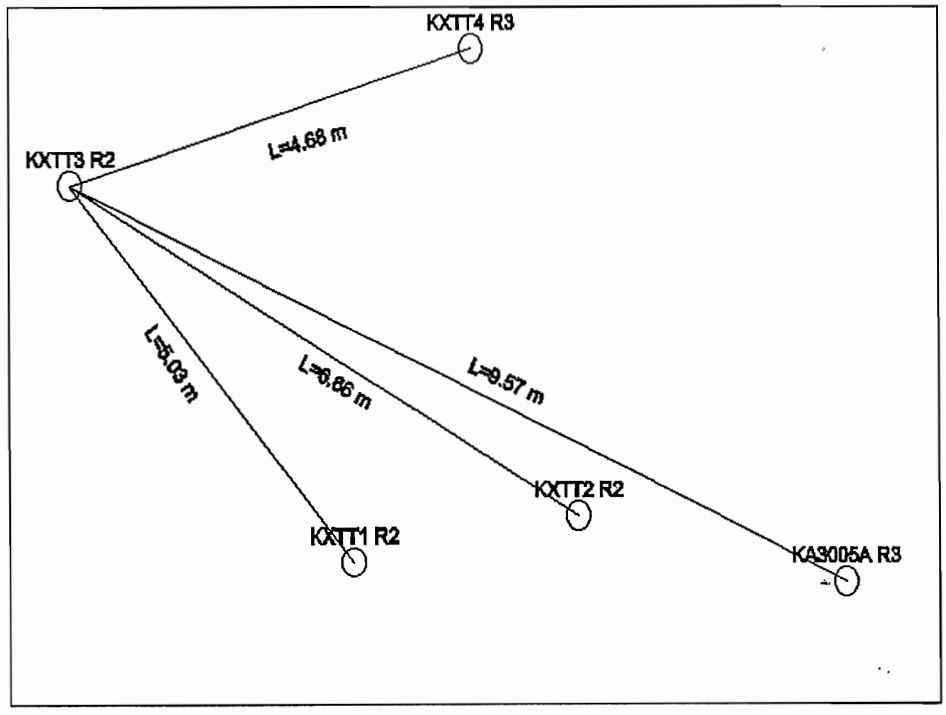

Figure 2-1 Borehole intersections with Feature A shown in the plane of the feature. Distances given in metres.

2.2 Experiments with non-sorbing tracers – Task 4C & 4D

During 1996 a series of tracer experiments in radially converging (RC-1) and dipole flow (DP1-DP4) configurations have been performed in Feature A using conservative fluorescent tracers and metal complexes. Furthermore, a set of complementary tests have been performed with the objective of providing final support for the planned tests with sorbing tracers (RC-2 and DP5-DP-6).

The objectives of the performed tests were specifically to:

- test transport connectivity within Feature A (RC-1),
- test flow heterogeneity within Feature A (DP1-DP4),
- determine and compare transport parameters for selected conservative tracers (RC-1, DP1-DP4),
- test techniques, tracers and equipment for injection and sampling of tracers in low-transmissive rocks (RC-1, DP1-DP4),

The modelling performed for Task 4C and Task 4D is being compiled into a report where the predictive modelling of the converging tracer tests and the dipole tests with non-sorbing tracers are evaluated. A draft Evaluation Report was discussed at the meeting and more comments solicited (Elert, M. 1999).

2.3 Experiment with sorbing tracers – Task 4E

The modelling teams presented their evaluation of the STT-1 experiment and predictive modelling of the STT-1b experiment. The contributions are compiled in Appendix B.

The STT1b experiment is performed in a radially converging configuration where tracers are injected in KXTT1 R2 and pumping takes place in KXTT3 R2 with 0.4L/min situated 5m away in feature A (Figure 4-1). A cocktail of ten different tracers (Table 2-1) were injected simultaneously as a finite pulse with a duration of 4 hours. Tracers were recovered in-line with a HpGe detector.

Table 2-1 STT-1b Injected tracers

Conservative tracers	Radioactive sorbing tracers
Uranine, HTO, Br, I	Na, K, Sr, Rb, Co, Tc

The following noteworthy points are summarised by the experimental team:

- From the source term sorption can be observed on the borehole wall
- In-line measurements give better description than samples
- A second peak after the exchange procedure was observed in the source-term it is attributed to a stagnant zone within the borehole volume
- Breakthrough was observed for nine tracers (not for Tc)
- The tracer arrival, t_5, vary between 5 and 285 hours
- HTO is somewhat delayed relative Uranine
- Recovery >90% for Uranine, HTO, Na and Rb
- Recovery <30% for Co
- A tracer recovery of >100% is obtained for the conservative tracers when the calculated flow rates are used. Since this is not possible it is suspected that volume of the borehole section is underestimated. A 100% recovery of uranine is achieved if the volume of the injection section is increased by 20%.

The TRUE-1 experimental team presented results from the STT-1b experiment which are included Appendix A. Predictive modelling results for the STT1b experiment are attached in Appendix B.2 and a comparative compilation of these modelling results is found in Appendix B.1.

2.4 Evaluation of STT1 predictions

BMBF/BGR and PNC/Golder also presented an evaluation of the predictive modelling for the STT1 experiment. These are included in the same report as the STT1b predictive modelling which is not included in Appendix B.2.

2.5 Predictive modelling of STT1b

The results of the predictive modelling are compiled in Appendix B and presented as:

- Tables of mass recovery differentiated between stochastic and deterministic modelling approach
- Bar charts of breakthrough time
- Breakthrough curves of absolute (Bq/h) and relative (%) massflow

The following general observations from the modelling are interesting to note:

- For most tracers (Uranine, HTO, K, Co, Rb) the experimental breakthrough curve fall within the range of the curves obtained by the modelling groups
- In all cases the modelled breakthrough time t_5 and t_{50} for tritiated water was similar to experiment while t_{95} was underestimated.
- Relatively similar breakthrough time in line with the experimental results was obtained by all modelling groups for Uranine, HTO, Na and Sr.
- There is considerable difference in the calculated massflow for all tracers but HTO and Uranine between the different modelleing groups. This might be accounted for by difference in calculated injected mass by the modelling groups, Figure 2-2.

Predicted breakthrough curves and mass recovery are dependent on the injected mass, this was calculated by each modelling group from the injection curve (see Appendix A) provided by the TRUE experiment team. The calculated injected mass from the modelling groups is compiled in Table 2-1 and in Figure 2-2.

Table 2-2 Calculated injected mass in experiment STT-1b, [MBq], uranine in [mg/L]

Tracer	NAGRA / PSI	BMBF/ BGR	SKB/ KTH-KAT	Experiment / Geosigma	SKB/TRUE	DOE/ Sandia	CRIEPI
Uranine	18.97	20.75	22.3	29.4	22.36	--	22.3
HTO	60.24	65.97	70.5	93.52	70.728	89.1	71.2
Na	0.514	0.56749	0.601	0.7976	0.6021	0.767	0.611
Sr	0.2594	0.28405	0.983	1.305	0.3035	0.386	0.309
Rb	0.8399	0.91983	0.303	0.4028	0.9861	1.26	0.983
K	0.5979	0.65487	0.7	0.9289	0.7056	--	--
Co	2.489	2.71905	2.91	3.864	2.915	3.67	--

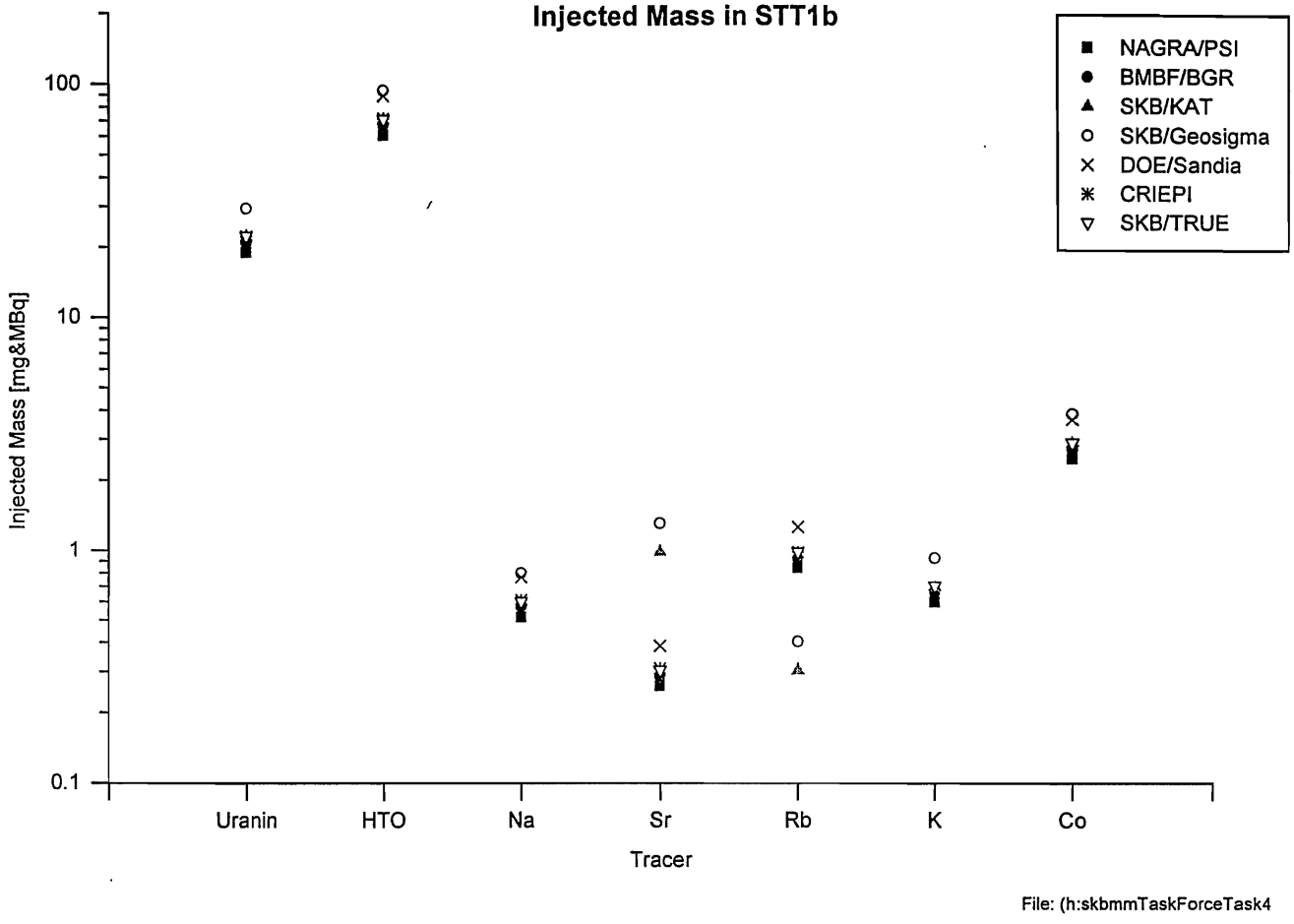

Figure 2-2 Calculated injected mass in experiment STT-1b

Some of the modelling groups also performed a predictive modelling where the injection was simulated with a Dirac pulse. Resulting curves of relative mass flow in this respect are from NAGRA/PSI, PNC/Golder and SKB/KTH-KAT are compiled at the end of Appendix B.1.

3 Task 5 – Integration of hydrochemistry and hydrogeology.

Task No 5 is a hydrological-hydrochemical model assessment exercise which specifically studies the impact of the tunnel construction on the groundwater system at Äspö. The task definition has been successively refined. The objectives are as follows:

- Assess the consistency of groundwater flow models and hydrochemical mixing-reaction models through integration and comparison of hydraulic and chemical data obtained before and during tunnel construction.
- Develop a procedure for integrating hydrological and hydrochemical information which could be used in the assessment of potential disposal sites.

Figure 3-1 illustrates the working sequence of the Modelling Task as well as the division into subtasks. Organisations participating in this modelling task are SKB, POSIVA, BMBF, PNC, CRIEPI and ENRESA.

Task 5 modelling results were presented by SKB/CFE, PNC/Golder, POSIVA/VTT, BMBF/BGR and CRIEPI. The reports are in Appendix C. ENRESA have not performed any modelling but presented their intended approach and tools for the task.

During the Task Force meeting there were five technical presentations from Task 5. Four modelling groups presented groundwater flow modelling results and one group on the groundwater chemical mixing proportions. The status of Task 5 has reached a preliminary modelling of the groundwater flow corresponding to level 5C of the concpetual workflow chart Figure 3-2. The discussion during the meeting led to feedback to level 5A on Data Compilation due to the issues of boundary conditions and control points that were covered.

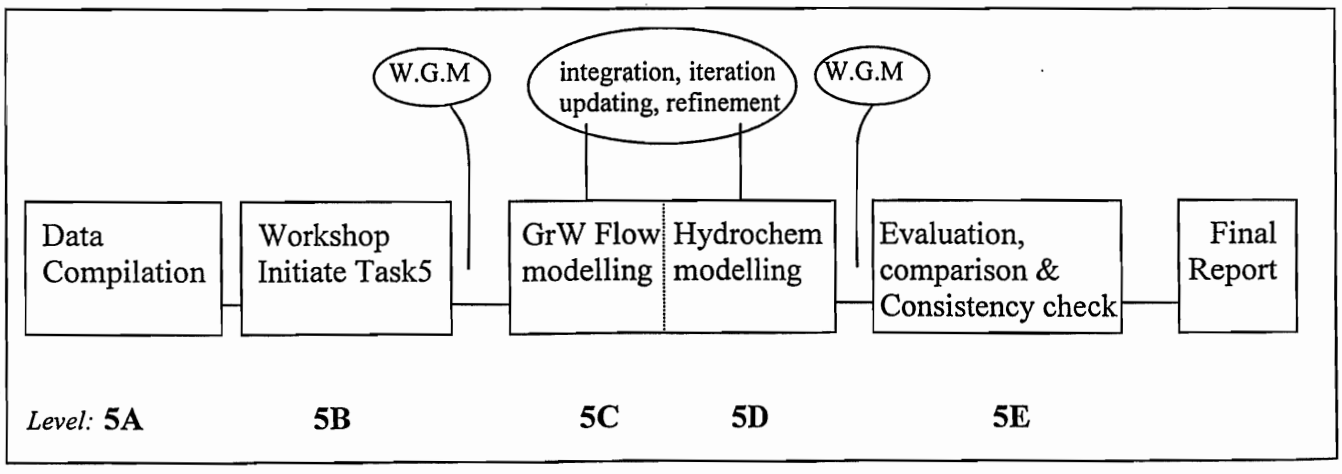

Figure 3-1 Flow chart of Task 5 illustrating subtasks and their dependencies. W.G.M= Work Group Meeting

During the technical session of the Task Force meeting the discussion focussed on boundary conditions, selection of control points and perfvormance measures. For the future planning the following was agreed upon.

- instructions should be issued to modelling groups on formulating concepts and models (September 1998)
- flow chart should be compiled illustrating how Task 5 intends to integrate hydrochemistry and hydrogeology in the modelling exercises (September 1998)
- groundwater mixing proportions should be recalculated based on a new Baltic seawater end member (October 1998)
- there should be a selection of control points along the tunnel section (October 1998)
- the modelling groups should submitt concepts and models to be used (December 1998)
- there should be further development of initial boundary conditions within specific hydrostructural features; conceptualism to be completed by January 1999
- an evaluation programme should be submitted by the modelling groups by March 1999
- there should be a prediction of hydraulic and chemical conditions ahead of 2900 m by April 1999
- there should be a data delivery to check predictions by May 1999

The next Modelling Group meeting was scheduled to January 1999 where the status of the modelling will be presented and more about initial and boundary conditions.

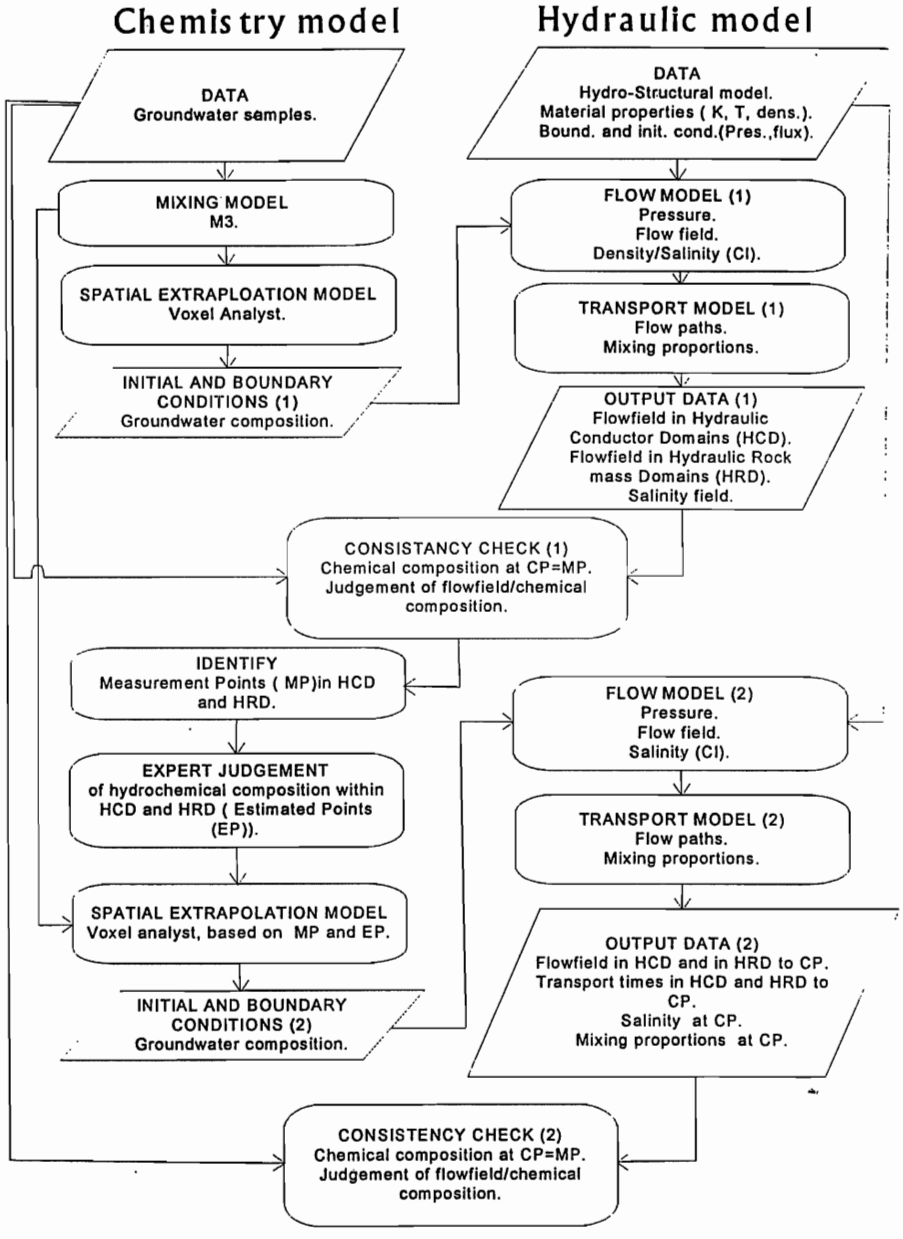

Figure 3-2 Example of flowchart showing modelling steps that should be included in reports from modelling teams.

4 References

Elert, M. (in preparation). Äspö Task Force on Modelling of Groundwater Flow and Transport of Solutes. Evaluátion of modelling of the TRUE-1 radially converging and dipole tests with conservative tracers. Äspö Task Force Task 4C and 4D. SKB HRL International Cooperation Report ICR ??-??.

Gustavsson, G., Ström, A., Vira, J. (1997). Evaluation report on Task No 3, the Äspö tunnel experiment. Äspö Task Force on Modelling of Groundwater Flow and Transport of Solutes. SKB International Cooperation Report ICR 97-06.

Tanaka, Y., Hasegawa, T., Kawanishi, M. (1997). Numerical analysis with FEGM/FERM for TRUE-1 non-sorbing tracer tests. Äspö Task Force on Modelling of Groundwater Flow and Transport of Solutes. SKB International Cooperation Report ICR 97-07.

Gylling, B. Khademi, B., Moreno, L. (1998). Modelling of the tracer retention understanding experiment Task 4C-D using the channel network model. Äspö Task Force on Modelling of Groundwater Flow and Transport of Solutes. SKB International Cooperation Report ICR 98-01.

Liedtke, L., Shao, H. (1997). Modelling of the Tracer experiments in feature A at Äspö HRL. Äspö Task Force on Modelling of Groundwater Flow and Transport of Solutes. SKB International Cooperation Report ICR 98-02.

Poteri, A., Hautojärvi, A. (1998). Modelling of the tracer tests in radially converging and dipole fields in the first phase of the TRUE project. Äspö Task Force on Modelling of Groundwater Flow and Transport of Solutes. SKB International Cooperation Report ICR 98-03.

Mahara, Y., Igarashi, T., Miyakawa, K., Kiho, K., Tanaka, Y., Hasegawa, T. (1998). Dynamic changes in groundwater conditions caused by tunnel construction at the Äspö Hard Rock Laboratory, Sweden. Äspö Task Force on Modelling of Groundwater Flow and Transport of Solutes. SKB International Cooperation Report ICR 98-04.

Appendix A – Experimental results from STT-1b

ACKNOWLEDGEMENTS

Eva Wass, GEOSIGMA, field operation, analyses

Mats Skålberg, Henrik Johansson, Gunnar Skarnemark, CTH; field operation, instrumentation, radioactive protection, analyses

Anders Winberg, Conterra; project manager

SKB Äspö HRL: funding, technical support

GEOSIGMA
MARK BERG VATTEN
MILJÖ

RESULTS FROM THE STT-1b TRACER EXPERIMENT

Presentation at the 11th Meeting of the Task Force on Modelling of Groundwater Flow and Transport of Solutes

Äspö Hard Rock Laboratory, Sweden
September 1-3, 1998

Peter Andersson
GEOSIGMA AB

GEOSIGMA
MARK BERG VATTEN
MILJÖ

PERFORMANCE

- Radially converging flow, injection in KXTT1 R2, pumping in KXTT3 R2 (Q=0.4 l/min)
- Simultaneous injection of 10 different tracers, 4 conservative (Uranine, HTO Br, I) and 6 sorbing radioactive isotopes (Na, K, Sr, Rb, Co, Tc)
- Injection performed as a finite pulse (4 hours) by exchange of tracer solution with water
- In-line measurement of source term for radioactive tracers (HpGe detector)

CONTENTS

GEOSIGMA
MARK BERG VATTEN
MILJÖ

STT-1b SOURCE TERMS

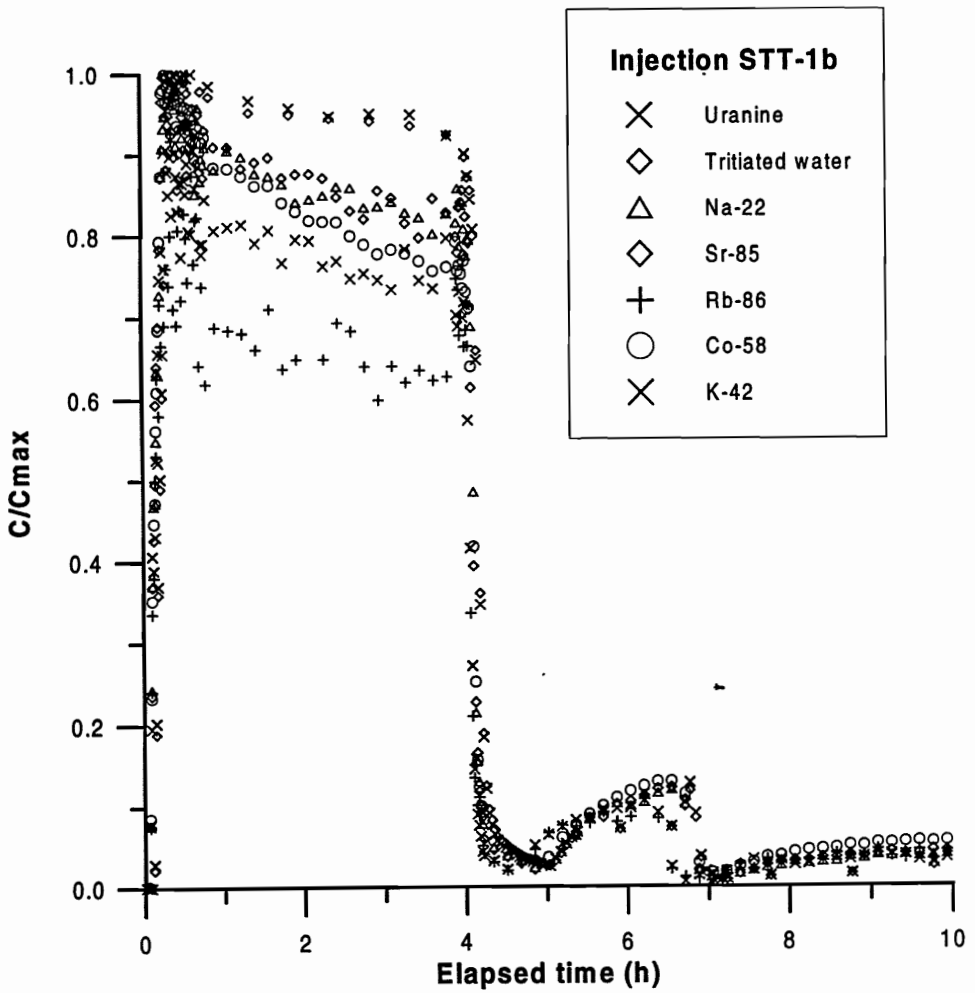

EXPERIMENTAL GEOMETRY STT-1b
(plane view of Feature A)

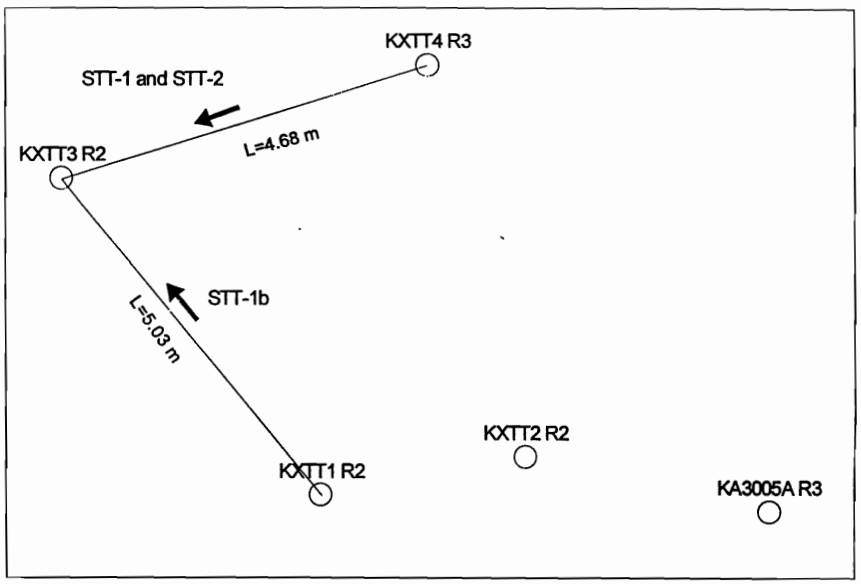

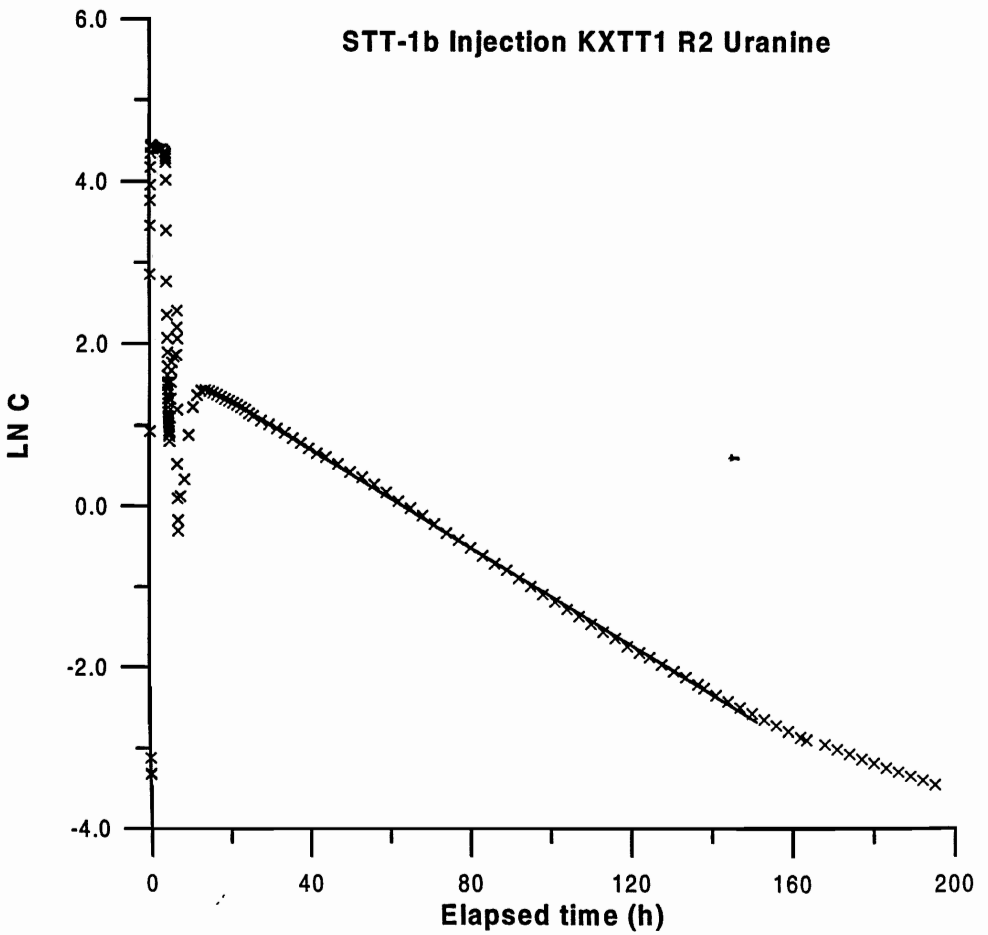

STT-1 SOURCE TERMS

- Sorption on borehole walls can be observed
- In-line measurements gives better description than samples
- Second peak after exchange procedure probably due to stagnant zones within the borehole volume
- Mass flux calculations based on Uranine data

GEOSIGMA
MARK BERG VATTEN MILJÖ

SUPPORTING DATA

- Hydraulic head and drawdown same as PDT-4 (same pumping)
- Head difference T1R2→T3R2 = 9.5 m
- Pumping rate constant 0.40 l/min
- Electrical conductivity sinking trend, i.e. "transient" water chemistry

GEOSIGMA
MARK BERG VATTEN MILJÖ

STT-1b SOURCE TERMS

Tracer	Elapsed time (h)	Flow (ml/h)	R
Uranine	0-4	41.9	0.9212
	20-151	58.1	0.9995
HTO	0-4	41.7	0.9142
	20-169	61.0	0.9997

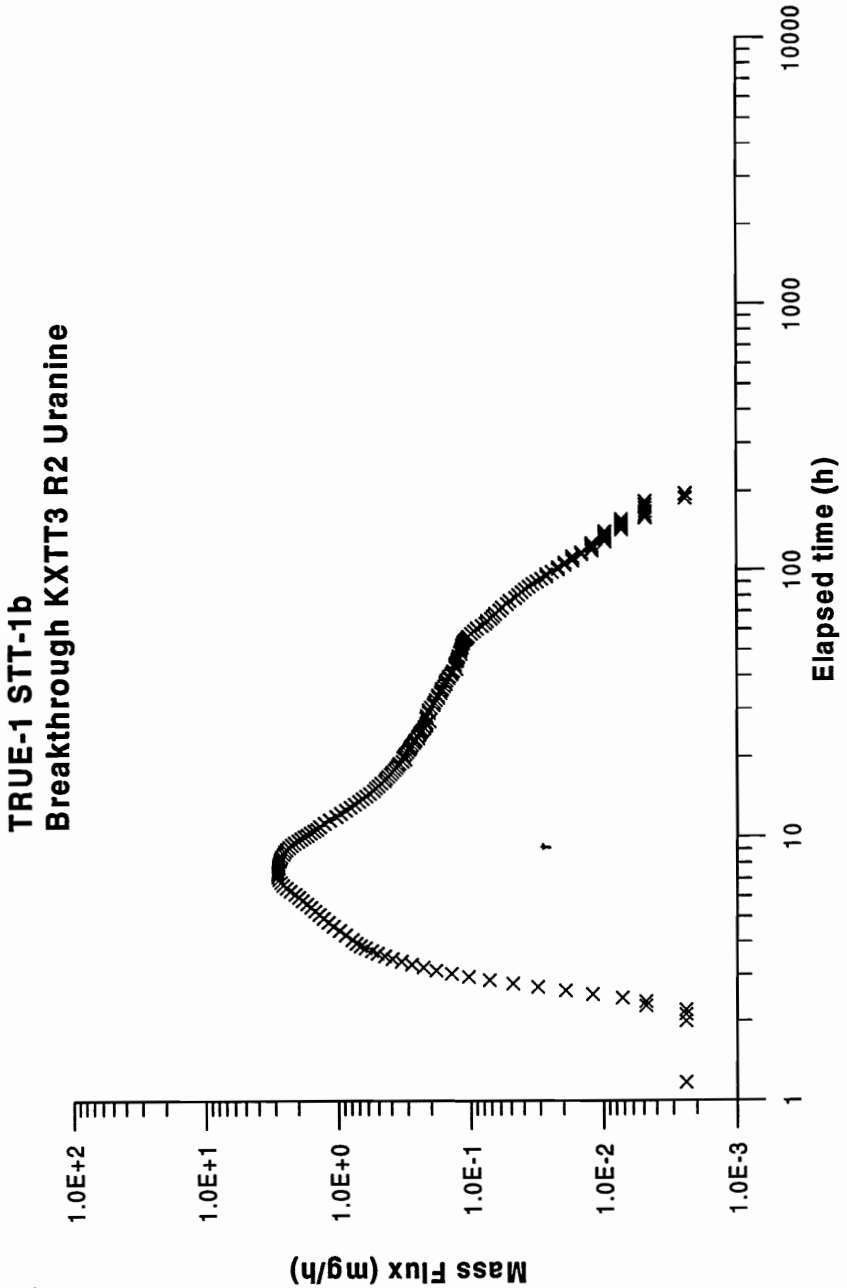

RESULTS

- Breakthrough of nine tracers monitored in pumping borehole (no Tc)
- Tracer arrival t_5 vary between 5.0 to 285 hours (based on injected mass)
- HTO seem to be somewhat delayed compared to Uranine!
- High recovery (>90%) for Uranine, HTO, Na, Rb
- Low recovery (<30%) for Co
-

GEOSIGMA
MARK BERG VATTEN MILJÖ

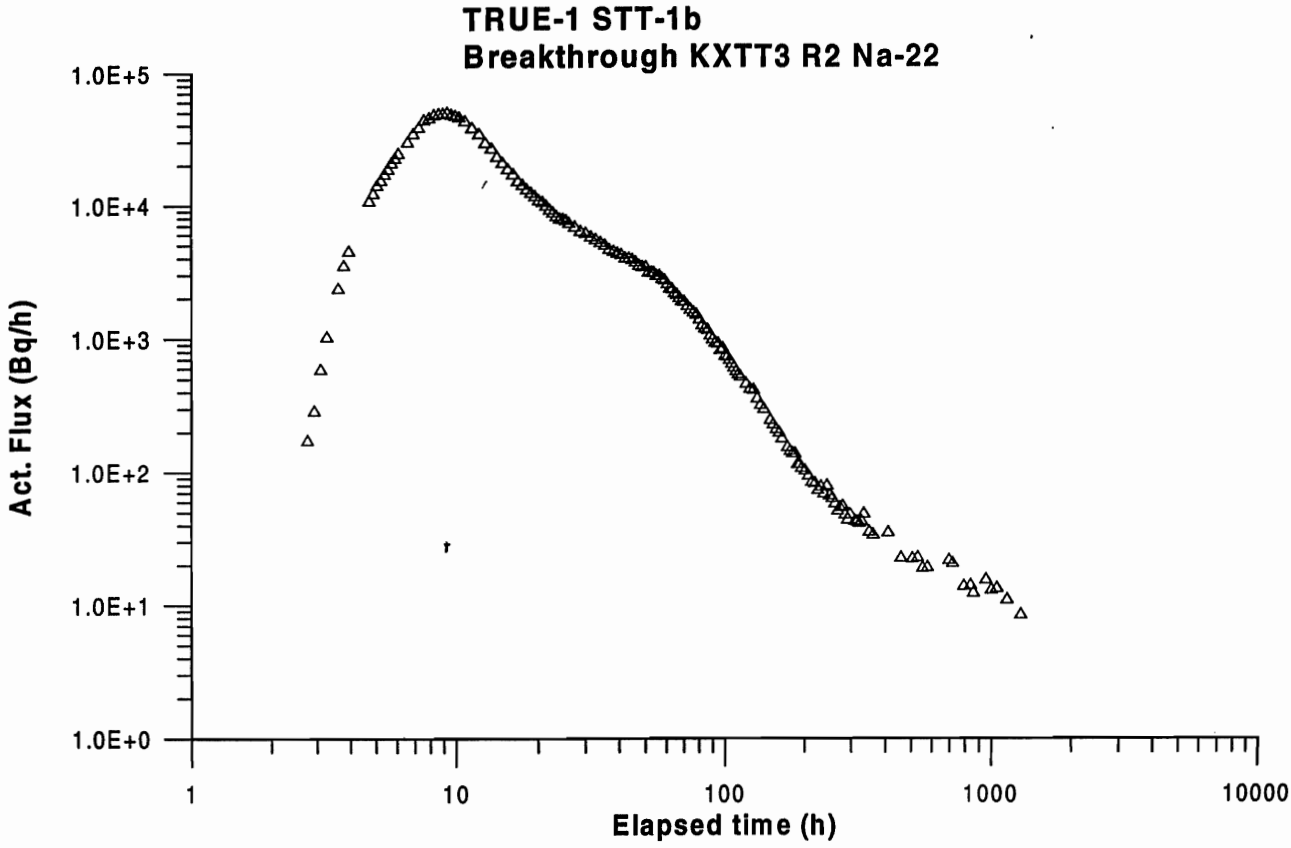
TRUE-1 STT-1b
Breakthrough KXTT3 R2 Na-22
Act. Flux (Bq/h)
1.0E+5
1.0E+4
1.0E+3
1.0E+2
1.0E+1
1.0E+0
1
10
100
1000
10000
Elapsed time (h)

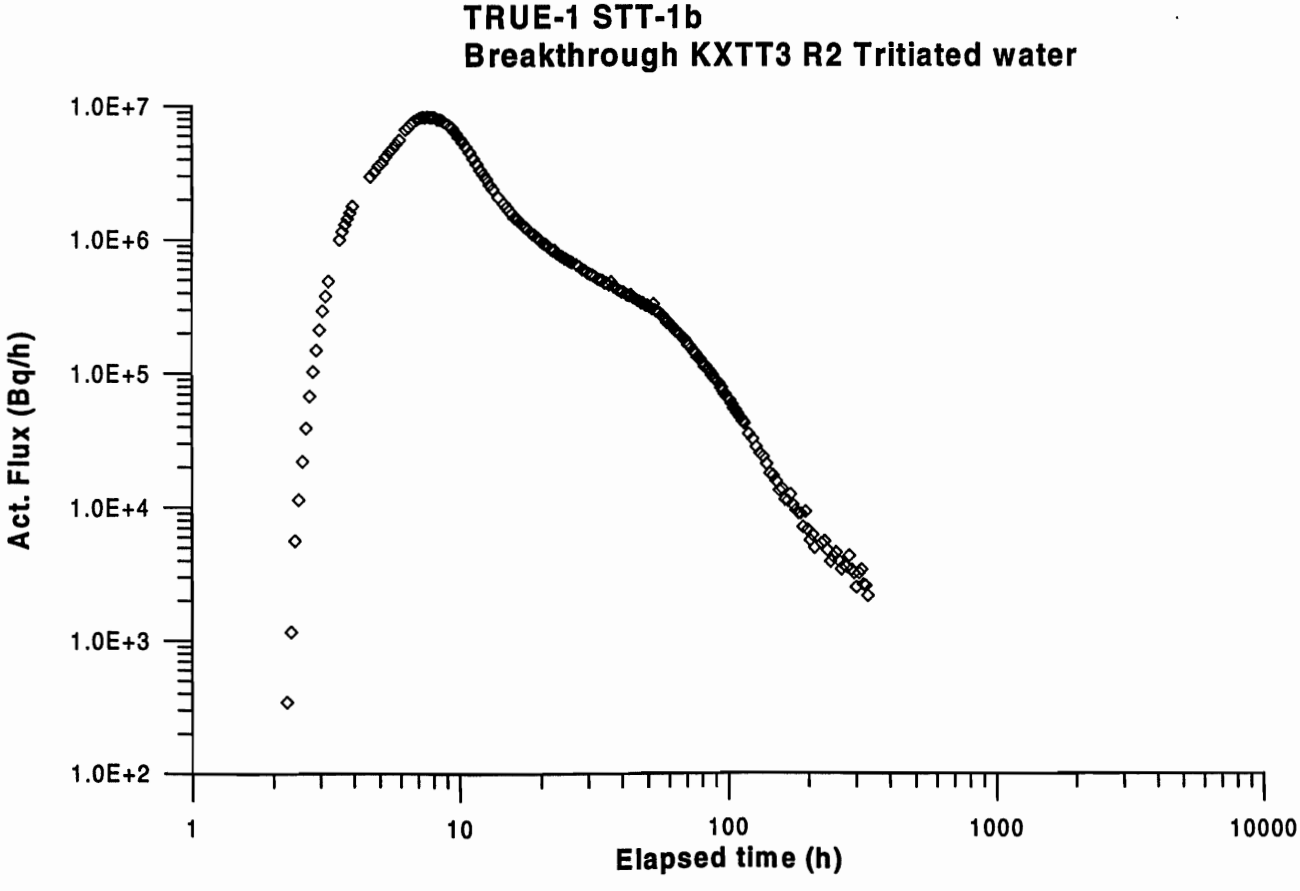
TRUE-1 STT-1b
Breakthrough KXTT3 R2 Tritiated water
Act. Flux (Bq/h)
1.0E+7
1.0E+6
1.0E+5
1.0E+4
1.0E+3
1.0E+2
1
10
100
1000
10000
Elapsed time (h)

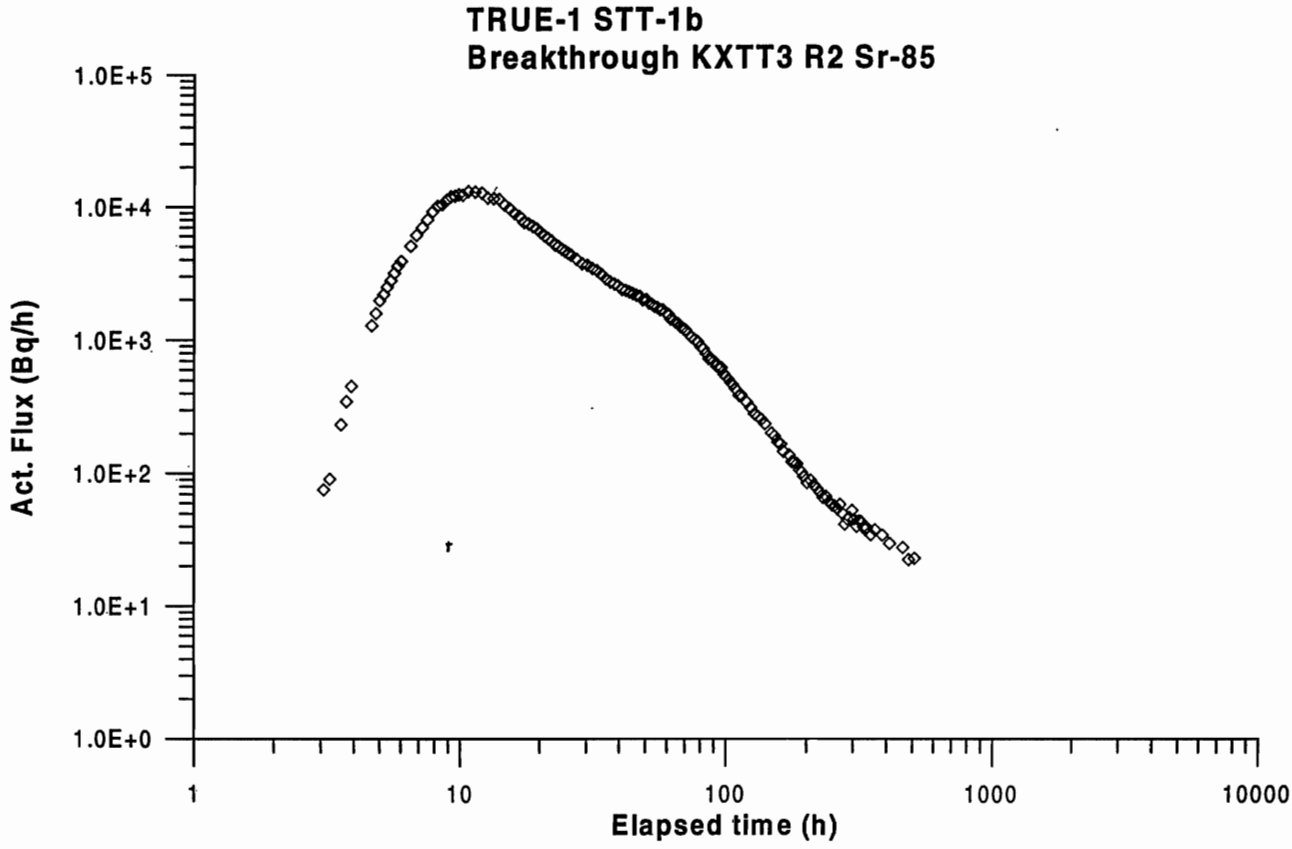
TRUE-1 STT-1b
Breakthrough KXTT3 R2 Sr-85
Act. Flux (Bq/h)
1.0E+5
1.0E+4
1.0E+3
1.0E+2
1.0E+1
1.0E+0
1
10
100
1000
10000
Elapsed time (h)

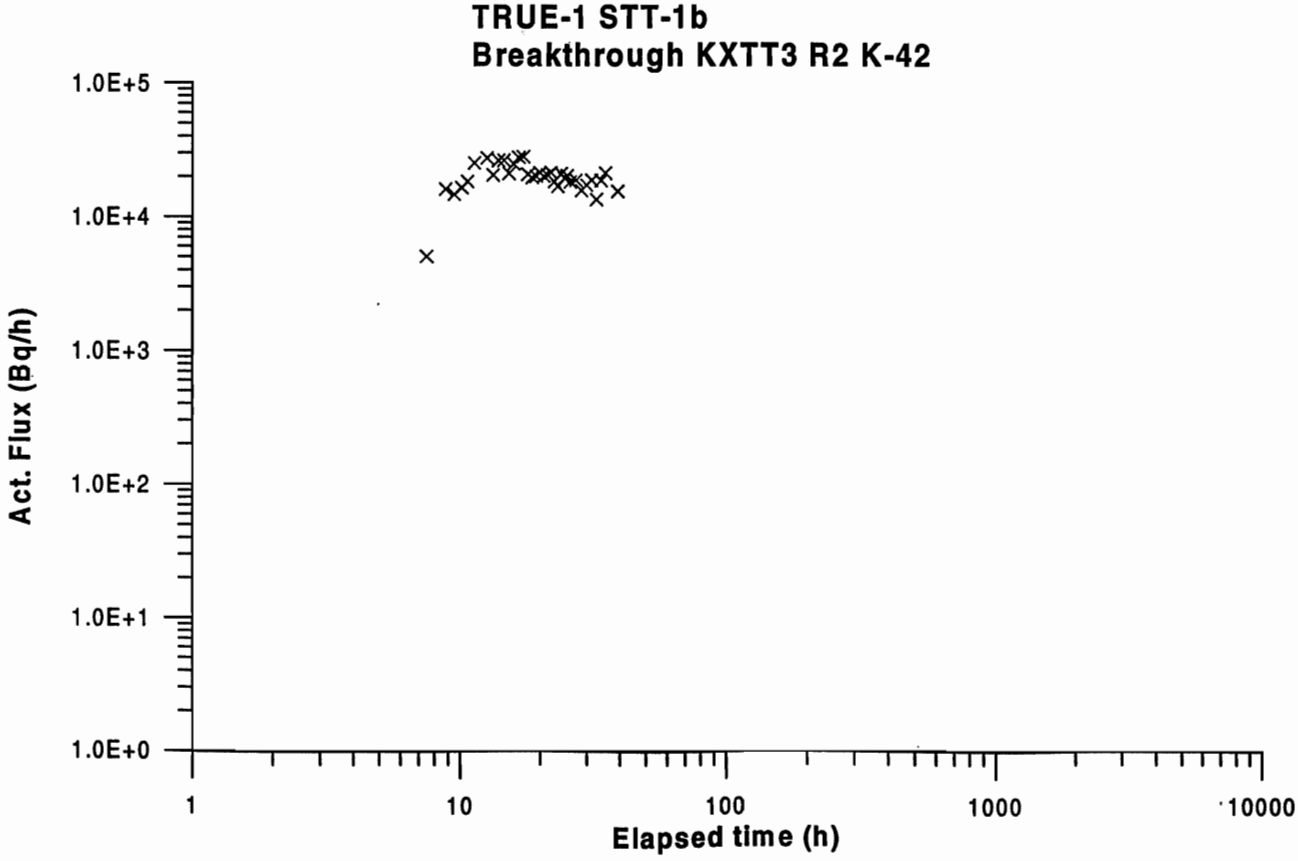
TRUE-1 STT-1b
Breakthrough KXTT3 R2 K-42
Act. Flux (Bq/h)
1.0E+5
1.0E+4
1.0E+3
1.0E+2
1.0E+1
1.0E+0
1
10
100
1000
10000
Elapsed time (h)

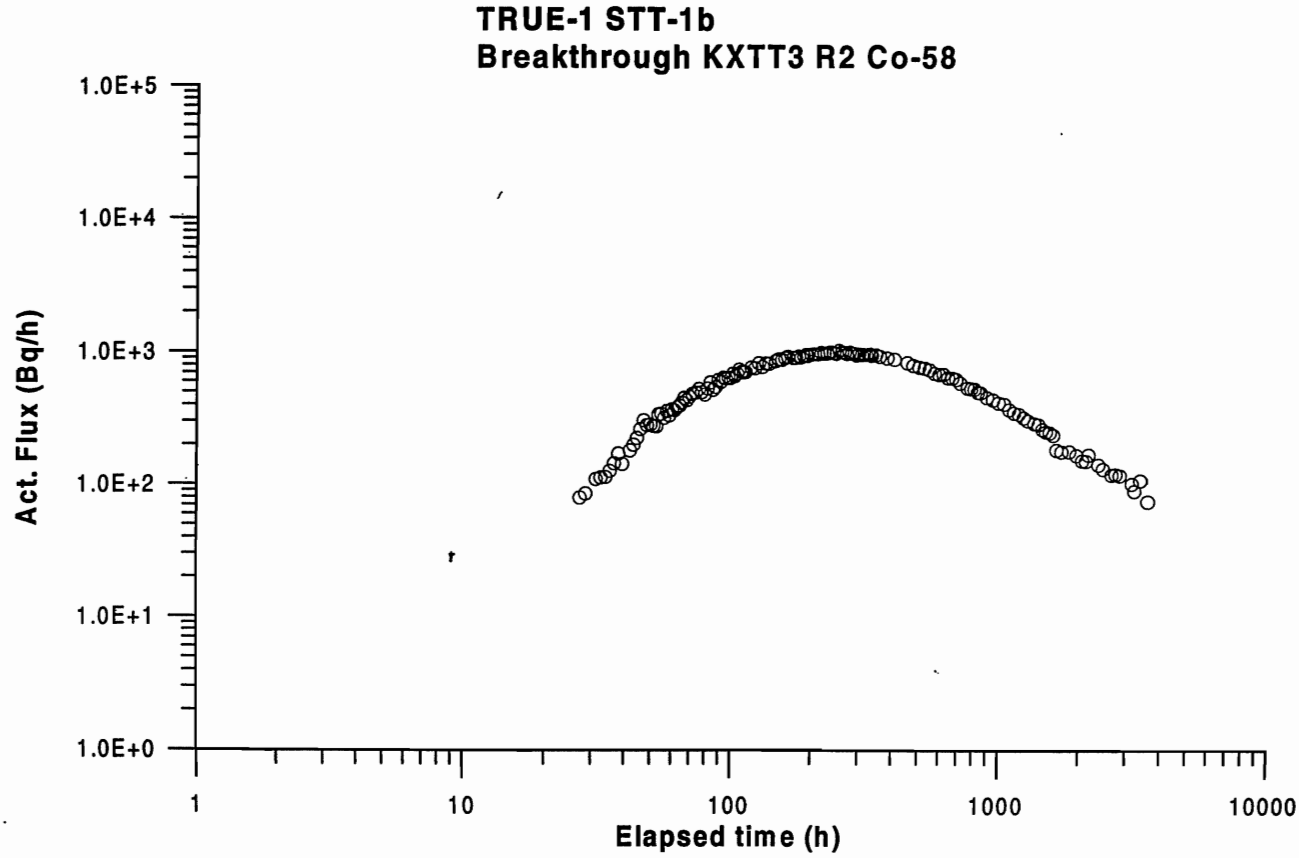
TRUE-1 STT-1b
Breakthrough KXTT3 R2 Co-58
Act. Flux (Bq/h)
1.0E+5
1.0E+4
1.0E+3
1.0E+2
1.0E+1
1.0E+0
1
10
100
1000
10000
Elapsed time (h)

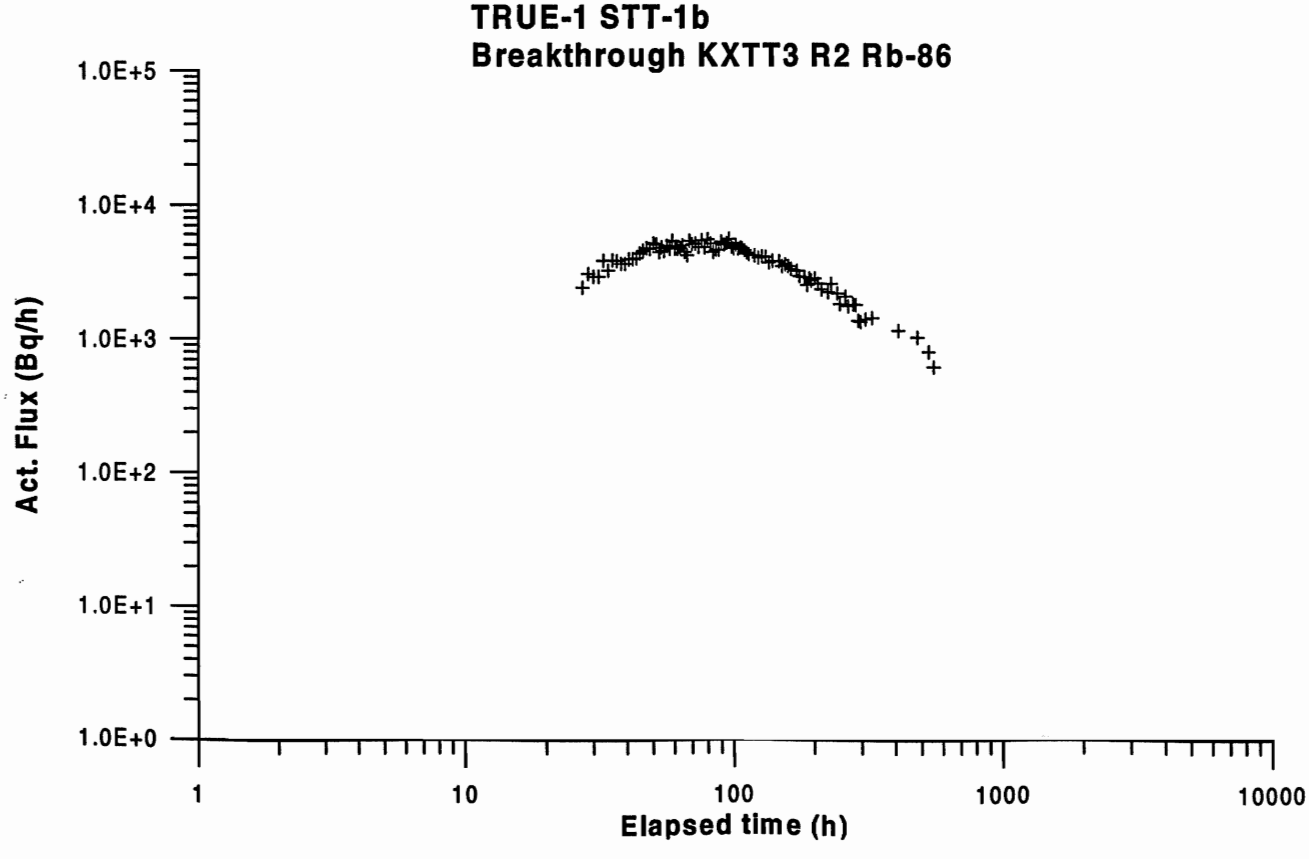
TRUE-1 STT-1b
Breakthrough KXTT3 R2 Rb-86
Act. Flux (Bq/h)
1.0E+5
1.0E+4
1.0E+3
1.0E+2
1.0E+1
1.0E+0
1
10
100
1000
10000
Elapsed time (h)

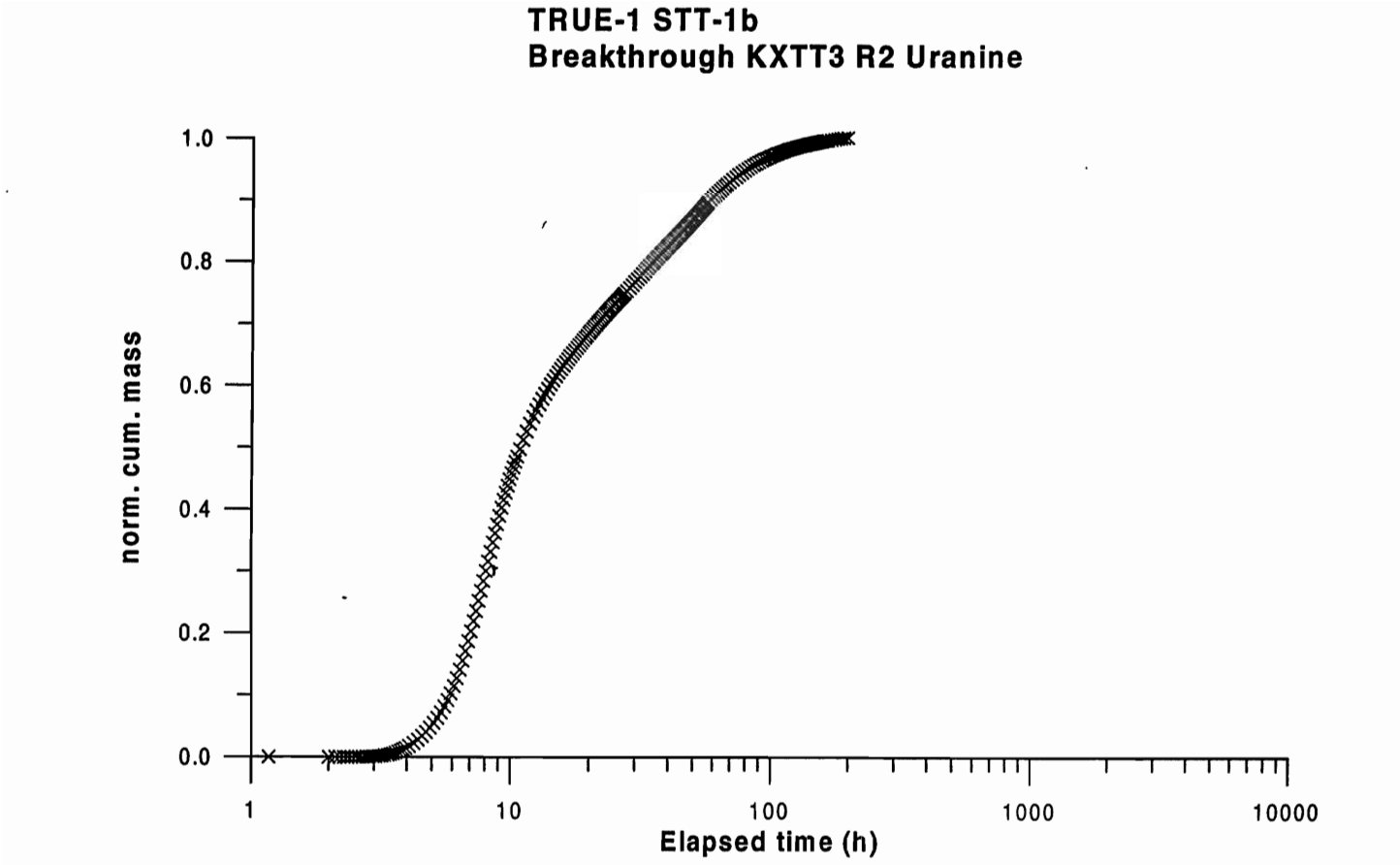
TRUE-1 STT-1b
Breakthrough KXTT3 R2 Uranine
norm. cum. mass
1.0
0.8
0.6
0.4
0.2
0.0
1
10
100
1000
10000
Elapsed time (h)

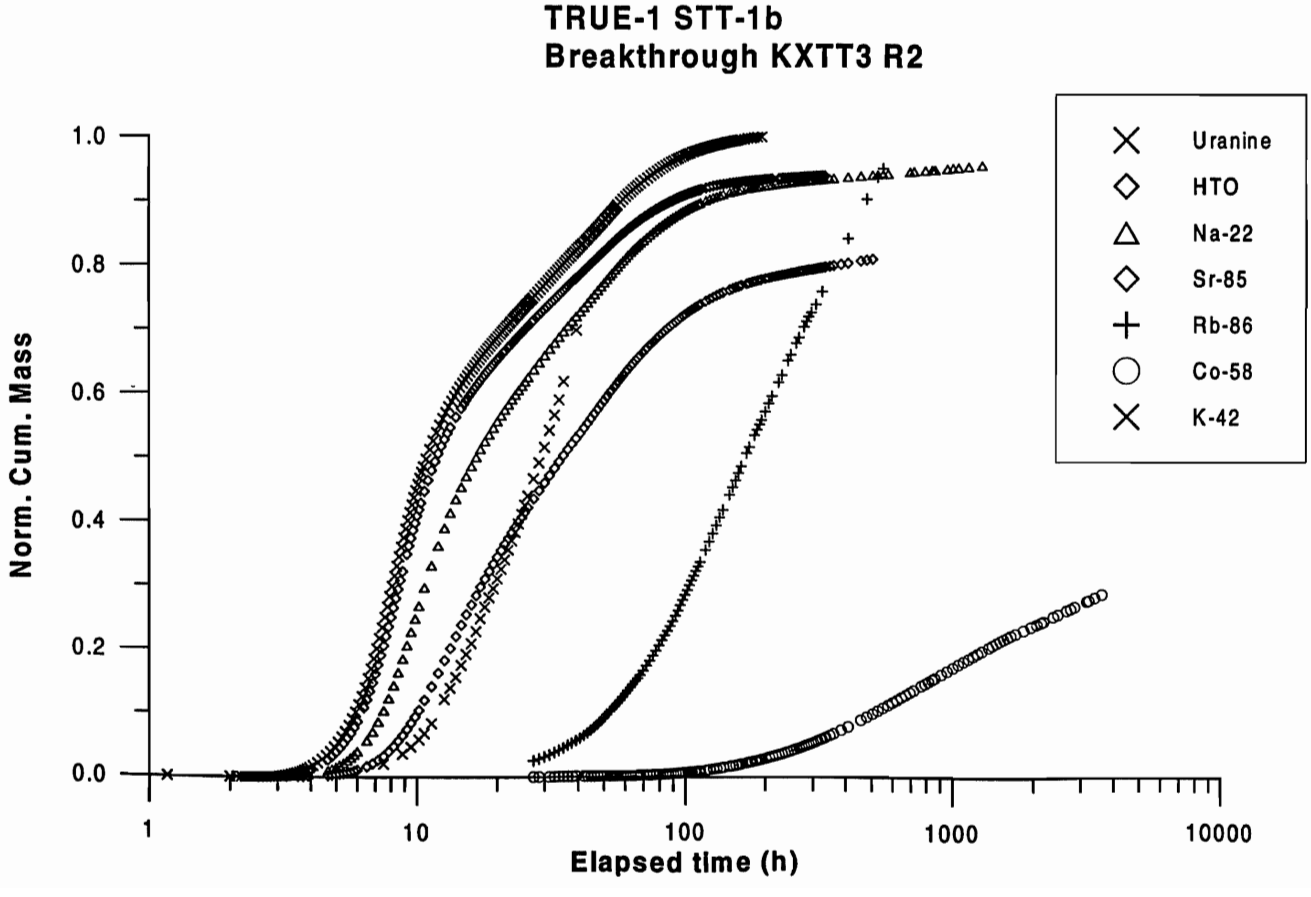
TRUE-1 STT-1b
Breakthrough KXTT3 R2
Norm. Cum. Mass
1.0
0.8
0.6
0.4
0.2
0.0
1
10
100
1000
10000
Elapsed time (h)
Uranine
HTO
Na-22
Sr-85
Rb-86
Co-58
K-42

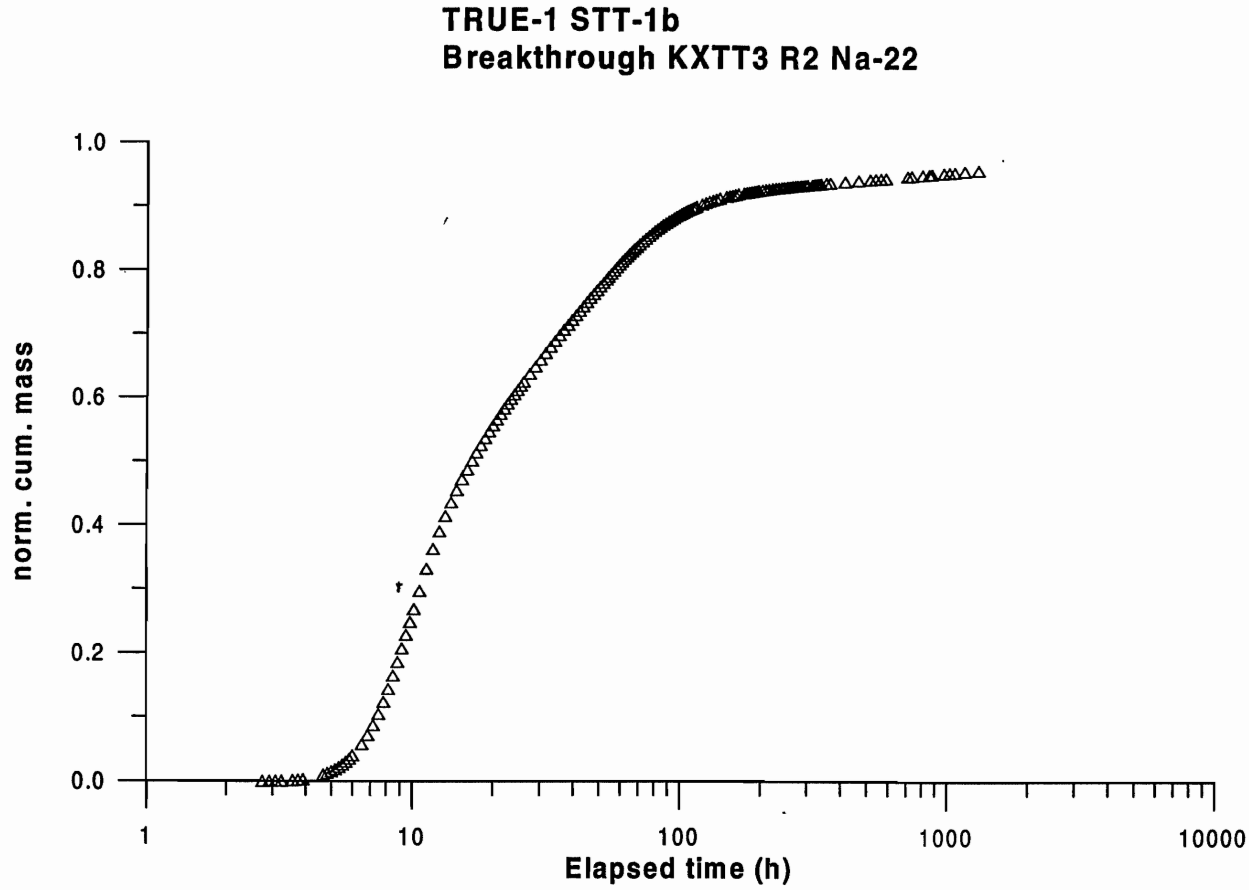
TRUE-1 STT-1b
Breakthrough KXTT3 R2 Na-22
norm. cum. mass
1.0
0.8
0.6
0.4
0.2
0.0
1
10
100
1000
10000
Elapsed time (h)

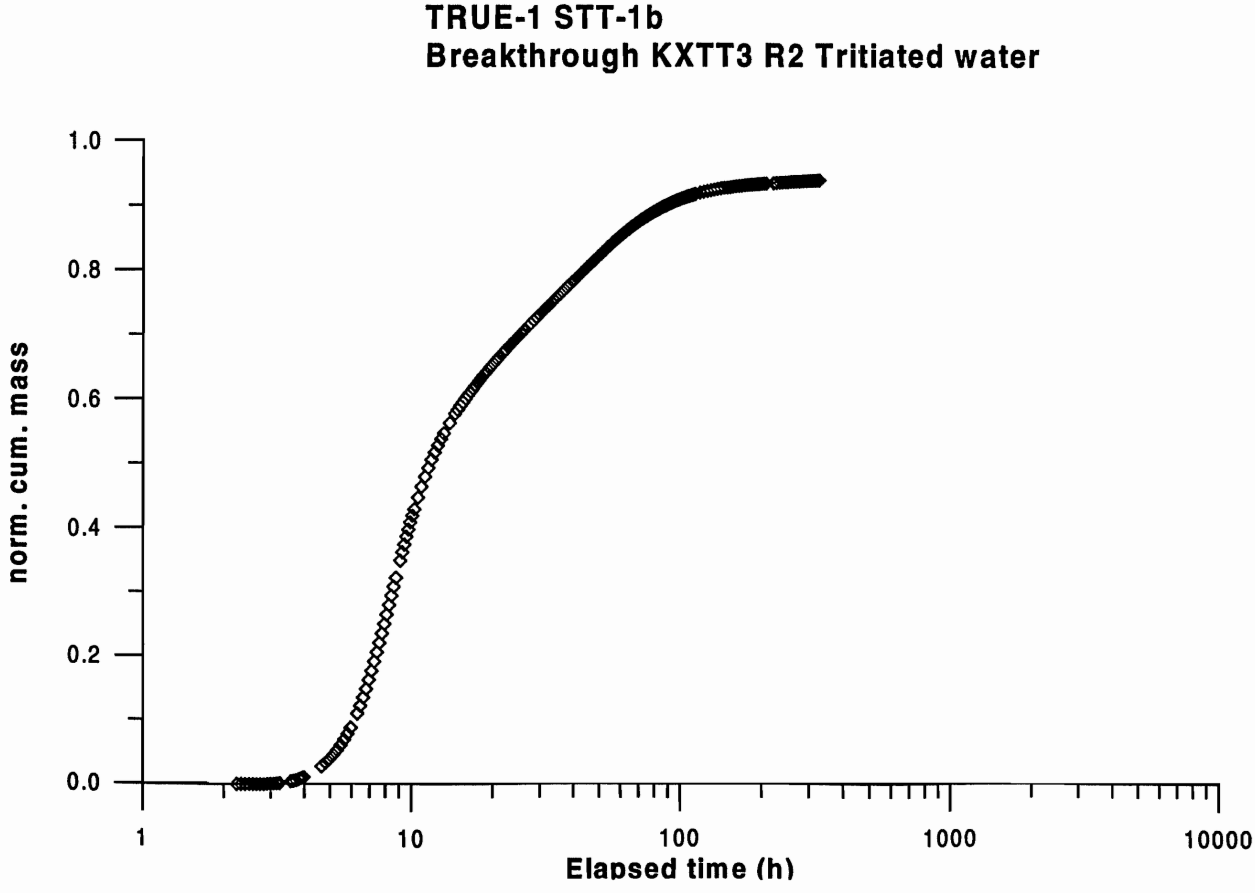
TRUE-1 STT-1b
Breakthrough KXTT3 R2 Tritiated water
norm. cum. mass
1.0
0.8
0.6
0.4
0.2
0.0
1
10
100
1000
10000
Elapsed time (h)

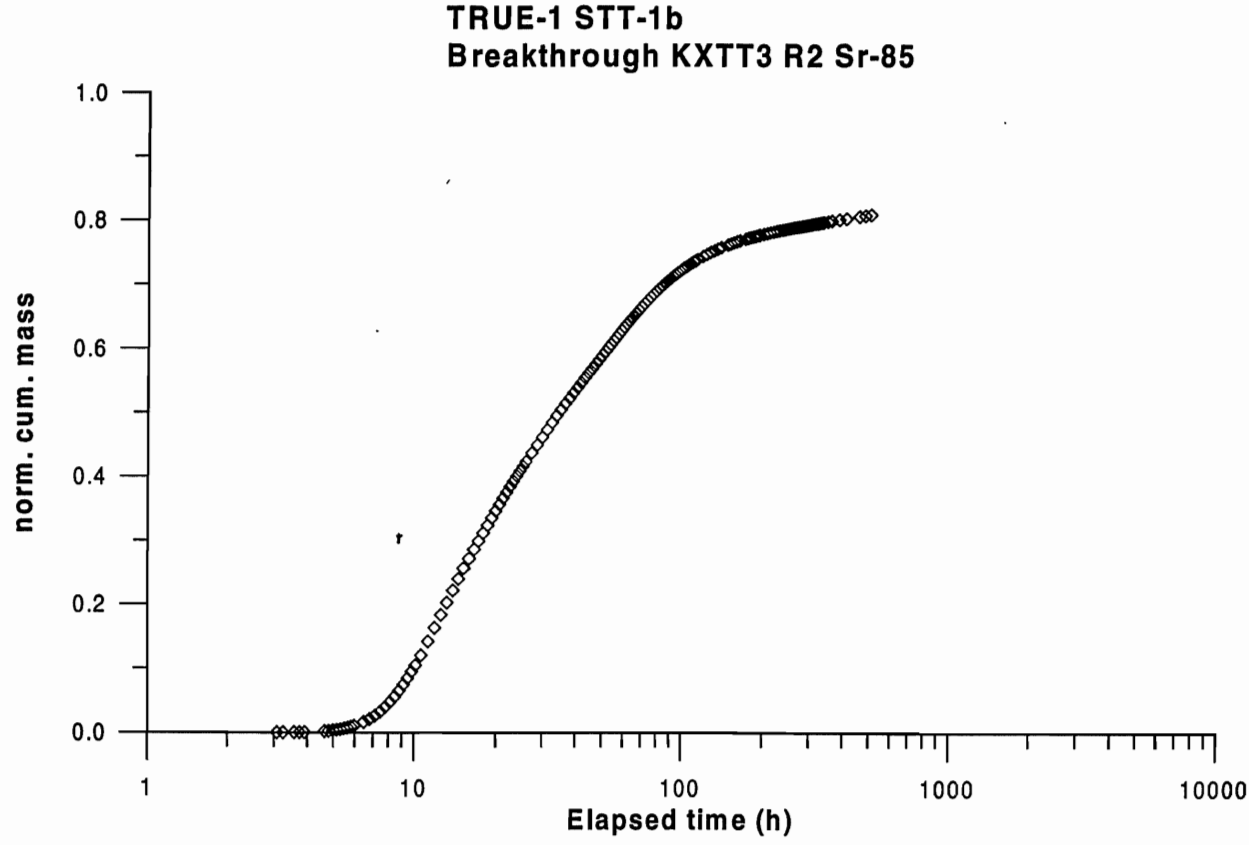
TRUE-1 STT-1b
Breakthrough KXTT3 R2 Sr-85
norm. cum. mass
1.0
0.8
0.6
0.4
0.2
0.0
1
10
100
1000
10000
Elapsed time (h)

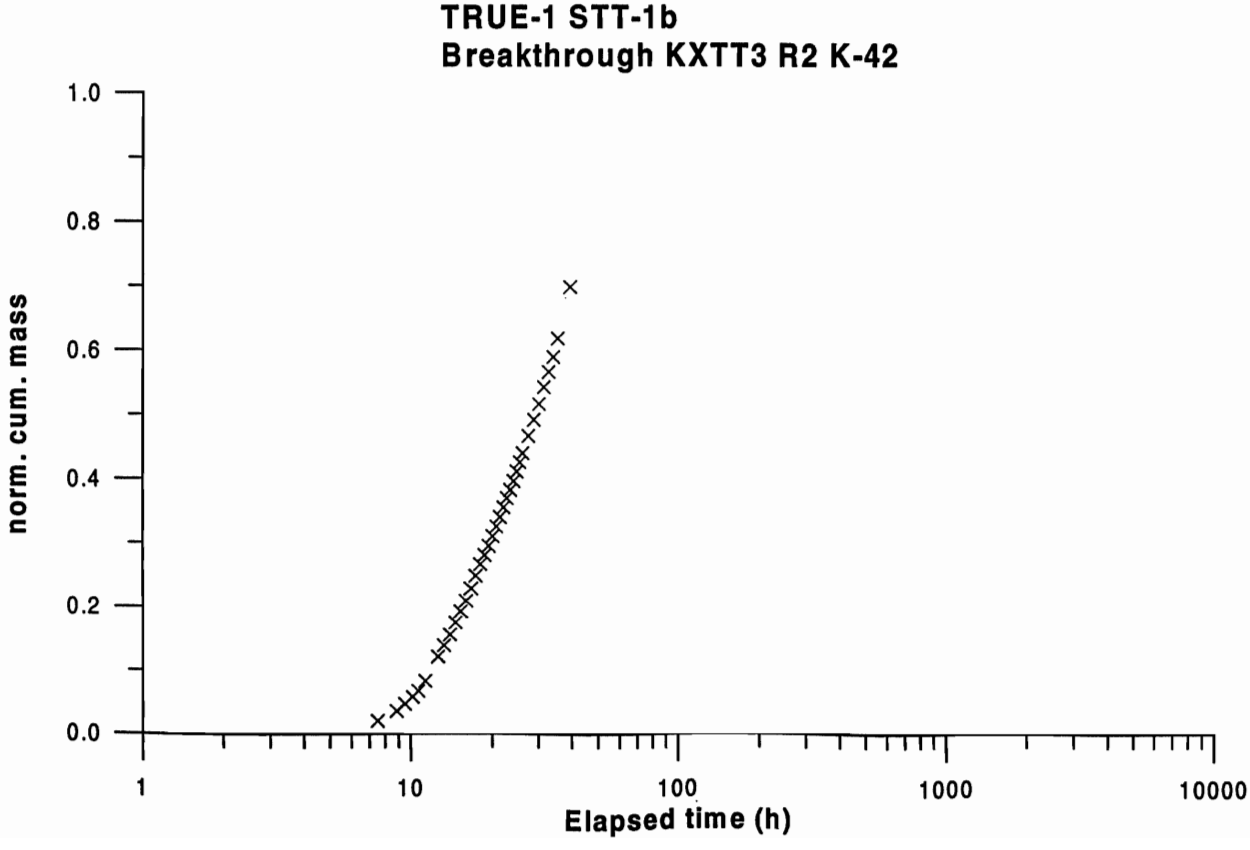
TRUE-1 STT-1b
Breakthrough KXTT3 R2 K-42
norm. cum. mass
1.0
0.8
0.6
0.4
0.2
0.0
1
10
100
1000
10000
Elapsed time (h)

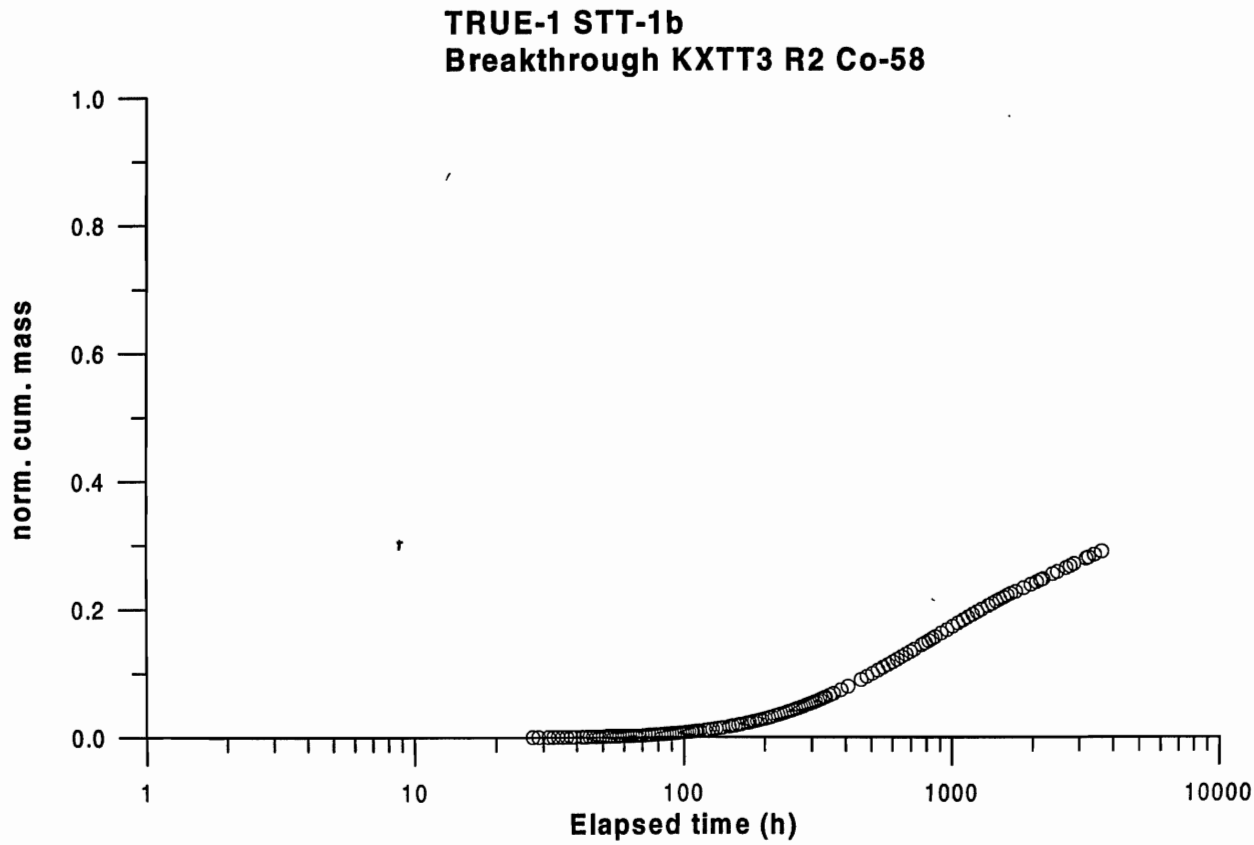
TRUE-1 STT-1b
Breakthrough KXTT3 R2 Co-58
norm. cum. mass
1.0
0.8
0.6
0.4
0.2
0.0
1
10
100
1000
10000
Elapsed time (h)

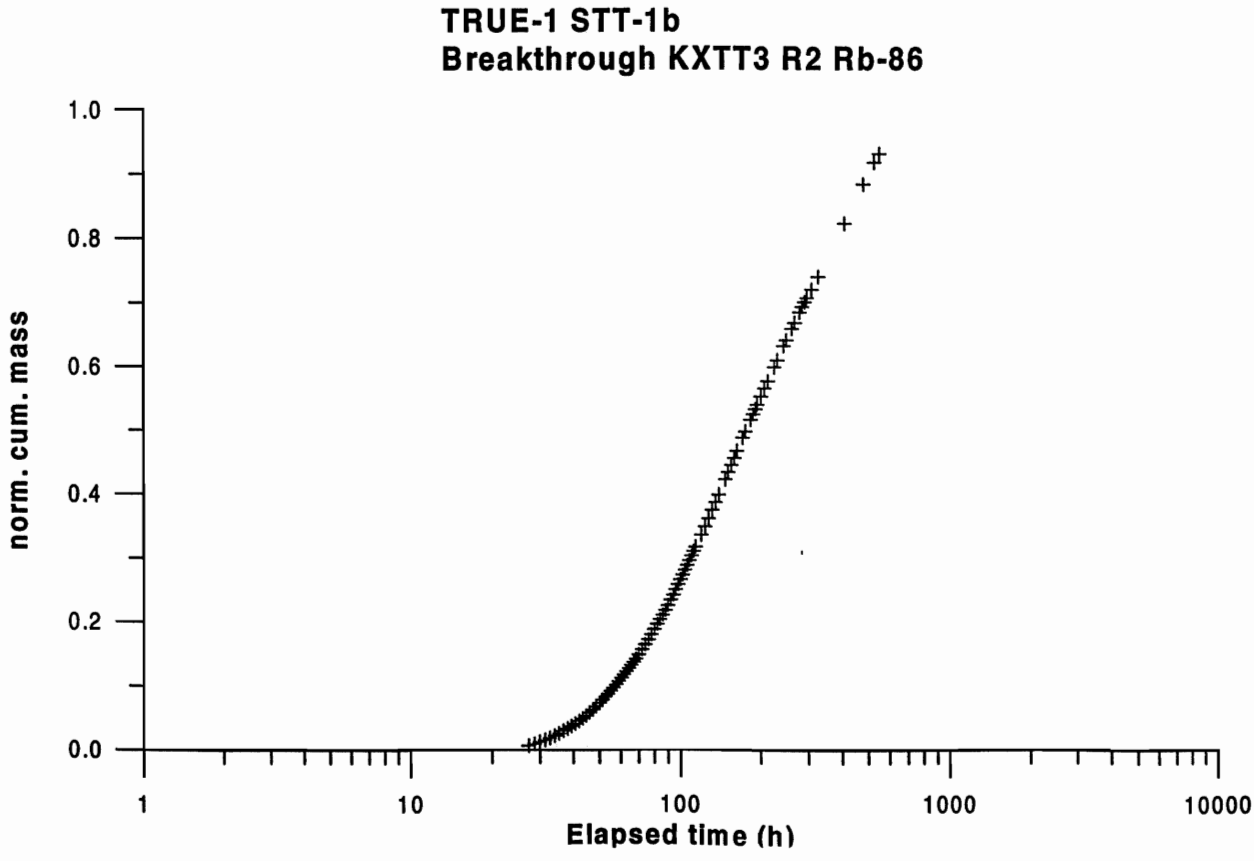
TRUE-1 STT-1b
Breakthrough KXTT3 R2 Rb-86
norm. cum. mass
1.0
0.8
0.6
0.4
0.2
0.0
1
10
100
1000
10000
Elapsed time (h)

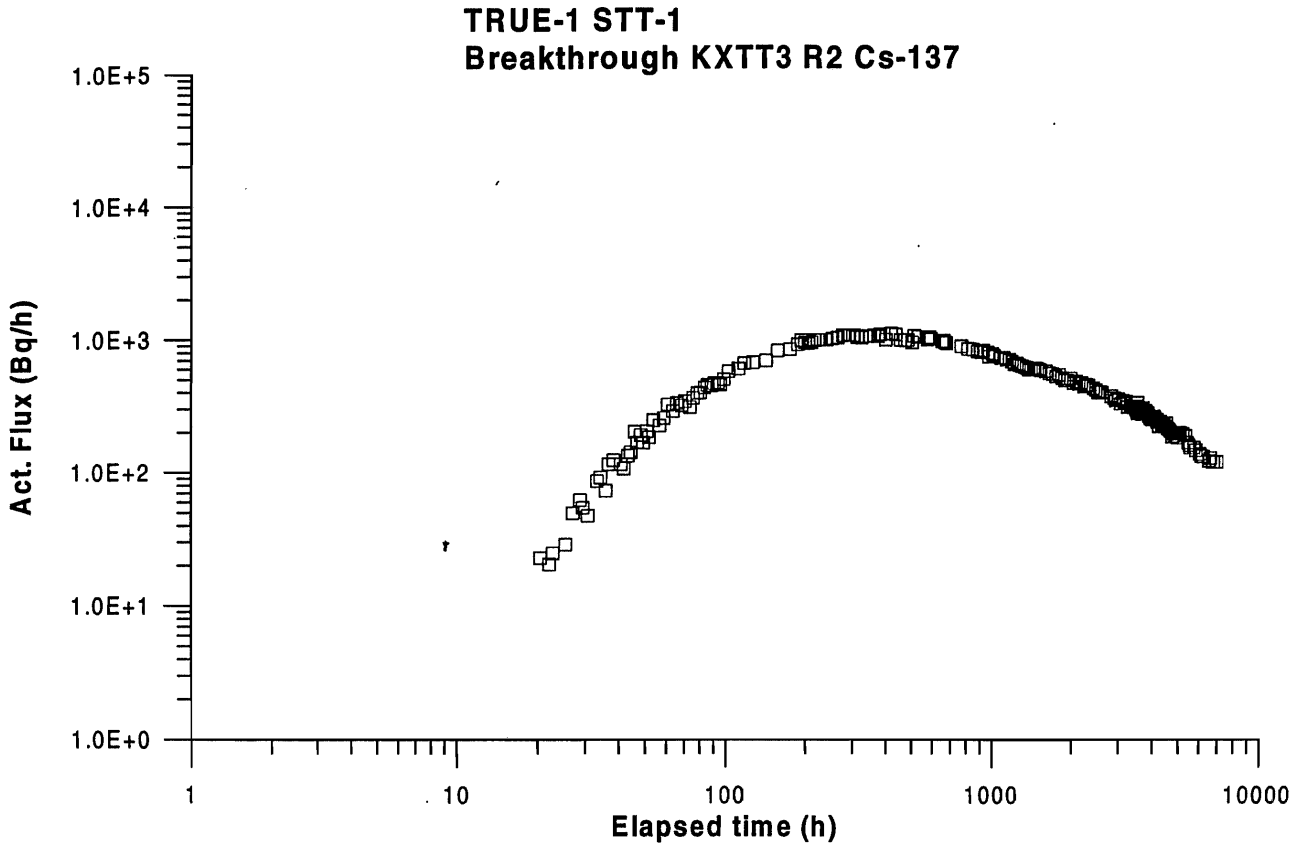
TRUE-1 STT-1
Breakthrough KXTT3 R2 Cs-137
Act. Flux (Bq/h)
1.0E+5
1.0E+4
1.0E+3
1.0E+2
1.0E+1
1.0E+0
1
10
100
1000
10000
Elapsed time (h)

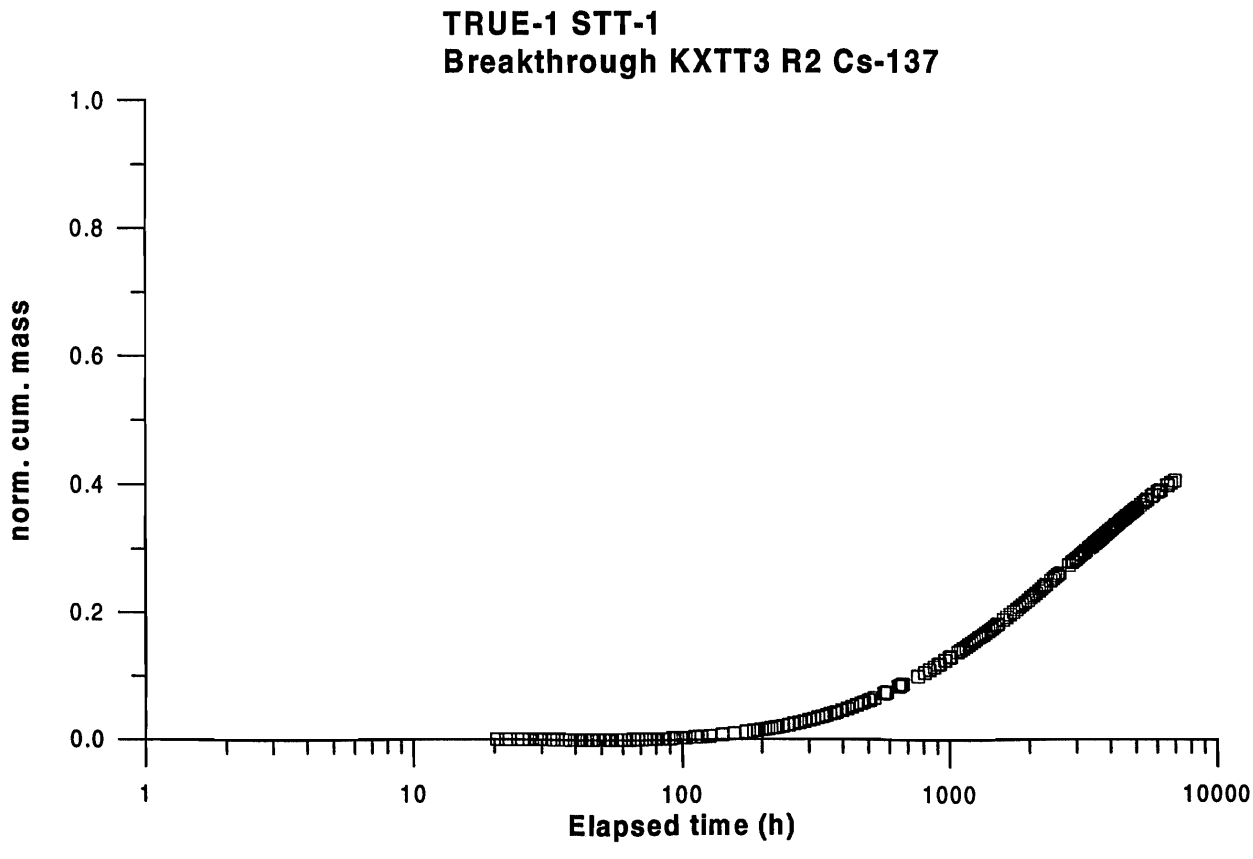
TRUE-1 STT-1
Breakthrough KXTT3 R2 Cs-137
norm. cum. mass
1.0
0.8
0.6
0.4
0.2
0.0
1
10
100
1000
10000
Elapsed time (h)

TRACER RECOVERY

- **Tracer recovery >100% for conservative tracers if caculated flow rates are used, not possible!**
- **Reason may be that borehole section volume is underestimated due to larger borehole diameter and/or smaller dummy diameter**
- **Recovery for Uranine set to 100% achieved by increasing the volume for injection section by 20%**

GEOSIGMA
MARK BERG VATTEN MILJÖ

Tracer travel times, t_5, t_{50} and t_{95} based on injected mass at t_{inj} for tracers injected during STT-1b.

Tracer	t_5 (h)	t_{50} (h)	t_{95} (h)	t_{inj} (h)
Uranine	5.0	11	80.5	192
HTO	5.3	12	-	186
Na-22	6.5	16.7	900	164
K-42	10	30	-	18
Sr-85	8.3	35	-	248
Rb-86	43	176	-	140
Co-58	285	-	-	1980
Cs-137 (STT-1)	426	-	-	595

NUMERICAL MODELLING

- 1D Advection-dispersion-linear sorption model (same as used in earlier tests)
- Automatic parameter estimation by non-linear least-square regression including error estimates
- Discretization of source term in 50 time steps
- Using standard error ($1/s^2$) as weight for each data point
- Modelling in two steps, first conservative tracers, then simultaneous run with conservative and sorbing tracers
- Parameters determined from step 1: mean travel time, t_m , dispersivity, D/v, proportonality factor, f
- Additional parameters determined from step 2: retardation coefficient, R, relative inj. concentration, f_c

GEOSIGMA
MARK BERG VATTEN MILJÖ

TRACER RECOVERY

Tracer	t_t (h)	Recovery (%)
Uranine	195	100
HTO	333	94
Na-22	1292	96
K-42	39	70
Sr-85	505	81
Rb-86	553	93
Co-58	3622	29
Cs-137 (STT-1)	5600	41

MODELLING RESULTS

- Values consistent with earlier model runs (RC-1 and PDT 1-3)
- Good fits to experimental data for Uranine, and Na using linear sorption
- Not possible to fit Sr, Rb and Co with linear sorption only
- Retardation coefficients vary between 1.4 (Na) and 58 (Cs)
- Values consistent with STT-1

GEOSIGMA
MARK BERG VATTEN MILJÖ

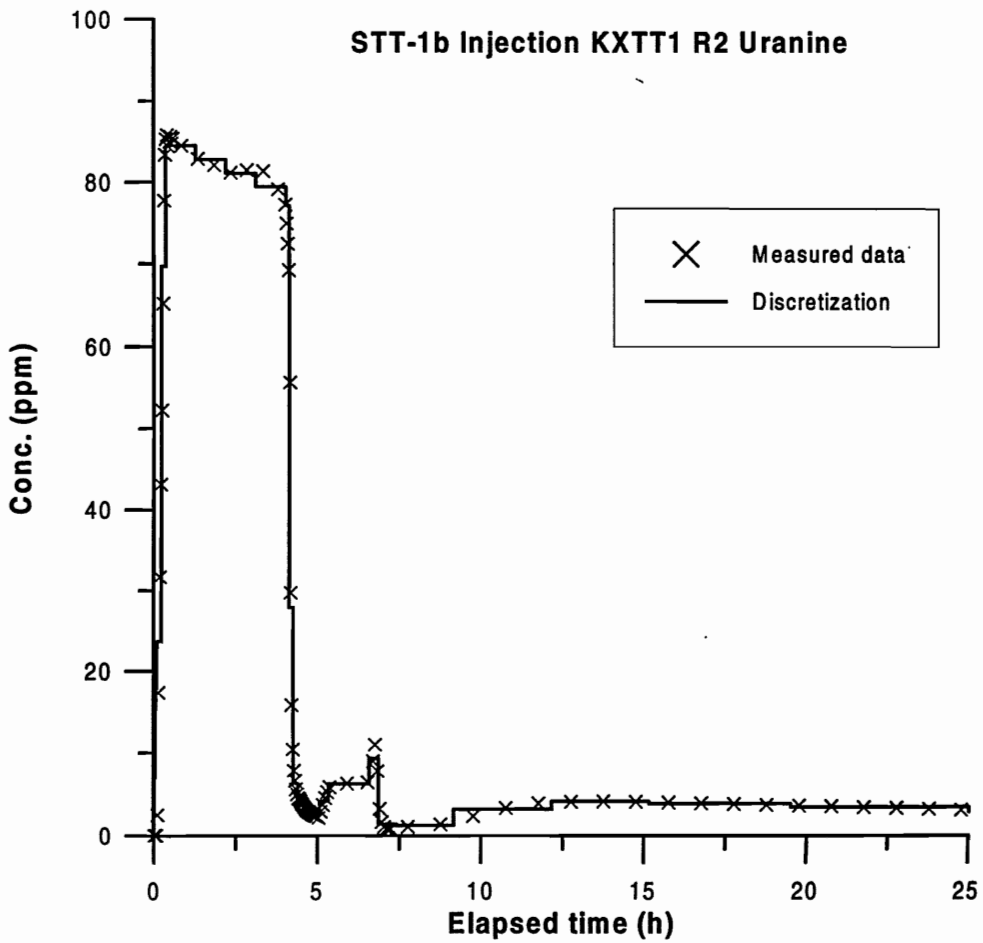

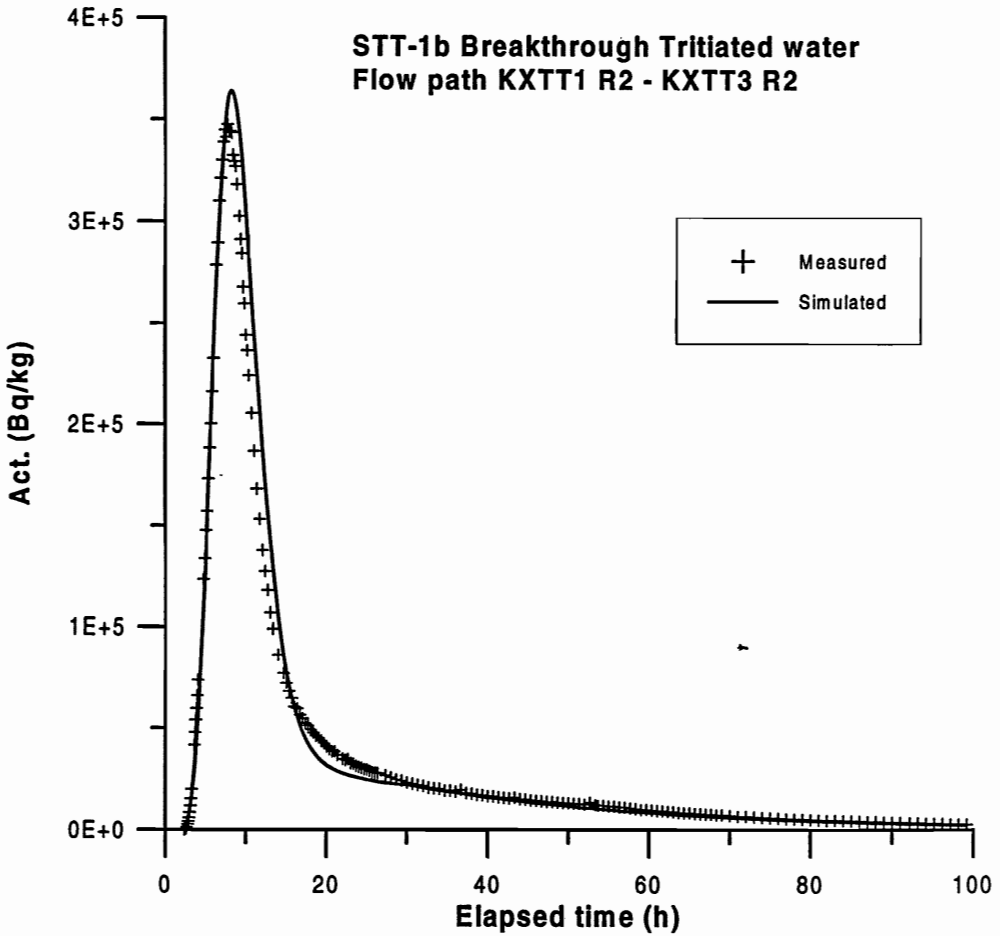
STT-1b Breakthrough Tritiated water
Flow path KXTT1 R2 - KXTT3 R2
Measured
Simulated
Act. (Bq/kg)
4E+5
3E+5
2E+5
1E+5
0E+0
0
20
40
60
80
100
Elapsed time (h)

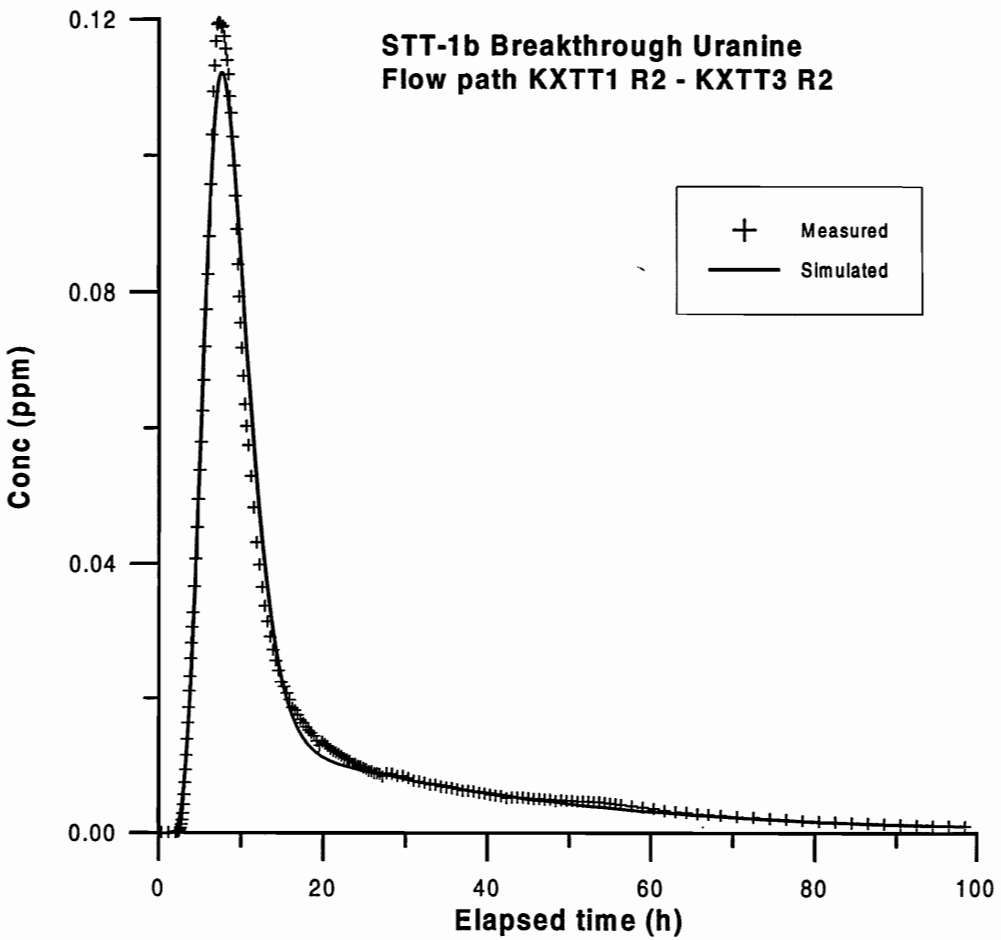
STT-1b Breakthrough Uranine
Flow path KXTT1 R2 - KXTT3 R2
Measured
Simulated
Conc (ppm)
0.12
0.08
0.04
0.00
0
20
40
60
80
100
Elapsed time (h)

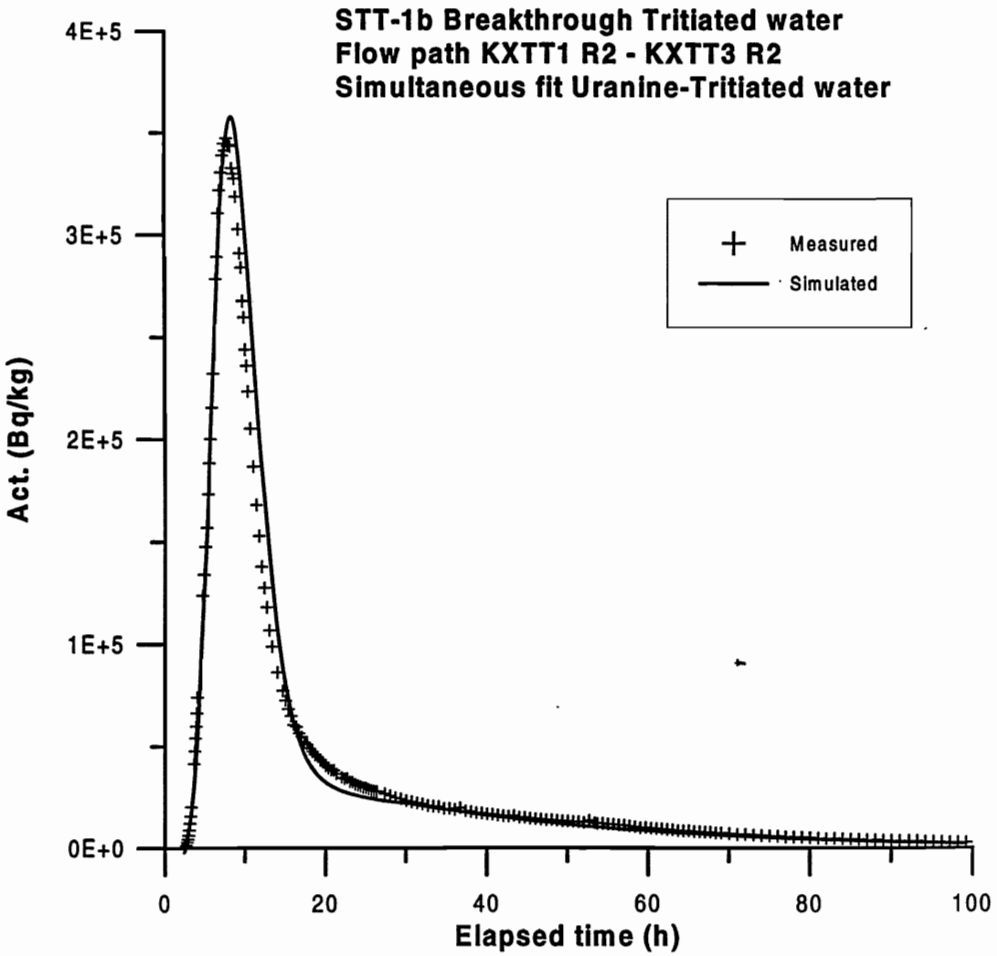
STT-1b Breakthrough Tritiated water
Flow path KXTT1 R2 - KXTT3 R2
Simultaneous fit Uranine-Tritiated water
Measured
Simulated
Act. (Bq/kg)
4E+5
3E+5
2E+5
1E+5
0E+0
0
20
40
60
80
100
Elapsed time (h)

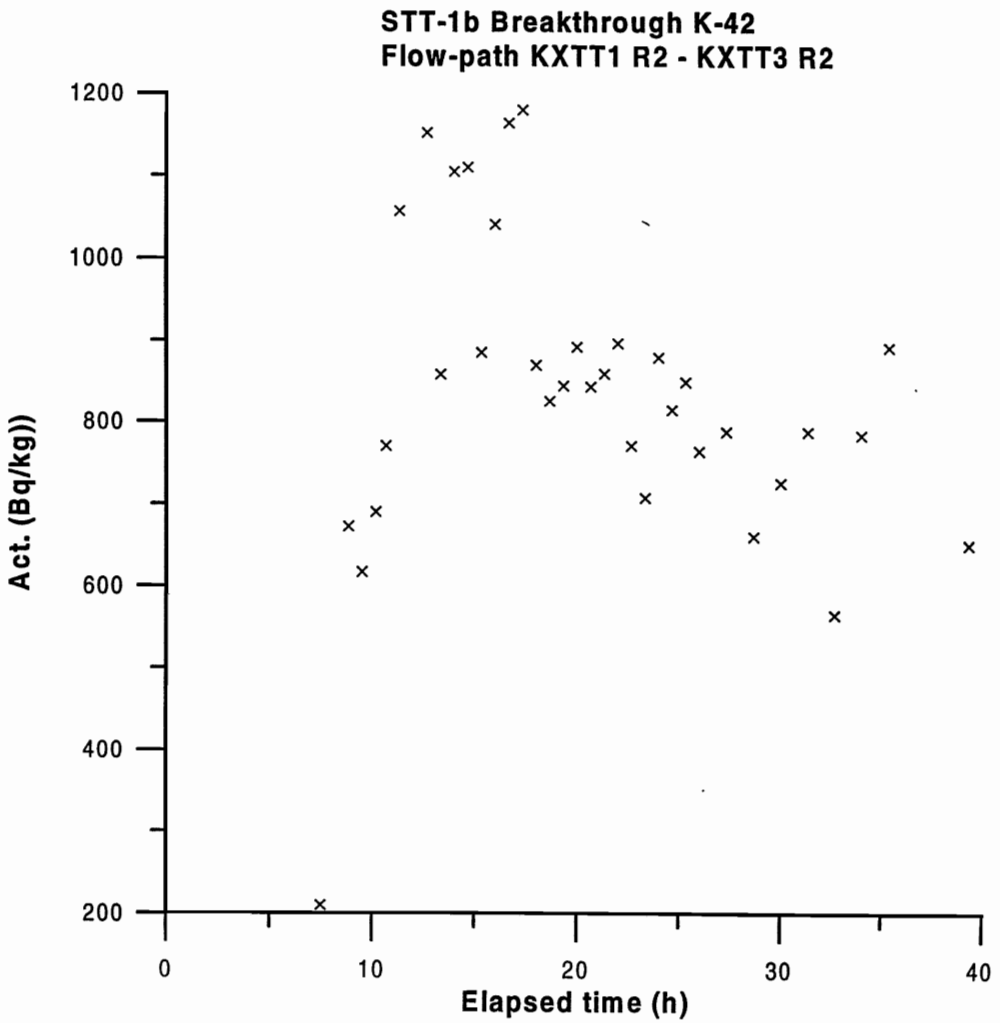
STT-1b Breakthrough K-42
Flow-path KXTT1 R2 - KXTT3 R2
Act. (Bq/kg))
1200
1000
800
600
400
200
0
10
20
30
40
Elapsed time (h)

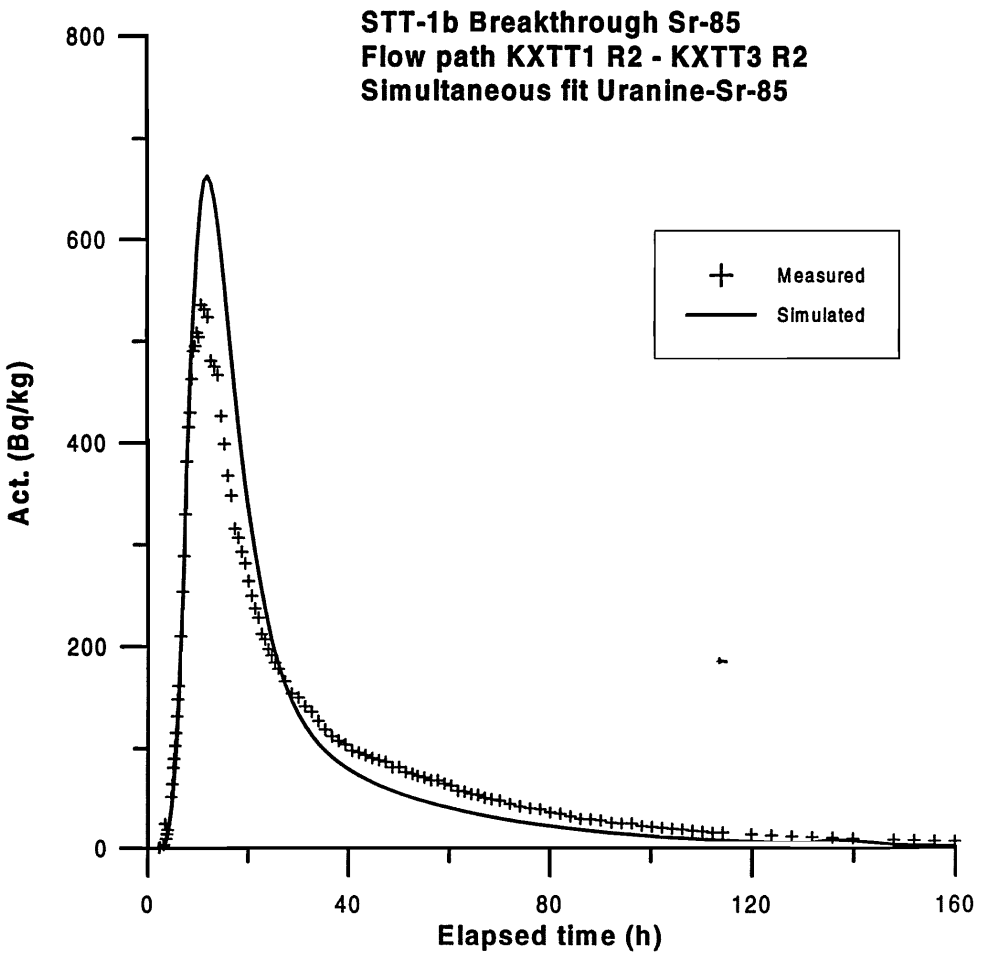
STT-1b Breakthrough Sr-85
Flow path KXTT1 R2 - KXTT3 R2
Simultaneous fit Uranine-Sr-85
Measured
Simulated
Act. (Bq/kg)
Elapsed time (h)
0
200
400
600
800
0
40
80
120
160

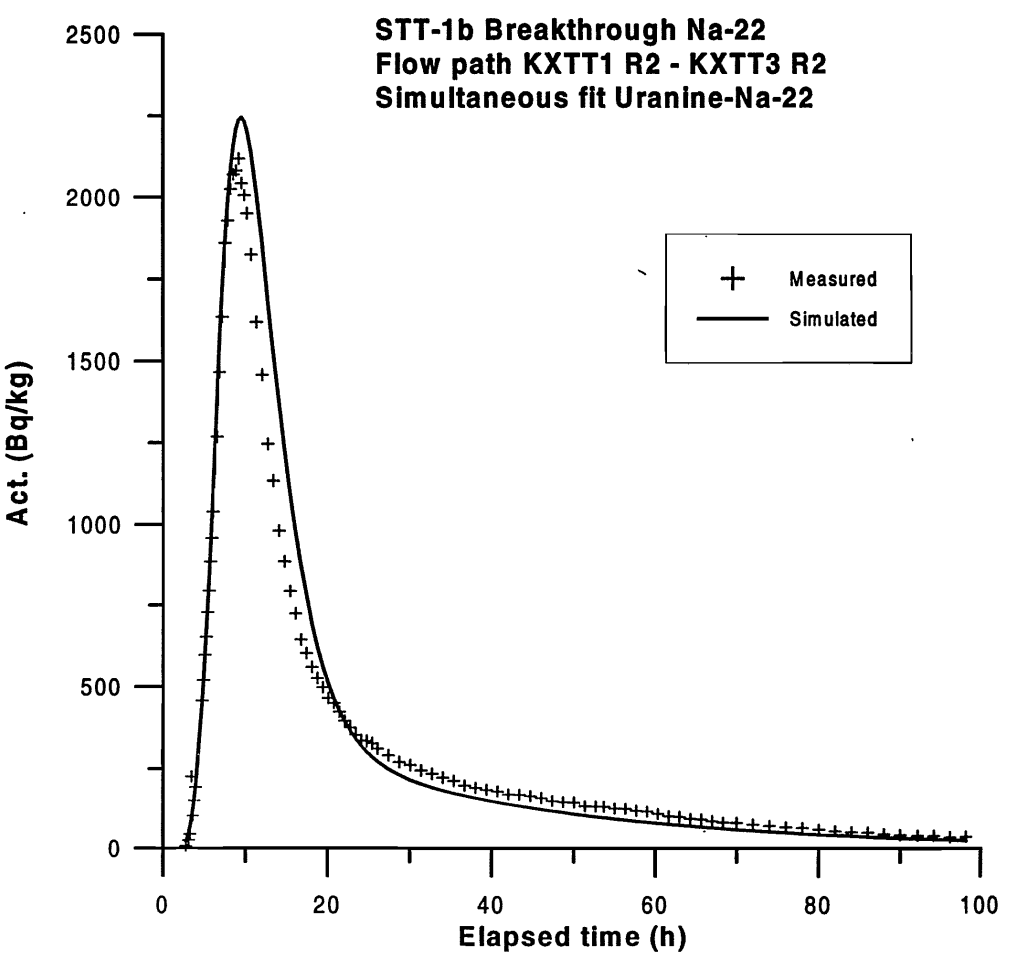
STT-1b Breakthrough Na-22
Flow path KXTT1 R2 - KXTT3 R2
Simultaneous fit Uranine-Na-22
Measured
Simulated
Act. (Bq/kg)
Elapsed time (h)
0
500
1000
1500
2000
2500
0
20
40
60
80
100

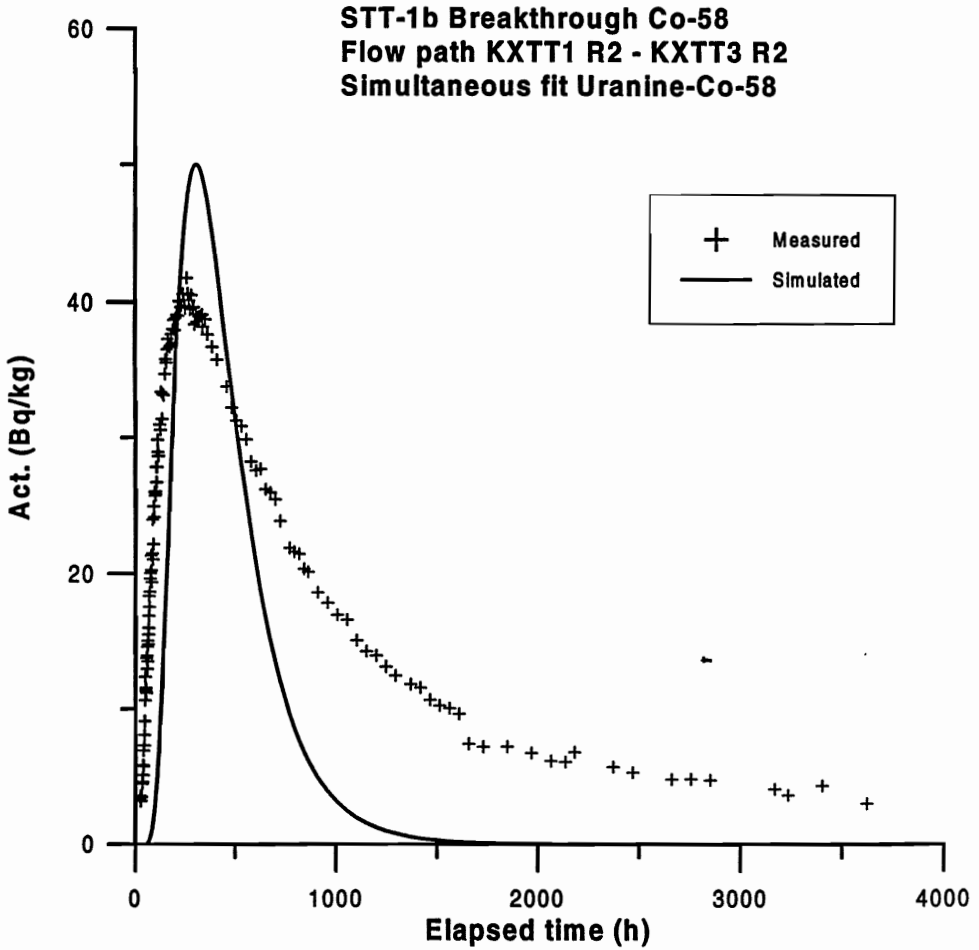
STT-1b Breakthrough Co-58
Flow path KXTT1 R2 - KXTT3 R2
Simultaneous fit Uranine-Co-58
Measured
Simulated
Act. (Bq/kg)
Elapsed time (h)
0
20
40
60
0
1000
2000
3000
4000

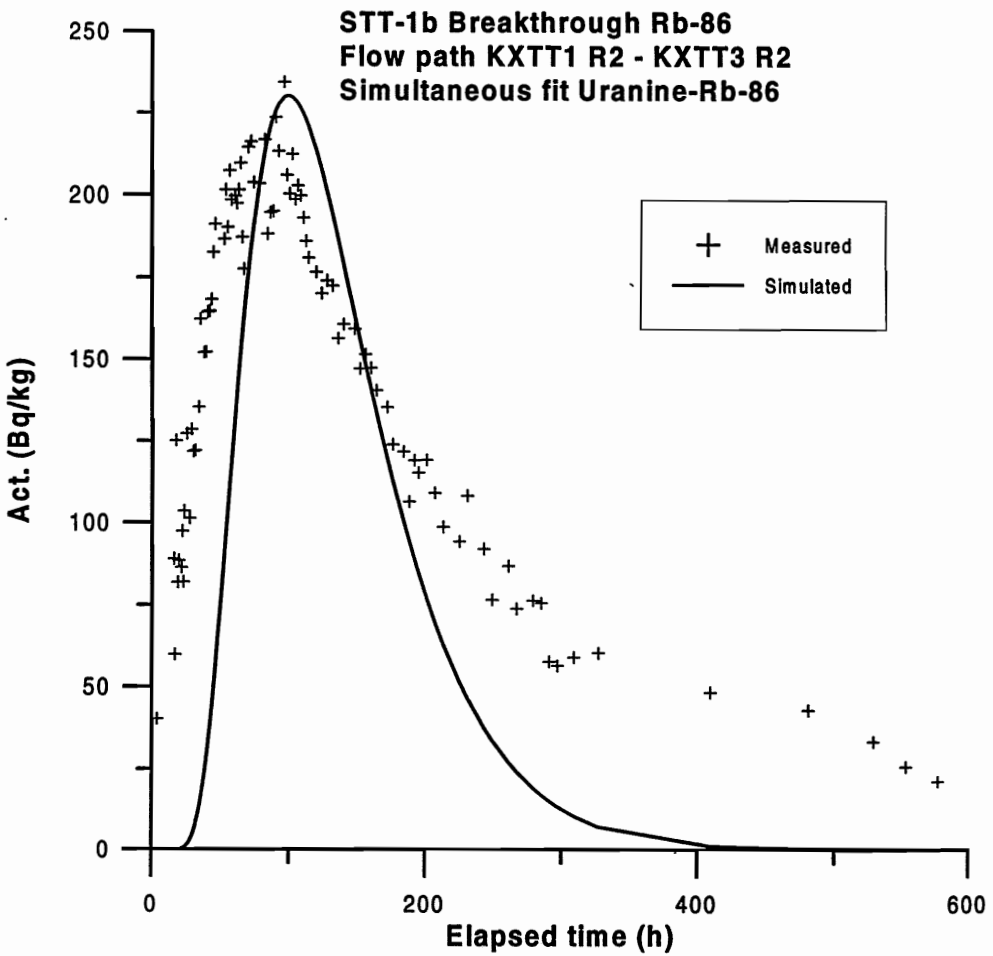
STT-1b Breakthrough Rb-86
Flow path KXTT1 R2 - KXTT3 R2
Simultaneous fit Uranine-Rb-86
Measured
Simulated
Act. (Bq/kg)
Elapsed time (h)
0
50
100
150
200
250
0
200
400
600

Evaluated parameters from PAREST (Advection-dispersion model)

Tracer	t_0 (h)	D/v	$F^*(10^{-2})$
Uranine	6.1	0.55	0.24
HTO	6.6	0.46	0.23
Na-22	8.6	0.69	0.22
Sr-85	14.9	1.9	0.17
Rb-86	123	3.9	0.21
Co-58	672	6.2	0.11

Evaluated parameters from PAREST (Advection-dispersion-linear sorption model). Simultaneous run Uranine and sorbing tracer.

Tracer	t_0 (h)	D/v	$F^*(10^{-2})$	R	f_c
Uranine	6.1	0.55	0.24	1	1
Na-22	6.2	0.59	0.24	1.37	0.95
Sr-85	6.2	0.60	0.24	1.86	0.78
Rb-86	6.1	0.56	0.24	17.0	0.49
Co-58	6.5	0.80	0.22	57.0	0.21

MODELLING RESULTS

Summary of measured and evaluated parameters for the flow path KXTT1 R2→KXTT3 R2 from STT-1b and for the flow path KXTT4 R3→KXTT3 R2 from STT-1.

Parameter	STT-1b Value	STT-1 Value
Travel distance, L (m)	5.03	4.68
Mean head difference, Δh (m)	9.5	6.8
Mean velocity, v (m/s)	$2.3 \cdot 10^{-4}$	$2.5 \cdot 10^{-4}$
Mean travel time, t_m (h)	6.1	5.1
First arrival, t_a (h)	2.3	1.3
Dispersivity, D/v (m)	0.55	2.0
Mass recovery, R (%)	100	100

Appendix B – Task 4E modelling results

B.1 Comparison of modelling results

B.2 Contributions of modelling results of Task 4E

- Modelling of reactive-radioactive and sorbing tracer tests in Feature A at Äspö HRL. Lutz Liedtke & Hua Shao (BMBF/BGR)
- Tracer tests with sorbing tracers. Task 4E-II: Analysis of STT-1 blind predictions and Task 4EIII: Predictions of STT-1b. T.T. Cladouhos, William S. Dershowitz, Ian Miller (Golder) and Masahiro Uchida (PNC)
- Modelling of the sorbing tracer tests by using the Channel Network model. B. Khademi &Luis Moreno (SKB/KTH-KAT)
- Numerical analysis with FEGM/FERM for TRUE-1 sorbing tracer tests. Yasuharu Tanaka, Toshifumu Igarashi, Motoi Kawanishi (CRIEPI)
- Predictions of the sorbing tracer test STT1b of the TRUE. Antii Poteri (POSIVA)
- Evaluation of STT-1 and prediction of STT-1b. Vladimir Cvetkovic, (SKB/TRUE)
- Modelling and blind predictions for STT-1b tracer test. Andreas Jakob (NAGRA/PSI)
- The interaction of sorbing and non-sorbing tracers with different Äspö rock types. Sorption and diffusion experiments in the laboratory scale. Johan Byegård, Henrik Johansson, Mats Skålberg (CTH), Eva Lena Tullborg (Terralogica)

B.1 Comparisons of modelling results

TASK NO 4E:2 – PREDICTIVE MODELLING OF THE STT-1b TRACER EXPERIMENTS WITHIN TRUE-1

Seven different groups have presented predictive modelling results for the STT-1b tracer experiment within TRUE-1. The modelling teams are presented in table 1.

Table 1 Modelling teams and their model approach to Task 4E:2.

MODELLING TEAM	MODEL APPROACH	AUTHOR
BMBF / BGR	Deterministic	Liedtke & Shao
CRIEPI	Deterministic	Tanaka et al
NAGRA / PSI	Deterministic	Jakob & Heer
PNC / Golder	Deterministic	Cladouhos et al
POSIVA / VTT	Stochastic	Poteri
SKB / KTH-KAT	Stochastic	Khademi & Moreno
SKB / TRUE	Deterministic	Cvetkovic et al
Experimental results	Results from field tracer experiments	Andersson et al

The modelling groups have predicted the breakthrough of the non-sorbing tracers; Uranine and tritiated water (HTO), and the sorbing radioactive tracers Na, Rb and Sr. All groups except CRIEPI and POSIVA/VTT have also modelled the sorbing tracers Co and K. Breakthrough times for the tracers are presented in tables and diagrams. The predictive breakthrough of the seven different tracers is shown in two different ways; as mass flux (Bq/h or mg/h) versus time (h) and as cumulative percentage versus time. The t_5, t_{50} and t_{95} for each tracer are shown as histograms and in tables. In the tables the results are differentiated between the stochastic and deterministic models. In the histograms both types of models are shown in the same diagram where data from the stochastic models are taken from the 50% column.

The groups NAGRA/PSI, SKB/KTH-KAT and PNC/Golder have also modelled all seven tracers with a Dirac pulse. The results are presented as diagrams with cumulative percentage versus time.

STOCHASTIC MODELS OF MASS RECOVERY - Task 4E:2

Table 1 Mass recovery of Cobalt. Unit for mass recovery is (%). The detection time (T_{100}) unit is hours.

Modelling team	F_c (5%)	F_c (50%)	F_c (95%)	T_{100} (h)
POSIVA / VTT	-	-	-	-
SKB / KTH-KAT	90	96	98	3622
Experimental results		*29*		*3622*

Table 2 Mass recovery of tritiated water (HTO). Unit for mass recovery is (%). The detection time (T_{100}) unit is hours.

Modelling team	F_c (5%)	F_c (50%)	F_c (95%)	T_{100} (h)
POSIVA / VTT	96	100	100	333
SKB / KTH-KAT	93	99	99	333
Experimental results		*94*		*333*

Table 3 Mass recovery of Potassium. Unit for mass recovery is (%). The detection time (T_{100}) unit is hours.

Modelling team	F_c (5%)	F_c (50%)	F_c (95%)	T_{100} (h)
POSIVA / VTT	-	-	-	-
SKB / KTH-KAT	71	86	95	39
Experimental results		*70*		*39*

Table 4 Mass recovery of Rubidium. Unit for mass recovery is (%). The detection time (T_{100}) unit is hours.

Modelling team	F_c (5%)	F_c (50%)	F_c (95%)	T_{100} (h)
POSIVA / VTT	96	100	100	553
SKB / KTH-KAT	48	66	84	553
Experimental results		*93*		*553*

Table 5 Mass recovery of Sodium. Unit for mass recovery is (%). The detection time (T_{100}) unit is hours.

Modelling team	F_c (5%)	F_c (50%)	F_c (95%)	T_{100} (h)
POSIVA / VTT	97	100	100	1292
SKB / KTH-KAT	94	99	99	1292
Experimental result		*96*		*1292*

Table 6 Mass recovery of Strontium. Unit for mass recovery is (%). The detection time (T_{100}) unit is hours.

Modelling team	F_c (5%)	F_c (50%)	F_c (95%)	T_{100} (h)
POSIVA / VTT	97	100	100	505
SKB / KTH-KAT	93	99	99	505
Experimental results		*81*		*505*

Table 7 Mass recovery of Uranine. Unit for mass recovery is (%). The detection time (T_{100}) unit is hours.

Modelling team	F_c (5%)	F_c (50%)	F_c (95%)	T_{100} (h)
POSIVA / VTT	96	100	100	195
SKB / KTH-KAT	93	98	99	195
Experimental results		*100*		*195*

DETERMINISTIC MODELS OF MASS RECOVERY - Task 4E:2

Table 1 Mass recovery of Cobalt. Unit for mass recovery is (%). The detection time (T_{100}) unit is hours.

Modelling team	F_c (%)	T_{100} (h)
BMBF / BGR	65.1	3622
CRIEPI	-	-
PNC / Golder	89.6	3620
NAGRA / PSI	5.2	3622
SKB / TRUE	73	3622
Experimental results	*29*	*3622*

Table 2 Mass recovery of tritiated water (HTO). Unit for mass recovery is (%). The detection time (T_{100}) unit is hours.

Modelling team	F_c (%)	T_{100} (h)
BMBF / BGR	99.9	333
CRIEPI	100	333
PNC / Golder	99.1	333
NAGRA / PSI	99.8	333
SKB / TRUE	109	333
Experimental results	*94*	*333*

Table 3 Mass recovery of Potassium. Unit for mass recovery is (%). The detection time (T_{100}) unit is hours.

Modelling team	F_c (%)	T_{100} (h)
BMBF / BGR	59.5	39
CRIEPI	-	-
PNC / Golder	88.5	39.3
NAGRA / PSI	35.9	39
SKB / TRUE	23	39
Experimental results	*70*	*39*

Table 4 Mass recovery of Rubidium. Unit for mass recovery is (%). The detection time (T_{100}) unit is hours.

Modelling team	F_c (%)	T_{100} (h)
BMBF / BGR	69.4	553
CRIEPI	100	553
PNC / Golder	81.2	553
NAGRA / PSI	71.2	553
SKB / TRUE	86	553
Experimental results	*93*	*553*

Table 5 Mass recovery of Sodium. Unit for mass recovery is (%). The detection time (T_{100}) unit is hours.

Modelling team	F_c (%)	T_{100} (h)
BMBF / BGR	92.3	1292
CRIEPI	99.99	1292
PNC / Golder	100	1292
NAGRA / PSI	100	1292
SKB / TRUE	103	1292
Experimental results	*96*	*1292*

Table 6 Mass recovery of Strontium. Unit for mass recovery is (%). The detection time (T_{100}) unit is hours.

Modelling team	F_c (%)	T_{100} (h)
BMBF / BGR	82.2	505
CRIEPI	99.99	505
PNC / Golder	96.9	505
NAGRA / PSI	99.8	505
SKB / TRUE	100	505
Experimental results	*81*	*505*

Table 7 Mass recovery of Uranine. Unit for mass recovery is (%). The detection time (T_{100}) unit is hours.

Modelling team	F_c (%)	T_{100} (h)
BMBF / BGR	85.9	195
CRIEPI	99.95	195
PNC / Golder	97.9	195
NAGRA / PSI	97.0	195
SKB / TRUE	106	195
Experimental results	*100*	*195*

STOCHASTIC MODELS OF BREAKTHROUGH TIME - Task 4E:2

Table 1 Breakthrough times for Cobalt in the stochastic models. Unit for measured input functions is hours. The experimental results are based on injected mass at 1980 h.

Modelling team	t5 (5%)	t5 (50%)	T5 (95%)	t50 (5%)	t50 (50%)	t50 (95%)	t95 (5%)	t95 (50%)	t95 (95%)
POSIVA / VTT	-	-	-	-	-	-	-	-	-
SKB / KTH - KAT	5.0	8.9	16.1	46.9	75.0	138.5	1755.4	1982.2	-
Experimental results		*285*			-			-	

Table 2 Breakthrough times for tritiated water (HTO) in the stochastic models. Unit for measured input functions is hours. The experimental results are based on injected mass at 186 h.

Modelling team	t5 (5%)	t5 (50%)	t5 (95%)	t50 (5%)	t50 (50%)	t50 (95%)	t95 (5%)	t95 (50%)	t95 (95%)
POSIVA / VTT	3.0	3.3	4.2	7.5	8.7	11	33	40	78
SKB / KTH - KAT	3.9	7.0	10.2	9.0	14.8	23.1	78.2	90.6	-
Experimental results		*5.3*			*12*			-	

Table 3 Breakthrough times for Potassium in the stochastic models. Unit for measured input functions is hours. The experimental results are based on injected mass at 18 h.

Modelling team	t5 (5%)	t5 (50%)	t5 (95%)	t50 (5%)	t50 (50%)	t50 (95%)	t95 (5%)	t95 (50%)	t95 (95%)
POSIVA / VTT	-	-	-	-	-	-	-	-	-
SKB / KTH - KAT	4.0	7.1	10.7	8.2	14.5	24.9	43.9	-	-
Experimental results		*10*			*30*			-	

Table 4 Breakthrough times for Rubidium in the stochastic models. Unit for measured input functions is hours. The experimental results are based on injected mass at 140 h.

Modelling team	t5 (5%)	t5 (50%)	t5 (95%)	t50 (5%)	t50 (50%)	t50 (95%)	t95 (5%)	t95 (50%)	t95 (95%)
POSIVA / VTT	7.8	9.0	9.3	22	24	28	62	71	208
SKB / KTH - KAT	7.2	20.6	51.0	56.2	217.7	-	-	-	-
Experimental results		*43*			*176*			-	

Table 5 Breakthrough times for Sodium in the stochastic models. Unit for measured input functions is hours. The experimental results are based on injected mass at 164 h.

Modelling team	t5 (5%)	t5 (50%)	t5 (95%)	t50 (5%)	t50 (50%)	t50 (95%)	t95 (5%)	t95 (50%)	t95 (95%)
POSIVA / VTT	2.7	3.3	4.2	7.5	8.7	11	32	40	73
SKB / KTH - KAT	4.2	7.6	11.7	10.7	20.5	37.1	123.8	405.6	-
Experimental results		*6.5*			*16.7*			*900*	

Table 6 Breakthrough times for Strontium in the stochastic models. Unit for measured input functions is hours. The experimental results are based on injected mass at 248 h.

Modelling team	t5 (5%)	t5 (50%)	t5 (95%)	t50 (5%)	t50 (50%)	t50 (95%)	t95 (5%)	t95 (50%)	t95 (95%)
POSIVA / VTT	3.0	3.3	4.2	7.8	9.6	12	36	43	76
SKB / KTH - KAT	4.4	8.2	13.2	14.4	30.3	53.8	249.8	-	-
Experimental results		*8.3*			*35*			-	

Table 7 Breakthrough times for Uranine in the stochastic models. Unit for measured input functions is hours. The experimental results are based on injected mass at 192 h.

Modelling team	t5 (5%)	t5 (50%)	T5 (95%)	t50 (5%)	t50 (50%)	t50 (95%)	t95 (5%)	t95 (50%)	t95 (95%)
POSIVA / VTT	3.0	3.3	4.2	7.8	9.3	12	37	45	79
SKB / KTH - KAT	4.0	7.1	10.3	9.6	15.7	24.8	92.9	105.0	-
Experimental results		*5.0*			*11*			*80.5*	

DETERMINISTIC MODELS OF BREAKTHROUGH TIME - Task 4E:2

Table 1 Breakthrough times for Cobalt in the deterministic models. Unit for measured input functions is hours. The experimental results are based on injected mass at 1980 h.

Modelling team	$t_{5\%}$	$t_{50\%}$	$t_{95\%}$
BMBF / BGR	124.1	562.2	3107.0
CRIEPI	-	-	-
PNC / Golder	45.7	283	-
PSI	3780	$5.54 \cdot 10^4$	$2.08 \cdot 10^6$
SKB / TRUE	103.0	597.0	-
Experimental results	*285*	-	-

Table 2 Breakthrough times for tritiated water (HTO) in the deterministic models. Unit for measured input functions is hours. The experimental results are based on injected mass at 186 h.

Modelling team	$t_{5\%}$	$t_{50\%}$	$t_{95\%}$
BMBF / BGR	4.4	16.9	150.3
CRIEPI	5.40	10.79	71.86
PNC / Golder	5.0	11.2	78.8
PSI	6.4	20.7	148
SKB / TRUE	5.5	16.0	97.0
Experimental results	*5.3*	*12*	-

Table 3 Breakthrough times for Potassium in the deterministic models. Unit for measured input functions is hours. The experimental results are based on injected mass at 18 h.

Modelling team	$t_{5\%}$	$t_{50\%}$	$t_{95\%}$
BMBF / BGR	4.55	9.9	31.9
CRIEPI	-	-	-
PNC / Golder	5.3	12.8	-
PSI	11.3	75.3	963
SKB / TRUE	21.6	64.3	173.0
Experimental results	*10*	*30*	-

Table 4 Breakthrough times for Rubidium in the deterministic models. Unit for measured input functions is hours. The experimental results are based on injected mass at 140 h.

Modelling team	$t_{5\%}$	$t_{50\%}$	$t_{95\%}$
BMBF / BGR	15.9	48.7	189.7
CRIEPI	61.79	116.40	232.07
PNC / Golder	21.2	98.8	-
PSI	23.5	193	2320
SKB / TRUE	32.5	113.2	-
Experimental results	*43*	*176*	-

Table 5 Breakthrough times for Sodium in the deterministic models. Unit for measured input functions is hours. The experimental results are based on injected mass at 164 h.

Modelling team	$t_{5\%}$	$t_{50\%}$	$t_{95\%}$
BMBF / BGR	4.8	13.5	882.1
CRIEPI	6.01	12.20	73.45
PNC / Golder	5.0	13.5	93.6
PSI	7.0	25.8	208
SKB / TRUE	6.5	22.2	113.0
Experimental results	*6.5*	*16.7*	*900*

Table 6 Breakthrough times for Strontium in the deterministic models. Unit for measured input functions is hours. The experimental results are based on injected mass at 248 h.

Modelling team	$t_{5\%}$	$t_{50\%}$	$t_{95\%}$
BMBF / BGR	4.8	13.5	882.1
CRIEPI	7.43	15.64	93.37
PNC / Golder	5.8	19.5	229
PSI	8.3	37.2	218
SKB / TRUE	8.2	31.4	168.8
Experimental results	*8.3*	*35*	-

Table 7 Breakthrough times for Uranine in the deterministic models. Unit for measured input functions is hours. The experimental results are based on injected mass at 192 h.

Modelling team	$t_{5\%}$	$t_{50\%}$	$t_{95\%}$
BMBF / BGR	4.65	13.2	129.5
CRIEPI	5.46	11.32	79.13
PNC / Golder	5.2	12.3	83.3
PSI	6.2	19.2	178
SKB / TRUE	5.6	18.0	109.5
Experimental results	*5.0*	*11*	*80.5*

TRUE-1 STT-1b Breakthrough Times for Cobalt

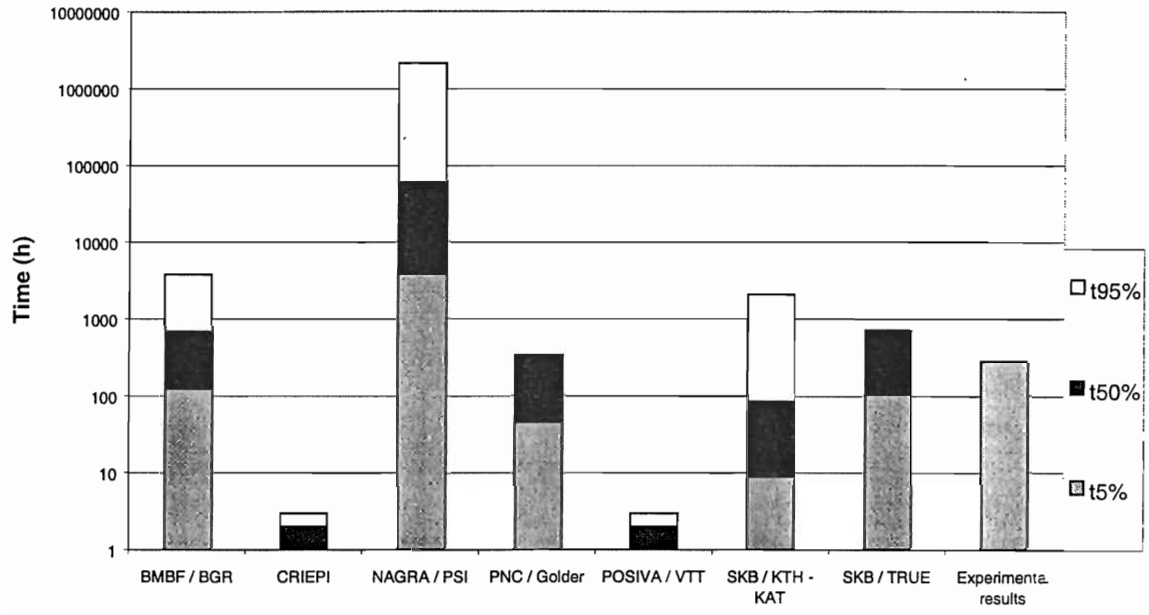

TRUE-1 STT-1b Breakthrough Times for Tritiated Water

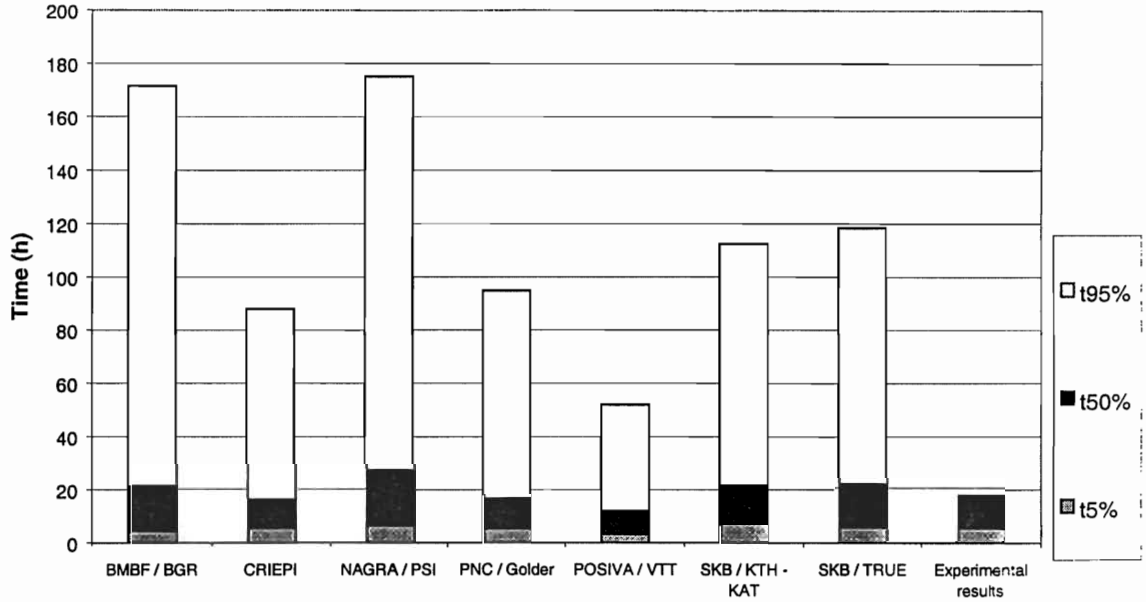

TRUE-1 STT-1b Breakthrough Times for Uranine

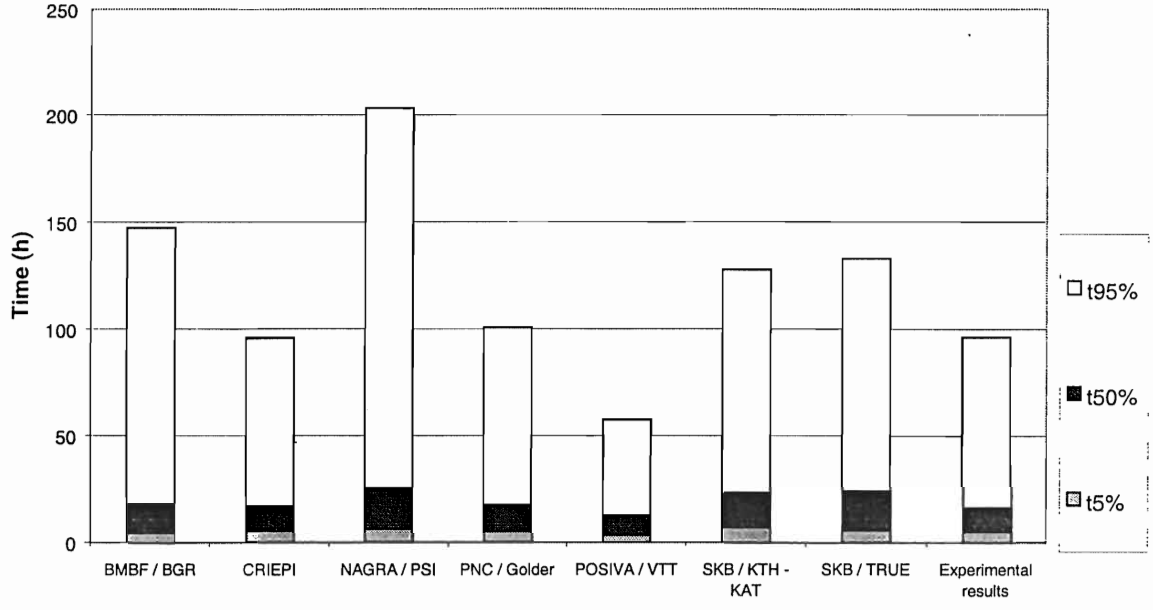

TRUE-1 STT-1b Breakthrough Times for Strontium

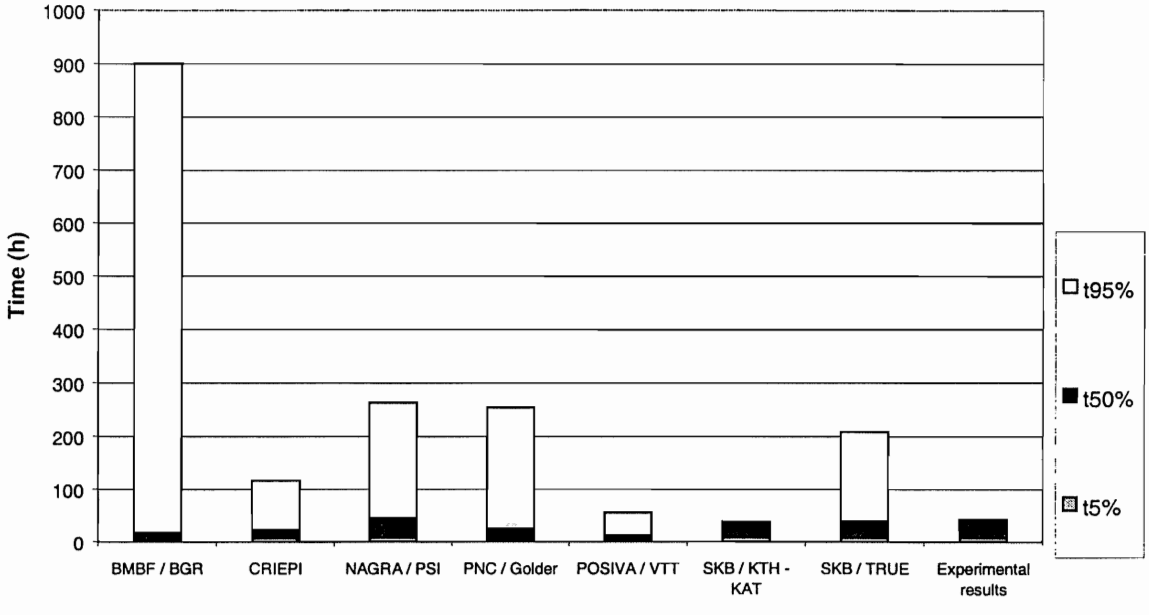

TRUE-1 STT-1b Breakthrough Times for Potassium

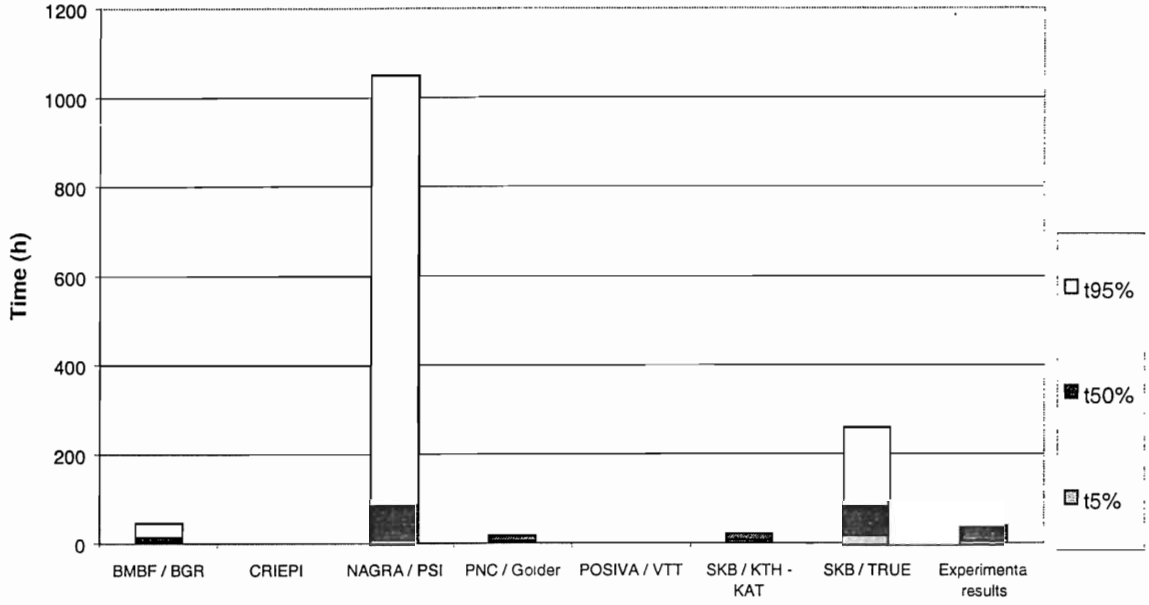

TRUE-1 STT-1b Breakthrough Times for Sodium

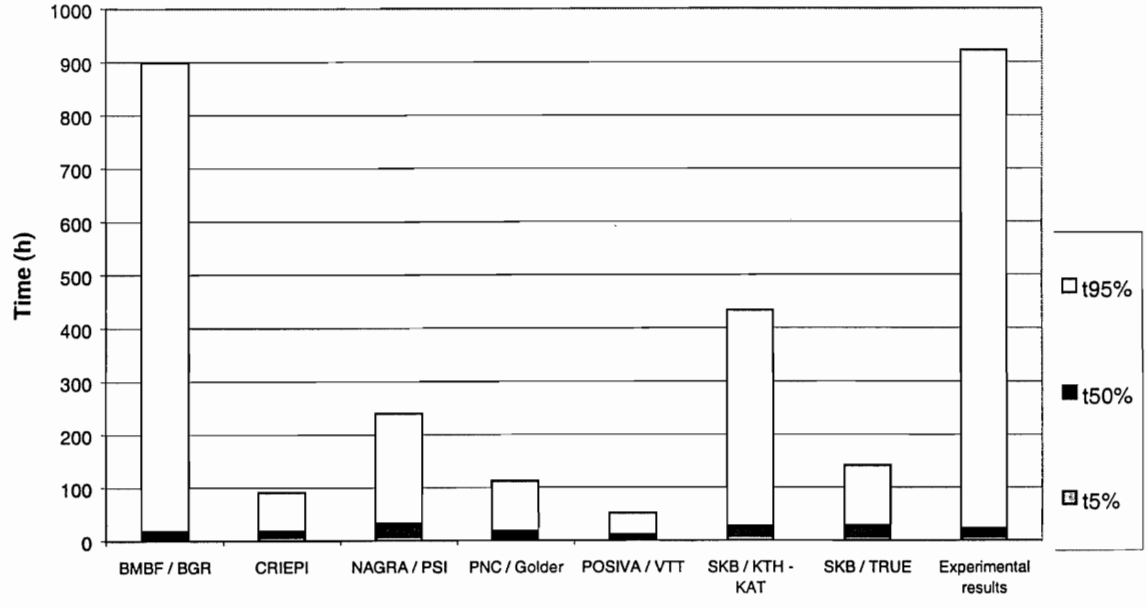

TRUE-1 STT-1b Breakthrough Times for Rubidium

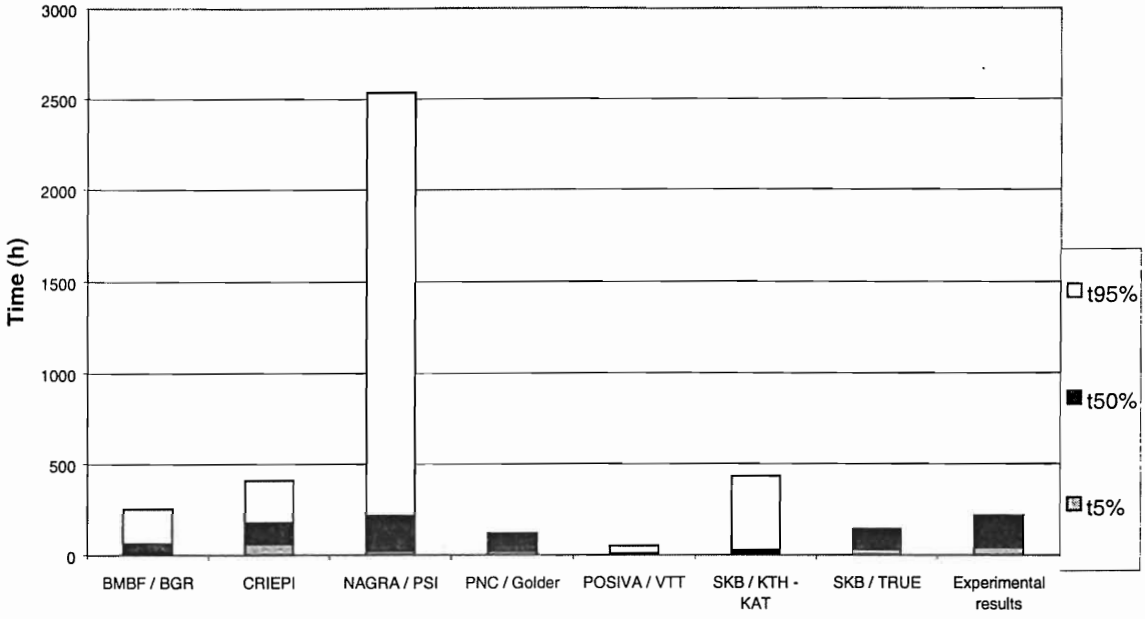

TRUE-1 STT-1b Mass Recovery (F50%)

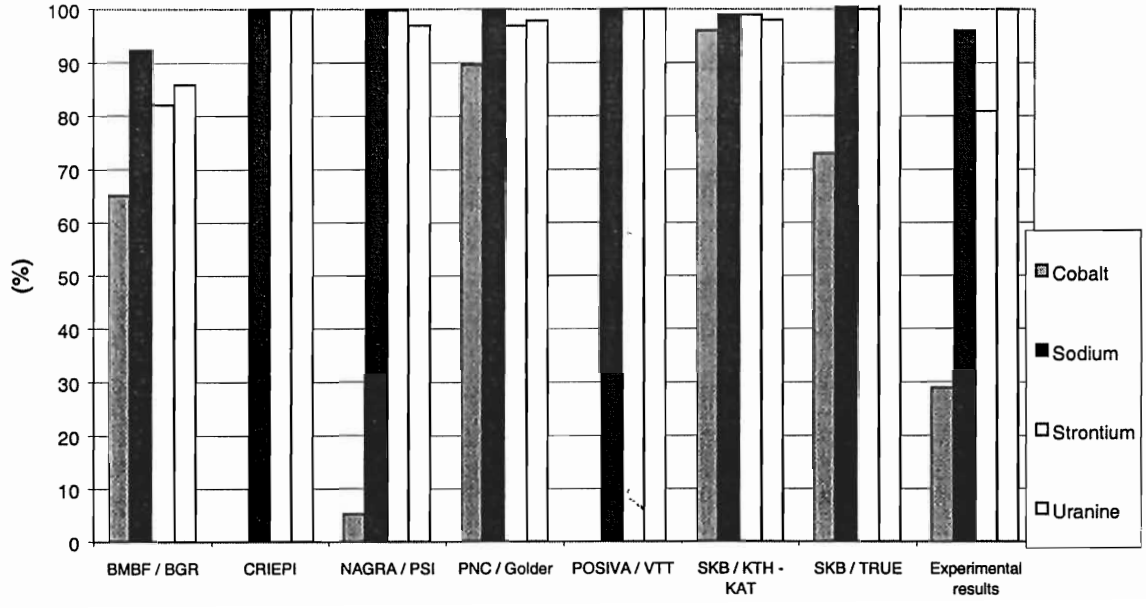

TRUE-1 STT-1b Breakthrough Curves for Tritiated Water

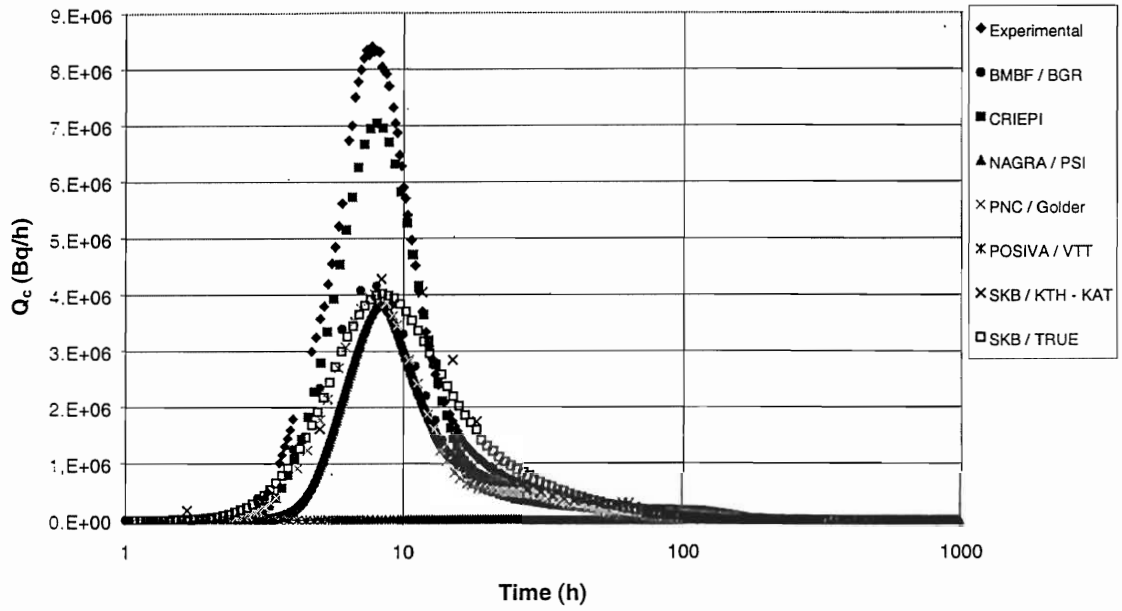

TRUE-1 STT-1b Breakthrough Curves for Sodium

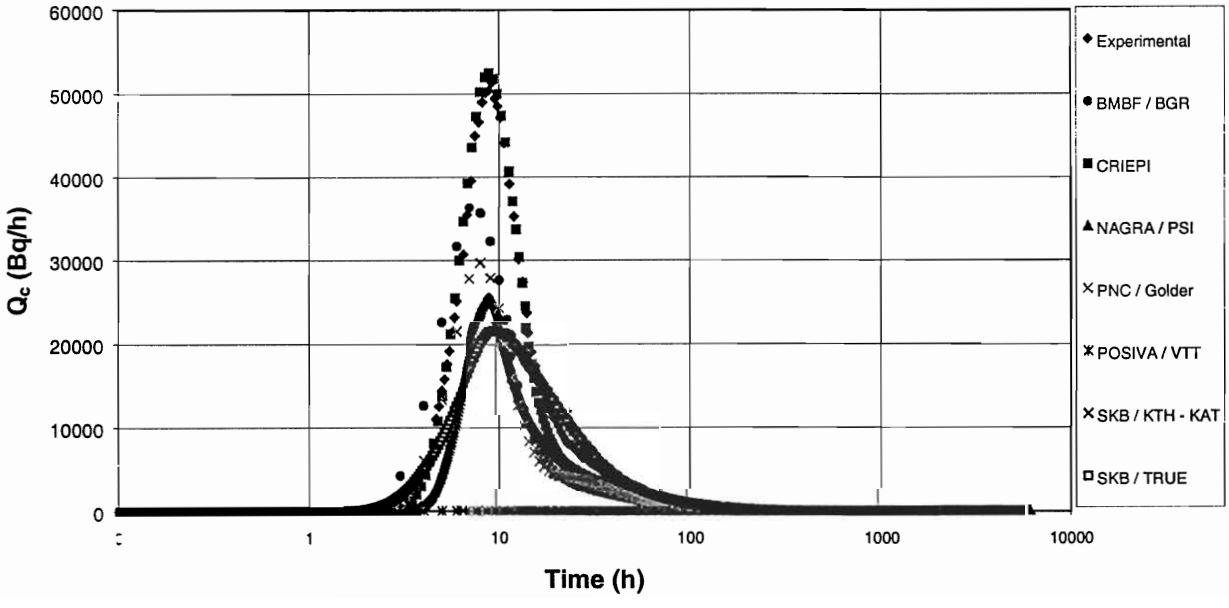

TRUE-1 STT-1b Breakthrough Curves for Cobalt

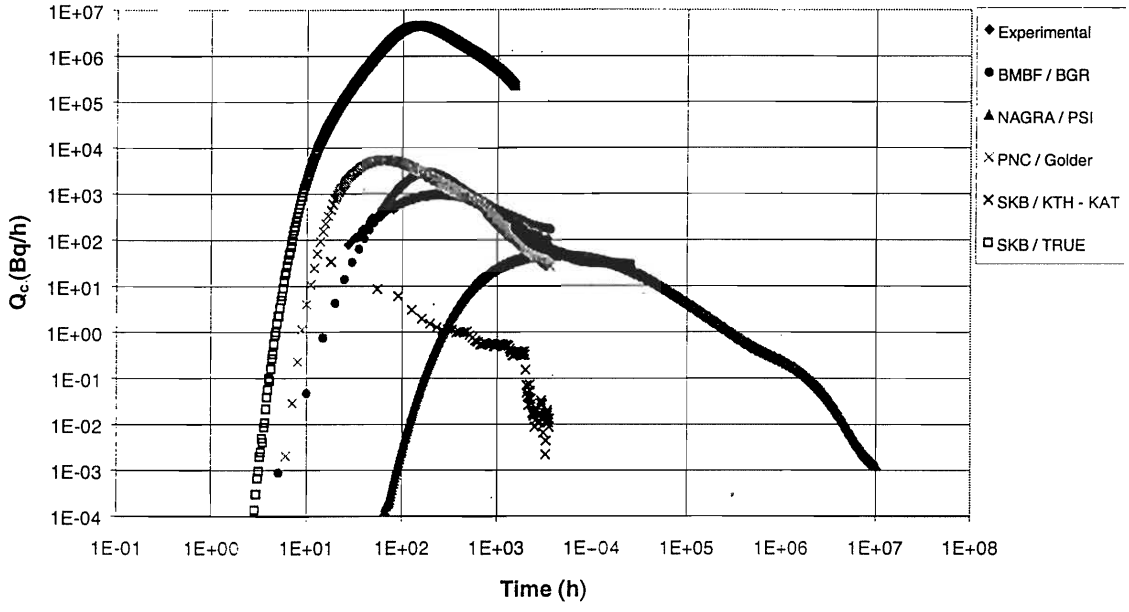

TRUE-1 STT-1b Breakthrough Curves for Potassium

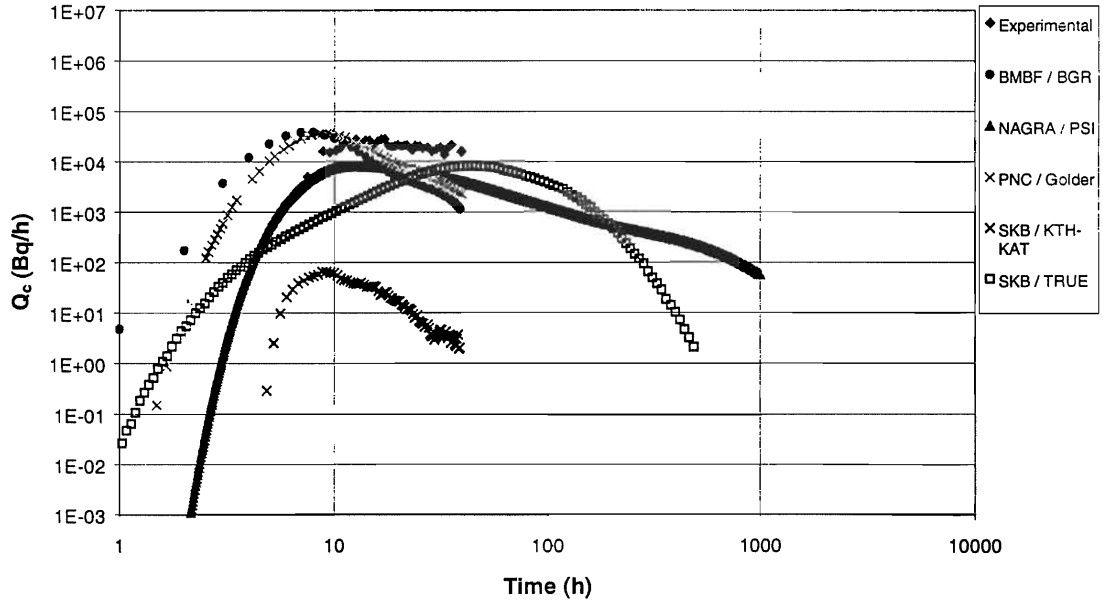

TRUE-1 STT-1b Breakthrough Curves for Rubidium

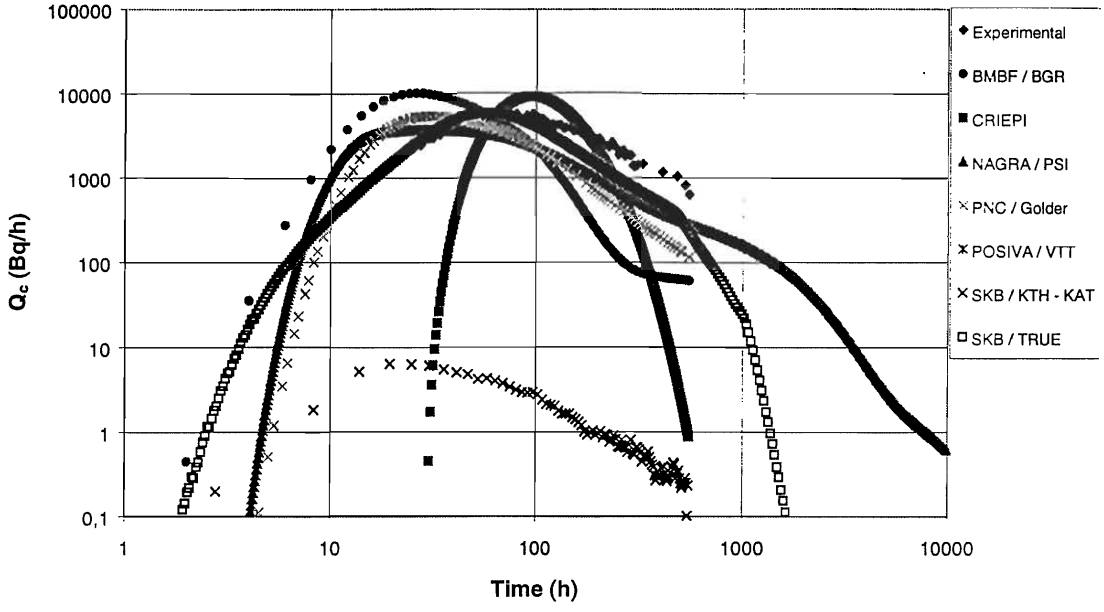

TRUE-1 STT-1b Breakthrough Curves for Strontium

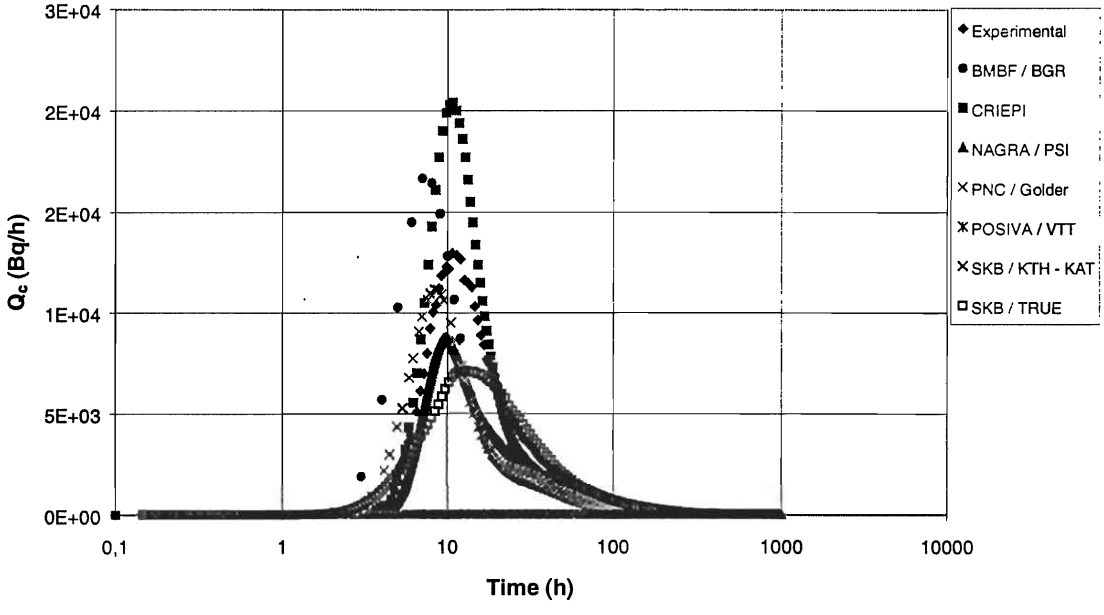

TRUE-1 STT-1b Breakthrough Curves for Uranine

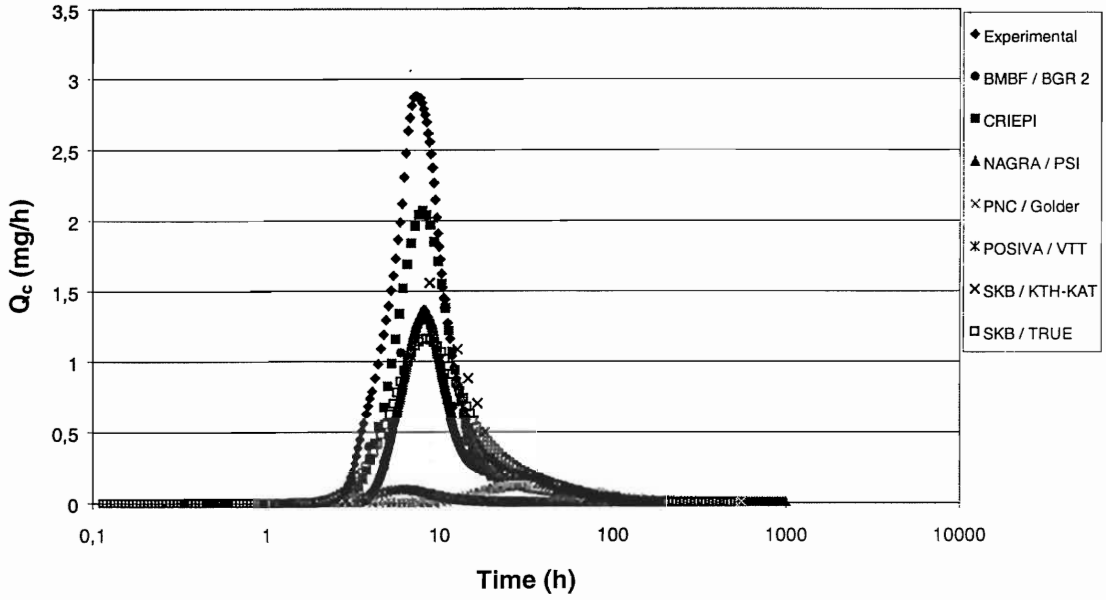

TRUE-1 STT-1b Breakthrough Curves for Cobalt

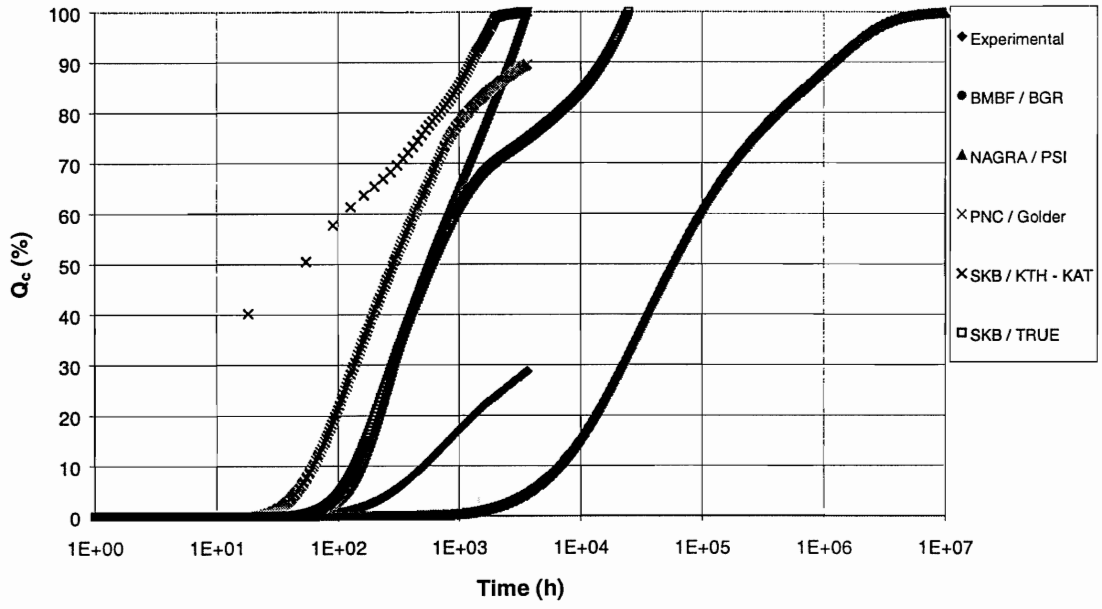

TRUE-1 STT-1b Breakthrough Curves for Sodium

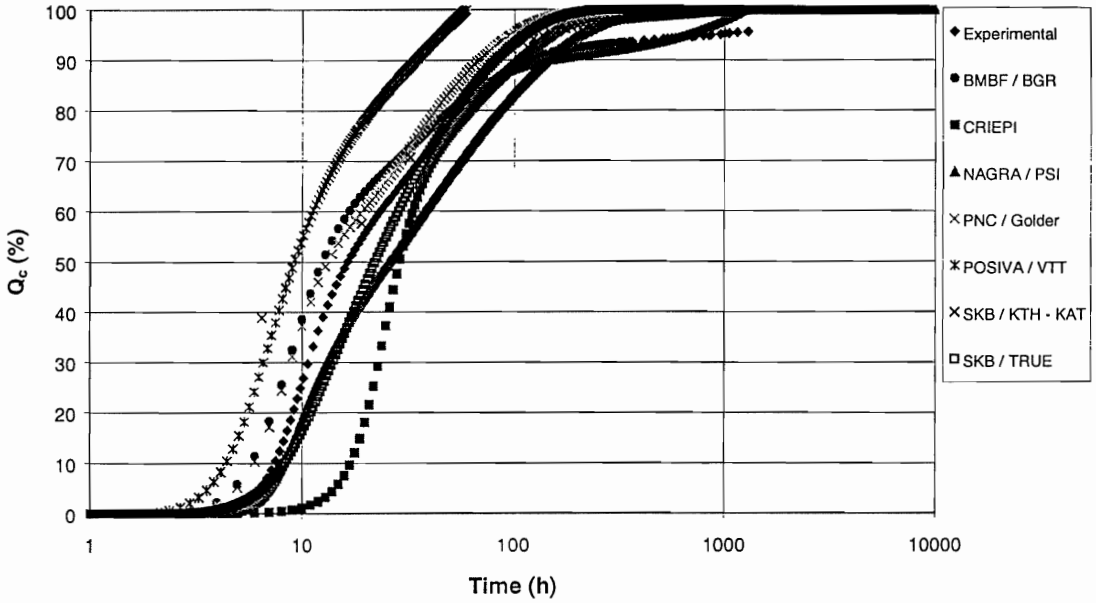

TRUE-1 STT-1b Breakthrough Curves for Rubidium

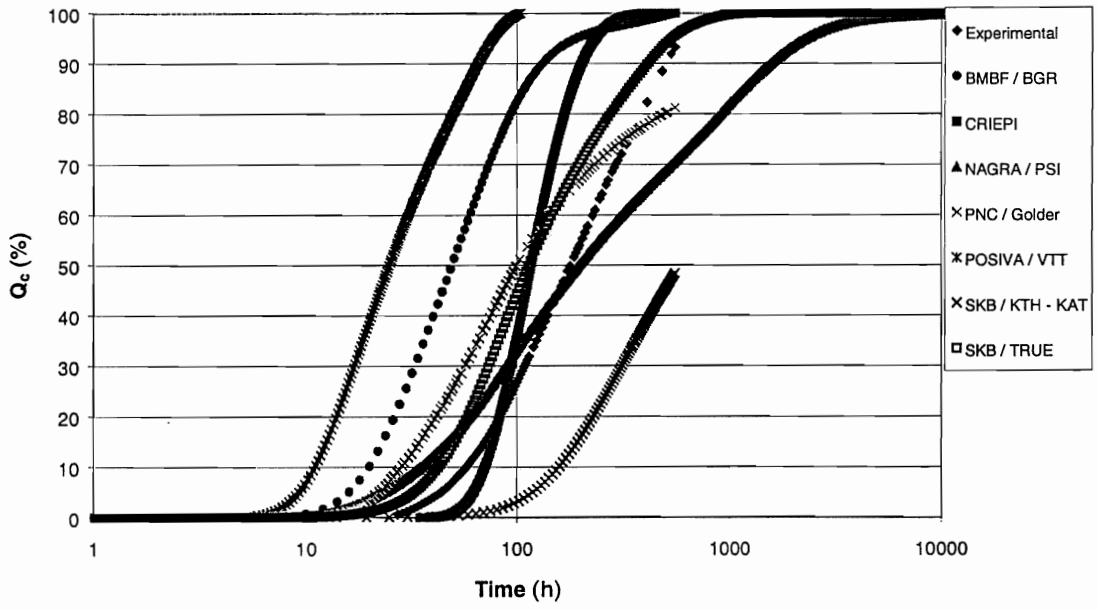

TRUE-1 STT-1b Breakthrough Curves for Tritiated Water

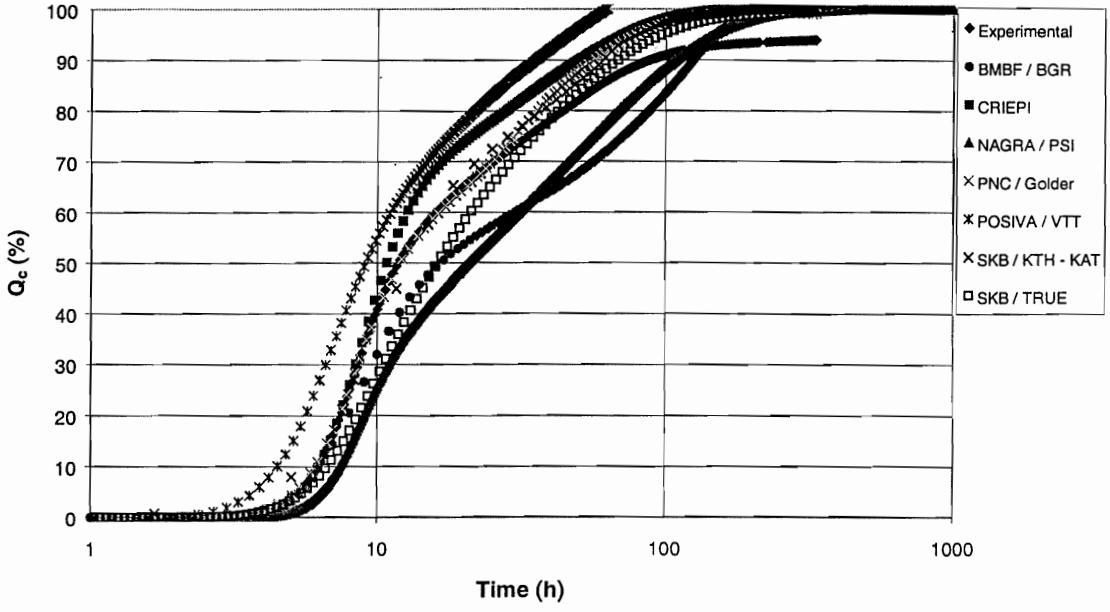

TRUE-1 STT-1b Breakthrough Curves for Potassium

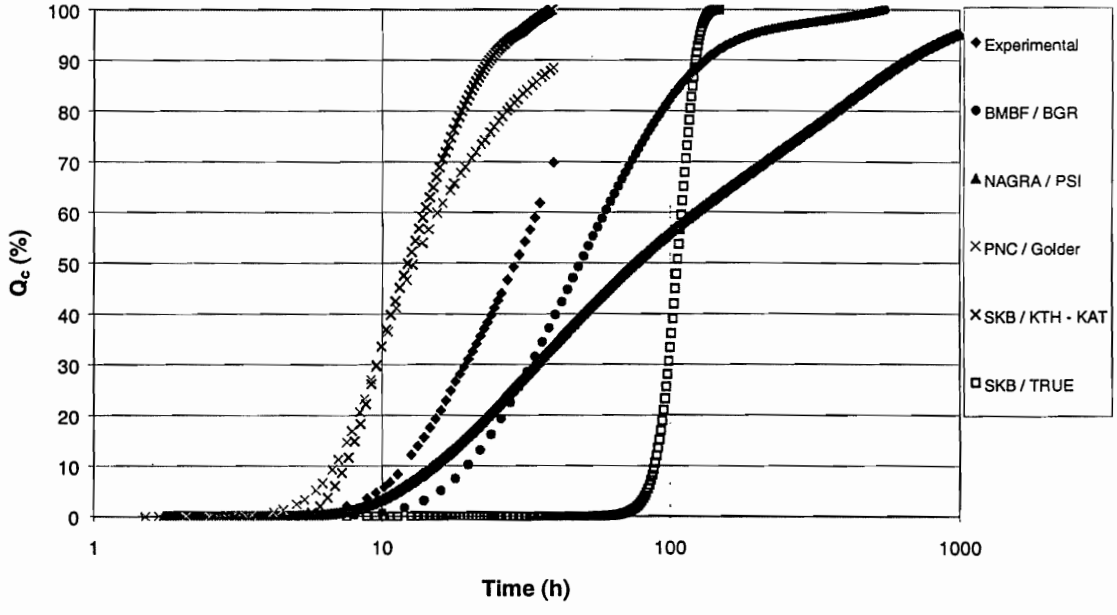

TRUE-1 STT-1b Breakthrough Curves for Strontium

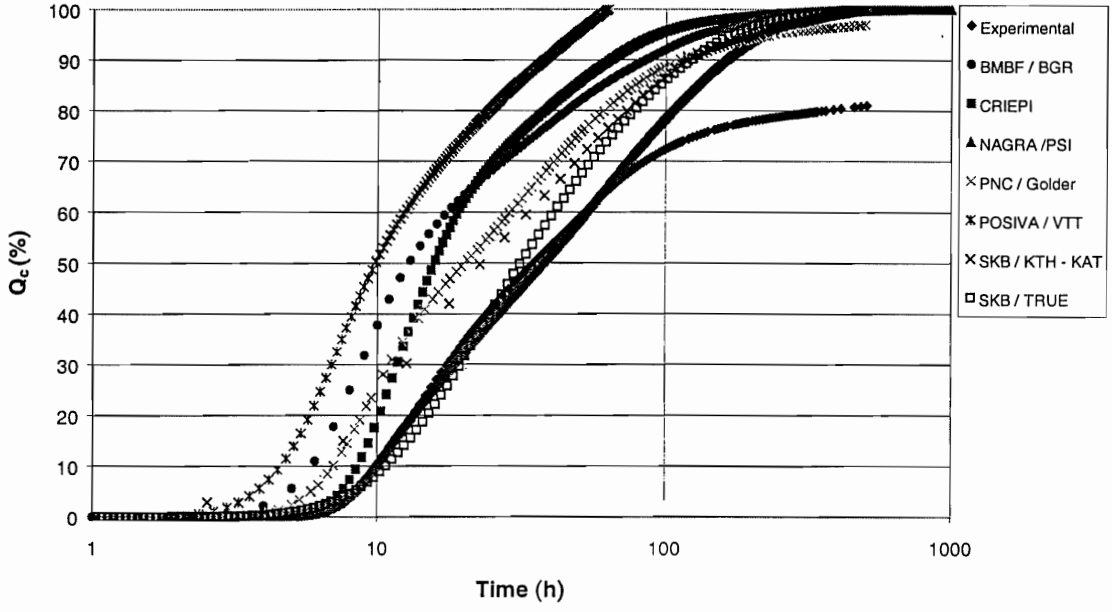

TRUE-1 STT-1b Breakthrough Curves for Uranine

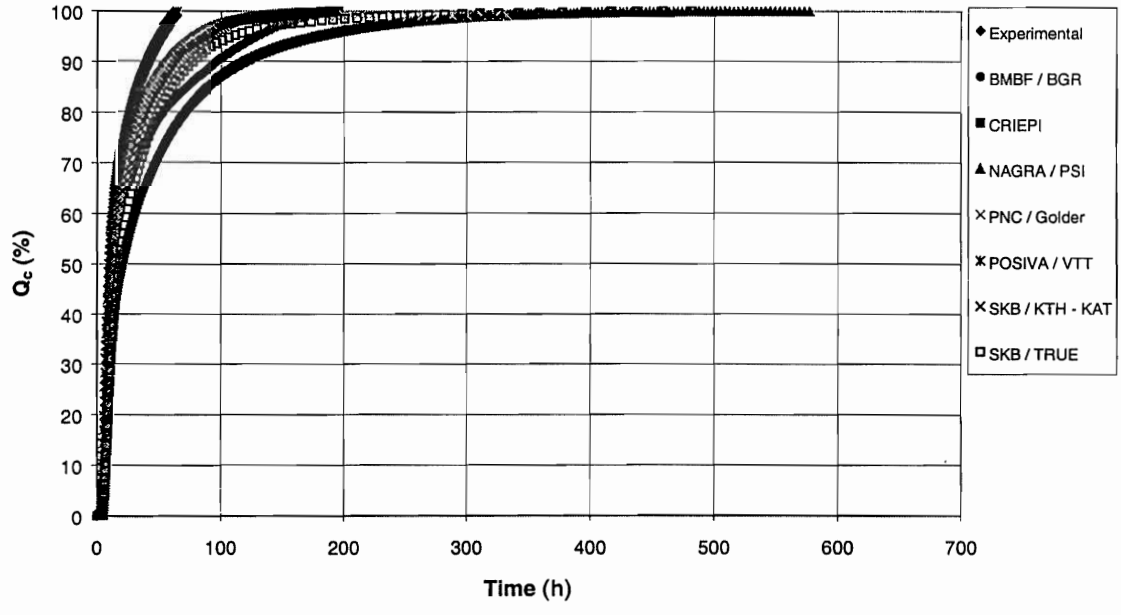

TRUE-1 STT-1b Breakthrough Curves for Strontium: DIRAC Pulse Modelling, Stochastic/Deterministic Determination and Experimental Result

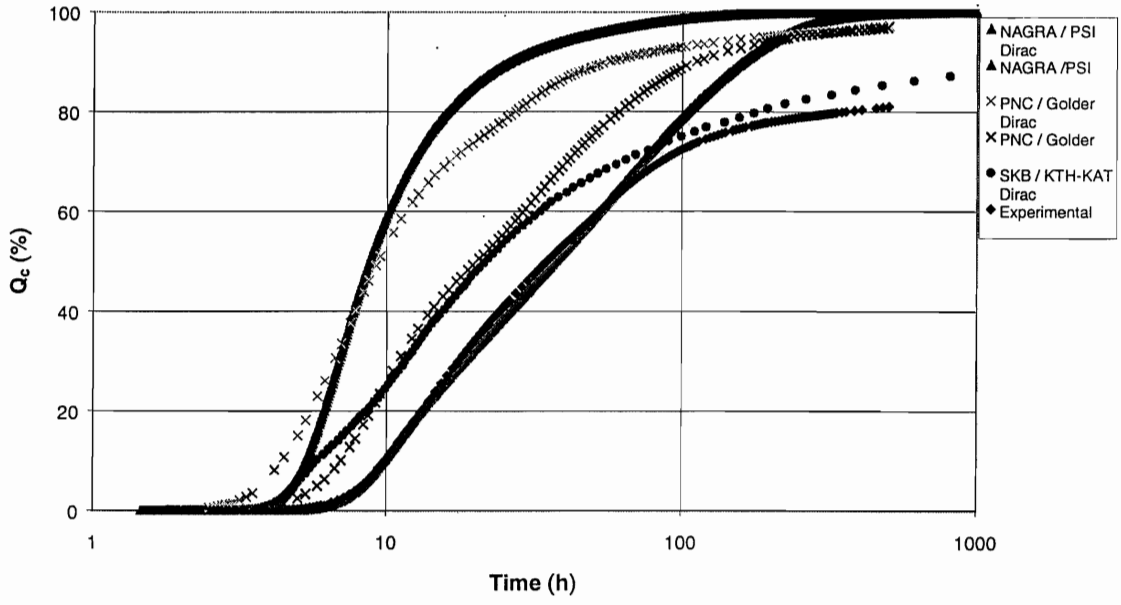

TRUE-1 STT-1b Breakthrough Curves for Cobolt: DIRAC Pulse Modelling, Stochastic/Deterministic Determination and Experimental Result

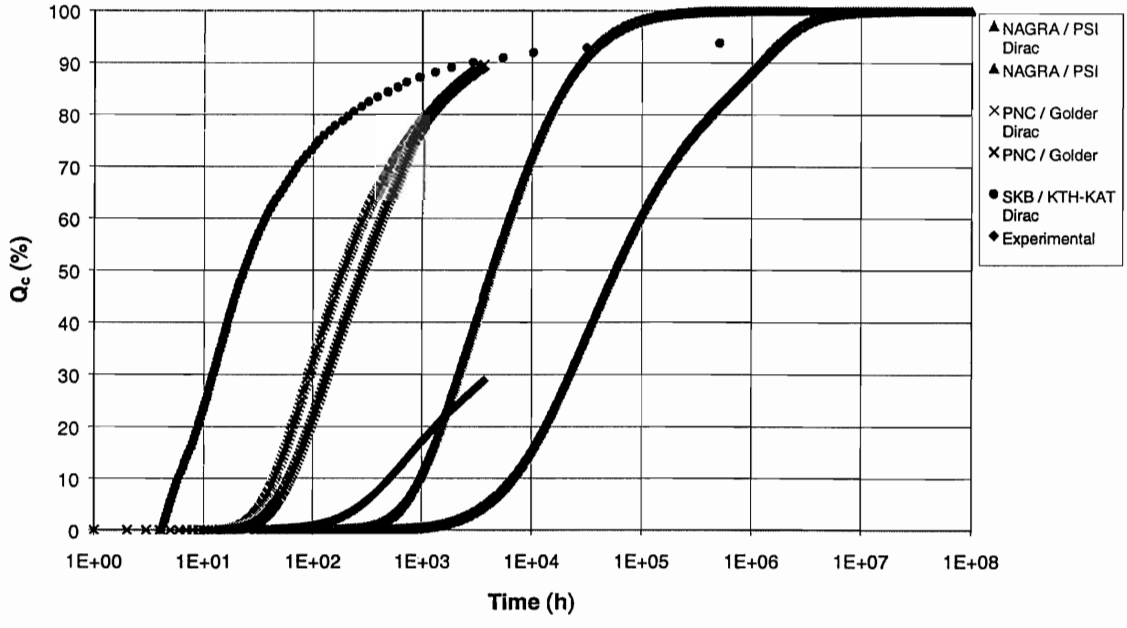

TRUE-1 STT-1b Breakthrough Curves for Tritiated Water: DIRAC Pulse Modelling, Stochastic/Deterministic Determination and Experimental Results

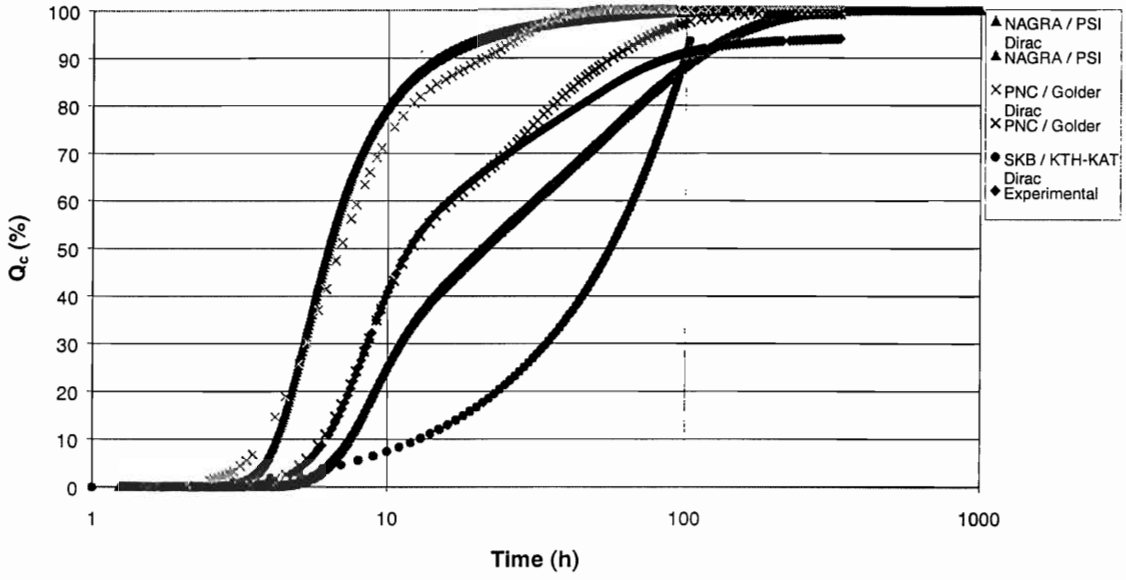

TRUE-1 STT-1b Breakthrough Curves for Potassium: DIRAC Pulse Modelling, Stochastic/Deterministic Determination and Experimental Result

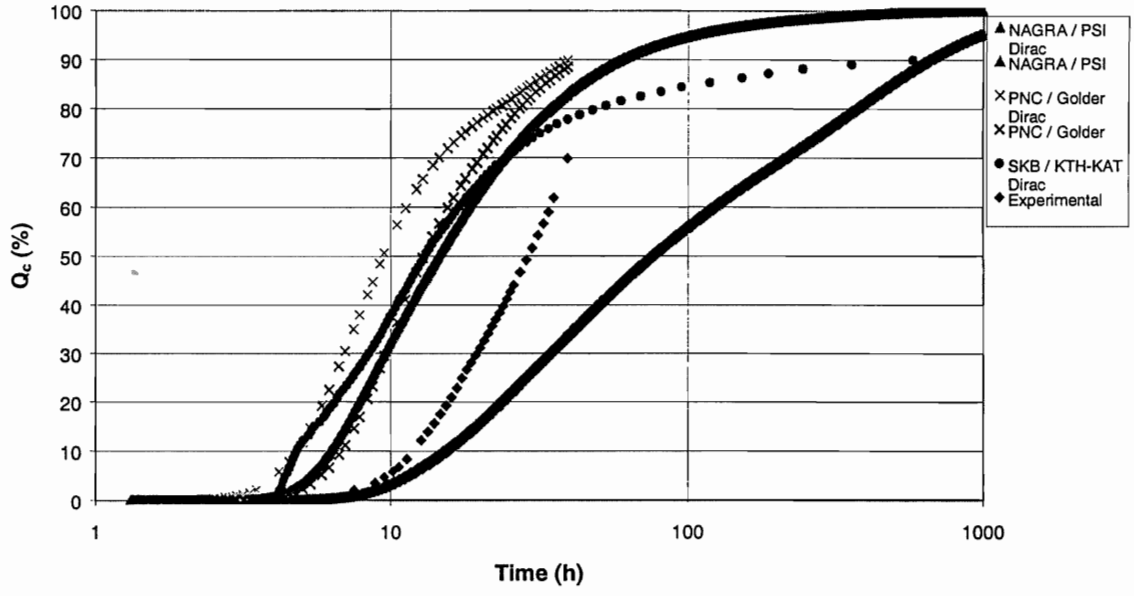

TRUE-1 STT-1b Breakthrough Curves for Sodium: DIRAC Pulse Modelling, Stochastic/Deterministic Determination and Experimental Result

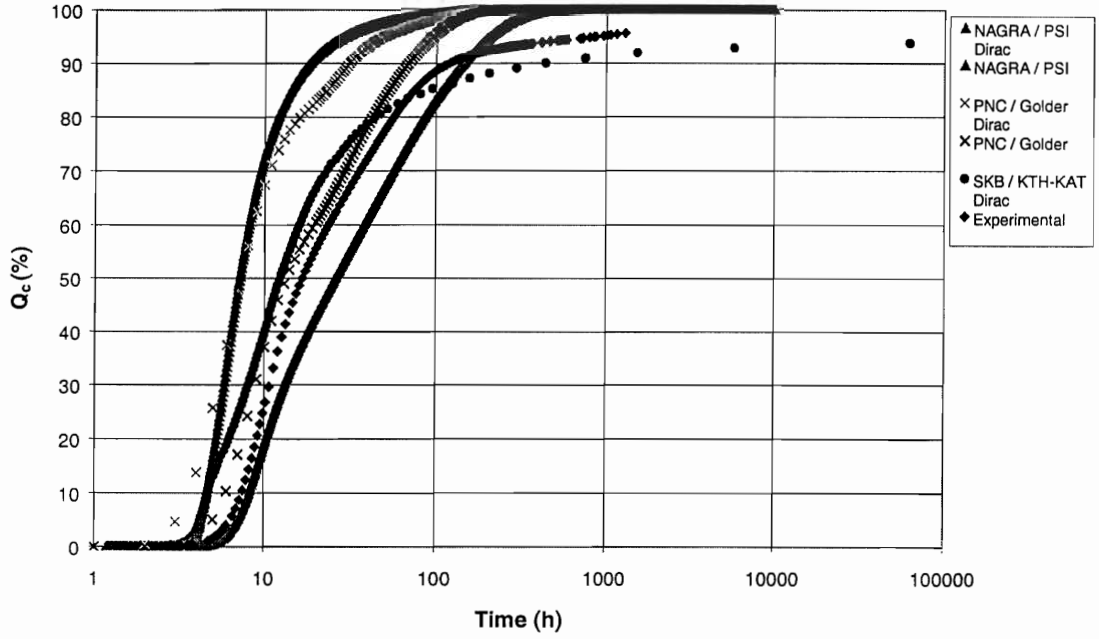

TRUE-1 STT-1b Breakthrough Curves for Rubidium: DIRAC Pulse Modelling, Stochastsic/Deterministic Determination and Experimental Result

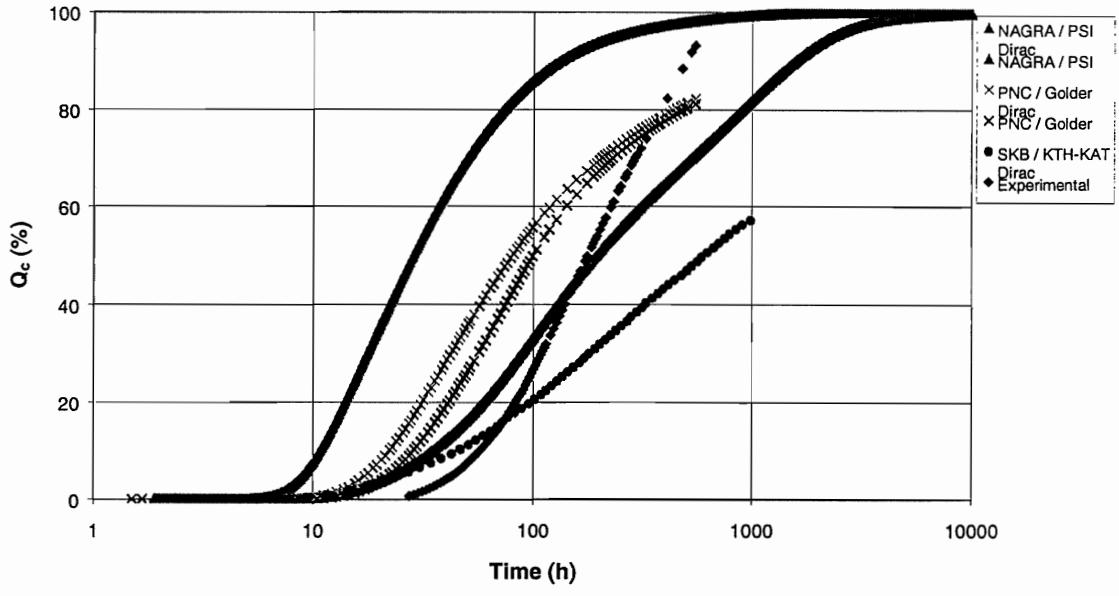

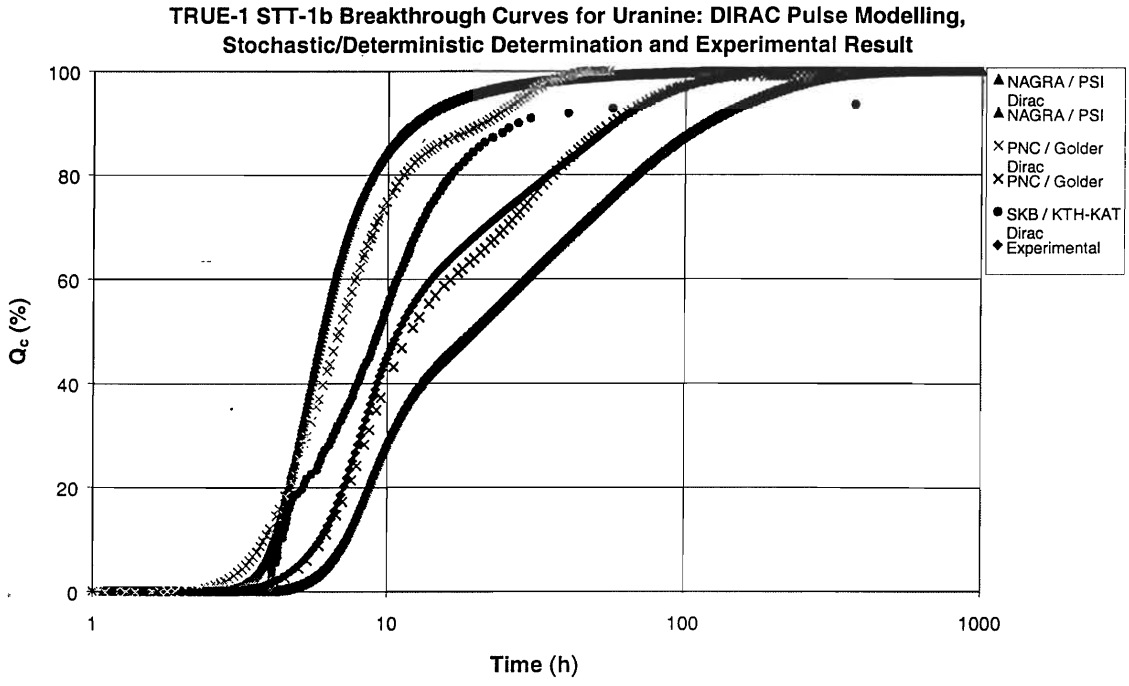
TRUE-1 STT-1b Breakthrough Curves for Uranine: DIRAC Pulse Modelling, Stochastic/Deterministic Determination and Experimental Result
100
80
60
40
20
0
Qc (%)
1
10
100
1000
Time (h)
NAGRA / PSI Dirac
NAGRA / PSI
PNC / Golder Dirac
PNC / Golder
SKB / KTH-KAT Dirac
Experimental

B.2 Contributions of modelling results of Task 4E

Modelling of reactive-radioactive and sorbing tracer tests in Feature A at Äspö HRL.

Lutz Liedtke & Hua Shao

(BMBF/BGR)

MODELLING OF REACTIVE - RADIOACTIVE AND SORBING TRACER TESTS IN FEATURE *A* AT ÄSPÖ HRL

Lutz Liedtke, Hua Shao

**Federal Institute for
Geosciences and Natural Resources (BGR)
Hannover, Germany**

August 1998

Supported by BMBF, Bonn, Germany

ABSTRACT

For the long-term safety analysis of a repository for high-level radioactive waste in hard rocks, SKB (Svensk Kärnbränslehantering AB, Sweden) are carrying out a series of in-situ tracer experiments using conservative and reactive tracers in a fairly well defined fracture system, Feature A in the Äspö Hard Rock Laboratory, within the framework of the TRUE-1 (Tracer Retention Understanding Experiment) project, to check and validate the numerical models developed and to determine the transport parameter values in the fractured rock.

Eight modelling groups from seven countries are participating in this project and carrying out the modelling work to support the in-situ experiments. BGR (Federal Institute for Geosciences and Natural Resources, Hanover) utilises the 3D numerical program DURST/Rockflow to simulate the flow and transport processes.

Within the 4C/4D Task, the natural hydrodynamic behaviour and tracer transport processes with conservative tracers in the converging and dipole flow geometry have been evaluated using a deterministic fracture model. Therefore, the fracture geometry, the hydraulic boundary conditions, and the transport parameter values for the conservative tracers have been determined step by step via a set of satisfactory interpretations of the experimental data.

In this report, the reactive chemical processes, radioactive decay and sorption processes (adsorption and desorption) in the fractured rock are discussed analytically, experimentally and numerically within the 4E Task. Based on the results from STT-1 (Sorbing Tracer Test), the transport processes of reactive tracers, especially the moderate sorbing tracer, were then modelled using a coupled fracture and matrix model. A satisfactory interpretation of the experimental results for tracers ^{86}Rb and ^{137}Cs in STT-1 was achieved. As a result the matrix effect on sorption and diffusion on the transport processes for the sorbing tracers in the fractured rock cannot be ignored.

TABLE OF CONTENTS

EXECUTIVE SUMMARY

The Federal Institute for Geosciences and Natural Resources (Bundesanstalt für Geowissenschaften und Rohstoffe, BGR), supported by the Federal Ministry of Education, Sciences, Research and Technology (Bundesministerium für Bildung, Wissenschaft, Forschung und Technologie, BMBF) began a program in the Äspö Hard Rock Laboratory (Sweden) in 1995 to characterise sites for the disposal of high-level radioactive waste in granite. This programme comprises two parts: participating in the Task Force project on modelling the groundwater flow and transport of solutes; and studying two-phase flow in water-saturated fractured rock.

During the last four phases (1984 – 1997) of the research work at the Grimsel Test Site, a 3D finite-element program code, DURST/Rockflow, based on the deterministic method was developed jointly by BGR and the Institute of Fluid Mechanics of the University of Hannover to simulate flow and solute transport in fracture systems. This program packet has been successfully used to study the hydraulic tests and tracer experiments in the Grimsel Rock Laboratory.

To test and validate the suitability of the developed methods and to establish confidence in the mathematical and numerical models, BGR, together with modelling groups from seven other countries, have carried out modelling work on in-situ tracer experiments with conservative and reactive tracers in a well characterised fracture system, Feature A in the Äspö Hard Rock Laboratory (Sweden).

Based on the geological analysis and hydraulic data, a deterministic model with a single fracture was built to model the tracer tests within the TRUE project. Two different meshes with variable hydraulic conductivity and fracture aperture were set up according to different calibration criteria. While in the second mesh, the pressure difference between the injection and pumping borehole and the tracer breakthrough time were used as criteria for model calibration, the matching of the hydraulic drawdown from the measurements was given more attention in the first mesh. Both yielded reasonably inhomogeneous fracture models

The complicated fracture geometry has been explained clearly step by step using the data from conservative tracer tests in TRUE 4C/4D. In addition it was also possible to determine the transport parameter values for the conservative tracers. The hydraulic conductivity of Feature A was estimated to be 1e-5 ~ 6e-4 m/s assuming an approximately constant fracture aperture of 1.4 mm (locally 0.3 - 1.0 mm, variable). For a transport distance 5 m, as in KXTT4 - KXTT3 or KXTT1 - KXTT3 used in the previous tests, the effective porosity amounted to 0.3 ~ 0.4, the longitudinal / transverse

dispersivity were 0.8 ~ 0.9 /0.08 ~ 0.09 m respectively, and the diffusion coefficient could be ignored for the conservative tracer (< 1e-7 m^2/s).

Using the calibrated flow and transport models and the determined parameter values, tracer test STT-1 (Sorbing Tracer Test) with reactive tracers was simulated within Task 4E. Because the flow path between KXTT4 - KXTT3 was relatively well established through calculation of the preliminary design tests PDT-1, PDT2 and PDT-3, the transport process modelling results for the conservative tracers (Uranine, HTO) and six weak sorbing tracers (^{22}Na, ^{85}Sr, ^{47}Ca and ^{133}Ba) were satisfactory. However the modelling results of moderate sorbing tracers were unsatisfactory (^{86}Rb and ^{137}Cs).

In fact, the flow and advection of solute transport occur in the fracture, while the matrix has a major effect on diffusion and sorption. The slower arrival time and the longer 'tailing' in the breakthrough curve clearly show these matrix effects. Therefore, for the moderate sorbing tracer, ignoring the matrix in the numerical modelling can produce a false result. Taking this into consideration, a coupled fracture and matrix model was built to model the transport processes of moderate sorbing tracers ^{86}Rb and ^{137}Cs. In the new model, the flow geometry and parameters estimated from the previous modelling work were not changed, only the matrix was formed by 3D finite elements, with a large storage volume for the diffusion and sorption processes. A satisfactory match was obtained by varying the distribution coefficients K_d in the fracture and the matrix.

Tracer solutions were injected as a finite pulse. The second peak measured in the injection hole may be explained by the desorption process between the borehole wall and the measuring equipment. Hence, a pulse function for the numerical model is not able to describe the actual mass flow into fractured rock. The modelling work for 4E was carried out only using the measured data as input function for the model.

For the description of the chemical sorption process, a physical parameter, distribution coefficient K_d, is introduced into the present numerical model. This parameter value can be estimated experimentally and numerically within the scope of Task 4E.

1 INTRODUCTION

The Federal Institute for Geosciences and Natural Resources (BGR, BUNDESANSTALT FÜR GEOWISSENSCHAFTEN UND ROHSTOFFE, HANNOVER), supported by the Federal Ministry for Education, Sciences, Research and Technology (BMBF, BUNDESMINISTERIUM FÜR BILDUNG, WISSENSCHAFT, FORSCHUNG UND TECHNOLOGIE, BONN), has been participating in a hydraulic and transport modelling project to characterise the fracture systems and to understand the transport mechanisms of conservative and non-conservative tracers with radioactive decay in the saturated fractured rock within the framework of TRUE-1 (Tracer Retention Understanding Experiments, First Stage) in the ÄSPÖ Hard Rock Laboratory (HRL) (Sweden)

The TRUE program in the ÄSPÖ HRL in Sweden has been divided into several stages, the first of which is currently in progress. Objectives of the first stage are identification and characterisation of Feature A, a fracture system 10 - 20 m from an existing drift, and understanding the solute transport mechanism in the known fractured rock. Tracer tests have been carried out step by step with several different non-sorbing and sorbing tracers with radioactive decay under different hydraulic conditions. A structural-hydraulic model of the rock volume studied was developed and one of the identified minor fracture zones was selected for tracer testing. The Task Force has recently been given all characterisation data for the site and has been modelling the tracer tests. Different model concepts and their ability to predict tracer transport have been tested by comparing the predictions from the modelling groups with the experimental results. Further tracer tests are to be suggested and optimised by the modelling group.

The initial objectives of participation in the Task Force are to check and extend our knowledge of flow and transport mechanisms in fractured rock and methods of studying them, and to exchange experience gained from in-situ experiments at the GRIMSEL Test Site (Switzerland) with the international partners looking into radioactive waste disposal in granite. Through the participation in Task 4E, the effects of sorption and radioactive decay on transport in fractured rock has been studied using different models.

This report deals with numerical modelling of solute transport taking into consideration sorption and radioactive decay carried out using the finite element program system DURST/ROCKFLOW within the scope of the 4E programs. A summary of the interpretation of the fracture system is also given.

2 THE DATA BASE

The geometry of the ÄSPÖ tunnel and Feature A of the TRUE-1 experiment was described in the modelling work of TRUE 4C/4D [Liedtke & Shao, 1998] using the structural model and available data received from SKB (Svensk Kärnbränslehantering AB, Sweden).

On the basis of the knowledge available, the following data sets delivered by SKB for the TRUE-1 4E programs were used in the following modelling task:

Data for Task No. 4E: Predictive modelling of the reactive tracer tests of TRUE-1:

No 1: Data set for the Preliminary Design Test 1 and 2 (PDT-1 and PDT-2) (breakthrough and injection curves) and hydraulic data (head and pump rate) as well as electrical conductivity of pumped water (08-97)

No 2: Data set for the Preliminary Design Test 3 (PDT-3) (injection and breakthrough curves) and injection data for the Sorbing Tracer Test - 1 (STT-1) (09-97)

No 3: Data set for the Preliminary Design Test No.4 (PDT-4) (breakthrough curve and injection curves) and Sorbing Tracer Test (STT-1) (breakthrough curves) (03-98)

No 4: Data set for the injection data of STT-1b (03-98)

No 5: Data set for the Radially Converging Test No. 3 (RC-3) (injection curve and breakthrough curve) (06-98)

Data for Task No. 4C/4D:

The data from the Radially Converging test 1 (RC-1) and Dipole Test - 1 (DP-1) were also analysed taking into consideration the flow path from KXTT4 to KXTT3 in test STT-1 and from KXTT1 to KXTT3 in test STT-1b.

3 REACTIVE PROCESSES

The reactive chemical processes can be classified as equilibrium (fast reaction) and non-equilibrium processes (slowly reaction: chemical equilibrium between sorbed and dissolved phases). The criterion on which this this classification is based is the relative velocity of the chemical reaction compared to the physical transport process. Every reaction can be divided into homogeneous and heterogeneous processes (Fig. 3-1). A reaction process is homogeneous if the reaction occurs within the same phase, and conversely, a process is heterogeneous if the reaction happens between the different phases, e.g. groundwater as fluid phase and rock as solid phase. The heterogeneous reaction process consists of surface reactions e.g. sorption process, and classic reactions, e.g. solution, precipitation, oxidation and reduction reactions.

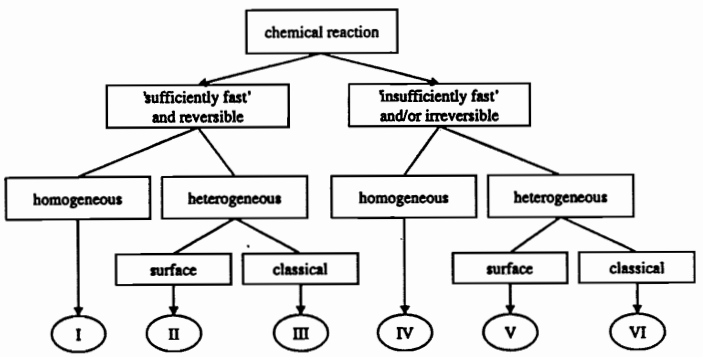

Figure 3-1: Classification of chemical reaction system (after RUBIN, [RUBIN, 1983])

Within the framework of Task 4E concerning the sorbing and radioactive tracer, we concentrated our study on the equilibrium heterogeneous surface reaction sorption process (case II in Fig. 3-1) and decay of the substance.

3.1 RADIOACTIVE DECAY OF THE SUBSTANCE

Radioactive decay can be described as a change in the composition of the nucleus, in which it emits a particle and/or electromagnetic radiation. There are different types of radioactive decay: decay through emission of negatrons or positrons and decay involving the emission of γ-radiation. Radioactive decay is therefore an irreversible process.

The decay of radioactive isotope is independent of temperature and can normally be written as (reaction with the first order and without decay chain):

$$\frac{\partial C}{\partial t} = -\lambda C \qquad (3\text{-}1)$$

where λ is decay rate. The integration of (3-1) reduces this to an exponential decomposition term:

$$C(t) = C_0 e^{-\lambda t} \qquad (3\text{-}2)$$

In practice, we express the decay value of a radioactive substance using the definition of 'half-life time' $T_{1/2}$. We obtain the relation from equation (3-2) taking into consideration $C=C_0/2$:

$$\lambda = \frac{\ln(2)}{T_{1/2}} \qquad (3\text{-}3)$$

The half-life time of the radioactive tracers used in the TRUE-experiment are listed below:

Table 3-1: Half-life time used in the modelling

	HTO	^{22}Na	^{47}Ca	^{86}Rb	^{85}Sr	^{133}Ba	^{137}Cs	^{42}K	^{58}Co
$T_{1/2}$	12.3 y	2.6 y	4.5 d	19 d	65 d	10.5 y	30.2 y	12.4 h	70.8d

3.2 SORBING PROCESSES IN THE FRACTURED ROCK

In the fractured rock flow and transport processes occur mainly in the more permeable fracture area. The matrix zone with lower permeability may have a great capacity of storage for diffusion and sorption processes of the substance dissolved in the groundwater flow. About the effect of diffusion in the fractured rock, which relates to the molecular movement, has been discussed in the last report [Liedtke & Shao, 1998a].

Sorption reactions are inter-phasic exchange processes between fluid phases and solid phases. Given the required change of chemical environment, the process is reversible, namely adsorption and desorption. Adsorption can be understood as a process of particle accumulation at the surface of a solid object, e.g. rock. Desorption is the reverse process of adsorption. The adsorbing substance is designated an adsorbate and the rock as adsorbent. The sorption reaction can be subdivided into physical or chemical sorption according to the type of binding of the adsorbent. These processes are dependent on the type of the adsorbate / adsorbent, pressure, temperature

and the nature of surface structures etc.. Fig. 3-2 summarises the possible sorption processes in the fracture system.

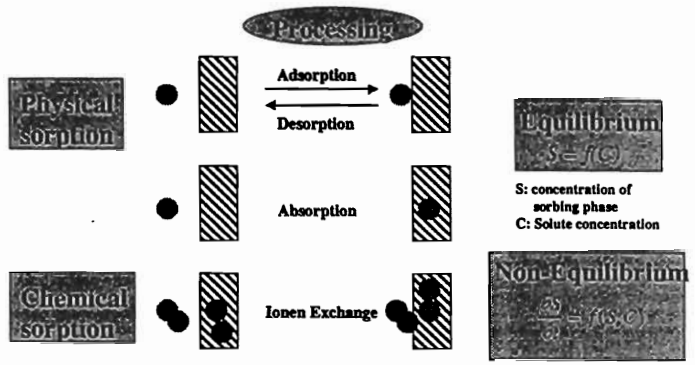

Figure 3-2: Example of sorption processes

In our study we concentrate on physical sorption under equilibrium conditions. In this case, the concentration of the sorbing phase can be expressed in algebraic form as:

$$S = f(C) \tag{3-4}$$

where S is the concentration of the sorbing phase and C is the concentration of the dissolved phase. Often in the practice, the linear relation from the HENRY - isotherm:

$$S = K_d C \tag{3-5}$$

is used, where K_d is the distribution coefficient [m³/kg].

The distribution coefficient k_d is material-dependent and varied by an order of magnitude between the laboratory experiment and through-diffusion experiments. The parameter values used in the modelling of sorbing tracer tests STT-1 and STT-1b in Feature A at ÄSPÖ Hard Rock Laboratory were provided by SKB (Tab. 3-2):

Table 3-2: Distribution coefficient used in the modelling

Tracer	K_d [m³/kg][1]	K_d [m³/kg][2]	comment
^{22}Na	< 2.8e-5	1.4e-6	weak
^{47}Ca	< 4.4e-5	5.2e-6	weak
^{86}Rb	1.4e-3 +/- 3.5e-4	4.0e-4	weak
^{85}Sr	< 2.3e-4	4.7e-6	weak
^{133}Ba	1.2e-3 +/- 1.2e-4	2e-4	weak
^{137}Cs	1.4e-2 +/- 1.2 e-3	6.0e-3	moderate
^{42}K		2e-4	weak
^{58}Co		2.4e-2/2.8e-3	moderate

1) from through-diffusion experiment carried out by SKB
2) estimated from laboratory experiment

3.3 ANALYTICAL SOLUTION OF 1-D TRANSPORT EQUATION

The generalised advection-dispersion equation for the transport of chemical substances taking into consideration the radioactive decay and sorption processes can be written as:

$$n_e \frac{\partial C}{\partial t} + \rho_r \frac{\partial S}{\partial t} + v_a \frac{\partial C}{\partial x_i} = n_e \frac{\partial}{\partial x_i}(D_{ij} \frac{\partial C}{\partial x_j}) - \lambda_c n_e C - \lambda_s \rho_r S, \quad i,j=1, 2, 3, \tag{3-6}$$

where x_i is the coordinate [m], i=1, 2, 3,
t is the time [s],
$C=C(x_i,t)$ is the concentration of substance in the dissolved phase [kg/m³],
S is the concentration of substance in the sorbed phase [kg/kg],
v_a is the DARCY velocity [m/s],
n_e is effective porosity [-],
ρ_r is the density of the rock [kg/m³],
λ_c is the decay rate of the substance in the dissolved phase [1/s],
λ_s is the decay rate of the substance in the sorbed phase [1/s] and
D_{ij} is the hydro-dynamic dispersion tensor [m²/s].

The tensor D_{ij} can be expressed [Bear, 1972] as:

$$D_{ij} = (\alpha_T |v| + \tau D_m)\delta_{ij} + (\alpha_L - \alpha_T)\frac{v_a^2}{|v|}, \quad i,j=1, 2, 3, \tag{3-7}$$

where α_L / α_T the longitudinal / transversal dispersivity [m], D_m the molecular diffusion tensor [m²/s], $|v| = \sqrt{\sum v_i^2}$ the velocity [m/s], τ the tortuosity and δ_{ij} the Delta-function.

Assuming that the decay rates in the dissolved and sorbed phases are the same, e.g. $\lambda_c = \lambda_s = \lambda$, and the reaction process can be described after linear HENRY - isothermal relation $S = K_d C$, then the equation (3-6) can be simply rearranged into:

$$\frac{\partial C}{\partial t} + \frac{v_a}{R}\frac{\partial C}{\partial x_i} = \frac{\partial}{\partial x_i}\left(\frac{D_{ij}}{R}\frac{\partial C}{\partial x_j}\right) - \lambda C, \quad i, j = 1, 2, 3, \tag{3-7}$$

where $R = 1 + \frac{(1-n_e)\rho_r}{n_e} K_d$ is designated the retardation factor and stays a constant in the case of HENRY - isotherm; K_d is called the distribution coefficient.

The equation (3-7) has be solved numerically and implemented in the program packet *ROCKFLOW - TM2*. In order to verify the numerical solution, the numerical results have been compared to the analytical solution developed by BEAR [Bear, 1972] for the 1D transport processes with constant material parameter values under stationary flow condition in the homogeneous and isotropic medium. Considering the initial and boundary conditions $C(x, t=0) = C_0$ and $\frac{\partial C}{\partial x}(x \to \infty, t) = C_I$ the analytical solution can be expressed as:

$$C = C_I + (C_0 - C_I) \bullet \frac{1}{2}\left[\exp\left(\frac{v_a x(1-\gamma)}{2D_{xx}}\right) erfc\left(\frac{x - v_a \gamma t / R}{2\sqrt{D_{xx} t / R}}\right) + \exp\left(\frac{v_a x(1+\gamma)}{2D_{xx}}\right) erfc\left(\frac{x + v_a \gamma t / R}{2\sqrt{D_{xx} t / R}}\right)\right] \tag{3-8}$$

where $\gamma = \sqrt{1 + 4\lambda R D_{xx} / v_a^2}$ and $D_{xx} = D_{11}$, if $i=j=1$.

Fig. 3-3 shows the verification of the numerical model with the analytical solution. Case D is the solution for conservative tracer.

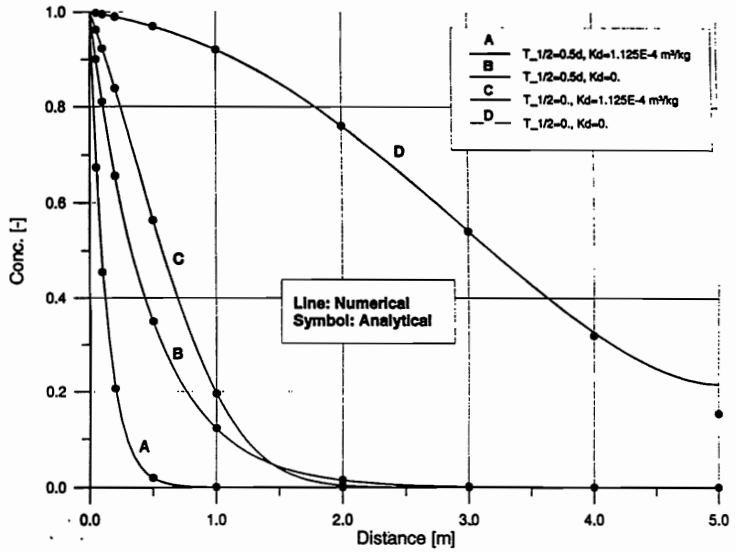

Figure 3-3: Verification of the numerical model with a 1D analytical solution (after t=10 [d] with D=1E-6 [m²/s] and v_a=3E-6 [m/s])

Identical results were gained for the distribution of concentration in the 1D fracture from the numerical calculations and the analytical solutions. Because there is no analytical solution for the transport processes (3-7) in the 2 or 3 dimensional cases, a synthetic analysis for the transport of non-conservative tracer with radioactive decay in a dipole flow field has been conducted.

4 CONCEPTUAL MODEL

Within the TRUE-1 test site, fractures have been identified on the basis of data from the five boreholes KXTT1 - KXTT4 and KA3005A. All fractures have a dominant NW orientation with a steep dip, corresponding to a major fracture zone, so that it is assumed that the fracture system in the test site may have a hydraulic connection to sea level through the 3rd order fracture zone [Winberg, et. Al, 1996].

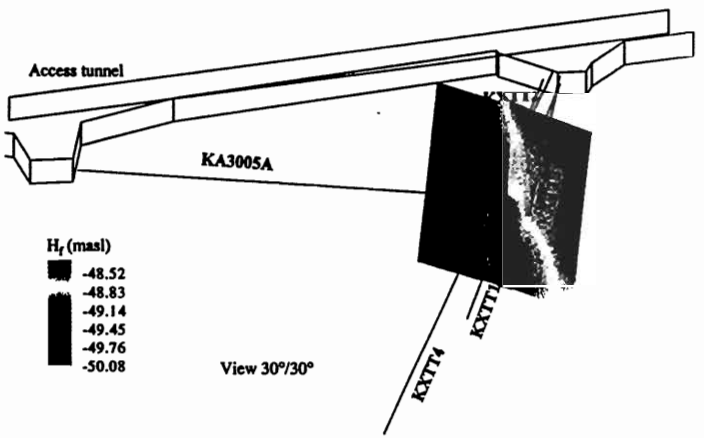

Figure 4-1: Natural hydraulic head distribution in Feature A (inhomogeneous fracture model)

The potentially water-bearing fractures identified in five boreholes were analyzed based on the deterministic description of the features. Different fracture system features have been classified. Appling the analysis of the geological structural model in the TRUE site [Winberg, et. Al, 1996] Feature A was interpreted as a single, steeply dipping NW trending plane structure. Feature B is connected in some way to Feature A, but the numerical investigation shows that the hydraulic influence of Feature B on Feature A can be ignored with the test configuration used [Liedtke & Shao, 1998].

4.1 FRACTURE MODEL

A single fracture model which was considered as heterogeneous by using a non-constant distribution of fracture aperture and hydraulic conductivity was established to carry out TRUE4C/4D [Liedtke & Shao, 1998]. A satisfactory

agreement between the predicted breakthrough curve and associated measurements was achieved when modeling the Radially Converging Test RC-1 and Dipole Tests DP#1-4. A fundamental data set for the transport parameter values (e.g. effective porosity, dispersivity) was then determined.

For the conservative tracer, transport is dominated by advection and dispersion processes, which are determined by flow velocity in the fracture. For a higher flow rate in the injection hole, a relatively fast flow velocity can be realized so that the transport time was restricted to a few days, hence, the influence of the matrix can be ignored. In this case, a single fracture model can be used to characterize the small scale hydraulic and transport properties in an area like Feature A.

If the complexity of the tracer test is increased by using sorbing tracer, the single fracture model cannot explain the transport phenomena such as the longer duration of the transport time and longer tailing because the sorption effect plays a major role in the matrix. Variation of the distribution coefficient K_d (ÄSPÖ granite $6 \cdot 10^{-3}$ - $1.4 \cdot 10^{-2}$ m³/kg) and numerical diffusion coefficient D (0 - 10^{-4} m²/s) in the fracture failed to satisfactorily model the effect of longer tailing in the breakthrough curve (Fig. 4-1). A coupled fracture and matrix model was therefore developed to model the transport of sorbing tracer.

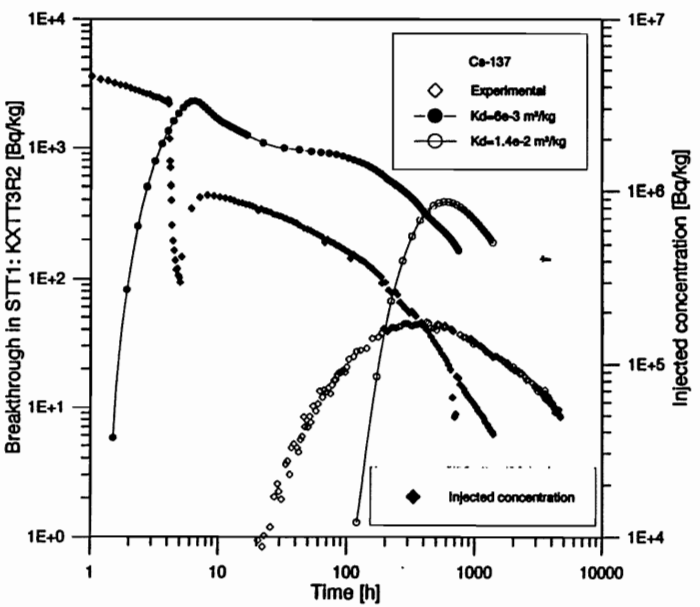

Figure 4-1: Modeling of the Sorbing Tracer Test STT-1: ^{137}Cs

4.2 COUPLED FRACTURE AND MATRIX MODEL

In order to find out the size of the sorption effect in the matrix area on the transport breakthrough curve (maximal concentration and breakthrough time) in the case of moderately sorbing tracers, a numerical experiment using a simplified model coupled with 1D fracture and 2D matrix was carried out. The results of the coupled model were compared with that from a 1D fracture model.

A distance of 5 m between injection point and observation point with a hydraulic pressure difference of 10 m was chosen for the experiment. The hydraulic conductivity of the fracture was 1e-4 m/s (flow rate 12 l/min in area 1 m² or aperture 10 cm) and that of the matrix was zero so that the flow and transport processes only occur in the fracture and diffusion and sorption only occur in the matrix. The natural flow field was not considered.

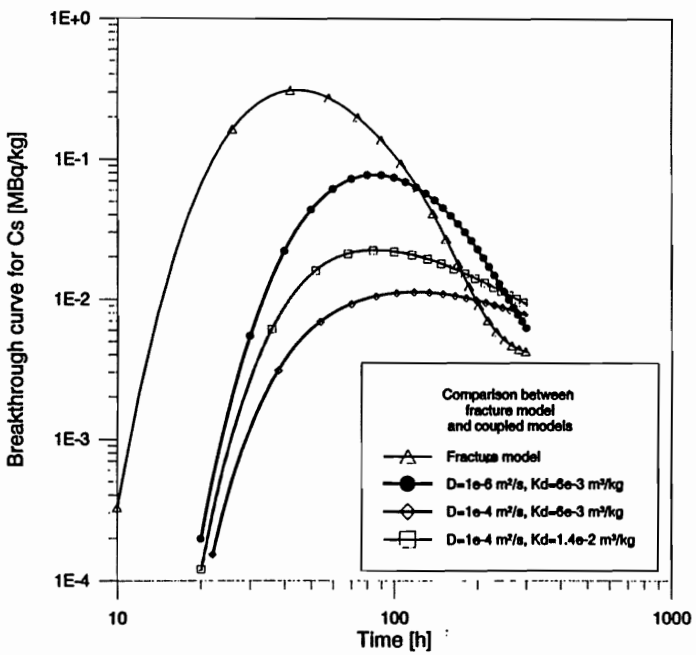

Figure 4-2: Influence of the diffusion and distribution coefficients in the matrix on the breakthrough curve in the observation hole

From Fig. 4-2 we can see that in this case the matrix area has a large influence on the transport processes. The curve in fracture model shows a fast rise in concentration (short breakthrough time, 10 h) and a short tailing

in the breakthrough curve. The diffusion coefficient in the matrix seems to have a large effect on the shape of the curve. That means that the tracer diffuses into the matrix and is adsorbed on the wall of the borehole. The different concentration gradients result in the sorbed tracer being de-sorbed into the pore space where it diffuses into the fracture again - so that the curve shows that a slower breakthrough time (20 h) and a longer tailing effect corresponding to the form of breakthrough curve for the sorbing tracer ^{137}Cs measured. Fig. 4-3 shows the distribution of tracer concentration in the matrix and Fig. 4-4 compares the concentration distribution along the fracture at various times in the two models. Agreement with experimental data will be discussed in the next chapter using a coupled model with an experimental configuration (natural flow field and pumping flow field) in a 3 dimensional calculation.

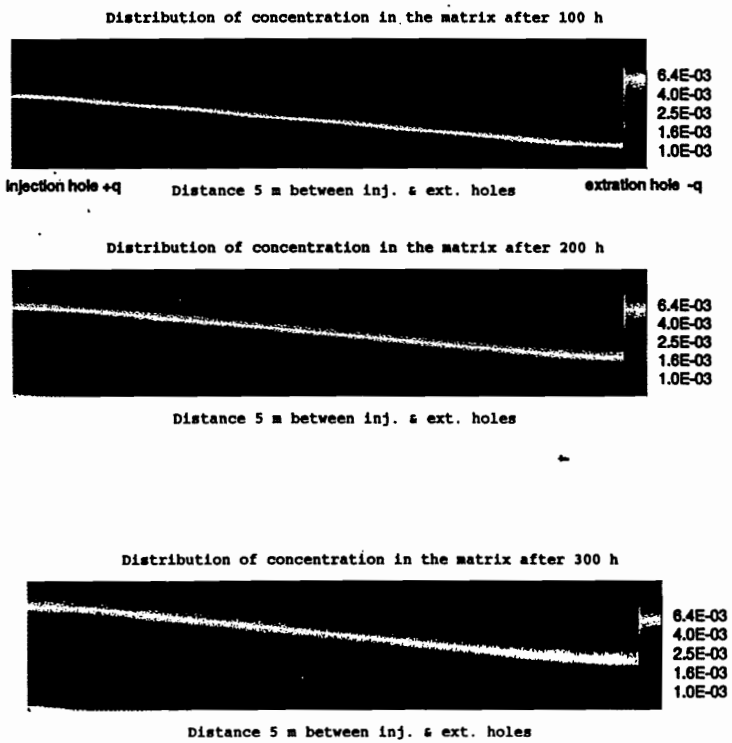

Figure 4-3: Distribution of concentration in the matrix through matrix diffusion and sorption [MBq/kg]

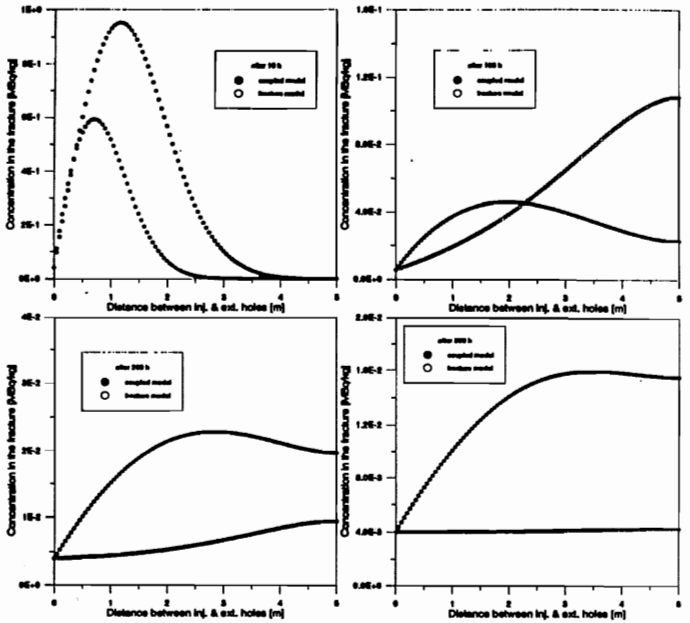

Figure 4-4 *Comparison of calculated concentration from fracture model and coupled model (displayed in different scale)*

don

5 SORBING TRACER TEST STT-1

The main objective of the tracer tests with sorbing tracers was primarily to test equipment and procedures for radioactive sorbing tracer tests to be carried out at later stages of the TRUE project, and secondly to increase the understanding of the transport and retention of sorbing substance types in crystalline rock and to obtain in situ data [Andersson, 1998].

STT-1 (Sorbing Tracer Test circle 1) was carried out in Feature A in a radially converging flow geometry between boreholes KXTT4 - KXTT3. The pumping rate was 400 ml/min in borehole KXTT3R2. Eight tracers, two conservative (Uranine and tritiated water) and six weak to moderate radioactive sorbing tracers (^{22}Na, ^{47}Ca, ^{85}Sr, ^{133}Ba, ^{86}Rb and ^{137}Cs) were injected as a finite pulse with a duration of four hours in borehole KXTT4R3. Tracer breakthrough in the pumping section was monitored for all eight tracers. For the predictive modeling, all input data from test STT-1 and information about 3 Preliminary Design Tests PDT-1 to PDT-3 (chapter 2) were available.

5.1 MODEL CALIBRATION: FLOW PATH KXTT4-KXTT3

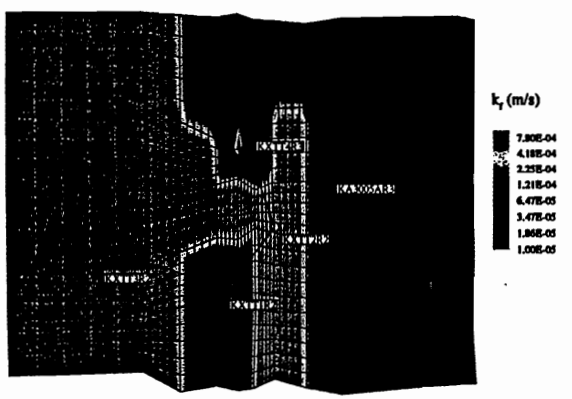

Figure 5-1: Distribution of hydraulic conductivity used in mesh 1 (after Liedtke & Shao, 1998)

Two finite element meshes were used to perform the transport calculation for STT-1. Different calibration criteria were used. Mesh 1 was calibrated using all the hydraulic data available, so that the distribution of the hydraulic conductivity around all 5 boreholes were relatively well determined (Fig. 5-

1) (aperture 0.14 mm and hydraulic conductivity 8e-4 ~ 1e-6 m/s). In mesh 2, the effective aperture and hydraulic conductivity were varied using the hydraulic data related to the test configuration and transport information from tracer tests (Dipole Test DP-6, Preliminary Design Test PDT-2/3). The results of drawdown from the calibrated model are summarised in table 5-1.

Table 5-1: Calculated and measured drawdown in Feature A

	Dip # 1 (102 ml/min)	Dip # 5 (102 ml/min)	Dip # 6 (202 ml/min)	PTT # 1 (100 ml/min)	PTT # 2 (200 ml/min)	PTT # 3 (400 ml/min)
KXTT1R2	1.5(1.2)			0.56(0.4)	0.99(0.8)	
KXTT3R2	-4.7(-4.6)	-2.1(-2.0)	-1.5(-0.8)	1.6(1.3)	3.36(3.1)	7.39(8.2)
KXTT4R3		1.5(1.1)	3.3(3.2)	0.5(0.2)	0.98(0.5)	1.89(1.2)
Drawdown	6.2(5.8)	3.6(3.1)	4.8(4.0)	1.1(1.1)	2.38(2.6)	5.5(7)

Values within brackets were measured by SKB

Considering the flow geometry KXTT4 - KXTT3 used in STT-1, two models were calibrated using data on pumping rate and transport time of conservative tracer Uranine from DP-6 and PDT-2. In order to maintain consistency with the parameters obtained from previous modeling results, the hydraulic and fundamental transport parameter values (conductivity, effective porosity and dispersivity etc.), which were calibrated in the modeling task TASK 4C/4D were only varied within a range of less than 10%. Acceptable results concerning the breakthrough curve (transport time and concentration values) were achieved (Fig. 5-2 and 5-3).

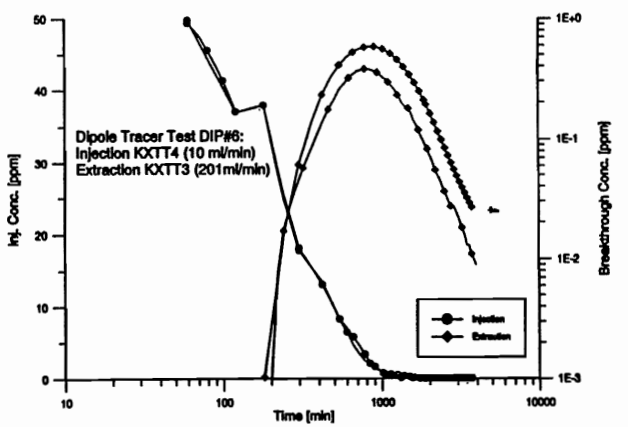

Figure 5-2: Model calibration using data from Dipole Test DP-6

The same experimental configuration as STT-1 was also used in PDT-3 with the same pumping rate of 400 ml/min in borehole KXTT3. The tracer solution included tritiated water (HTO), two short-life γ-emitting tracers (^{82}Br and ^{24}Na), and a fluorescent dye (Uranine). Injection and breakthrough

data for Uranine were available for use in the model for calibration of the flow geometry (Fig. 5-4).

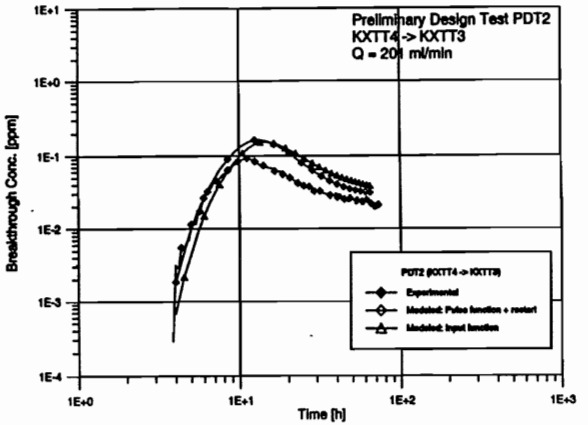

Figure 5-3: Model calibration using data from PDT-2

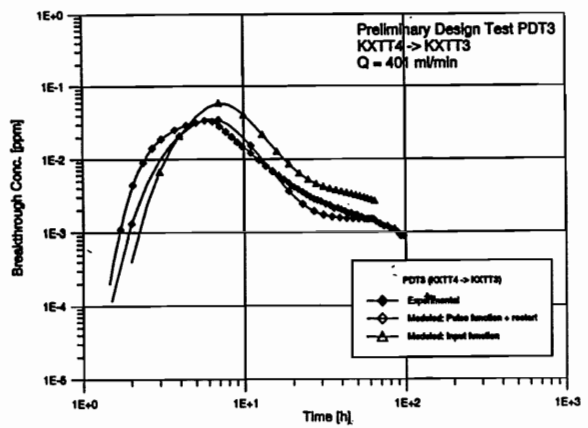

Figure 5-4. Comparison of the measured and modeled breakthrough curve in PDT-3.

The calibrated parameter values for modeling STT-1 are slightly different to the data used in the report on Task 4C/4D.

The model parameters used in mesh 1 and 2 are summarised in table 5-2.

Table 5-2: Parameter values used in the modeling of STT-1

Parameter	Mesh - 1	Mesh - 2
Conductivity	Variable	Partially variable
Porosity	0.4 [-]	0.3 [-]
Dispersivity	0.5 - 0.9 [m]	0.83 [m]
Diffusion	1.e-7 [m²/s]	0

5.2 SENSITIVITY OF THE MODEL PARAMETER (K_d)

We have discussed the sensitivity of transport parameters, e.g. effective porosity, dispersivity and diffusion coefficient earlier in Liedtke & Shao, 1998. In this report we want to discuss the sensitivity of the transport parameter K_d, which is an important value for the sorbing tracer.

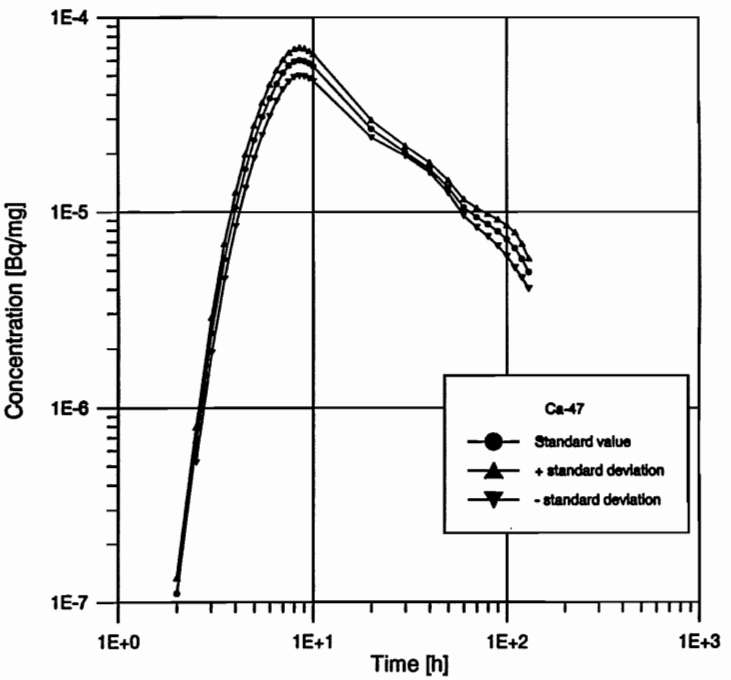

Figure 5-5: Sensitivity of the input concentration function to the breakthrough curve

The radioactive tracers were measured by gamma-spectrometry using HpGe-detector. Due to uncertainty concerning the measurement, the error for the input function and breakthrough curve were represented using one standard

deviation. For a specific tracer, e.g. ^{47}Ca, the calculations were carried out using standard input function x and an injection concentration with 68% probability $\pm\varepsilon$ (ε=68% αx). With the constant K_d=4.4e-5 m³/kg, a slight difference in breakthroughs is observed (Fig. 5-5). Compared to the influence of the another parameter values this effect can be ignored.

The distribution coefficient K_d used in the prediction of in situ experiments is determined in the laboratory. The parameter values can be quite different depending on the different test methods used, e.g. the K_d of ^{137}Cs is 1.4e-2 m³/kg from through-diffusion experiments and 6.0e-3 m³/kg from laboratory experiments. The sensitivity of the distribution coefficient to the breakthrough curve was therefore investigated. Three typical values of K_d for ^{137}Cs (extreme case: 1.4e-7 m³/kg, 8e-3 m³/kg and 1.4e-2 m³/kg) were chosen. The result shows that this parameter not only influences the transport time but also the maximum concentration (Fig. 5-6).

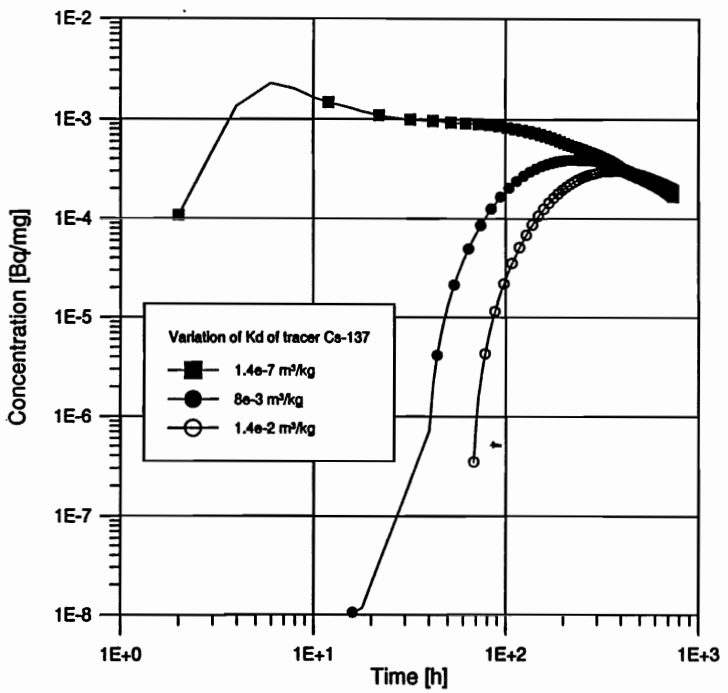

Figure 5-6: Sensitivity of the distribution coefficient K_d to the breakthrough curve of ^{137}Cs

5.3 MODELING OF SORBING TRACER TEST STT-1

The experimental setup for STT-1 was identical to the one used for PDT-3. However the head difference between injection and pumping sections increases significantly during STT-1 under the same pumping rate of 400 ml/min. The measured head difference was 9.5 m while the calculated value amounts to 7 m (drawdown 1.2 m in hole KXTT4 and 8.2 m in hole KXTT3. Although the hydraulic values between measured and calculated are some different, the predictive modeling of transport processes for the conservative tracers (Uranine and HTO) shows a satisfactory result thanks to the introduction of effective porosity and transport dispersivity (Fig. 5-7).

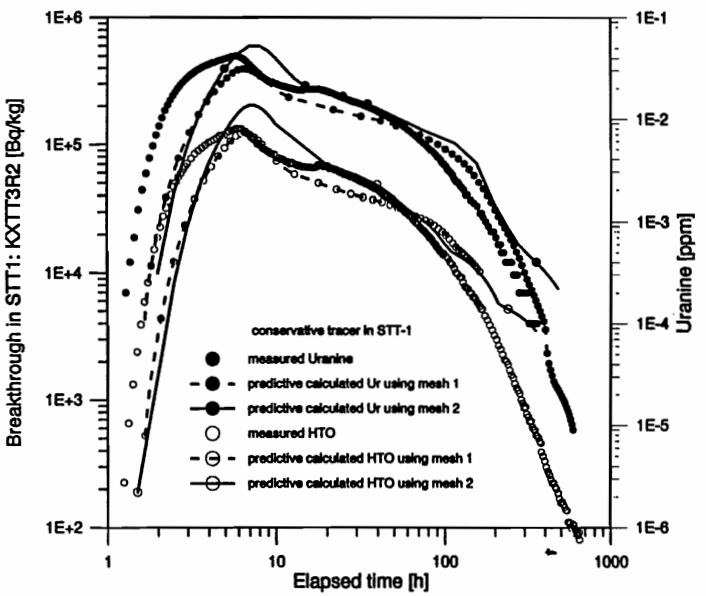

Figure 5-7: Measured and Modelled breakthrough curves for the conservative tracers in STT-1

There are no basic differences between the results from the two meshes. Analysis of the modeling results shows that the general adjustment of the distribution of hydraulic conductivity in mesh 1 has a better transport time and maximal concentration if the transport parameter values were varied slightly. Mesh 1 was therefore chosen to carry out the on-going tracer test modeling, but the transport parameters calibrated in mesh 2 were used. The results seem to be more satisfactory using the new parameter values in mesh 1 (Fig. 5-8). Hence the flow structure and geometry of Feature A was determined.

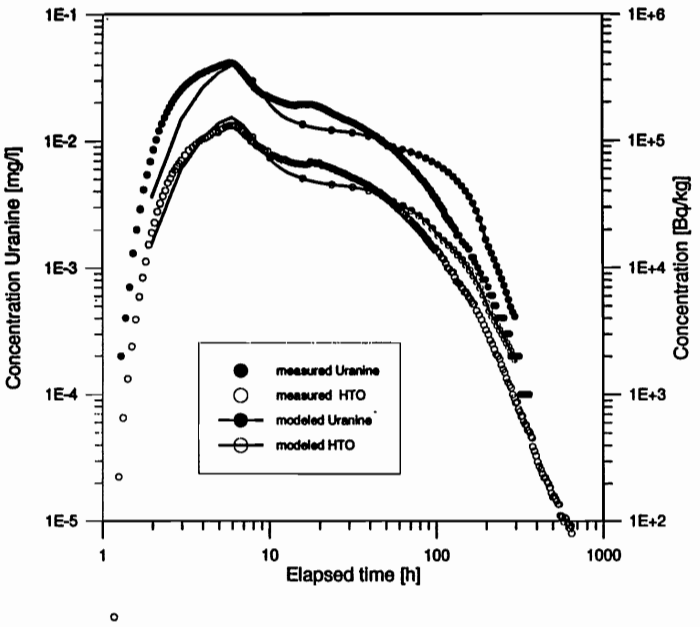

Figure 5-8: *Measured and calculated (mesh 1) breakthrough curves for conservative tracers in STT-1*

The predictive calculation of transport for weak and moderate sorbing tracers , e.g. ^{86}Rb (K_d = 4e-4 - 1.4e-3 m³/kg) and ^{137}Cs (K_d = 6e-3 - 1.4e-2 m³/kg) appears to be more problematic. Based on the flow geometry calibrated by conservative tracer tests, no satisfactory results can be achieved even with a wide spectrum of K_d values (Fig. 5-9).

Fig. 5-9 indicates that the shape of the breakthrough curve for the reactive tracer is different to that of the conservative tracer. The transport time and maximum concentration cannot be obtained by only varying the distribution coefficient in the numerical model. Therefore, a coupled fracture and matrix model was used to interpret the transport processes of the reactive tracers. The influence of the matrix effect on the breakthrough curve has been discussed in capital 4.2.

The fracture properties were not changed in the coupled model with a view to maintaining the consistency of the model and the parameters. The matrix parameter was varied. Taking the natural flow field into consideration, a coupled fracture matrix model, which combined a two dimensional fracture system with a three dimensional rock block, was displayed in Fig. 5-10. While the parameter values in the fracture remain unchanged, i.e. K_d = 1e-3 m³/kg for casium, the K_d in the matrix was varied until a best-fit curve was reached (Fig. 5-11). In this case K_d is 2.5e-3 m³/kg.

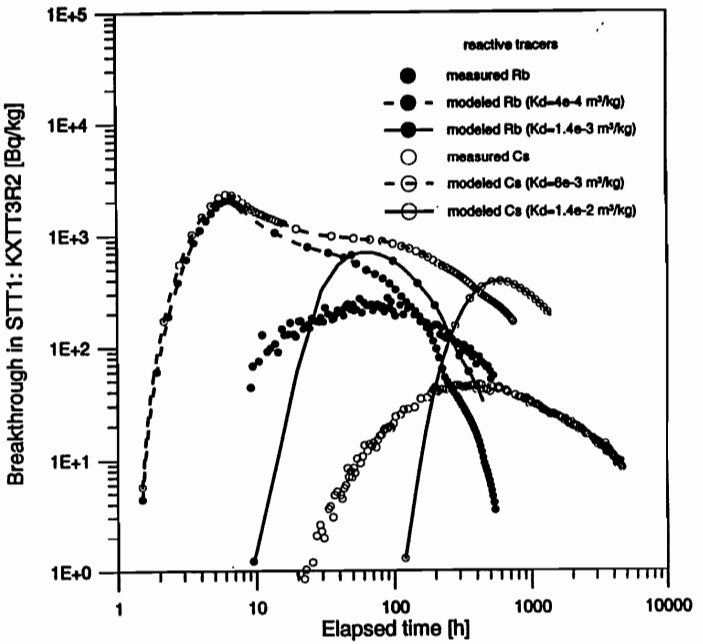

Figure 5-9: *Measured and modelled breakthrough curves for the reactive tracers (casium and rubidium) in STT-1*

As examples, the transport of sorbing tracers (casium and rubidium) were recalculated using the coupled fracture and matrix model. The parameters used are listed in table 5-3.

Table 5-3: Transport parameters used in evaluation of STT-1

Parameter	^{137}Cs	^{86}Rb
Porosity (matrix)	0.01	0.01
Porosity (fracture)	0.3	0.3
Dispersivity [-]	0.9/0.09	0.9/0.09
Matrix sorption K_d [m³/kg]	1e-4	2e-4
Fracture sorption K_a [m³/kg]	2.5e-3	5e-5
Diffusion [m²/s]	1.e-7	1.e-7

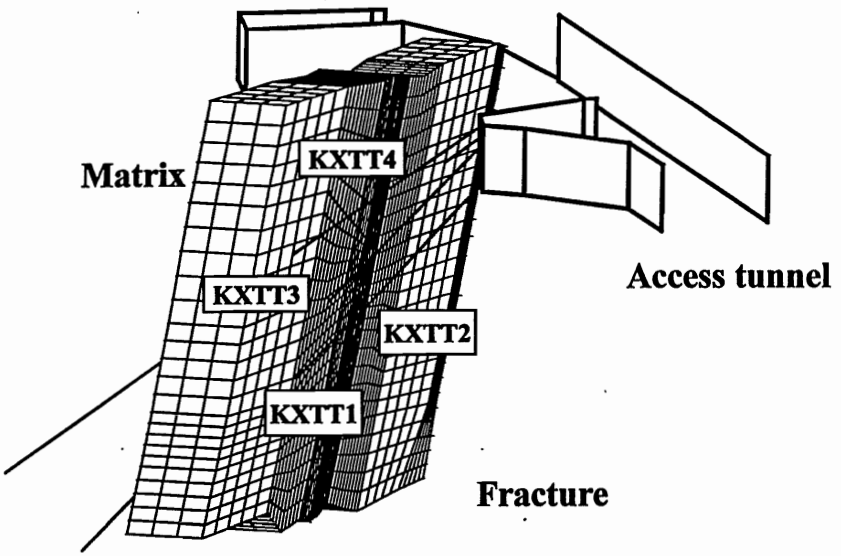

Figure 5-10: 3-dimensional coupled fracture matrix model for Feature A in TRUE-4E

The recalculation of the tracer tests with weak or moderate sorbing tracers shows that a satisfactory result has been achieved. That means that the rock surrounding Feature A has an influence attributable to adsorption and desorption on the transport time and solute concentration. It makes the transport process slower and reduces the maximum concentration. Table 5-3 compares the volume / surface distribution coefficient used in the numerical model and quoted from experimental data.

Table 5-4: Distribution coefficient for casium and rubidium [m³/kg]

	K_a (model)	K_a (laboratory experiment)	K_d (model)	K_d (laboratory experiment)
^{137}Cs	1e-3	5e-4~1e-2	2.5e-3	6e-3 ~ 1.4e-2
^{86}Rb	5e-5	6.e-5~1e-3	4e-4	4e-4 ~1.4e-3

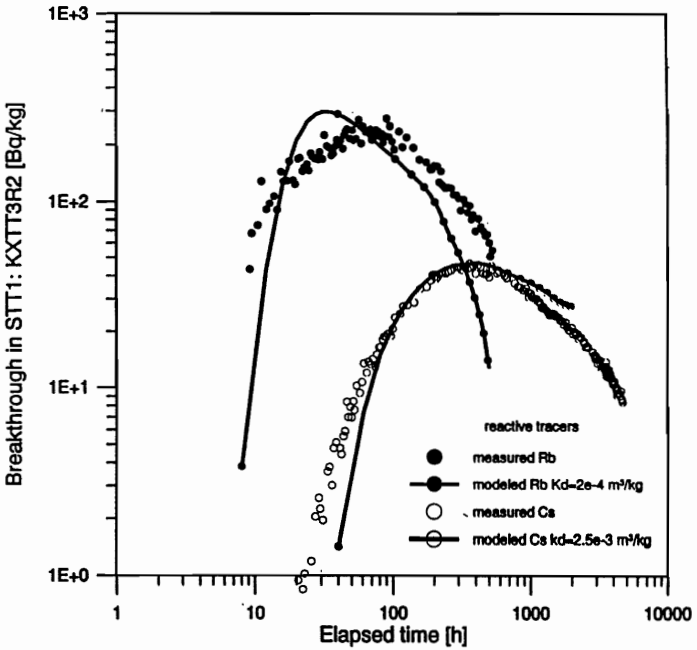

Figure 5-11: Comparison of the calculated breakthrough curve using the coupled model with experimental data.

6 SORBING TRACER TEST STT-1B

In order to prove the results of tests with the moderate sorbing tracers from the sorbing tracer test (STT-1), another series of tracer tests (STT-1b) was designed to be carried out in Feature A - also with a radially converging flow geometry between boreholes KXTT1 - KXTT3. The pumping rate was equivalent to 400 ml/min in borehole KXTT3R2. Seven tracers, two conservative (Uranine and tritiated water) and five weak to moderate radioactive sorbing tracers (^{22}Na, ^{85}Sr, ^{42}K, ^{86}Rb and ^{58}Co) were injected as a finite pulse with a duration of four hours into borehole KXTT1R3. Tracer breakthrough in the pumping section was monitored for all seven tracers. Prior to the test, a preliminary design test PDT-4, with the same experimental conditions as STT-1b, was carried out to give the modeler adequate information on the flow geometry from KXTT1 to KXTT3.

6.1 MODEL CALIBRATION: FLOW PATH KXTT1-KXTT3

The finite element mesh used for the calculation of tracer test STT-1b was calibrated with respect to the hydraulic data e.g. pumping rate and drawdown, and tracer transport information, breakthrough time and maximal concentration and mass balance from preliminary design test PDT-4. This involved varying the hydraulic conductivity and fracture aperture in the flow model, as well as effective porosity in the transport model near borehole KXTT1. This was done so that the remaining domains, especially the domains which were calibrated for the flow path KXTT4-KXTT3, have the same model parameter values as previously. The corrected model parameter values in the vicinity of borehole KXTT1 with a diameter of about 2.5 m are listed below:

Table 6-1: Parameter values near the bore hole KXTT1 for STT-1b

	Old	New
Hydraulic conductivity (m/s)	1e-4 ~ 5e-4	6.5e-5 ~ 4e-4
Fracture aperture (mm)	1.4	0.3 ~ 1.0
Effective porosity (-)	0.3	0.4 ~ 0.5

Using this set of parameter values, the tracer tests PDT-1, PDT2 and PDT-4, which are related to the flow path from KXTT1 to KXTT3, were again calculated. All tests used the same conservative tracer Uranine and different pumping rates in the extraction hole (0.1 l/min in PDT-1, 0.2 l/min in PDT-2 and 0.4 l/min in PDT-4).

The head difference between KXTT1 and KXTT3 from the model was 8.87 m and was acceptable compared to the measured value of 8.5 m at the end of

November 1997. Figures 6-1 and 6-2 show the comparison between the modelling results of the breakthrough curve with the experimental data for PDT-4 and PDT-2.

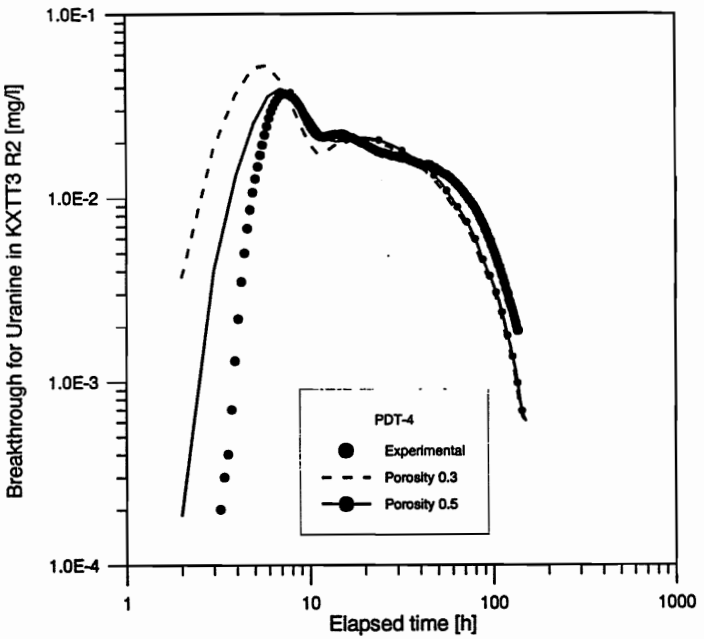

Figure 6-1: Tracer breakthrough in KXTT3 R2 during PDT-4

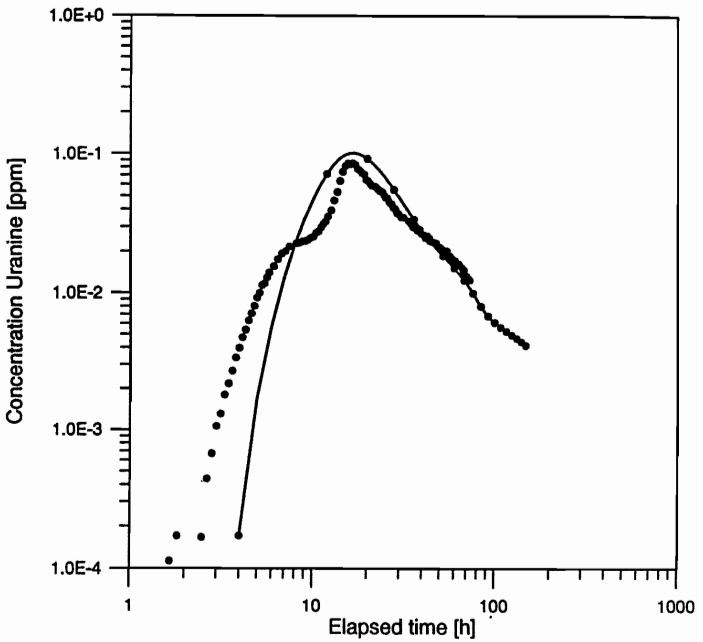

Figure 6-2: Tracer breakthrough in KXTT3 R2 during PDT-2

6.2 MODELS FOR STT-1B IN FEATURE A

Based on the results from the previous work, two models were used to carry out the modelling for sorbing tracer test STT-1b.). The fracture model can be used to calculate transport times and mass balances for conservative tracers (Uranine and tritiated water) and weak sorbing tracers (the distribution coefficient K_d estimated in the laboratory < 1.e-4 m^3/kg) because the matrix has less influence on the transport processes. For the moderate sorbing tracer with a distribution coefficient K_d > 1.e-4 m^3/kg, the coupled fracture matrix model should be used because the use of surface sorption process on the fracture surface alone cannot explain the retardation of these types.

Complete 3 dimensional modelling demands considerable CPU time and computer capacity. An analogue model - here called the Brush model - can be employed to estimate transport processes. This model combines 2-D finite elements for the fracture and 1-D finite elements instead of 3-D elements for the matrix (Fig. 6-3). The advantages of this concept are that the main physical characteristics of the different transport mechanisms in the

fracture and the rock matrix are maintained at the same time as dramatically reducing the amount of computer time required [Lege & Shao, 1996]. The 1-D elements are localised perpendicular to the fracture plane and coupled to the 2-D fracture elements through common nodes. A chain of 1-D elements is attached to every node of the 2-D mesh. The mass exchange between chains of 1-D elements has thus been deliberately ignored. The cross-sectional area of the 1-D elements is equivalent to the area surrounding the nodes of the corresponding 2-D mesh. Due to the symmetrical geometry, only half of the fracture aperture was considered.

Figure 6-3: The coupled fracture-matrix model presented by 1-D and 2-D finite elements

6.3 PREDICTIVE MODELLING OF SORBING TRACER TEST STT-1B

In STT-1b, seven tracers were injected in the form of mixed solutions into borehole section KXTT1R2, with an interval volume of 1548 ml. The concentration in the injection hole was registered by on-line measurement and measured through sampling in the laboratory. The sampling rate of 3 ml/h has be considered by calculating the mass balance.

The transport of conservative tracers (HTO and Uranine) and three weak sorbing tracers (^{22}Na, ^{85}Sr, ^{42}K) was modeled using the single fracture model. The transport of moderate sorbing tracers (^{86}Rb and ^{58}Co) was simulated using the coupled fracture matrix model so that the large adsorption and desorption processes in the matrix could be incorporated.

The predicted drawdown of STT-1b for all sections can be calculated by subtracting the natural head from the head deduced from the pumping process in the extraction hole. The modelled values are listed in table 6-2.

Table 6-2: Predicted drawdown in STT-1b

	Natural head (masl)	Head in STT-1b (masl)	Drawdown (m)
KXTT1R2	-53.0880	-54.5612	1.4732
KXTT2R2	-52.8809	-55.6365	2.7556
KXTT3R2	-52.5959	-63.4351	10.8392
KXTT4R3	-52.8884	-53.2976	0.4092

Table 6-3 shows all the predicted breakthrough times with the respect to the time at which recording stopped.

Table 6-3: Modeled breakthrough time of all tracers in STT-1b

	$t_{5\%}$ (h)	$t_{50\%}$ (h)	$t_{95\%}$ (h)	$T_{100\%}$ (h)
HTO	4.4	16.9	150.3	333
Uranine	4.65	13.2	129.5	195
^{22}Na	4.8	13.5	882.1	1292
^{86}Rb	15.9	48.7	189.7	553
^{85}Sr	4.8	13.05	171.7	505
^{42}K	4.55	9.9	31.9	39
^{58}Co	124.1	562.2	3107.0	3622

Fig. 6-4 shows all of the breakthrough curves carried out for STT-1b.

The tracer mass recovery was calculated for all eight tracers by integrating the breakthrough curves for the mass flux (mg/h for Uranine or Bq/h for the other tracers) against time (h). The injected mass was determined in the same way by integrating the measured concentration in the injection interval against time. For the calculation of the injected mass, it is important to determine the flow rate through the injection interval. A mean flow rate of 41 ml/h in the model was used. Table 6-4 lists all the predicted mass recoveries taking into consideration the time recording stopped.

Table 6-4: Predicted mass recovery in STT-1b

	$t_{100\%}$ (h)	Injected Mass [Bq]	Recovered Mass [Bq]	Recovery rate [%]
HTO	333	65.97e+6	65.91e+6	99.9
Uranine	195	20.775 [mg]	17.85 [mg]	85.9
^{22}Na	1292	562749	519434.8	92.3
^{86}Rb	553	919830	638670	69.4
^{85}Sr	505	284052.3	233437.1	82.2
^{42}K	39	654869.6	389541	59.5
^{58}Co	3622	2719054.4	1769685	65.1

A comparison of the modelled and measured results will followed after publication of the experimental data in the 11th Task Force meeting in Äspö.

Figure 6-4: Predicted breakthrough curves in the Sorbing Tracer Test STT-1b

7 DISCUSSION AND CONCLUSION

The tracer tests with reactive tracers in a radially converging flow geometry were carried out within the scope of TRUE-4E to understand the decay effects and sorption processes of reactive tracers in fractured rock.

Using the program packet DURST/Rockflow we have modelled and evaluated conservative and weak / moderate sorbing tracer transport in tracer tests STT-1 and STT-1b. Prior to the modelling work, the developed model was verified with the analytical solution for the 1D solute transport equation taking diffusion, decay and sorption into consideration.

A fracture model, which was previously calibrated by the experimental data from conservative tracer tests within Task 4C and 4D, was used to calculate the sorbing tracer transport. For the weak sorbing tracer, a satisfactory result was obtained using the same fracture model. However, the breakthrough curve of the moderate sorbing tracer cannot be reproduced using the fracture model. The special form of the breakthrough curve, e.g. slower arrival time and longer 'tailing' compared to the conservative tracer cannot be obtained by merely varying the distribution coefficient K_d, which describes the sorption process in the physical model.

Taking the fact into consideration that the flow and advection processes generally occur in the fracture, and that the diffusion and sorption processes occur in the matrix, a coupled fracture matrix model was built to model the moderate sorbing tracer transport. The results of the modelling of ^{86}Rb and ^{137}Cs were satisfactory. However, a statement on the validation of the linear K_d concept for the retardation effect would only be possible on the basis of more data from tracer tests, especially with strong sorbing tracer.

The decay of radioactive isotope can be adequately described using the half-life time. ^{47}Ca, which has a half-life time of several days, and can also be modelled satisfactorily.

.....

ACKNOWLEDGEMENTS

This work was supported by the Federal Minister for Education, Science, Research and Technology (Bundesministerium für Bildung, Wissenschaft, Forschung und Technologie, BMBF). The German work is coordinated by Werner Bechthold (Forschungszentrum Karlsruhe, KFK).

We would like to thank the SKB Task Force Team and Mr. Anders Ström for the excellent organisation and data delivery.

APPENDIX:

MODELLING QUESTIONAIRE FOR TASK 4E

Draft

1. SCOPE AND ISSUES

a. What was the purpose for your participation in Task 4E?

The purpose of our participation in the Task Force 4E is:

- to understand transport mechanisms for different solutes in fractured rock, especially for the solutes with sorbing and radioactive effects,
- to test our numerical models developed jointly by BGR and University Hanover during GRIMSEL project in the last years, and
- to exchange experience gained from in-situ experiments at the GRIMSEL Test Site (Switzerland) with the international partners in the field of radioactive waste disposal in granite.

b. What issues did you wish to address through participation in Task 4E?

TRUE-1 is very good designed for the understanding the transport of radioactive nuclides in the fracture system. Through participation in Task 4E we wish to address the influence of sorption effect of sorbing tracer in the fractured rock, e.g. whether the physical kd concept is suitable to describe the fast chemical reaction (mass equilibrium reaction).

2. CONCEPTUAL MODEL AND DATA BASE

a. To what extent have you used the data sets delivered?

Based on the data delivered in Task 4C/4D we used additionally following data in the modelling of Task 4E:

Task 4E:I: Data Distribution #1-3

Task 4E:III: Data Distribution #4...

b. Specify more exactly what data in the data sets you actually used?

In the predictive modelling of STT-1 (4E-I) we used the measurement of hydraulic draw-down, the tracer test information from DP5/6 (Dipole Test), PDT1/2/3 (Preliminary Design Test) for the test configuration KXTT4 - KXTT3. For the blind calculation of STT-1b (4E-III) with a test configuration KXTT4 - KXTT1, the data sets from PDT4, Preliminary

Tracer Test (PTT), Radial Converging Test (RC) and Dipole Test - 1 have been used and analysed.

c. What additional data did you use if any and what assumptions were made to fill in data not provided in the Data Distributions but required by your model?

evtl. Kd-Werte

3. MODEL GEOMETRY/STRUCTURAL MODEL

a. How did you geometrically represent the TRUE-1 site and its features / zones?

On the basis of the structural-hydraulic model described by SKB, PNC/GOLDER and USDOE/LBNL, we analysed the fracture system using the data from the bore hole cores and hydraulic tests. Depending on the location and orientation of the fractures, the potentially water-bearing fractures have been combined into the fracture system.

Matrix?

b. Which features were considered the most significant for the understanding of flow and transport in the TRUE-1 site, and why?

The analyse of geological data and hydraulic tests shows that there is a weekly connection between Feature A and B, and they have quite different hydraulic conductivity. The numerical calculation shows that any hydraulic influence of Feature B on Feature A may be neglected for the configuration used in the tracer tests in Feature A.

c. Motivate selected numerical discretisation in relation to used values of correlation length and/or dispersion length

###?

4. MATERIAL PROPERTIES

a. How did you represent the material properties in the hydraulic units used to represent the TRUE-1 site?

The three factors, hydraulic conductivity, fracture aperture and special storage coefficient are important to represent the hydraulic behaviour in the fracture system. A water saturation state was assumed in the TRUE-1 experimental site and the hydraulic conductivity and fracture aperture were varied in our models in order to describe the hydraulic flow field reasonably.

b. What is the basis for your assumptions regarding material properties?

The special storativity has be assumed to be zero if the gas saturation in the pore and water compressibility could be neglected when the hydraulic pressure magnitude in the experiments didn't differ from the natural condition.

c. Which assumptions were the most significant, and why?

In the homogenous model the fracture aperture was often considered as a constant. Actually this is a most significant factor, which influences the distribution of flow field on the one hand, and consequently the transport velocity of tracer on the other hand.

5. BOUNDARY CONDITIONS

a. What boundary conditions were used in the modelling of the TRUE-1 tests?

The piezometric head in all boundaries of the Feature A was used to definite the hydraulic pressure distribution. The NEUMANN Boundary condition - flow rate was used in the injection and pumping situation.

b. What was the basis for your assumptions regarding boundary conditions?

We used a double great calculation area than the experimental site so that we assumed that the boundary condition in the outer boundary has no influences on the experiments.

c. Which assumptions were the most significant, and why?

The correctly application of the pumping rate in the experimental bore holes was important because it determines the flow configuration of the experiments.

6. MODEL CALIBRATION

a. To what extent did you calibrate your model on the provided hydraulic information? (steady and transient hydraulic head etc.)

We have calibrated our flow model with a steady hydraulic head under the natural flow condition and under the condition of the preliminary tracer test in the 4C and additionally under the condition of the radial converging tracer test in the 4D.

b. To what extent did you calibrate your model on the provided 'transport data'? (breakthrough curves etc.)

Based on the flow field calibrated by hydraulic head the breakthrough curve from the preliminary and radial converging tracer tests (breakthrough time, maximal concentration and tailing form of the curve) have been calibrated in the transport model.

c. What parameters did you vary?

We varied the local distribution of the hydraulic conductivity and fracture aperture as well as flow porosity, dispersivity and diffusion in order to match the experimental breakthrough curve.

d. Which parameters were the most significant, and why?

The flow geometry and the hydraulic conductivity were the most significant because they determined the tracer transport path and time in the experimental area.

e. Compare the calibrated model parameters with the initial data base, comments?

##

7. SENSITIVITY ANALYSIS

Identify the sensitivity in your model output to:

a) the discretisation used

b) the transmissivity (distribution) used

c) transport parameters used

Two different meshes were used to identify the sensitivity of the discretisation of the finite element, in which the hydraulic conductivity and fracture aperture have been varied. Additionally transport parameters, e. g. flow porosity, dispersivity and diffusion coefficient were checked in order to determine their influences on the transport phenomena.

8. LESSONS LEARNED

a. Given your experience in implementing and modelling the TRUE-1 site, what changes do you recommend with regard to:

- experimental site characterisation?
- experimental design?

- presentation of characterisation data?
- performance measures and presentation formations?

The experimental site of TRUE was very good characterised.

b. What additional site specific data would be required to make a more reliable prediction of the tracer experiments?

The additional measurement of the concentration in the other bore holes and / or in the interval of Feature B will give us more detail information about tracer distribution in the fracture system.

c. What conclusions can be made regarding your conceptual model utilised for the exercise?

Feature A could be considered as a planar fracture system regarding our conceptual model. But the channelling effect may exist and it could be described as one dimensional element in a two dimensional model.

d. What additional generic research results are required to improve the ability to carry out predictive modelling of transport experiments on the detailed scale?

On the detailed scale one can use another geo-scientific method, e.g. radar tomograph to detect the distribution of tracer concentration during the tracer test so that it could be as additional information for the modeller.

9. RESOLUTION OF ISSUES AND UNCERTAINTIES

a. What inferences did you make regarding the descriptive structural-hydraulic model on the block and detailed scale for the TRUE-1 site?

b. What issues did your model application resolve?

c. What additional issues were raised by the model application?

In the fracture system Feature A, which was quite well-known, the tracer tests were interpreted by numerical model. The consistency of the geological model and the numerical model were proved. The tracer transport parameter (effective porosity, dispersivity and diffusion coefficient) were determined by the modelling of the tracer tests under different test configurations. The numerical models ROCKFLOW (flow model and transport model) have been tested their applicability. The question is if the model and parameter can be used in a large scale consideration. The extrapolation of the result from detailed scale to large (real) scale should be investigated in the next step.

Tracer tests with sorbing tracers. Task 4E-II: Analysis of STT-1 blind predictions and Task 4EIII: Predictions of STT-1b.

T.T. Cladouhos, W.S. Dershowitz, I. Miller (Golder)

and

Masahiro Uchida (PNC)

TRACER TESTS WITH SORBING TRACERS

Task 4e-II: Analysis of STT-1 blind prediction and Task 4e-III: Predictions for STT-1b

Trenton T. Cladouhos[1]
William S. Dershowitz[1]
Ian Miller[1]
Masahiro Uchida[2]

[1]Golder Associates, Inc., Redmond, WA, USA
[2]Power Reactor and Nuclear Fuel Development Corporation (PNC/GOLDER), Tokai, Japan

August 29, 1998

EXECUTIVE SUMMARY

This report describes analysis of sorbing tracer experiments carried out within the Äspö TRUE-1 rock block for the Äspö Modeling Task Force (AMTF) meeting of September, 1998. Task 4eII was an analysis of transport parameters and processes for "Feature A" of the "TRUE-1" rock block based on the results of the SST-1 sorbing and non-sorbing tracer breakthrough measurements. Task 4eIII was a prediction of the SST-1b sorbing and non-sorbing tracer breakthrough based on an improved understanding of transport processes and parameters. Both of these analyses were carried out using a combination of discrete feature network flow modeling and Laplace Transform Galerkin transport modeling.

TABLE OF CONTENTS

LIST OF TABLES

LIST OF FIGURES

1. INTRODUCTION AND BACKGROUND

The Tracer Retention Understanding Experiments (TRUE) are part of a research program at Äspö, the Swedish Hard Rock Laboratory, designed to study the transport of radionuclides in crystalline rock. The first series of tracer tests (TRUE-1) have been performed on a single fracture or fracture zone known as Feature A. Task 4e involved using the results of a non-sorbing radial convergent tracer test (PDT-3) to create and calibrate models and then make blind predictions of sorbing tracer tests (STT-1). Seven modeling groups took this challenge, using a variety of tools and approaches.

The PNC/GOLDER modeling group used stochastic discrete feature network (DFN) models to make the STT-1 predictions. First, multiple DFN realizations of a Feature A geologic conceptual model were generated. Flow simulations of the DFN models provided simulated drawdowns and, via particle tracking, simulated non-sorbing tracer breakthrough curves. Acceptable models were chosen by comparing the measured drawdowns and breakthrough curves of PDT-3 to the model results. Accepted models were then used to predict STT-1 by calculating a retardation factor for each sorbing tracer.

The results of the STT-1 tests were made available in March 1998 (Andersson et al., 1998). Task 4e:II, described in the first part of this report, involves comparison of the measured and predicted tracer breakthrough curves followed by critical evaluation of the concepts used to make the predictions in light of the experimental results.

In the fall of 1997, two new tracer tests were performed using the same experimental setup as STT-1 but a different pathway. First, a non-sorbing tracer test, PDT-4, was run in order to provide information on the new pathway. Then, a cocktail of sorbing tracers was injected (STT-1b). Task4e:III, described in the second half of this report, involves using the refinements suggested by the evaluation of STT-1 and a transport model of the pathway derived from PDT-4, to predict the sorbing tracer transport on the new pathway (STT-1b).

2. TASK 4E:II

2.1 Goals of Task 4e:II

The goals of Task 4e:II are stated in the minutes of Cherbourg Meeting of February 4-6, 1997, "Compare experimental results from the performed sorbing tracer test (STT-1, STT-2, and STT-3) with blind predictions. Evaluate consistency of values for model parameters, e.g. field-scale sorption coefficients and/or flow-wetted surface/β etc. derived from the three experimental breakthroughs in STT-1, STT-2, and STT-3. Compare the derived values with the values used for the prediction. Evaluate validity of basic model concepts and assumptions, processes affecting the experimental result, consistency and realism of parameters values, and relevance and completeness of data base provided."

"Task 4e:II thus should result in 1) estimates of flow-wetted surface (or β, etc.) and/or field scale diffusion/sorption parameters, and 2) a critical evaluation of concepts, assumptions and evaluated parameters values obtained."

2.2 PNC/Golder strategy for Task 4e:II

The PNC/Golder team strategy for Task 4e:II attempted to determine transport parameters and processes which better explain the observed STT-1 breakthroughs than the processes considered in our Task 4e:I predictive modeling. The processes considered in our predictive modeling were:

- multiple stochastic pathways through stochastic continuum transmissivity fields within fracture networks,
- advective transport
- dispersion within fracture planes
- surface sorption
- matrix diffusion

Graphical and quantitative analyses were carried out to assess the possible importance of alternative processes of:

- matrix sorption
- advective exchange between mobile and immobile zones
- single and dual pathways

Comparison between predictions and observations generally indicated that pressure response as measured by drawdown, and advective transport, as measured by median breakthrough time t50 were well modeled in our SST-1 predictions. However, since our models relied on surface sorption for retardation, the initial breakthrough t_5 was shifted for our predictions, while it was not significantly effected in the measurements. In addition, the tail t_{95} of the measured breakthrough curves was longer than could be explained by

dispersion without incorrectly flattening the initial breakthrough. This indicated the possible importance of matrix sorption or other immobile zone exchange processes.

Examination of the measured breakthrough curves also indicated that the breakthroughs could be explained by one to two pathways or average pathways, due to the lack of additional peaks in the breakthrough curves.

Based on these observations, the PNC/Golder team applied the FracMan/PAWorks LaPlace Transform Galerkin (LTG) transport code to derive transport parameters for one and two path models including matrix sorption, and the RIP model to derive transport parameters for models including advective immobile zone exchange.

2.3 STT-1 Injection curves and flow geometry

Andersson et al. (1998) gives details of the experimental setup results. The preliminary design test for the KXTT4 R2 to KXTT3 R2 pathway was PDT-3. The STT-1 test was to have been identical to PDT-3 except that the former included sorbing tracers; however, there were two important differences.

In PDT-3, the tracer concentration in the borehole was held constant for 4.0 hours, and then successfully flushed from the system. In contrast, the injection curve for STT-1 had two peaks (Figure 1). The first peak lasted 4 hours. Due to sorption in the borehole (Andersson et al., 1998) the concentration did not remain constant during this initial peak; for non-sorbing Uranine the concentration dropped to 92% of the peak and for strongly sorbing Cesium, it dropped to 57% of the peak. Between 4 and 5.2 hours the fluid in the borehole was exchanged with unlabelled water, thus the concentrations of all tracers dropped to near zero during this period. However, after 6 hours the tracer concentrations climbed up to about 20% of the peak and then slowly decayed for several hours. It is thought that the exchange process was not effective due to incomplete mixing in the borehole (Andersson et al., 1998); stagnant volumes of labeled water were not flushed out during the exchange process. This problem with the injection makes it more difficult to distinguish the effects of multiple transport pathways from the effect of the injection curve. However, the fact that the breakthrough curves do not show a steep drop between the two parts of the injection curve indicates clearly that an immobile zone transfer process must be occurring.

The second difference between PDT-3 and STT-1 is the head change from the injection to pumping well. In PDT-3, the pumping rate was steady at 0.4 l/min for 100 hours, and a head difference between the pumping and injection well held steady at 6.8 m. In contrast, the pumping rate in STT-1 was steady for 140 days (0.4 l/min) but the head difference increased from 7.2 m to 10.5 m. Andersson et al. (1998) suggest this is either due to clogging (change in transmissivity) in the pumping section or boundary effects. Neither the previous or new model attempts to reproduce the transient behavior of the transmissivity; rather, steady-state heads are assumed.

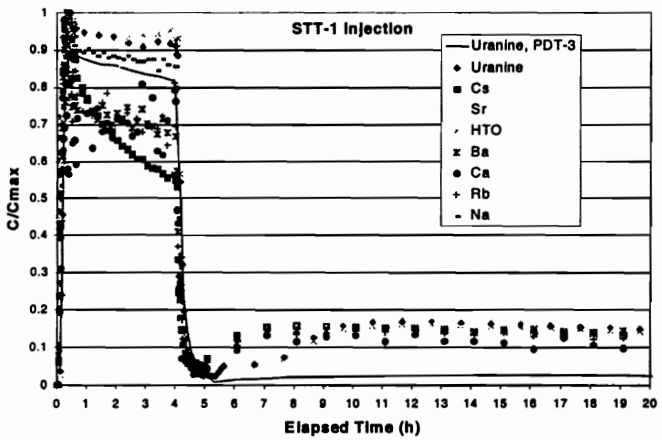

Figure 1 Injection curve for STT-1 tracers. Notice in-borehole sorption of moderately sorbing tracers (Cs, Rb, etc.) and incomplete flushing of wellbore after 6 hours.

2.4 STT-1 breakthrough curves

The breakthrough curves of STT-1 are shown in Figure 2, an arithmetic plot to 100 hours in which the concentrations have been normalized to the injection concentration at 4 hours and Figure 3, a log-log plot of entire monitoring period. An important general observation can be made from inspection of Figure 2; the two lightly sorbing tracers, Strontium (Sr) and Sodium (Na), reach peak concentration in the extraction well after just 7 hours, the same time that non-sorbing Uranine (Ur) and titrated water (HTO) reached the peak concentrations. This implies that the Sr and Na tracers were not retarded along the primary transport pathway. Even the moderately sorbing Barium (Ba), reached a concentration near its eventual maximum in just seven hours. This implies that fracture surface sorption along the primary transport pathway was not a critical process in STT-1.

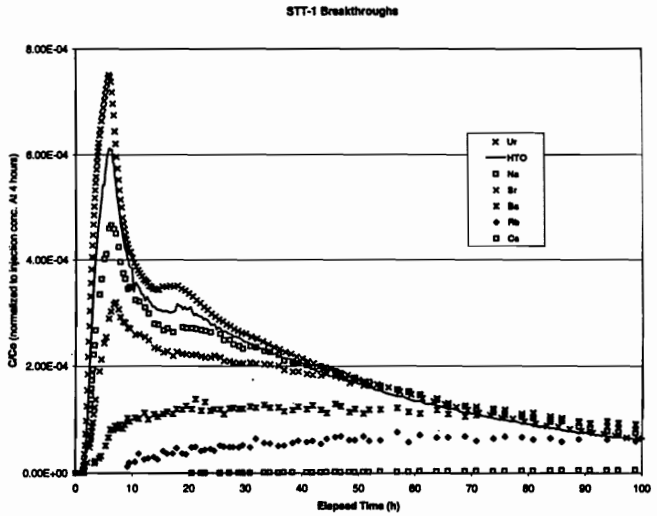

Figure 2 Tracer breakthroughs for STT-1, arithmetic plot.

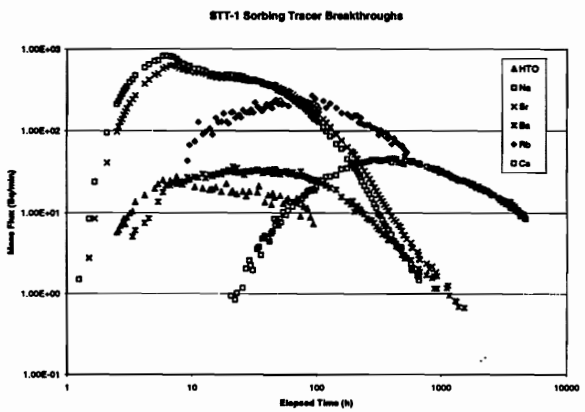

Figure 3 Tracer breakthroughs for STT-1, log-log plot.

2.5 Comparison of PNC/Golder blind predictions to actual results

Figure 4 and Table 1 compare the PNC/Golder predictions with the measured STT-1 results. The strontium and sodium predictions and the barium and rubidium predictions are combined on the same plots because the same retardation values were used for these predictions (Table 5 and 6). Therefore, the shapes of the predicted breakthrough curves are the same, only the mass flux (vertical axes), which depends on the injection mass flux, are different.

For all five sorbing tracers shown in Figure 4, the relationship between the prediction and the measured curves are similar; the measured curves are more stretched out in time than the predictions. In other words, while t_{50} (median breakthrough times) were well predicted, the times of initial (t_5) and tail (t_{95}) breakthrough were over-predicted and under-predicted, respectively.

The November 1997 PNC/Golder predictive model simulated dispersion, matrix diffusion, and fracture surface sorption. The difference between each set of tracers was the fracture retardation values. By increasing the retardations from 1.0 (Uranine) to 1.25 (Sr/Na) to 10 (Ba/Rb), the predictive curves maintained their basic shape and translated toward longer times (Figure 4). Clearly, additional processes in addition to surface sorption on the fracture walls, will be necessary to increase the time lag between the first (t_5) and last (t_{95}) tracer arrival.

Table 1 PNC/Golder Prediction and actual breakthrough curves for sorbing tracer test based on injected mass.

	T5 predicted	T5 measured	T50 predicted	T50 measured	T95 predicted	T95 measured
Uranine	8.3	4.5	35.8	36	98.3	175.0
Na, Sr, Ca	13.8	6.2 – 8.0	52.1	50 – 68	156.7	>527
Ba, Rb	100.8	21 – 42	216.7	206 – 360	610.8	>595
Cs	325.8	465	666.7	> 595	869.2	>595

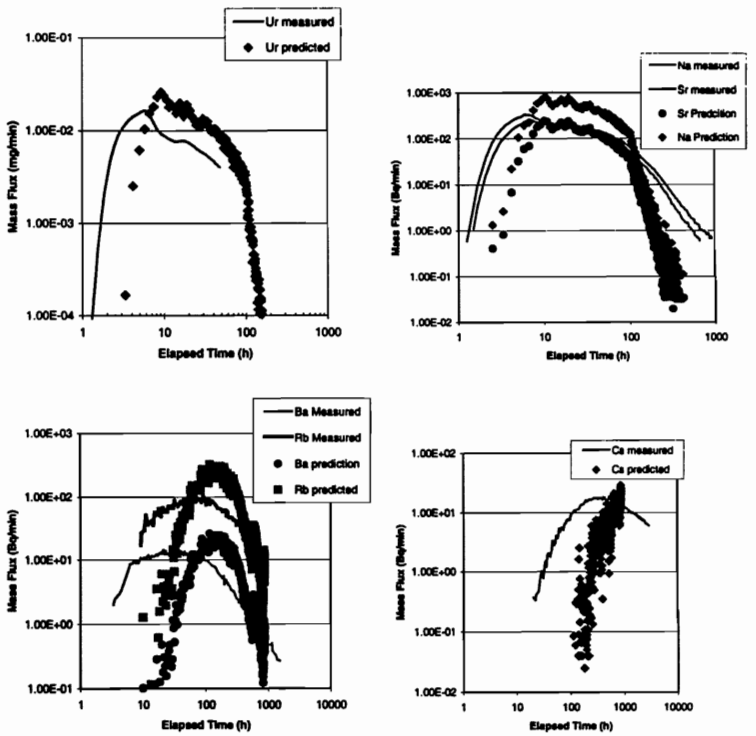

Figure 4 Comparison of PNC/Golder predictions of STT-1 and measured breakthrough curves.

2.6 Comparison of tracer recovery

The PNC/Golder predictions of the STT-1 tracer recovery are not directly comparable to the actual measured recoveries, because the total times of actual and simulated sampling were different. As the total sampling time was not specified prior to the blind prediction, a total time of 100 hours was assumed for all seven tracers. In retrospect, the assumed 100 hour test duration was much too short and resulted in low recovery of all tracers. The resulting predictions of mass recovery were 66 – 75% for the non-sorbing and lightly sorbing tracers and less than 1% for the moderately and strongly sorbing tracers (Table 2). The actual sampling times were much longer than the assumed time of 100 hours and consequently the mass recoveries were much higher; > 90% % for the non-sorbing and lightly sorbing tracers and 26 - 82%

for the moderately and strongly sorbing tracers.

Table 2 Predictions of mass recovery

Tracer	Measured R_t (%)	T100 (h)	Predicted Mean recovery % for T100 = 100 h
Uranine	100	360	75.4
HTO	96	228	75.4
Na-22	94	526	66.6
Sr-85	91	526	66.6
Ba-133	82	1350	0.8
Rb-86	60	526	0.8
Ca-47	97	132	66.6
Cs-137	26	3170	0.0

2.7 Comparison of drawdown predictions

The PNC/Golder strategy for predicting the STT-1 breakthrough curves was to condition and then screen multiple stochastic DFN models to PDT-3. Because the two tests were run at the same pumping rate (0.4 l/min), assuming steady-state heads, the drawdowns for PDT-3 and STT-1 should have been the same. Thus, the drawdowns presented in Table 3-5 of Dershowitz et al. (1997) are not predictions, but the results of conditioning and screening of the November 1997 PNC/Golder model to the PDT-3 drawdowns. Nevertheless, it is in instructive to compare the model results to the actual results. The drawdown screening criteria for the DFN models was +/- 3.5 m from the PDT-3 drawdowns for KTXX2 and KTXX3 and +/- 1.5 for the other three wells. A larger range was allowed for the pumping well (KTXX3) and KTXX2, the well connected by the high transmissivity Feature A*, because it was hypothesized that a local skin could be causing the higher drawdowns at these wells. Thirty stochastic DFN models passed these criteria. In general, the model drawdowns were smaller than the PDT-3 measured drawdowns (Table 3), thus it is no surprise that the model also "under-predicted" the STT-1 drawdowns. It is surprising that the drawdowns increased significantly from PDT-3 until the end of STT-1 (see discussion in section 2.3). Of course, this could not be predicted as the model did not include a time-varying transmissivity at the pumping well; rather, steady state heads was assumed.

Table 3 Predictions of drawdowns ([1]12 June 1997; [2]15 July, 1998 ; [3]30 Nov. 1998)

Well	Prepump Heads	PDT-3 [1] drawdown	Model drawdowns		STT-1 start[2] drawdown	STT-1 end[3] drawdown
			Mean	Accept. Range		
KTXX1	-53.0	1.9	2.2	0.4 – 3.4	2.6	5
KTXX2	-53.0	6.6	4.0	3.1 – 10.1	7	12
KTXX3	-52.6	8.1	5.3	4.3 – 11.6	9	14
KTXX4	-52.9	1.1	1.7	0.1 – 3.6	1.1	3.5
KA3005 A	-53.6	1.3	1.4	0.3 – 2.8	1.6	5

2.8 Comparison of other modeling groups results to actual results

Andersson et al. (1998) fit the breakthrough curves using a 1D advection-dispersion equation with linear sorption (herein called the Geosigma model). First, the fit was done for each curve individually by varying the dispersivity (D) and dilution factor. Nice fits were obtained for all curves but physically unreasonable dispersion values (D= 2.0 to 23.4 m) were required. This fit has no real physical meaning since all processes are included in the dispersivity term. Second, simultaneous fits of Uranine and each sorbing tracer were modeled to determine each retardation coefficients. However, the fits for Ba, Rb and Cs were poor (particularly in the tails), indicating that a linear sorption model cannot explain the results.

Six other modeling groups made STT-1 predictions. All other models employed stochastic continuum simulators with variable transmissivity on the surface of Feature A. Various assumptions about the importance of background flow, matrix retardation, diffusion, and secondary features were made. Table 4 below summarizes the relevant aspects of each model and Table 5 compares each group's prediction with the measured results. Most groups suffered from the same problem as PNC/Golder; namely, for the moderately sorbing tracer (Ba, Rb, and Cs) first arrival times (t_5) were over-predicted and final arrival times (t_{95}) were under-predicted. Most groups focused on the spatial distribution of transmissivity on Feature A and the flow field between the injection and pumping well. With the exception of SKB/KTH and CEA, issues of tracer sorption and diffusion were not explored.

Table 4 Approaches and parameters of other modeling groups (NR: Not reported NA: Not applicable)

Team	CODE	Aperture	dispersion	Matrix Porosity and/or effective diffusivity	T on Feature A	Assumptions
PNC/GOLDER	Fracman/MAFIC	e= 0.5sqrt (T)	α_L=0.5 m α_t=0.05 m	Dw=1x10^{-13} m^2/	7.0x10^{-4} m^2/s Conditioned to T at wells, POCS correction applied	
CRIEPI	FEGM/FERM	0.46 mm	0.65 m	NA	Lognormal kriged from T at boreholes. Correlation length = 1 m	Hydraulic gradient =0.125 @ 57. Flow only through features.
BGR	DURST/Rockflow	1.4 mm	α_L=0.6 m α_t=0.12 m	4x10^{-5} m^2/s	KhA = 2.4e-4 m/s KhB = 5.9e-4 m/s	2.1xQ, sp=5.0 m, delH=24m Double-porosity continuum mode
CEA	CASTEM2000	1.4 mm	1.6 m	0.001	log (mean T) = -7.4	1D advection disp. transport equa 1D matrix diffusion & surface retardation. Gradient and transverse disp. negl fracture and matrix retardation us
Nagra/PSI	NR	NR	NR	0.15 diffusion depth = 1 mm (fault gouge)	NR	Uniform time-independent backgr flow Homogeneous and isotropic transmissivity field
GeoSigma	PAREST	1.8 mm	2.0 m	NR	NR	Retardations: Na=1.5, Sr=2.1, Rb= Constant pump rate of .401 l/min
SKB/KTH	CHAN3D	NR	NR	5 layers: 1mm gouge (infinite D) 1mm alt rock1 (0.05) 5 mm alt rock2 (0.015) 25 mm alt rock3 (0.015) virgin rock (0.004)	NR	NR
VTT/ Posiva	FEFLOW/ TFIELD/ BTSIMU	e_{max} = .7 mm e_{min} = .05mm e_{avg}=.25 mm	Disp. Coeff. = 10^{-4} m^2/s	Dw=1x10^{-9} m^2/s	Isotropic; Heterogeneous; Lognormal; calculated from boreholes with correlation length = 0.4 m T inside of .1m radius from borehole = 5x10^{-5} m^2/s	Dispersion assumed instead of diff

Table 5 Modeling group predictions (shaded cells are within 25% of the measured times in bottom row).

		Uranine			*HTO*			*Na-22*			*Sr-85*		
Modeling Group	**Model Features**	t5 (hrs)	t50 (hrs)	t95 (hrs)	t5 (hrs)	t50 (hrs)	t95 (hrs)	t5 (hrs)	t50 (hrs)	t95 (hrs)	t5 (hrs)	t50 (hrs)	t95 (hrs)
CRIEPI	Variable T on Feat. A								29.8	165.5	4.7	30.4	170.1
BGR Mesh 1	Feature A & B, flow field	6.5	56.0	316.0	6.2	55.0	270.0		60.0	370.0		30.0	105.0
BGR Mesh 2	is paramount	6.3	57.0	225.0		49.0			62.0		5.5	43.0	144.0
SKB/KTH	5 layered fractures	34.6		62.6	35.6		387.0	33.6		77.4	31.1	39.2	
Nagra/PSI	Surface and Matrix Sorption				6.6				33.0	168.3		35.8	175.0
VTT/Posiva													
PNC/Golder POCS	Rough Feature A & Backgr. Fracs	7.9		99.2	7.9		99.2		11.0	42.0		11.0	42.0
PNC/Golder KT	Background Fractures	5.8		101.7			101.7	8.0	19.0	60.0		19.0	60.0
Measured (based on injected mass)		4.5	36.0	175.0	5.0	40.0	217.0	6.2	52.0		8.0	68.0	
Measured (based on recovered mass)		**4.5**	**36.0**	**175.0**	**4.9**	**37.0**	**161.0**	**6.0**	**48.0**	**240.0**	**7.5**	**60.0**	**304.0**

	Ca-47			*Ba-133*			*Rb-86*			*Cs-137*		
Group	t5(hrs)	t50(hrs)	t95(hrs)	t5(hrs)	t50(hrs)	t95(hrs)	t5(hrs)	t50(hrs)	t95(hrs)	t5(hrs)	t50(hrs)	t95(hrs)
CRIEPI	4.6	28.2	114.0	9.5	52.1	510.7	13.6	57.7	244.3		404.7	
BGR Mesh 1		60.0	360.0	35.0				115.0	330.0	320.0		
BGR Mesh 2	6.5	66.0	203.0	7.0	66.0	354.0	6.2	58.0	270.0	12.6	198.0	654.0
SKB/KTH	32.6	34.3	51.8	30.7	60.1	303.0				29.4	71.2	391.0
Nagra/PSI	6.0	34.2	123.5	41.3		643.3	134.0	350.0	715.0	635.0	1816.7	3750.0
VTT												
PNC/Golder P	6.0	11.0	42.0	60.0	185.0	530.0	60.0			250.0		
PNC/Golder K	8.0	19.0	60.0	85.0	185.0	600.0	85.0		600.0	335.0		
Measured (inj)	7.0	50.0	120.0			205.0	42.0	360.0		465.0		
Measured (rec)	**14.0**	**300.0**	**507.0**	**19.0**	**146.0**	**930.0**	**31.0**	**177.0**	**470.0**	**150.0**	**640.0**	**1265.0**

2.9 (Re)Calibration to STT-1 Uranine and Strontium Breakthrough

A goal of Task 4e:II is to explain the differences between the results of our November 1997 predictions and the actual sorbing tracer measurements. A slightly different approach was taken this time. The measured breakthrough curves do not show evidence of multiple pathways; therefore, the importance of background fractures to the tracer paths may not be as important as previously thought. In addition, the shapes of the breakthrough curves and the inability of most groups to make successful predictions, suggests that processes not previously modeled (i.e. matrix sorption) could be operative. Therefore, we decided to continue to use the DFN approach for simulating the flow field and to use FracMan/PAWorks (Foxford et al., 1998). PAWorks transforms 3D discrete feature network models to 3D pipe network models and solves transport by the Laplace Transform Galerkin (LTG) including the possibility of multiple immobile zones and matrix sorption.

An iterative process was followed in which first the Uranine breakthrough curve was fit allowing the flow (advective velocity, flow width) and transport (aperture, porosity) parameters to be solved. Then, by adjusting the free water diffusivity, and surface and matrix retardations only, an attempt to fit the strontium breakthrough curve was made. This process was first attempted with a single path model. Iterating between the Uranine and strontium curves quickly led to quite high values of porosity (10%) in order to fit both the non-sorbing and sorbing curves (Table 6). In addition, a single path model led to very high dispersivity (1.5 m) and an inability to fit the breakthrough curve in the 10-15 hour range. Then, we switched to a two path model and found that a two path model with parameters as listed in Table 6 can reproduce a better fit to the non-sorbing breakthrough curve of STT-1 (Figure 5). Table 6 also compares the transport properties used for the November 97 predictions, the revised properties derived using LTG, and the properties derived for the Geosigma model (Andersson et al., 1998).

Table 6 Comparison of STT-1 predictive model with fitted models (Uranine and Strontium)

Parameter	FracMan /MAFIC Model (11/97)	PAWORKS/LTG Fitted			Geosigma Fitted Model
		One path Model	Two Path Model		
			Path 1	Path 2	
Aperture	0.00013 m	.001 m	0.0007 m	0.0007 m	0.0018 m
Path Length	many paths >4.68	4.7 m	4.7 m	6.0 m	4.68 m
Path Width	~2 m	3.5 m	45%x 3.5 m	55% x 3.5 m	not reported
Dispersivity	0.5 m/ 0.05 m	1.5	0.8	0.8	2.0
Porosity	0.0001	0.1	0.015	0.015	0.0015

Mean Velocity	L/t_{50}= 0.85 m/hr	1.3 m/hr	1.3 m/hr	0.45 m/hr	0.9 m/hr
Transmissivity of A (for ΔH = 7.2m)	$10x10^{-7}$ m²/s	$2.4x10^{-7}$ m²/s	$1.7x10^{-8}$ m²/s	$0.7x10^{-7}$ m²/s	$7.6x10^{-7}$ m²/s

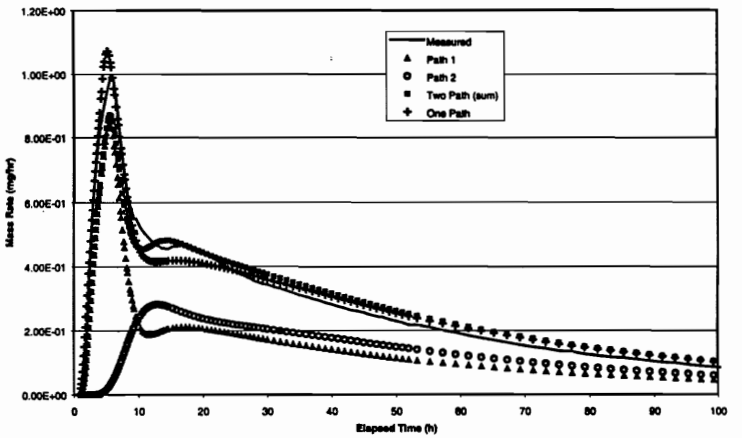

Figure 5 STT-1 Uranine breakthrough curve and fit with 2 pipe LTG model

2.10 Calibration to STT-1 Sodium and Rubidium Breakthrough

After obtaining a fit to the non-sorbing breakthrough curve and the Sr curve, two additional sorbing tracer tests, Na and Rb were modeled using LTG. These two tracers (as well as Sr) were chosen for reanalysis because they were also used in STT-1b. Although LTG significantly simplifies the geometry of the flow network, it provides an important advantage, the ability to independently simulate both surface sorption and matrix sorption. Initial values of surface retardation was calculated from

$$R_a = 1 + 2K_a / e \qquad (1)$$

where e is the fracture aperture and K_a the surface sorption coefficient. Initial values of matrix retardation was calculated from

$$R_m = 1 + \rho K_d / n \qquad (2)$$

where ρ is the density of the rock, K_d the matrix sorption coefficient, and n the porosity.

LTG models using retardation values calculated from the laboratory sorption coefficients failed to reproduce the long tails observed in the experimental data; therefore, the retardation values were increased until the tails on the breakthrough curves were fit (Tables 7 and 8). Andersson et al. (1998) also concluded that the laboratory values were too low (Tables 7 and 8). Figures 6 and 7 show the best fits to two of the sorbing tracer tests. Table 9 and 10 compare the initial, median, and tail breakthrough times for the actual experiment to the best one and two path LTG fits.

Table 7 Comparison between matrix and surface sorption (Ka and Kd) from lab and fitting STT-1.

Tracer	FracMan/ MAFIC Model) Ka (m) (e=0.0013)	PAWORKS/LTG Fitted Ka (m) (e=0.0007 m)	PAWORKS/LTG Fitted Kd (m^3/kg) (n=0.1 / 0.015)	Lab Ka (m)	Lab Kd (m^3/kg)	Geosigma fitted Ka (m) (e=0.0018 m)
Na	1.6e-5	1.3e-5	3.6 e-5 / 2.7e-5	5e-6	2.8e-5	4.5e-4
Sr	1.6e-5	5e-5	4.0e-4 / 2.35e-4	2e-5	2.3e-4	9.0e-4
Rb	6.0e-4	2.5e-3	6.9e-4/ 3.5 e-3	1e-3	1.4e-3	1.3e-2

Table 8 Comparison between retardation coefficients determined from laboratory data and evaluation of STT-1. For the LTG fitted model the first number is for the one path model (n=0.1) and the second number is for the two path model (n=0.015).

Tracer	FracMan/MAFIC Model (11/97)	PAWORKS/LTG Fitted		Lab (e=0.0007)	Lab (n=0.015)	Geosigma fitted
	Surface R	Surface R	Matrix R	Surface R	Matrix R	Surface R
Na	1.25	1.04	2.0 / 6.0	1.01	6.1	1.5
Sr	1.25	1.14	12 / 44	1.06	43.1	2.1
Rb	10	8.1	20 / 640	3.9	258	15.0

Table 9 Comparison of breakthrough statistics for STT-1 (one path model). Based on recovered mass at t100.

Tracer	t_5 measured	t_5 LTG fit	t_{50} measured	t_{50} LTG fit	t_{95} measured	t_{95} LTG fit	t_{100}
Ur	4.5 h	4.3 h	36 h	42 h	175 h	171.5 h	360 h
Na	6.0	5.8	48.0	53.8	240.0	348	527
Sr	7.5	8.3	60	80.8	304	398	527
Rb	31	22.2	177	127	470	434	527

Table 10 Comparison of breakthrough statistics for STT-1 (two path model). Based on recovered mass at t100.

Tracer	t_5 measured	t_5 LTG fit	t_{50} measured	t_{50} LTG fit	t_{95} measured	t_{95} LTG fit	t_{100}
Ur	4.5 h	5.0 h	36 h	43 h	175 h	171.5 h	360 h
Na	6.0	5.3	48.0	49.3	240.0	223.0	527
Sr	7.5	6.2	60	60.8	304	312	527
Rb	31	36.8	177	127	470	434	527

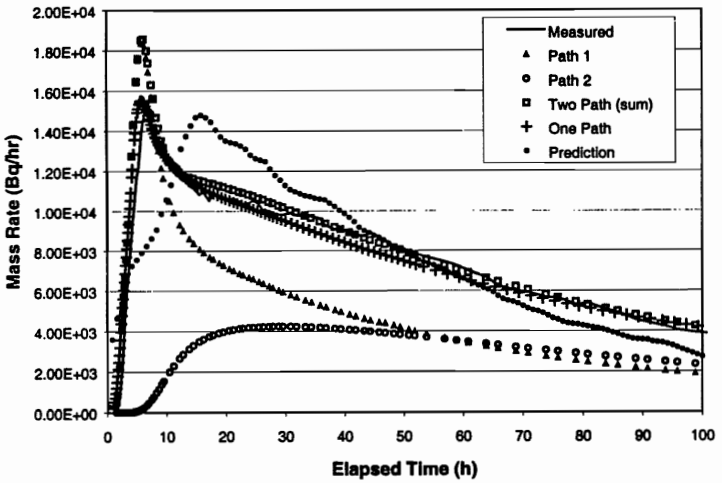

Figure 6 Strontium breakthrough curve, one pipe fit, two pipe and previous prediction.

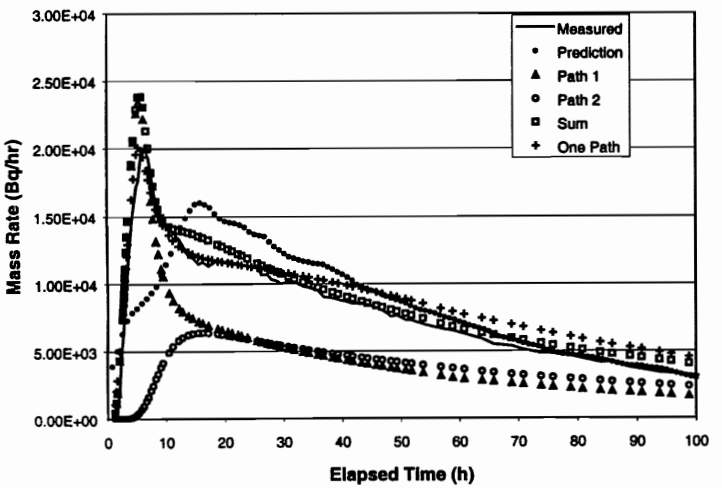

Figure 7 Sodium breakthrough curve, one pipe fit, two pipe and previous prediction.

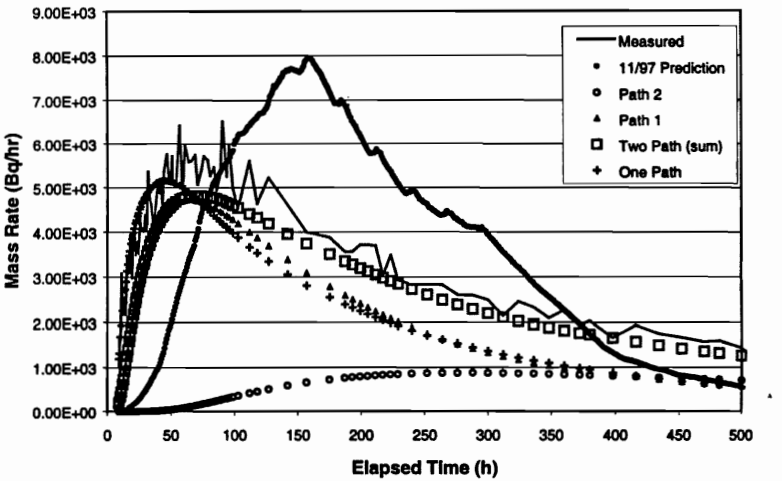

Figure 8 Rubidium breakthrough curve, one pipe fit, two pipe and previous prediction.

Table 11 Comparison of recovery statistics for STT-1

Tracer	% recovery measured	Injected Mass (model at 45 ml/hr	% recovery fitted (one path model)	% recovery fitted (two path model)
Ur	100	36.0 mg	98.9	99.2
Na	94	1.15×10^{-6} Bq	97.8	94.0
Sr	91	1.30×10^{-6} Bq	78.3	90.8
Rb	60	2.81×10^{-6} Bq	37.8	49

2.11 Alternative Transport Conceptual Model

The shape of the measured breakthrough curves is notable in three ways:

1. initial breakthrough is sharp for both sorbing and non-sorbing tracers, indicating little dispersion at least along the fastest transport path.

2. there is little retardation of the initial breakthrough, although t50 and t95 are strongly effected by sorption,

3. the breakthrough curves do not drop off as steeply as the injection curves between the two peaks of the injection curves.

These three observations strongly indicate a mixture of mobile and immobile zone transport with different sorption properties. The FracMan/PAWorks studies above address the possibility to explain these phenomena as a combination of higher matrix sorption and multiple pathways.

Another possible explanation is the use of the Miller (1998) transport approach which replaces dispersion and matrix diffusion by an advective exchange process between mobile and immobile zones. In this conceptual model the mobile zone is the portion of the fracture plane in which the advective velocity is directly related to the flux, gradient, aperture, and transmissivity of the fracture. In other words, in the mobile zone the flow field can be easily solved from the fracture geometry and boundary conditions. In contrast, the immobile zone is the portion of the fracture plane in which the advective velocity is extremely low, so that the turnover of water and tracer in these pockets in very slow. Immobile portions of the fracture could be caused by eddies in the flow, open, stagnant pores, dead-end fractures, or any geometry that causes the main flow to bypass a region. The difference between this conceptual model and that of LTG is that in LTG the tracer diffuses into the rock matrix (the immobile zone), whereas in this model tracer advects into the immobile zone.

The Miller (1998) conceptual model has been implemented in RIP: Integrated Probabilistic Simulator for Environmental Systems (Golder Associates, 1997). Like LTG, a pathway in RIP is modeled by specifying advective velocity, path length, transport aperture, and matrix porosity. Two further variables describe the relative importance of the mobile and immobile zones. The fraction of immobile volume in the fracture (f_{im}) is simply the ratio of the immobile portion of the fracture to the total volume of the fracture. The immobile fraction (f_{im}) and mobile fraction (f_m) must sum to 100%. The second variable is the exchange rate between the immobile and mobile portions of the fracture. This rate, denoted by β, is expressed in number of exchanges per meter.

First, the STT-1 Uranine breakthrough curve was fit with RIP (Figure 9); Table 12 lists the pathway parameters used. The best fit included an immobile fraction of 72.5% and an exchange rate of 0.6 m^{-1}. Then the STT-1 Sr and Rb breakthrough were fit (Figures 10 and 11). In order to properly fit the sorbing tracer curves, it was found that the matrix sorptions had be significantly reduced from the laboratory values: for strontium to about 1% of the lab value and for rubidium to about 3% of the lab value. However, even with these changes to the sorption/retardation values, the overall shape of the curve was not well fit.

The results of the sorbing tracer fits shown in Figures 10 and 11 suggest that the Miller (1998) conceptual model needs a further refinement. In the original concept, retardation occurs both in the mobile and immobile zones. As noted

earlier in Section 2.4, a distinctive characteristic of the sorbing tracer breakthroughs is the fast initial arrival (t_5) even for moderately sorbing tracers like rubidium. Therefore, a simple modification to the model is suggested: retardation which does not occur in the mobile zone, but does in the immobile zone. Theoretically this is similar to assuming that the tracer solution does not reach equilibrium with the fracture walls in the mobile zone because sorption requires some residence time at the sorption sites. Practically, this change will produce

Table 12 RIP pathway parameters

Parameter	Value
Aperture	1.06 mm
Path Length	4.7 m
Path Width	3.5 m
Dispersivity	0
Porosity	0.015
Mean Velocity	1.8 m/hr
F_{IM}	0.725
Beta	0.6 1/m

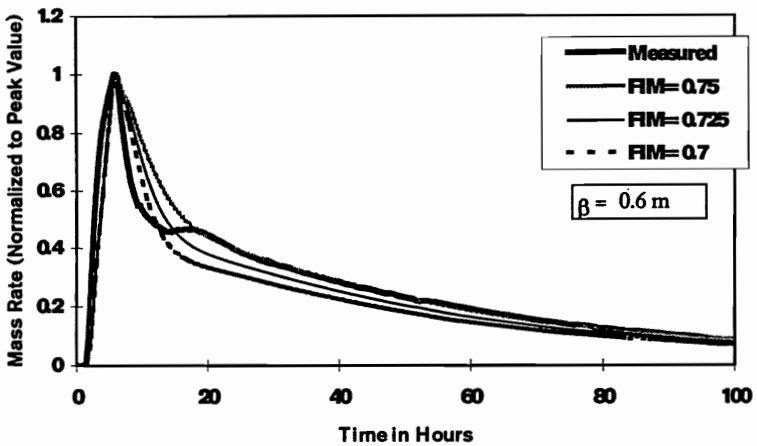

Figure 9 STT-1 Uranine breakthrough, Miller Model fits

both a sharp initial peak (due to unretarded tracer which traveled only in the mobile zone on the journey to the extraction well) and a large tail (due to retarded tracer which traveled into the immobile zone at some point during the journey). Figures 12 and 13 show the result of the non-equilibrium mobile zone transport simulation for strontium and rubidium. Even with no sorption in the mobile zone, the Miller Model fits are still

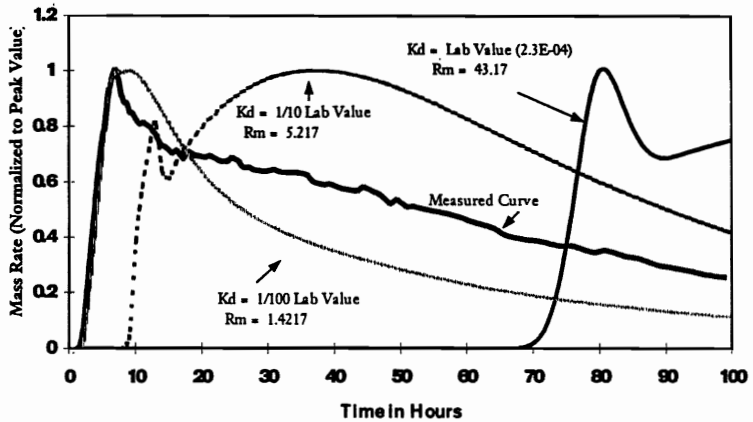

Figure 10 STT-1 strontium breakthrough, Miller model fit.

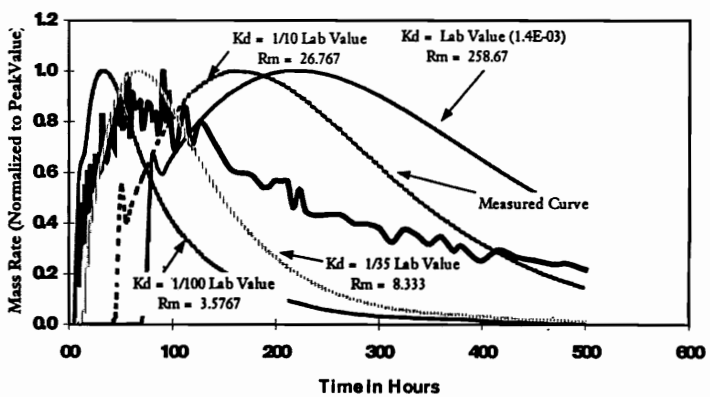

Figure 11 STT-1 Rubidium breakthrough curve, Miller Model fit.

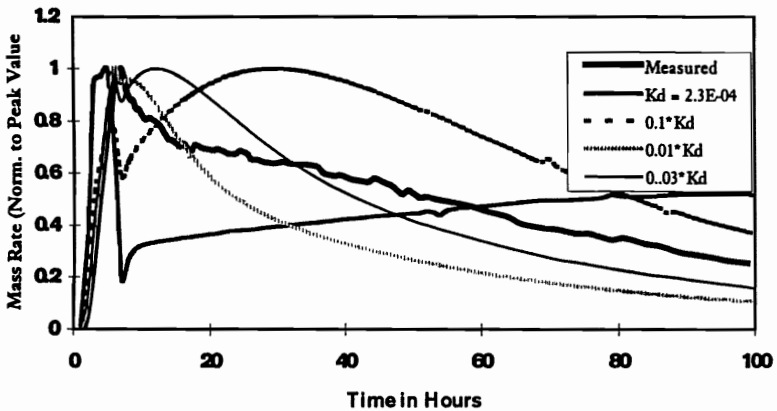

Figure 12 STT-1 strontium breakthrough, Miller Model, no sorption in mobile zone.

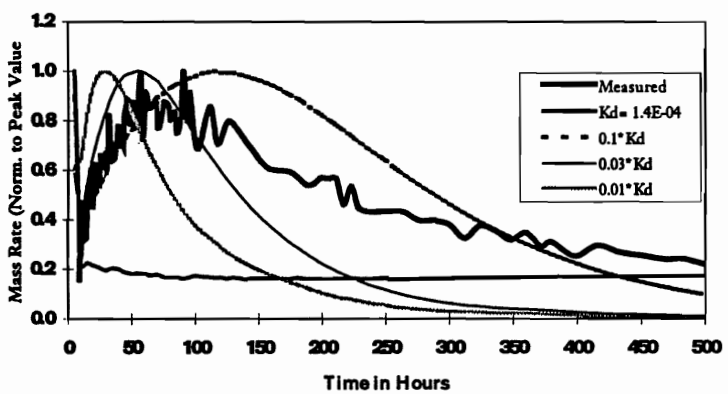

Figure 13 STT-1 rubidium breakthrough, Miller model, no sorption in mobile zone.

worse than the two path LTG fits. Therefore, although we believe that there is much promise in alternative conceptual models of tracer transport of the Miller (1998) type, the STT-1b predictions will be based upon the LTG model fits.

A final alternative conceptual model to explain the STT-1 curves is colloidal transport. In this model, dust particles (sub-micron sized) of rock or waste could be entrained in the flow. If some tracer sorbs onto a particle, it will be on a fast path to the extraction well. This scenario seems unlikely for the TRUE-1 tests.

2.12 Conclusions from Task 4e:II

1. The analysis of the head field, drawdown, and advective transport (t_{50}) for the SST-1 predictions adequately address the observed behavior
2. Immobile zone sorption is necessary to explain the observed breakthrough of sorbing tracers (t_5, t_{95})
3. The effective surface and matrix sorption (Kd and Ka) are approximately 2.5 times the laboratory values for the SST-1 tracers
4. Immobile zone/mobile zone transport can be explained using either a Fickian diffusion (LTG model) or an advective exchange (Miller, 1998) model. The Miller model provides a good match for the shape of the non-sorbing Uranine breakthrough without relying on matrix diffusion.
5. Assuming Fickian diffusion with the reported injection curves, it is necessary to define two transport pathways to match the measured breakthrough curves between the two peaks. This model will be carried forward to the STT-1b predictions in the next section of this report. Alternatively, the measured curves can be explained as an error in the measurement of the injection curve or alternative processes such as advective exchange between mobile and immobile zones.

3. TASK 4E:III

3.1 Goals of Task

The goals of this task can be found in the Äspö quarterly report (HRL 98-04). "A new Task 4e:III was defined as a straightforward extension of the present modeling task (Task 4e:I). Another injection of tracers, except Cs, will be performed. Another flow path will be studied (borehole KXTT1->KXTT3). The models utilized should be the same, i.e. there should be no updating of the structural model implemented or calibration on available experimental results from STT-1."

3.2 PNC/Golder Strategy for Task 4e:III

The PNC/Golder strategy for this task combine the strategies of Task4e:I and 4e:II. First, a flow simulation of the PDT-4 pumping geometry was performed on the Task4e DFN model (Dershowitz et al., 1998). In order to simulate the larger drawdowns observed for this test (Andersson et al. 1998), the transmissivity of Feature A in the model had to be modified slightly. Next, the non-sorbing Uranine tracer test was simulated using particle tracking in MAFIC. Here the strategy differed from that previously used; instead of trying to match the PDT-4 curve with a particle tracking, the primary goal was to determine a flow-path width and mean velocity. Thus, matrix diffusion was turned off. Next , LTG was used to fit the non-sorbing breakthrough curve of PDT-4. Both a 1 path model and a 2 path model were fit with transport properties similar to those found for STT-1 (Table 6). Finally, the results of the two methods of estimating flow width and velocity, one derived from particle tracking in MAFIC and the other from an LTG fit of the non-sorbing tracer test, were compared.

Like the STT-1 LTG models presented in the previous section, both a one path and a two path model were fit to the PDT-4 Uranine breakthrough curve. Although the two path model does not provide a significantly better fit than the one path model there are two reasons for continuing to use the two path model. First, the single path model has a high, possibly unrealistic, porosity compared to the two path curve. Second, in STT-1 it was found that the two path model provided better fits to the sorbing tracer breakthrough curves.

To predict the sorbing tracer breakthrough curves either the field scale sorptions derived from Task 4e:II (Table 7) or, for tracers not used in STT-1 (K, Co), from the laboratory derived sorptions. The injection history for each tracer was used to scale the breakthrough curves. Sorbing tracers were predicted using FracMan/PAWorks in order to address the importance matrix sorption process identified in Task 4e:II.

3.3 PDT-4 injection of non-sorbing Uranine

A dilution rate for PDT-4 of 50 ml/hr was derived from the slope of the injection curve (Figure 14) and the volume of the injection section (1560 ml). However,

this injection rate results in greater than 100% recovery. A similar observation was made during the analysis of PDT-3. In that case a 13% change in the volume of the injection borehole corrected the mass recovery to less than 100%. For the PDT-4 test, monitoring at the pumping well lasted 137 hours with the total mass received at the pumping well (concentration converted to mass with a pumping rate of 0.4 l/min = 24 l/hr) was 34.9 mg. Integrating the concentration curve of PDT-4, we find that a dilution rate of 33.3 ml/hr would inject 34.9 mg in 97 hours. Therefore, assuming 100% recovery of Uranine in this time frame the borehole volume is 1040 ml. This issue is not of the utmost importance, as the final results will be normalized to the injected mass.

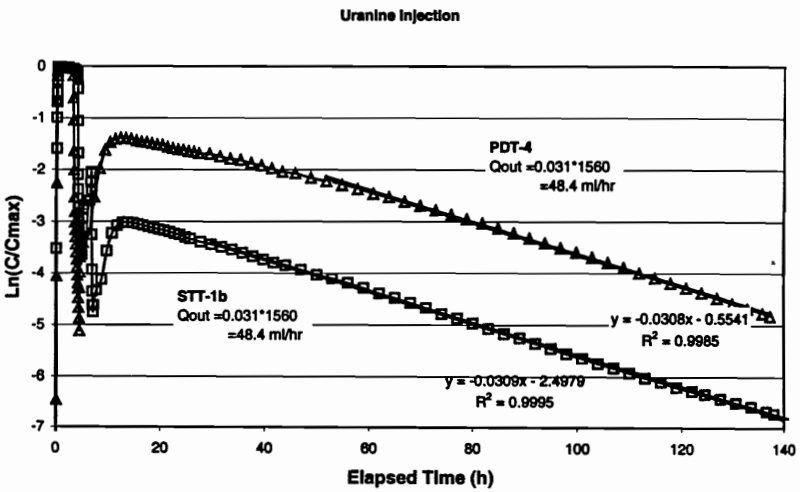

Figure 14 Natural log plot of concentration in injection section used to determine dilution rate.

3.4 FracMan/MAFIC Model

The primary goal of using the Task 4e:I FracMan DFN model for simulating PDT-4 is to establish a basis for comparison to the LTG models that will be used for the new sorbing tracer predictions. To achieve this goal, a MAFIC model that reproduced the observed heads was constructed and then the tracer test simulated using the particle tracking algorithm of MAFIC.

For this exercise, the Task 4e:I DFN model was modified in a few ways. First, the model was meshed with a finer mesh on Feature A, including symmetric meshing around the boreholes. The better mesh should result in more even release of particles from the injection borehole and less stuck particle in

elements with long aspect ratios. Second, instead of proceeding with both a constant transmissivity and POCS transmissivity field on Feature A as was done for the STT-1 predictions (Dershowitz et al., 1997), transmissivity on Feature A was simply conditioned to the at borehole values. This simplification was followed, because one conclusion of the STT-1 prediction task was that the spatial structure of transmissivity on Feature A did not seem to have a larger effect on the breakthrough curves. Third, the transmissivity of the background fractures was reduced to lessen the fluxes through the background fracture network . This was done because it was discovered that in the old model, many if not most of the particles left Feature A near the injection well, traveled along a network of background fractures, and then re-entered Feature A near the extraction well. Reduction of the background fracture transmissivities reduced the number of transport pathways to be more consistent with the results of Task 4e:II. However, a side effect of the change is that the drawdowns in Feature A significantly increased, as the storativity of the background network became less accessible. To counteract the side effect, the storativity of feature A and the background features were increased. Lastly, in order to fine tune the drawdowns in Feature A to those observed, the at borehole transmissivities were decreased (Table 13). Table 13 summarize the hydraulic parameters of the new DFN model described in this paragraph.

Table 13 New Hydraulic Parameters in MAFIC

Feature	Parameter	Task4e:III DFN	11/97 DFN
Background Fracture	Transmissivity	Mean = 1.0 x10^{-8} m^2/s Stdev = 5.0 x10^{-9} m^2/s	Mean = 3.98 x10^{-8} m^2/s Stdev = 5.17 x10^{-8} m^2/s
	Storativity	Mean = 2x10^{-8} m^2/s Stdev = 1x10^{-8} m^2/s	= 0.001$T^{0.5}$
	Aperture	Mean = 0.1 mm StDev = 0.05 mm	= 0.5$T^{0.5}$
Feature A	Transmissivity	Conditioned to well values (1x10^{-8}, 1x10^{-8}, 7x10^{-7}, 3x10^{-7}, 7x10^{-8} m^2/s for wells 1, 2, 3, 4, 5)	POCS or constant (7x10^{-8} m^2/s)
	Storativity	3x10^{-7} m^2/s	= 0.001$T^{0.5}$
	Aperture	1 mm	= 0.5$T^{0.5}$

The drawdowns simulated by the new DFN model are shown in Table 14 and Figure 15. Similar to the Nov. 1997 DFN model, the drawdowns at KTXX2 and KTXX3 are under-predicted by most of the realizations. Also similar to the old DFN model, there is a relatively large intra-realization variation of heads (4 m) at the pumping well. This variability is due to the stochastic background fractures near the pumping well for each realizations.

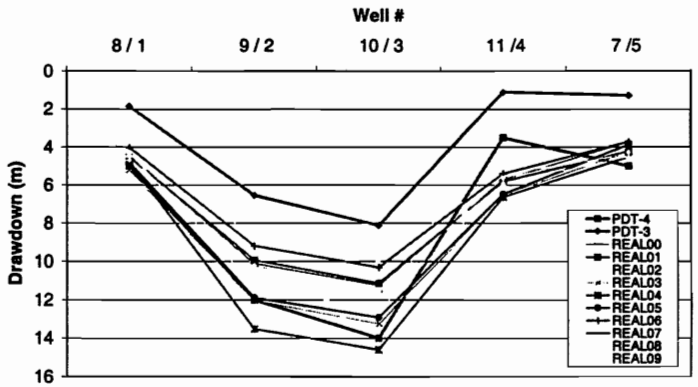

Figure 15 Drawdowns of PDT-4

Table 14 Drawdowns predicted by MAFIC model compared to measured drawdowns and heads.

Well	Measured* 98/12/1	MAFIC predictions		
		5th percentile	50th percentile	95th percentile
KTXX1	5 m	4.1 m	4.6 m	5.0 m
KTXX2	12	8.9	10.8	12.9
KTXX3	14	10.1	12.0	14.1
KTXX4	3.5	5.4	5.9	6.6
KA3005A	5	3.7	4.2	4.5

*From Figure 3-12 of Andersson et al. 1998 assuming -53 m initial head at all wells.

Once 10 stochastic models with acceptable drawdowns were found, particle tracking was run in MAFIC in order to simulate the tracer tests. Approximately, 1300 particles were released in KTXX4. To simulate the irregular injection curve of PDT-4, slug superposition was used with 27 slugs of varying amplitude.

The results of the MAFIC particle tracking are shown in Table 14 and Figures 16 and 17.
Three conclusions can be made from these simulations:

1. Particle paths are heavily influenced by Feature A*, the highly transimissive connection between KTXX2 and KTXX3 (Figure 17).

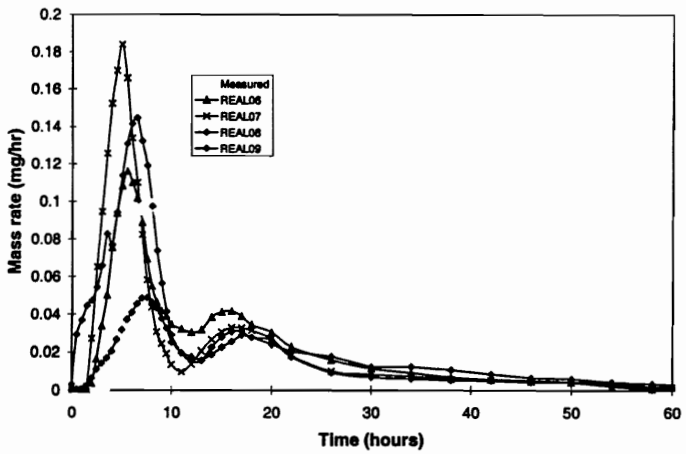

Figure 16 MAFIC Breakthrough curves. Simulations were run with no matrix diffusion in order to obtain mean unretarded flow velocity, thus poor fit on tail was expected.

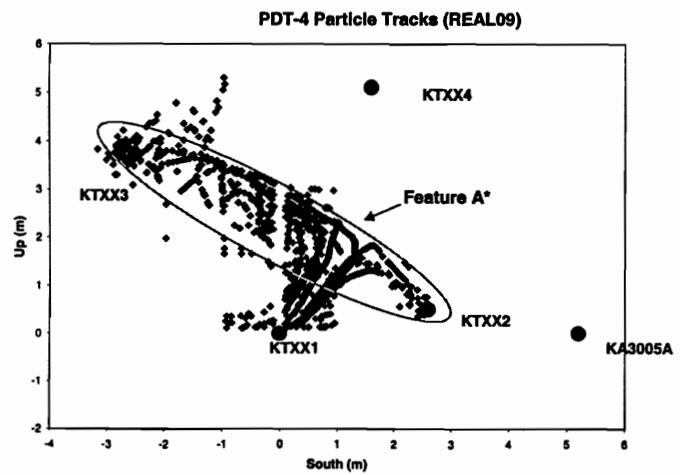

Figure 17 Flow paths in DFN model.

2. Missing the tail of the PDT-4 curve is not worrisome as matrix diffusion has been turned off and we wouldn't expect to match the large tail without matrix diffusion (Figure 16).
3. Mean velocity calculated from t_{50} is 0.6 – 2.5 m/hr. High velocities are due to Feature A* velocities.

Table 15 Breakthrough statistics for MAFIC simulations

realization #	t_5 (h)	t_{50} (h)	t_{95} (h)
5	8	22	82
6	4	12	42
7	2	7	38
8	2	8	38
9	4	18	54
median	4	12	42
measured*	7.2	36.8	86.3

* matrix diffusion was not modeled in MAFIC; however, matrix diffusion is affecting the measured data

3.5 One path model

After creating a DFN model with a rough fits to the drawdowns and breakthrough curves, attention turned to creating pipe models of the transport pathways. The simple shape of the PDT-4 breakthrough curve indicates a model with relatively few transport paths. Thus, we started with a single path LTG model to fit the PDT-4 Uranine breakthrough curve. A single path model generally matches t_5, t_{50}, and t_{95}, but does not match the trough between the two peaks of the breakthrough curve (Figure 19). A possible explanation for the lack of a trough is that the injection curve was not exactly as shown in Figure 18, but had a minor second spike as shown by the dotted line.

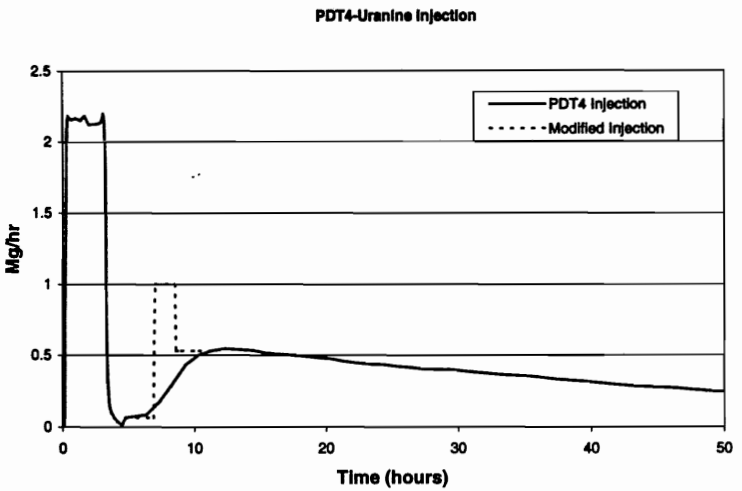

Figure 18 PDT Uranine injection. Dashed curve shows a modification of the measured injection that could explain breakthrough shape.

Table 16 PDT-4 fit parameters

	One Path	Two path model	
Parameter	Model	Path 1	Path 2
Aperture	0.004 m	0.002 m	0.005 m
Path Length	5.5 m	5.0 m	5.8 m
Path Width	2.75 m	90%x3.5 m	10% x 1.0 m
Dispersion	0.4 m	0.5 m	0.2 m
Porosity	0.1	0.015	0.015
Advective Velocity	0.8 m/hr	0.75 m/hr	0.4 m/hr
Transmissivity of A (from ΔH=9.3 m)	5.3×10^{-7} m^2/s	2.2×10^{-7} m^2/s	5.5×10^{-7} m^2/s
Dilution Rate	30 ml/hr		

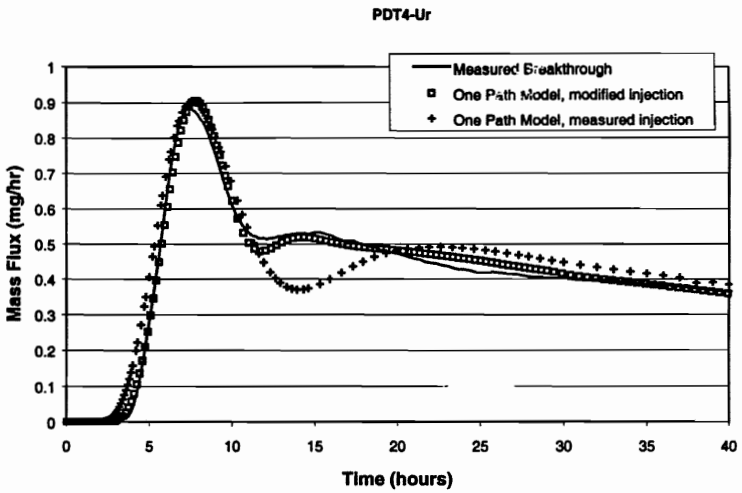

Figure 19 One path fits to PDT-4 Uranine breakthrough.

3.6 Two path model

The PDT-4 Uranine curve was also fit with a 2 pipe LTG pathway model was used. The parameters used for the two path LTG model of PDT-4 (Table 16) are similar to those used in STT-1 (Table 6). Figure 20 compares the LTG fit against the measured breakthrough curve. Although the two path model does not provide a significantly better fit than the one path model there are two reasons for continuing to use the two path model. First, the single path model has a high, possibly unrealistic, porosity compared to the two path curve. Second, in STT-1 it was found that the two path model provided better fits to the sorbing tracer breakthrough curves.

Table 17 LTG Uranine breakthroughs

	t5 measured	t50 measured	t95 measured
Measured	7.2 h	36.8 h	86.3 h
One Path LTG	7.5	42.0	165
Two Path LTG	7.5	34.3	86.3

Modelling of the sorbing tracer tests by using the Channel Network model.

B. Khademi & L. Moreno (SKB/KTH-KAT)

MODELLING OF THE SORBING TRACER TESTS

BY USING THE CHANNEL NETWORK MODEL

TASK 4E. Part II.

B. Khademi and L. Moreno

Department of Chemical Engineering and Technology
Royal Institute of Technology
Stockholm, Sweden

September 1998

ABSTRACT

The TRUE (Tracer Retention Understanding Experiments) experiment comprises a series of flow and transport experiments performed at different scales. The goal of these tracer tests is to give and develop a better understanding of radionuclide migration and retention in fractured rocks. In earlier experiments, the transport of non-sorbing tracers was studied. Task 4E comprises two sets of tracer tests with sorbing species. Here, predictions of the second set of tracer tests performed with sorbing tracer are reported. A tracer experiment with a non-sorbing species was used to re-calibrate the model. The Channel Network model, CHAN3D, was used to analyse these experiments.

1. INTRODUCTION

The first stage of the TRUE project at Äspö involved interference tests, dilution tests, flow loggings, pressure build-up tests and preliminary tracer tests. After this, the radially converging tracer test (RC-1) and a dipole experiment including four tests (DP 1-4) were performed. These experiments correspond to the Tasks 4C and 4D respectively. In order to test eventual changes in the hydraulic conditions several tracer tests with non-sorbing tracers were performed (RC-2, DP 5-6 and PDT 1-3) previous to the experiments with sorbing species.

The first set of experiments with sorbing tracers (STT1a) was performed with injection at KXTT4-3 and extraction at KXTT3-R2. Due to the low recovery of Cesium, the collection of the tracers was maintained for a longer time. It was then decided to perform a new experiment with sorbing tracers with injection at KXTT1-R2 and extraction at the section KXTT3-R2. Previous to the tests with sorbing tracers a tracer tests with a non-sorbing tracer (PDT 4) was carried out for calibration purposes.

This report presents the predictions of this second set of tests with sorbing tracers, STT1b.

2. MODEL CONCEPT

In the modelling of TRUE we have used the codes CHAN3D-flow and CHAN3D-transport, which both are based on the Channel Network model. First, the geometric information and boundary conditions were inserted to the flow model and the resulting flow distribution was then used in the transport model. A schematic picture of the features and the boreholes are shown in Figure 1.

2.2 The flow model

In the flow model, the tunnel with the niche, all the boreholes, the Feature A and the Feature B planes were included. The feature A was extended to the boundaries and the feature B fractures were treated as confined fracture planes. Regarding the boundary conditions, a given head was used on the top, on the bottom and on the right side of the rock block. No flow was assumed on the sides perpendicular to the tunnel. The head in the tunnel was taken as boundary condition on the left side, for the other region on this side, no flow condition was imposed. The withdrawal flow rate in the extraction section is also taken as a boundary condition. The conductance of the channels that connect the rock with the tunnel and the niche were reduced to simulate a skin effect. The size of the modelled rock volume was 30 x 30 x 40 meters in the direction longitudinal to the tunnel, the horizontal direction and the vertical direction respectively (Figure 1).

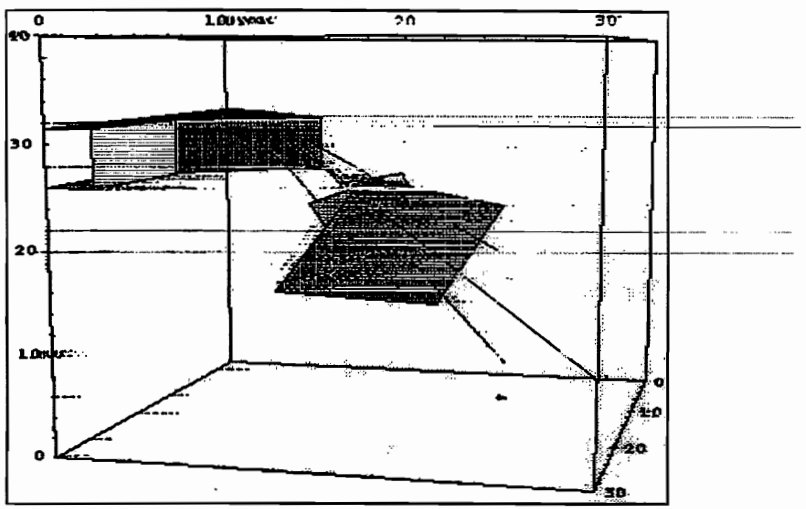

Figure 1. Feature A, the boreholes, the tunnel, and the niche. Behind feature A some of the feature B planes may be seen. For visualisation purposes the features are limited in extension. The feature A is extended to the borders of the model. The boreholes KXTT1, KXTT2, KXTT3, KXTT4 and KA3005A. are denoted as T1, T2, T3, T4 and K5, respectively.

The intersection points between Feature A and the boreholes were kept in the centre of the model to avoid the influence of the boundaries. The flow system was solved and the calculated flow field was used in the transport model. The mean transmissivity values for the different features were assigned from the experimental data. No conditioning of the transmissivity values around the intersection points was made.

2.3 The transport model

The transport in one channel member is by advection. Solute in the channel may diffuse into the rock matrix and be sorbed onto the microfissure surfaces. No hydrodynamic dispersion is assumed in the channel. The dispersion of the solute is caused by the heterogeneity of the flow field when the solute is transported with different velocities in different channels in the network. The volume of the channels was calculated assuming that the conductance of the channels is proportional to the cubed channel aperture. The value of the proportionality constant is determined by matching the volume of the channels with the desired flow porosity. The specific flow wetted surface was estimated to be 1.0 m^2/m^3. For channel lengths of 0.7 m the corresponding channel width is 0.25m.

3. DESCRIPTION OF THE EXPERIMENTS

3.1 Preliminary tracer tests.

In order to recalibrate the models, a tracer experiment was performed, PDT4. A radially converging geometry was used in this experiment with extraction at section KXTT3-R2 and injection of the tracer at KXTT1-R2. Experimental data are shown in Table 1.

Table 1. Experimental information for the tracer test PDT4.

	PDT-4
Injection section	KXTT1-R2
Tracer	Uranin
Extraction section	KXTT3-R2
Extraction rate, l/min	0.101
Sampling flow, ml/h	2.9
Inject-sect volume, l	1.56
Extract-sect volume, l	1.915
Cut-off, hrs	137.5

3.2 Sorbing tracer tests.

The tracer tests with sorbing species were carried out in a radially converging flow field. Two non-sorbing tracers, uranin and HTO, were also injected together with the sorbing species. The following weakly and intermediately sorbing tracers were used: Na^+, Rb^+, Sr^{2+}, K^+, and Co^{2+}. Sorption constants and effective diffusivities for the injected tracers are shown in Table 2.

As we discussed in a earlier report (Khademi et al. 1997), it was found that sorption and diffusion of some sorbing radionuclides (e.g., strontium and cesium) are higher at the fracture filling material and matrix close to the fracture. Since the travel times of these tracer experiments are rather long, the filling material and the rock matrix close to the fracture play an important role in the retardation of the tracers.

Table 2. Half-life, sorption constant and effective diffusivity for the tracer used in the tracer tests.

Species	K_d, m^3/kg	D_e, m^2/s	Increased by
Uranin	-	1.2E-13	1
HTO	-	1.2E-13	1
Na^+,	1.4E-06	6.7E-14	200
Rb^+	4.0E-04	1.0E-13	140
Sr^{2+}	4.7E-06	4.0E-14	580
K^+	2.0E-04	1.0E-13	1
Co^{2+}	3.2E-03	4.0E-14	1

In the first set of experiments, the sorbing species showed longer breakthrough times than the times predicted by using the diffusion and sorption values shown in Table 2. These differences were used to "calibrate" the values of diffusion and sorption. For the tracer tests with Na^+, Rb^+, and Sr^{2+} the values of the product K_dD_e were increased by a factor of 200, 140 and 580 respectively.

4. PREDICTION OF THE SORBING TRACER TESTS.

4.1. Steady-state drawdown

The steady-state drawdowns at the injection and extraction sections are shown in Table 3.

Table 3. The steady-state drawdown.

Section	S (5%), m	S (50%), m	S (95%), m
KXTT1-R2	2.99	3.38	3.77
KXTT2-R2	2.67	3.02	3.29
KXTT3-R2	8.62	11.42	16.57
KXTT4-R3	3.52	4.03	4.48
KA3005A-R3	2.20	2.44	2.7

4.2 Prediction of breakthrough curves

The breakthrough curves for a realisation are shown in Figure 1 and 2. Figure 1 shows the breakthrough concentration expressed as the fraction of the injected mass (activity) per unit time (hour). Figure 2 shows the cumulative curve for the mass (activity) arriving to the extraction section as a function of the injected mass (activity).

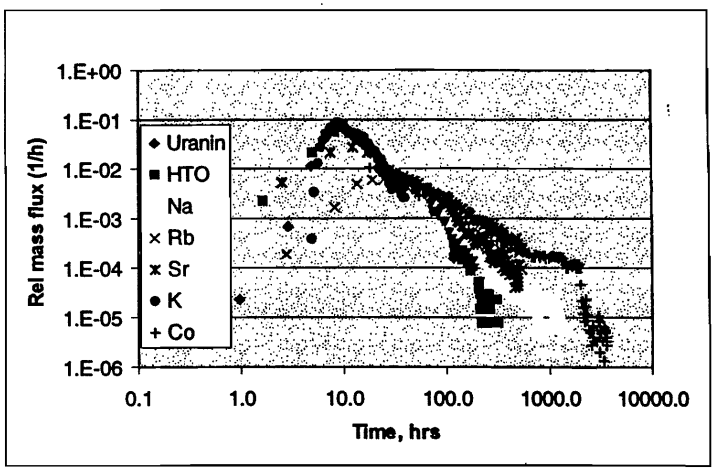

Figure 1 Mass flux into the extraction section for one realisation.

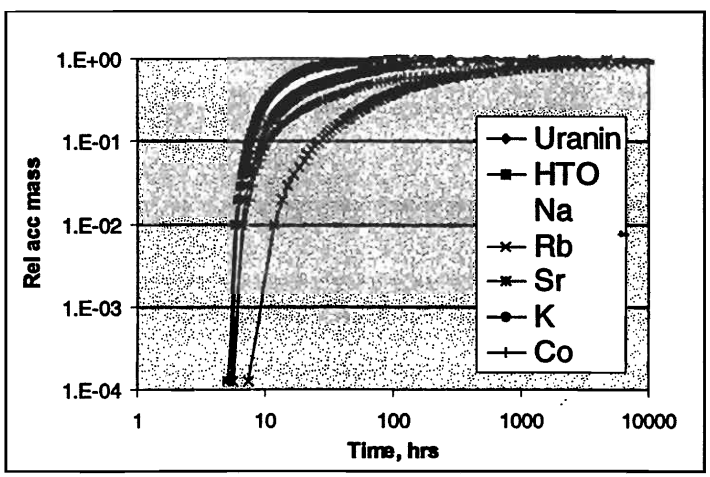

Figure 2 Cumulative mass arriving to the extraction section for one realisation. Curves for Rb, Ba and Cs are shown by using different type of lines.

4.2.2 Breakthrough times

The times to recover 5, 50 and 95 % of the injected mass are shown in Tables 4a, 4b and 4c, for the different tracers. The injections were carried out in the section KXTT1-R2 and the extraction at the section KXTT3-R2.

Table 4a Breakthrough times, T_5 [hr] of the injected tracer.

Tracer test	T_5(5%), hrs	T_5(50%), hrs	T_5(95%), hrs
STT1b-Uranin	4.0	7.1	10.3
STT1b-HTO	3.9	7.0	10.2
STT1b-Na	4.0	7.0	10.2
STT1b-Rb	4.2	7.6	12.0
STT1b-Sr	4.0	7.1	10.2
STT1b-K	4.0	7.1	10.7
STT1b-Co	5.0	8.9	16.1
New K_dD_e			
STT1b-Na	4.2	7.6	11.7
STT1b-Rb	7.2	20.6	51.0
STT1b-Sr	4.4	8.2	13.2

Table 4b Breakthrough times, T_{50} (median) [hr] of the injected tracer.

Tracer test	T_{50}(5%), hrs	T_{50}(50%), hrs	T_{50}(95%), hrs
STT1b-Uranin	9.6	15.7	24.8
STT1b-HTO	9.0	14.8	23.1
STT1b-Na	9.2	15.1	23.5
STT1b-Rb	11.6	22.2	38.4
STT1b-Sr	9.8	15.9	24.5
STT1b-K	8.2	14.5	24.9
STT1b-Co	46.9	75.0	138.5
New K_dD_e			
STT1b-Na	10.7	20.5	37.1
STT1b-Rb	56.2	217.7	-
STT1b-Sr	14.4	30.30	53.8

Table 4c Breakthrough times, T_{95} [hr] of the injected tracer.

Tracer test	T_{95}(5%), hrs	T_{95} (50%), hrs	T_{95} (95%), hrs
STT1b-Uranin	92.9	105.0	-
STT1b-HTO	78.2	90.6	-
STT1b-Na	77.7	89.4	-
STT1b-Rb	113.2	450.5	-
STT1b-Sr	95.6	110.5	-
STT1b-K	43.9	-	-
STT1b-Co	1755.4	1982.2	-
New K_dD_e			
STT1b-Na	123.8	405.6	-
STT1b-Rb	-	-	-
STT1b-Sr	249.8	-	-

4.2.2 Breakthrough times for a hypothetical pulse injection, Dirac pulse.

The times to recover 5, 50 and 95 % of the injected mass for a hypothetical pulse injection (Dirac pulse) are shown in Tables 5a, 5b and 5c, for the tracers used in the experiment. All the injections were carried out in the section KXTT1-R2 and the extraction at the section KXTT3-R2.

Table 5a Breakthrough curves, t_5 [hr] for pulse (Dirac) injection.

Tracer test	t_5(5%), hrs	t_5(50%), hrs	t_5(95%), hrs
STT1b-Uranin	2.5	5.4	7.7
STT1b-HTO	2.5	5.4	7.6
STT1b-Na	2.5	5.4	7.7
STT1b-Rb	2.6	5.6	8.8
STT1b-Sr	2.5	5.4	7.7
STT1b-K	2.5	5.6	8.5
STT1b-Co	2.6	5.8	9.9
New K_dD_e			
STT1b-Na	2.6	5.6	8.9
STT1b-Rb	4.3	13.7	40.7
STT1b-Sr	2.7	5.9	10.0

Table 5b Breakthrough curves, t_{50} [hr] for pulse (Dirac) injection.

Tracer test	t_{50}(5%), hrs	t_{50}(50%), hrs	t_{50}(95%), hrs
STT1b-Uranin	4.8	9.9	16.5
STT1b-HTO	4.8	9.9	16.5
STT1b-Na	4.8	9.9	16.7
STT1b-Rb	5.6	13.0	23.9
STT1b-Sr	4.8	10.0	16.7
STT1b-K	5.3	12.2	21.1
STT1b-Co	6.2	16.5	33.1
New K_dD_e			
STT1b-Na	5.4	13.0	23.7
STT1b-Rb	34.5	200.6	623.9
STT1b-Sr	6.3	16.9	33.7

Table 5c Breakthrough curves, t_{95} [hr] for pulse (Dirac) injection.

Tracer test	t_{95}(5%), hrs	t_{95}(50%), hrs	T_{95}(95%), hrs
STT1b-Uranin	16.3	29.6	-
STT1b-HTO	14.7	29.4	-
STT1b-Na	15.2	29.9	-
STT1b-Rb	68.9	428.7	-
STT1b-Sr	15.1	30.1	-
STT1b-K	38.7	-	-
STT1b-Co	181.9	1210.0	-
New K_dD_e			
STT1b-Na	70.0	379.7	-
STT1b-Rb	-	-	-
STT1b-Sr	213.7	-	-

4.2.4 Recovered mass

Table 5 shows the calculated recovered mass during the experiment. In the predictions, the recovered mass was calculated for the observation times shown in Table 5.

Table 5 Recovered mass as a fraction of the injected mass (activity).

Tracer test	Observation Time, hrs	Recov.(5%)	Recov.(50%)	Recov.(95%)
STT1b-Uranin	195	0.93	0.98	0.99
STT1b-HTO	333	0.93	0.99	0.99
STT1b-Na	1292	0.94	0.99	0.99
STT1b-Rb	553	0.89	0.96	0.98
STT1b-Sr	505	0.93	0.99	0.99
STT1b-K	39	0.71	0.86	0.95
STT1b-Co	3622	0.90	0.96	0.98
New K_dD_e				
STT1b-Na	1292	0.91	0.97	0.98
STT1b-Rb	553	0.48	0.66	0.84
STT1b-Sr	505	0.84	0.92	0.96

5. References

Khademi, B and L. Moreno, Modelling of the sorbing tracer tests by using the Channel Network model. Task 4E, Presented at the Task Force meeting at Kamaishi, Japan, November 11-13, 1997.

Numerical analysis with FEGM/FERM for TRUE-1 sorbing tracer tests.

Yasuharu Tanaka, Toshifumu Igarashi, Motoi Kawanishi
(CRIEPI)

NUMERICAL ANALYSIS WITH FEGM/FERM FOR TRUE-1 SORBING TRACER TESTS

Yasuharu Tanaka
Toshifumi Igarashi
Motoi Kawanishi

Abiko Research Laboratory,
Central Research Institute
of Electric Power Industry,
Abiko, Japan

September 1998

Keywords: numerical analysis, tracer test, fracture, sorption, dispersion, radionuclide, pumping, transmissivity, drawdown

1. Introduction

In this study, we performed numerical analyses for STT-1b by using our developed groundwater and transport models, FEGM/FERM. Before the analyses for STT-1b, we calibrated our model of Feature A on basis of the data of the previous tracer tests. First the spatial distribution of transmissivity in Feature A was estimated by kriging from drawdowns observed in the previous tracer tests. Secondly the average hydraulic gradient under the natural condition was estimated from the hydraulic heads observed prior to start of PDT-3 in order to determine the hydraulic boundary conditions. Thirdly the fluid flux through the tracer injection sections were estimated from the tracer concentration curves in the sections in order to calculate the mass flux of the tracers injected into Feature A. Fourthly simulations of the tracer migration were performed for PDT-3 and PDT-4 so that the aperture of Feature A and the longitudinal dispersivity were estimated through the simulations by try and error. Furthermore simulations of the tracer migration were performed for STT-1 and the surface related sorption coefficients were identified through the simulations. Finally simulations for STT-1b were performed by using the above mentioned conditions.

2 SIMULATION METHOD

2.1 NUMERICAL MODEL

We applied the groundwater and transport models, FEGM/FERM (Igarashi *et al.*, 1994 and Kawanishi *et al.*, 1987), to this analysis.

The governing equation for groundwater flow is expressed as follows;

$$\frac{\partial}{\partial x_i}\left(T\frac{\partial h}{\partial x_i}\right)+Q=0 \qquad 2\text{-}1$$

where T is the transmissivity, h the hydraulic head and Q the sink or source of the fluid.

In this study, we consider only surface sorption about sorption phenomena and do not consider decay of the radioactive tracers. Therefore the governing equation for solute migration is expressed as follows;

$$b\left(1+\frac{2K_a}{b}\right)\frac{\partial C}{\partial t}+\frac{\partial V_i C}{\partial x_i}-\frac{\partial}{\partial x_i}\left(D_{ij}\frac{\partial C}{\partial x_j}\right)-M=0 \qquad 2\text{-}2$$

where b is the fracture aperture, K_a the surface related sorption coefficient, C the concentration of the solute, V_i the component of the darcian velocity in the direction x_i and M the sink or source of the solute. And D_{ij} is the tensor of dispersion coefficient of which the ij-th component is expressed as follows;

$$D_{ij}=\alpha_T\frac{|V|}{b}\delta_{ij}+(\alpha_L-\alpha_T)\frac{V_iV_j}{b|V|} \qquad 2\text{-}3$$

where α_T is the longitudinal dispersivity, α_L the transverse one, δ_{ij} Kronecker delta and V the darcian velocity vector.

2.2 MODELING OF FEATURE A

In this study, groundwater and the tracers were assumed to move only in Feature A. Matrix diffusion was not taken into consideration. Therefore Feature A was modeled as a single flat square of which the length of the side was 30 meters. Figure 2-1 shows the finite element mesh used in the analysis. All the elements are quadrilateral. The total numbers of elements and nodes are 3,855 and 3,955 respectively. The boreholes were expressed as cavities.

The hydraulic heads were fixed on the surrounding boundaries of the model and no flux of the tracers were assumed to cross the boundaries. The time-varying mass flux of the tracers was prescribed at the injection boreholes.

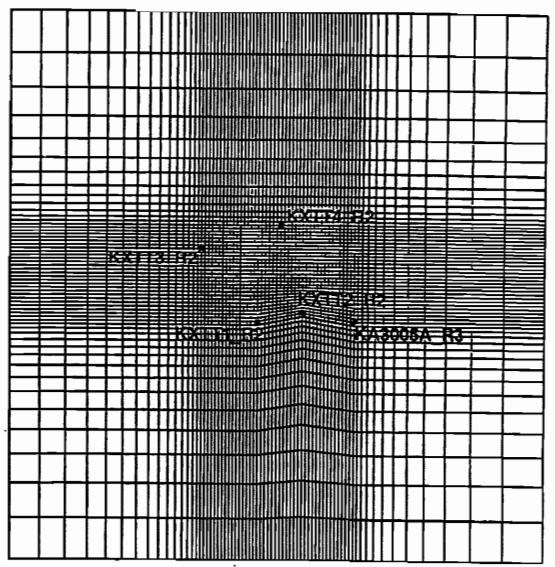

30m×30m
3,855 elements 3,955 nodes

Figure 2-1. Finite element mesh for the numerical analysis.

2.3 TRANSMISSIVITY IN FEATURE A

Transimissivities in Feature A were assumed to show a normal distribution in the logarithmic scale and to be distributed spatially with correlation. The spatial distribution of the transmissivity in Feature A was estimated by kriging on the basis of the transmissivities at the five borehole sections.

By kriging method, the estimation at the point x, T^*, can be obtained as the linear sum of the values at the measurement point x_i, T_i (de Marsily, 1986).

$$T^*(x)=\sum_{i=1}^{n}\lambda^i(x)\cdot T_i \qquad 2\text{-}4$$

where n is the number of the measurement points and $\lambda_i(x)$ the weights of the kriging estimator. The following condition is required in order to have an unbiased estimator.

$$\sum_i \lambda^i(x)=1 \qquad 2\text{-}5$$

And the errors of estimation must be minimal so that the estimator is optimal.

$$E\left[\{T^*(x)-T(x)\}^2\right] \text{ minimum} \qquad 2\text{-}6$$

where E represents the expectation of the value in parenthesis. The values of $\lambda_i(x)$ which satisfy the conditions 2-5 and 2-6 can be obtained by solving the following simultaneous equations.

$$\begin{aligned}&\sum_j \lambda^j(x)\gamma(x_i-x_j)+\mu=\gamma(x_i-x_0) \quad i=1,\cdots,n\\&\sum_i \lambda^i(x)=1\end{aligned} \qquad 2\text{-}7$$

where μ is an unknown, called a Lagrange multiplier. And γ is the variogram defined by the following equation.

$$\gamma(h)=\frac{1}{2}\mathrm{var}[Y(x+h)-Y(x)] \qquad 2\text{-}8$$

where var represents the variance of the value in parenthesis. In this study, the following exponential model was used to express variogram.

$$\gamma(h)=\sigma^2\cdot\left\{1-exp\left(-\frac{h}{a}\right)\right\} \qquad 2\text{-}9$$

where σ^2 is the variance of the logarithmic transmissivity, h the distance and a the correlation length.

3 CALIBRATION OF MODEL

3.1 TRANSMISSIVITY IN FEATURE A

The transmissivities at all the borehole sections except for KA3005A R3 were identified so that the sum of the squares of normalized errors between the calculated drawdowns and the observed ones, S_d, would be minimal.

$$S_d = \sum_{i=1}^{17} \left(\frac{\Delta h^i_{cal} - \Delta h^i_{obs}}{\Delta h^i_{obs}} \right)^2 \qquad 3\text{-}1$$

where Δh^i_{obs} is the i-th observed drawdown at the withdrawal or injection section. And Δh^i_{cal} is the i-th drawdown calculated by using the spatial distribution of transimissivity in Feature A which is estimated by kriging on basis of the transmissivities at the five borehole sections. In the kriging estimation, the correlation length was assumed to be 1 meter and the value determined from the flow- and pressure build-up test (Winberg, 1996) was used as the transmissivity at KA3005A R3. The identified transmissivities are given in Table 3-1. And Figure 3-1 shows the spatial distribution of transmissivity in Feature A estimated on basis of the identified section transmissivities. The drawdowns calculated by using the estimated transmissivity distribution are given in Table 3-2. In this study, we used this estimated transmissivity distribution as the spatial distribution of transmissivity in Feature A.

3.2 HYDRAULIC BOUNDARY CONDITION

The hydraulic heads were fixed on the surrounding boundaries of the model as mentioned in 2.2. The hydraulic heads on the boundaries were identified so that the sum of the squares of normalized errors between the calculated heads and the observed ones at the five borehole sections under the natural condition, S_h, would be minimal.

$$S_h = \sum_{i=1}^{5} \left(\frac{h^i_{cal} - h^i_{obs}}{h^i_{obs}} \right)^2 \qquad 3\text{-}2$$

where h^i_{obs} is the observed hydraulic head at the i-th section under the natural condition and h^i_{cal} the calculated one. The identified parameters were the hydraulic head at the point A, h_A, the magnitude of the average hydraulic gradient, I, and the angle between the direction of the average hydraulic gradient and the side AB, θ, *see* Figure 3-2. Table 3-3 gives the identified values of these parameters for the hydraulic head prior to start of PDT-3.

3.3 MASS FLUX AT INJECTION SECTION

The fluid flux through the tracer injection section, Q_{bh}, is obtained theoretically by the following equation (Winberg, 1996 and Andersson, 1996).

$$Q_{bh} = -\frac{V}{t} ln(C/C_0) - Q_{sam} \qquad 3\text{-}3$$

where V is the volume of the tracer injection section, t the elapsed time, C_0 the initial concentration of the tracer in the injection section, C the concentration at the time t and Q_{sam} the sampling flow rate. Figure 3-3 to 3-6 show the measured concentration of Uranine at the injection section during each tracer test and the straight lines for approximation. Table 3-4 shows the fluid flux through the injection section estimated by using the equation 3-3 from the slope of the straight lines. In this calculation, the borehole volume of KXTT4 R3 was supposed to be 2154 ml (Andersson et al., 1998). The fluid flux was not constant. The natural hydraulic gradient probably changed. The fluid flux for Uranine were used for the calculation of the mass flux injected into Feature A.

The product of the tracer concentration and the fluid flux was used as the mass flux of the tracer injected into Feature A for the tracer migration analysis of each tracer test.

3.4 APERTURE AND DISPERSIVITY

Simulations for the migration of Uranine in Feature A were performed for PDT-3 and PDT-4 on basis of the above-mentioned conditions. The aperture of Feature A, b, and the longitudinal dispersivity, α_L, along the travel path in each tracer test were estimated through the simulation. The ratio of longitudinal dispersivity to transverse one was fixed at 10:1 in the simulations.

The best-fit run for each test is shown in Figure 3-7 and 3-8 respectively. The identified aperture of Feature A and the longitudinal dispersivity are shown in Table 3-5. The calculated breakthrough curve agreed approximately with the measured one. The following factors are considered to cause the slight difference between the calculated result and the experimental one. First the concentration values measured in the injection section in the early stage of the experiment were not accurate due to delay and dispersion in the sampling line (Andersson, 1996). Accordingly the

input tracer flux in the early stage used in the simulation might be different from the one in the experiment. Secondly the natural hydraulic gradient was estimated on basis of the hydraulic heads at only five borehole sections. So the hydraulic boundary condition used in the simulation might be different from the one in the experiment. Thirdly the transmissivities at the five borehole sections were identified so that they would satisfy the drawdowns observed in all the tracer tests properly at the same time. Consequently the calculated drawdowns did not exactly agree with all the observed ones, see Table 3-2.

3.5 SORPTION COEFFICIENT

Simulations for the tracer migration in Feature A were performed for STT-1 on basis of the above-mentioned conditions. Only surface sorption was considered about sorption phenomena. The surface related sorption coefficients of Na-22, Sr-85 and Rb-86 were identified through the simulations.

Figure 3-9 and 3-10 show the simulated results for Uranine and HTO. Figure 3-11 to 3-13 show the results of the best-fit runs for Na, Sr and Rb. The identified values of the sorption coefficient are shown in Table 3-6. The calculated maximum concentration is larger than the measured one. And in the tail part the calculated concentration decreases more speedily than the measured one. Such tendency becomes remarkable with increasing sorption coefficient. It might be impossible to model the retardation of Na, Sr and Rb only by surface sorption.

Table 3-1. Transmissivities at borehole sections identified on basis of drawdowns at borehole sections during tracer tests.

Borehole Section	Transmissivity (m^2/s)
KXTT1 R2	9.58×10^{-9}
KXTT2 R2	3.90×10^{-9}
KXTT3 R2	6.30×10^{-2}
KXTT4 R3	2.29×10^{-8}
KA3005A R3	$4.20\times10^{-8*}$

* Not identified but determined from flow- and pressure build-up tests

Table 3-2. Drawdowns at injection and withdrawal sections calculated by using the estimated spatial distribution of transmissivity in Feature A.

Test#	Injection section		Withdrawal section	
	Observed	Calculated	Observed	Calculated
RC-1			3.1	2.72
DP-1	-4.6	-6.01	1.2	1.31
DP-2	-18	-15.4	40	25.9
DP-3	-5	-5.32	44.5	26.0
DP-4	-15	-15.6	11	12.1
DP-5	-2	-2.06	1.1	1.30
DP-6	-0.8	-0.70	3.2	2.67
RC-2			27	32.3
PDT-1			1.3	1.37
PDT-2			3.1	2.73
PDT-3			8.2	5.45

Unit:mH_2O

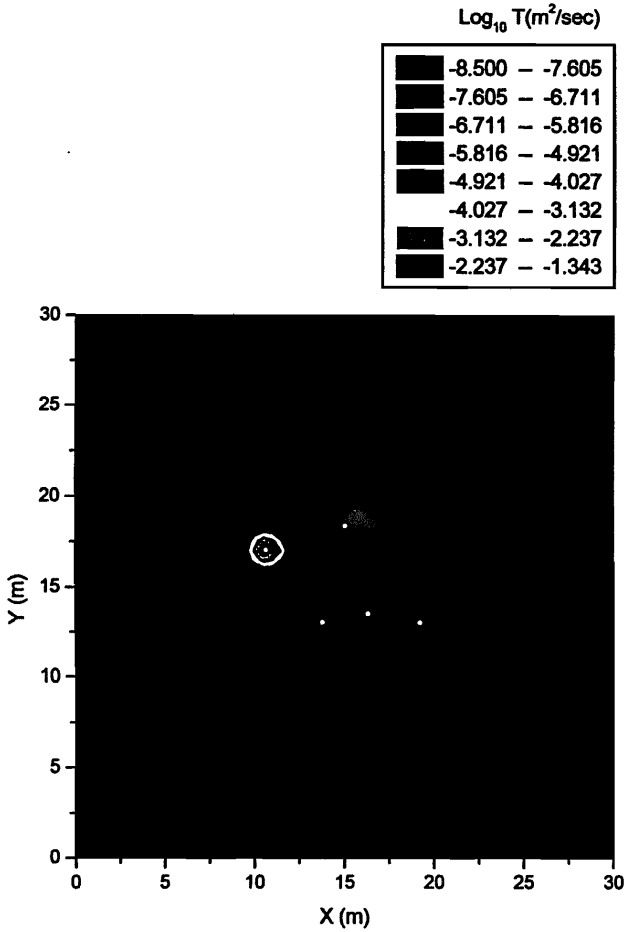

Figure 3-1. Spatial distribution of logarithmic transmissivitiy in Feature A estimated by kriging on basis of the identified transmissivities at the five borehole sections. (KXTT1 R2:(X,Y)=(13.78, 13.04), KXTT2 R2:(16.32, 13.53), KXTT3 R2:(10.63, 17.04), KXTT4 R3:(15.06, 18.35), KA3005A R3:(19.22, 13.03))

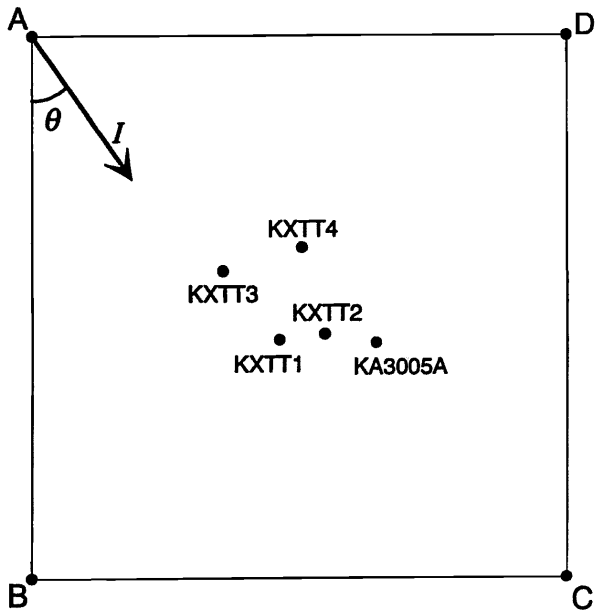

Figure 3-2. Schematic diagram for parameters defining hydraulic boundary conditions.

Table 3-3. Identified values of parameters for natural hydraulic head prior to start of the Preliminary Design Test, PDT-3.

Parameters	Identified value
Hydraulic head, h_A	-51.7mH_2O
Magnitude of hydraulic gradient, I	0.125
Direction of hydraulic gradient, θ	57.6°

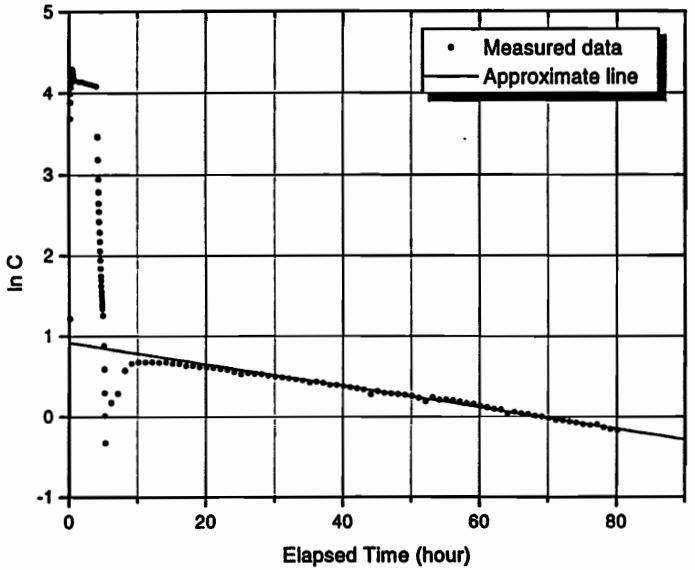

Figure 3-3. Injected concentration of Uranine (ln C) in KXTT4 R3 during PDT-3.

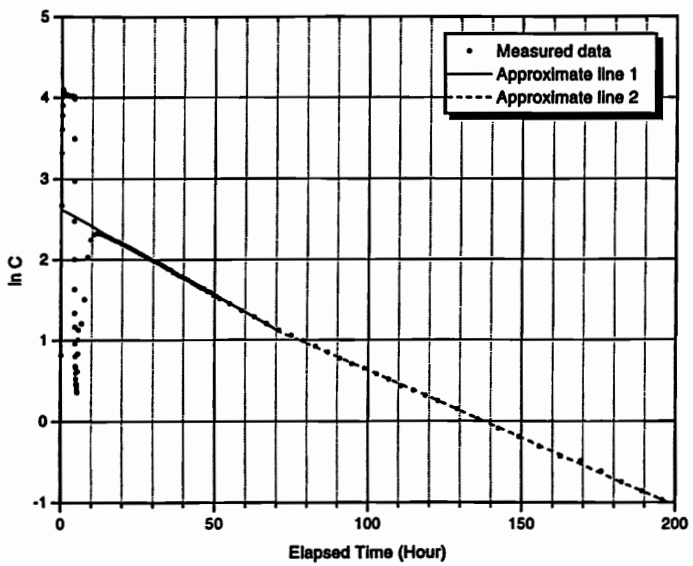

Figure 3-4. Injected concentration of Uranine (ln C) in KXTT4 R3 during STT-1.

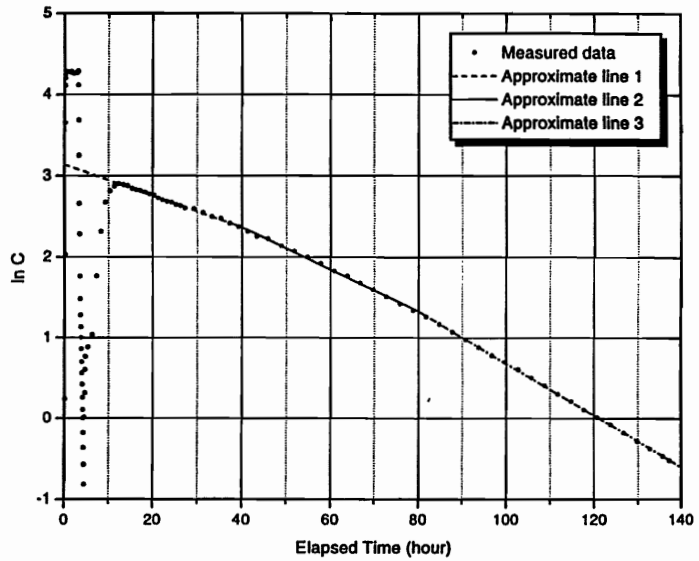

Figure 3-5. Injected concentration of Uranine (ln C) in KXTT1 R2 during PDT-4.

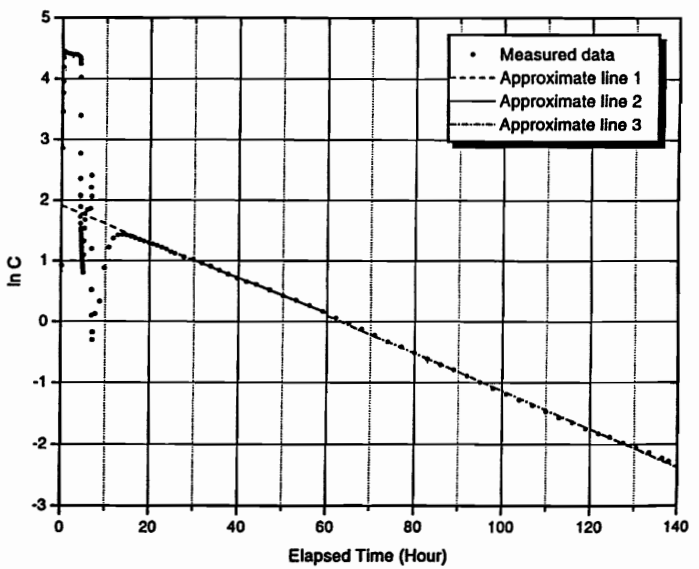

Figure 3-6. Injected concentration of Uranine (ln C) in KXTT1 R2 during STT-1b.

Table 3-4. Fluid flux through the tracer injection section during PDT-3, PDT-4, STT-1 and STT-1b estimated from the dilution of Uranine and HTO.

Test#	Inj. section	Tracer	Elapsed time (h)	Fluid flux (ml/min)
PDT-3	KXTT4 R3	Uranine	40-80	0.430
STT-1	KXTT4 R3	Uranine	20-70	0.720
			70-200	0.550
		HTO	20-70	0.698
			70-200	0.544
PDT-4	KXTT1 R2	Uranine	20-40	0.449
			40-80	0.624
			80-140	0.792
STT-1b	KXTT1 R2	Uranine	20-30	0.752
			30-60	0.701
			60-140	0.754
		HTO	20-30	0.701
			30-60	0.739
			60-140	0.813

Table 3-5. Aperture of Feature A, b, and longitudinal dispersivity, α_L, between KXTT3 R2 and KXTT4 R3 or KXTT1 R2 identified through simulations for PDT-3 and PDT-4.

Test#	Injection section	Withdrawal section	b (mm)	α_L (m)
PDT-3	KXTT4 R3	KXTT3 R2	0.51	1.0
PDT-4	KXTT1 R2	KXTT3 R2	0.328	0.215

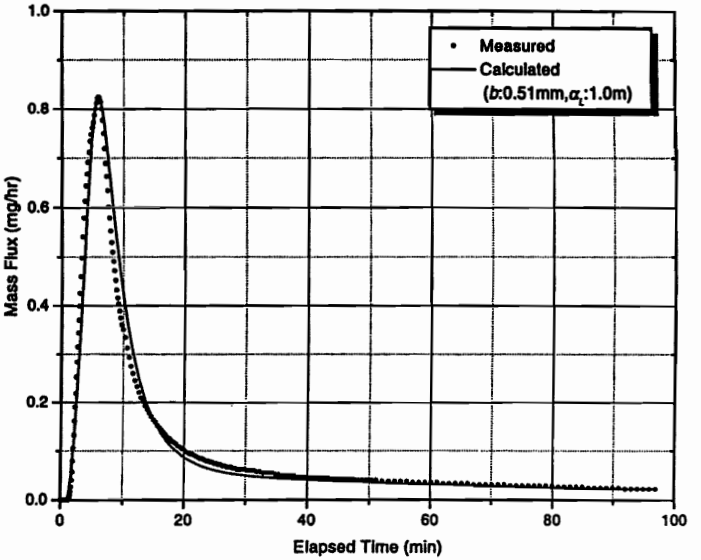

Figure 3-7. Measured breakthrough curve of Uranine in pumping section during PDT-3 and result of the best-fit run.

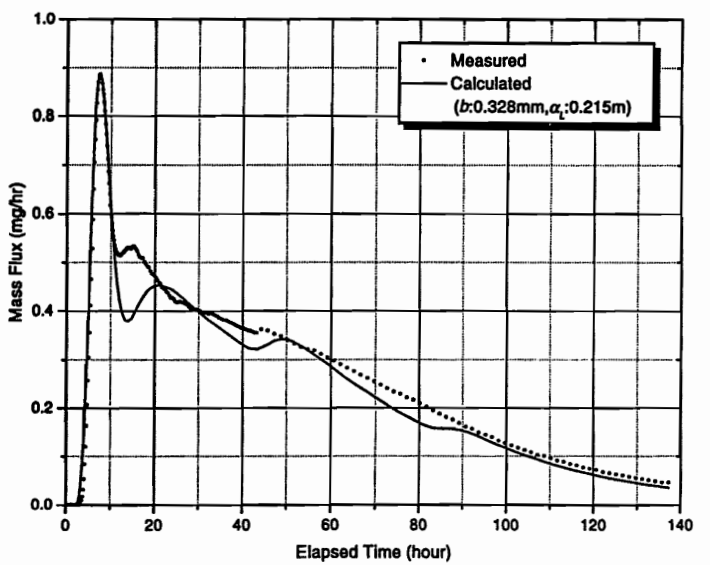

Figure 3-8. Measured breakthrough curve of Uranine in pumping section during PDT-4 and result of the best-fit run.

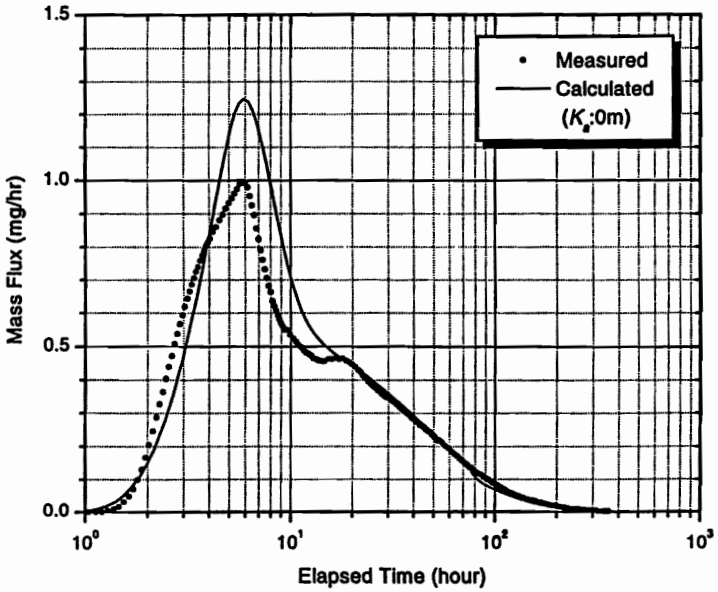

Figure 3-9. Measured and simulated breakthrough curves of Uranine in pumping section during STT-1.

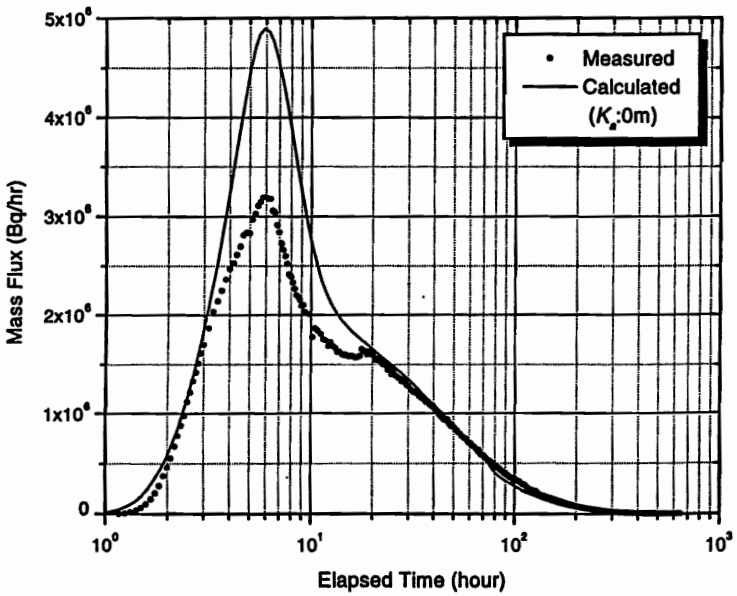

Figure 3-10. Measured and simulated breakthrough curves of HTO in pumping section during STT-1.

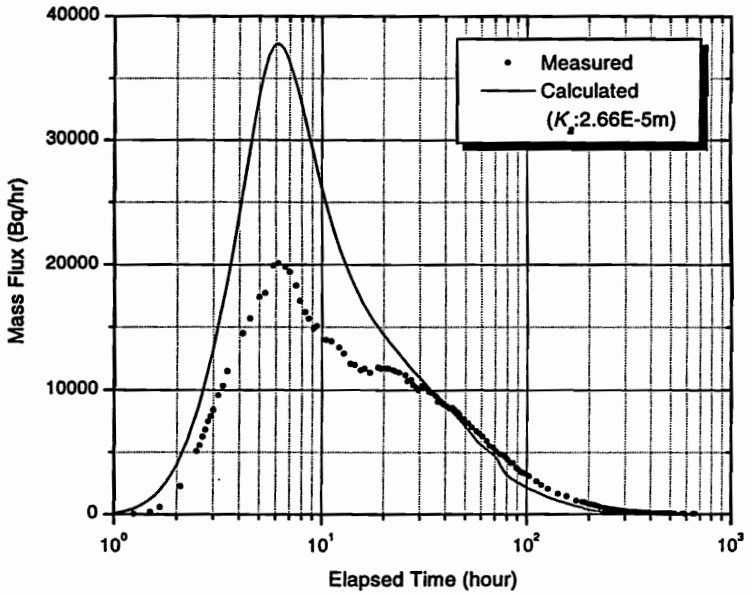

Figure 3-11. Measured breakthrough curve of Na-22 in pumping section during STT-1 and result of the best-fit run.

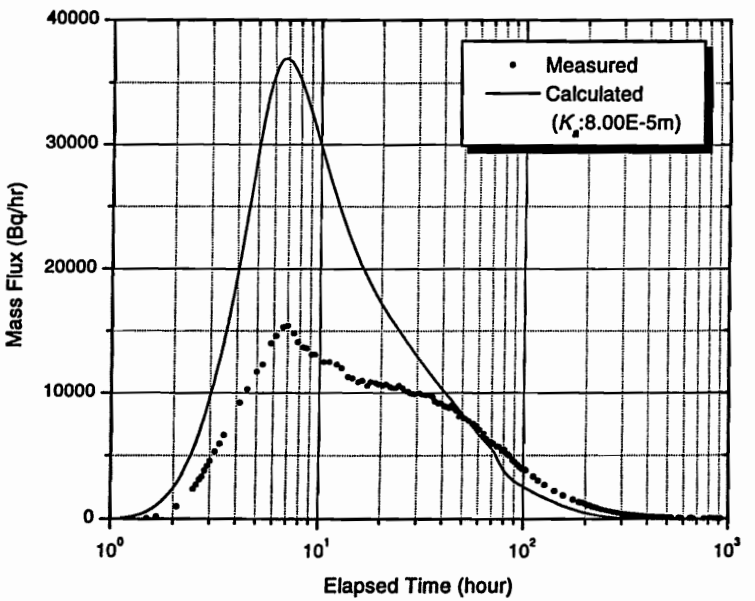

Figure 3-12. Measured breakthrough curve of Sr-85 in pumping section during STT-1 and result of the best-fit run.

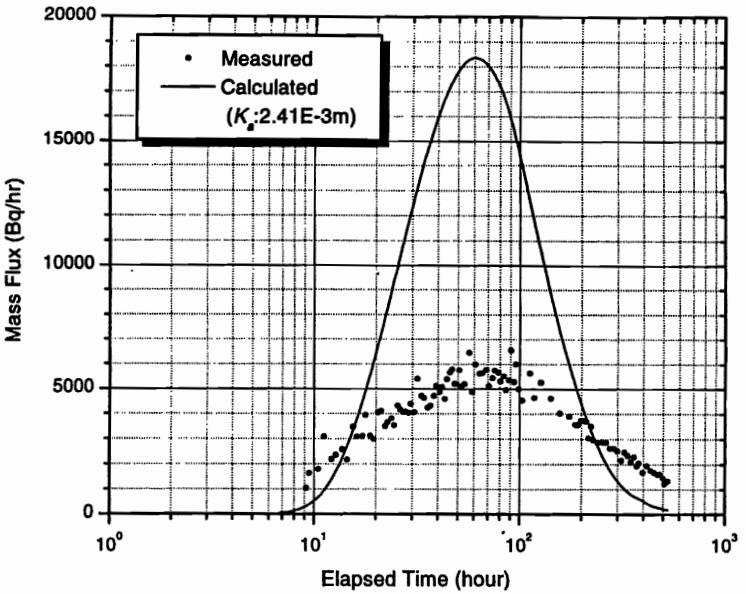

Figure 3-13. Measured breakthrough curve of RB-86 in pumping section during STT-1 and result of the best-fit run.

Table 3-6. Surface related sorption coefficients identified through simulations for STT-1.

Tracer	K_a (m)
Na-22	2.66E-5
Sr-85	8.00E-5
Rb-86	2.41E-3

4 SIMULATED RESULTS

Simulations were performed for STT-1b. Firstly, the drawdown in Feature A was calculated. The transmissivity distribution shown in Figure 3-1 was used in the calculation. The parameter values for the natural hydraulic head were assumed to be identical to the ones given in Table 3-3. The calculated drawdowns at the five boreholes are shown in Table 4-1.

Secondly the tracer migration in Feature A was simulated for the pulse input. The values for PDT-4 in Table 3-5 were used as the aperture of Feature A and the longitudinal dispersivity. The surface related sorption coefficients were assumed to be identical to the ones in Table 3-5. Figure 4-1 and 4-2 show the mass flux and the cumulative mass flux in the pumping section respectively. These figures are normalized to the injected mass. Table 4-2 gives the tracer travel times, t_5, t_{50} and t_{95}, defined as times when 5, 50 and 95 % of the recovered mass respectively had arrived. And Table 4-3 gives the tracer recoveries. The mass recoveries were 100 % at the ending time of simulation for all the tracers. The breakthrough curve of Uranine is the same as the one of HTO because both tracers are not adsorbed on Feature A and the same input condition, pulse input, was used. The maximum concentration becomes small with increasing sorption coefficient.

Finally the tracer migration in Feature A was simulated for the measured input. The products of the tracer concentration in the injection section and the fluid flux for Uranine in Table 3-4 were used as the mass flux of the tracers injected into Feature A. Figure 4-3 and 4-4 show the normalized mass flux and the normalized cumulative mass flux respectively. Table 4-4 and 4-5 give the tracer travel times and the tracer recoveries. The mass recoveries were almost 100 % at the ending time of simulation for all the tracers.

Table 4-1. Calculated drawdons at five boreholes during STT-1b.

Borehole Section	Drawdown (mH_2O)
KXTT1 R2	3.519
KXTT2 R2	2.316
KXTT3 R2	5.432
KXTT4 R3	3.658
KA3005A R3	3.658

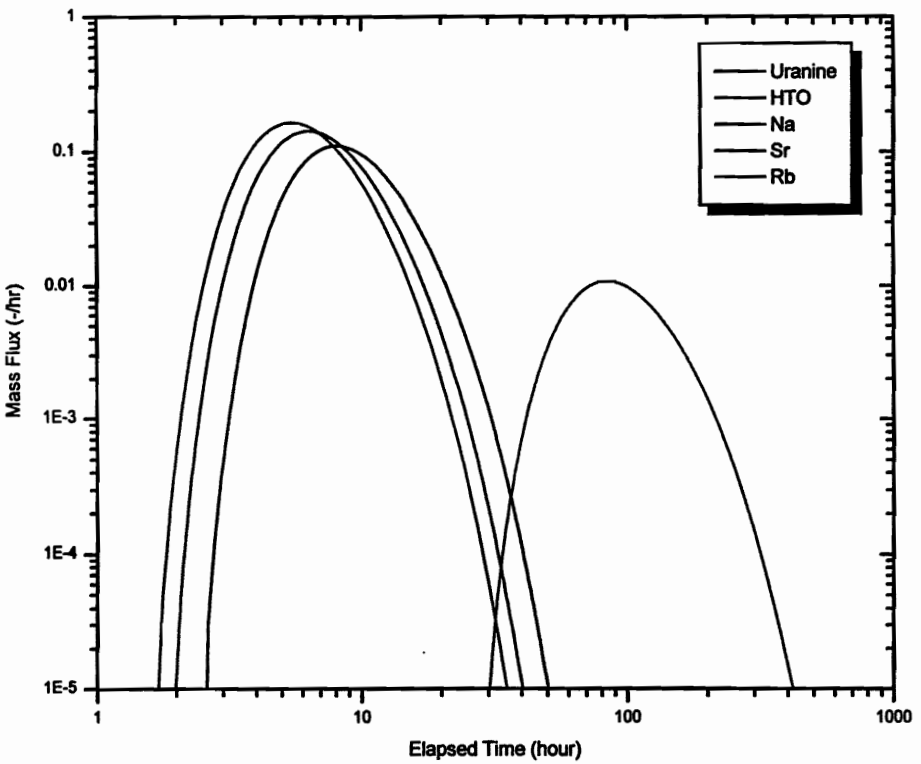

Figure 4-1. Calculated tracer breakthrough curves in pumping section during STT-1b. Y-axis on the right is for Uranine and Y-axis of the left is for radionuclides.

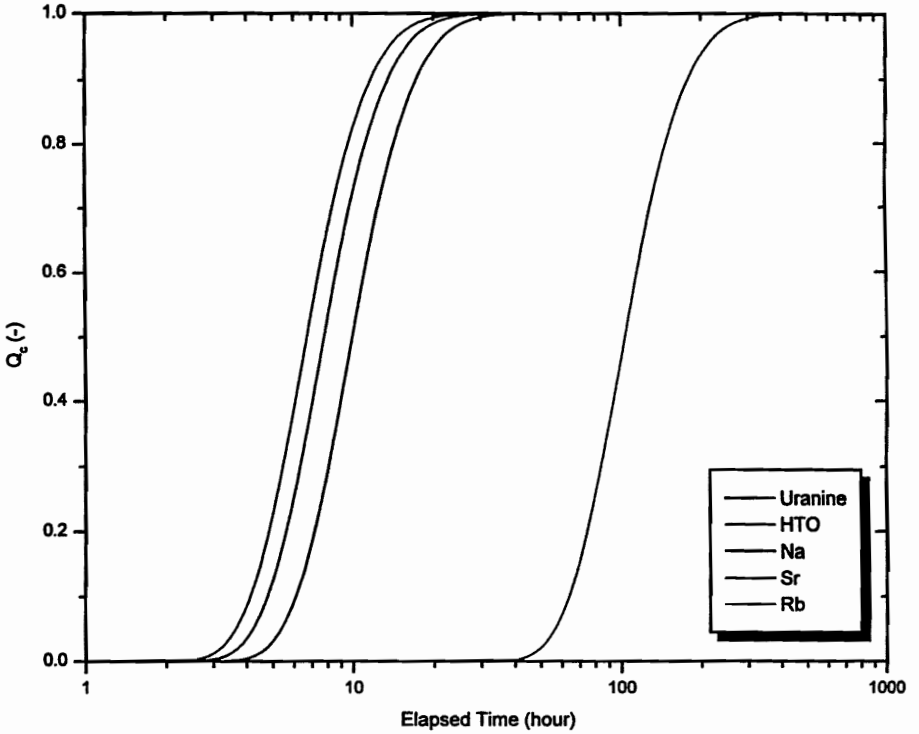

Figure 4-2. Normalized cumulative mass flux in pumping section for pulse input of STT-1b.

Table 4-2. Calculated tracer travel times for pulse input of STT-1b.

Tracer	t_5	t_{50}	t_{95}
Uranine	3.64	6.72	13.70
HTO	3.64	6.72	13.70
Na-22	4.21	7.80	15.88
Sr-85	5.38	9.95	20.24
Rb-86	56.28	103.05	209.45

Unit : hour

Table 4-3. Calculated tracer recoveries at the time, t_r, for pulse input of STT-1b. t_r represents the time of termination of monitoring.

Tracer	t_r (hour)	Recovery (%)
Uranine	195	100
HTO	333	100
Na-22	1292	100
Sr-85	505	100
Rb-86	553	100

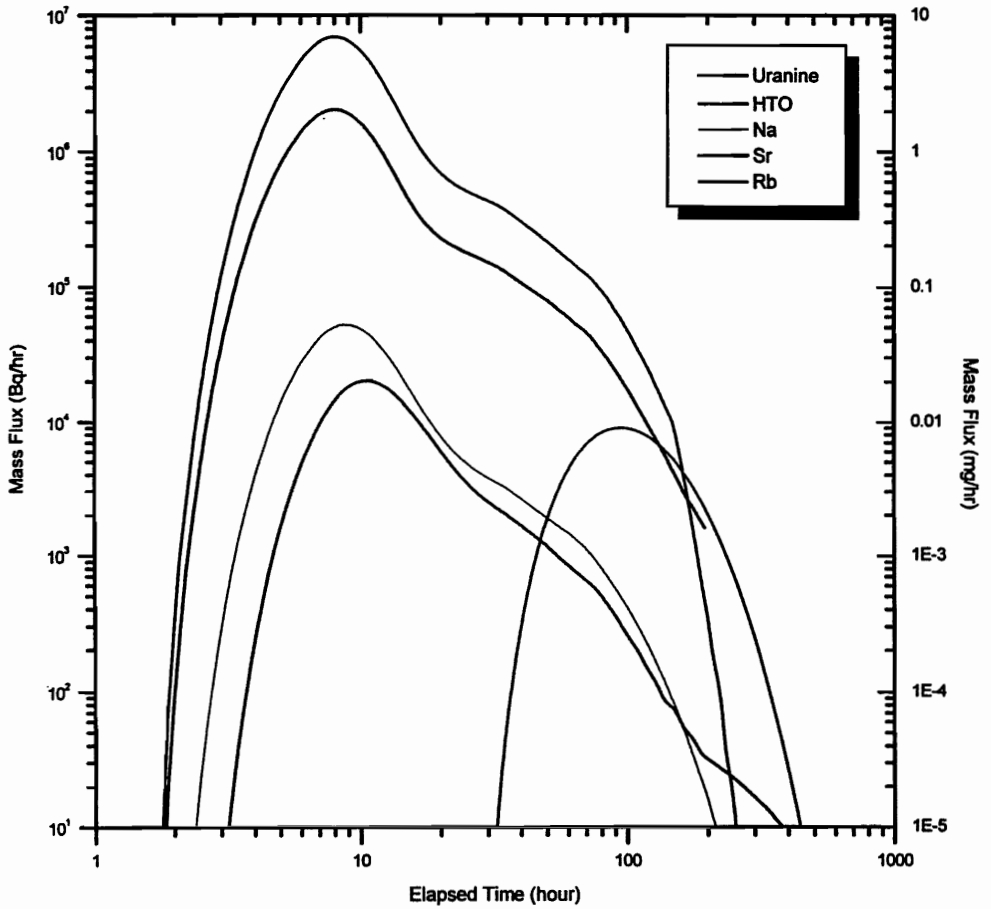

Figure 4-3. Calculated tracer breakthrough curves in pumping section for measured input of STT-1b. Y-axis on the right is for Uranine and Y-axis of the left is for radionuclides.

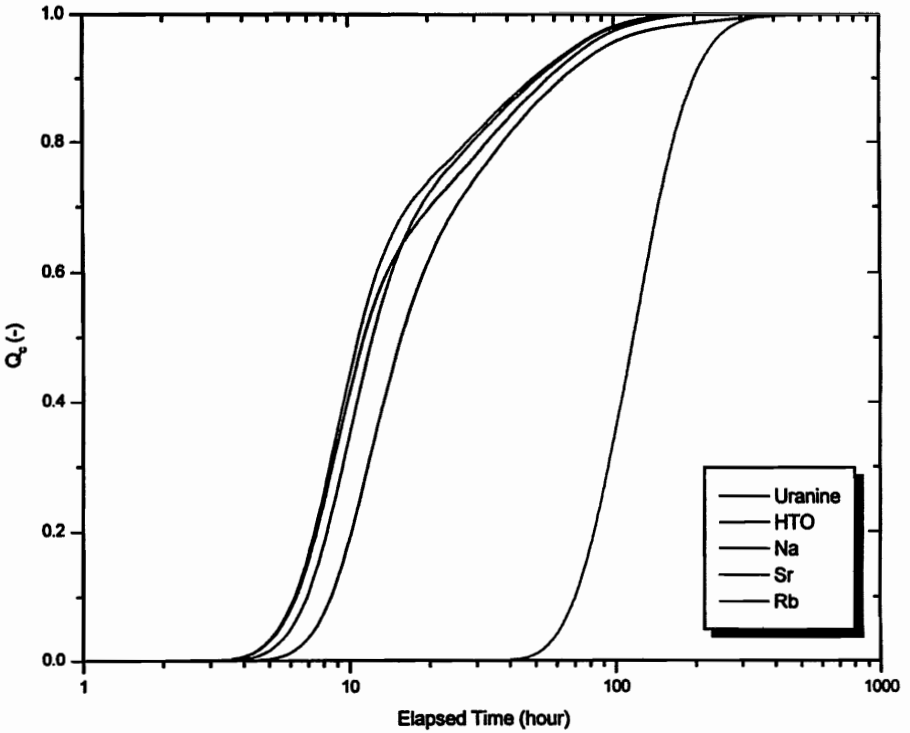

Figure 4-4. Normalized cumulative mass flux in pumping section for measured input of STT-1b.

Table 4-4. Calculated tracer travel times for measured input of STT-1b.

Tracer	t_5	t_{50}	t_{95}
Uranine	5.46	11.32	79.13
HTO	5.40	10.79	71.86
Na-22	6.01	12.20	73.45
Sr-85	7.43	15.64	93.37
Rb-86	61.79	116.40	232.07

Unit : hour

Table 4-5. Calculated tracer recoveries at the time, t_r for measured input of STT-1b. t_r represents the time of termination of monitoring.

Tracer	t_r (hour)	Recovery (%)
Uranine	195	99.95
HTO	333	100
Na-22	1292	99.99
Sr-85	505	99.99
Rb-86	553	100

REFERENCES

Igarashi T, Tanaka Y, Kawanishi M, 1994. Application of three-dimensional smeared fracture model to the groundwater flow and the solute migration of LPT-2 experiment. SKB International Cooperation Report ICR 94-08.

Kawanishi M, Igarashi T, Mahara Y, Komada H, Maki Y, 1987. Computer models for safety assessment on land disposal of low-level wastes. Waste Management '87, 3, Tucson, Arizona, pp. 175-180.

de Marsily G, 1986. Quantitative Hydrogeology. Academic Press, INC..

Winberg A, 1996. Descriptive structural-hydraulic models on block and detailed scales of the TRUE-1 site. SKB International Cooperation Report ICR 94-08.

Andersson P, 1996, TRUE 1st stage tracer test program. Experimental data and preliminary evaluation of the TRUE-1 radially converging tracer test (RC-1). Äspö Hard Rock Laboratory Progress Report HRL-96-24.

Andersson P, Nordqvist R, Jönsson S, 1997. TRUE 1st stage tracer test program. Experimental data and preliminary evaluation of the TRUE-1 dipole tracer tests (DP-1 – DP-4). Äspö Hard Rock Laboratory Progress Report HRL-97-13.

Andersson P, Byegård J, Cvetkovic V, Johansson H, Nordqvist R, Selroos J, Winberg A, 1997. TRUE 1st stage tracer test program. Experimental plan for tests with sorbing tracers at the TRUE-1 site. Äspö Hard Rock Laboratory Progress Report HRL-97-07.

Andersson P, Johansson H, Nordqvist R, Skarnemark G, Skålberg M, Wass E, 1998. TRUE 1st stage tracer test program. Tracer tests with sorbing tracers, STT-1. Experimental description and preliminary evaluation.

Predictions of the sorbing tracer test STT1b of the TRUE.

Antii Poteri (POSIVA)

PREDICTIONS OF THE SORBING TRACER TEST STT1B OF THE TRUE 4E

Antti Poteri
VTT ENERGY

August 1998

Supported by POSIVA Oy

TABLE OF CONTENTS

1 INTRODUCTION

This memorandum summaries the modelling work to predict the breakthrough curves of the sorbing tracers in the Task 4E II (STT1B test) of the first phase of the TRUE program.

The STT1B test is a continuation of the earlier STT1 test. The pumping borehole and the pumping rate were maintained from the STT1. This means that the flow field should be exactly the same as in the STT1 assuming that the surrounding environment of the test site stays in the same state. The injection borehole in the STT1B was the KXTT1 instead of the KXTT4 applied in the STT1 test. This means that instead of the about 4.6 meters migration distance in the STT1 test there is about 5 metres migration distance in the STT1B test.

2 Modelling approach

2.1 Conceptual model

All the tracer tests of the Task 4 have been performed in the feature A. The characterization of the feature A also shows rather planar nature of the of the feature (Winberg, 1996). In this study the basic assumption have been that the feature A can be modelled as a two dimensional plane of varying transmissivity and that the migration of the tracers between the injection and extraction sections takes place only in the feature A. The transmissivity field on the fracture plane is assumed to be isotropic.

The processes modelled are the advection due to the flow field, dispersion, matrix diffusion and sorption. The approach is semianalytical. Matrix diffusion and sorption are modelled by applying analytical solution of the one dimensional matrix diffusion equation (Hautojärvi, 1989). The advective flow field was calculated numerically.

2.2 Simulation procedure

The simulation procedure can be simplified into following steps:

1. Solve the head field.
2. Release (2000) particles at the injection position. Track them in the advection field and integrate the transport times. Transport times are then multiplied by 11 to take into account the correct volume aperture. The factor of 11 have been derived by simulating the PDT3-test. This stage results breakthrough curves for the impulse source term.
3. Take into account the sorption and possible matrix diffusion. This stage results breakthrough curves for impulse source term of individual tracers.
4. Convolute the impulse responses with the measured source terms to get the final breakthrough curves.

3 Input data used

3.1 Properties of the

The feature A is modelled as a 15 m x 11 m rectangle. Transmissivity field over the fracture plane is isotropic and heterogeneous. Transmissivities are assumed to follow a lognormal distribution and they are correlated according to a spherical correlation function. Correlation length of 0.4 metres was applied in this model. This is consistent with the estimates based on the site geology (Winberg, 1996).

Transmissivity field applied in the modelling was a lognormal distribution of μ=-7.1 and σ=1.0. The standard deviation of the transmissivity field was not estimated from the field data, but the maximum standard deviation giving stabile head solution was used. The estimation of the mean transmissivity was based on the simulation of the drawdowns in the tracer tests. A total number of 16 different tests were simulated with 800 different transmissivity fields. The mean transmissivity was calibrated using the all the simulation results. For the transport simulations 30 best matching realisations were selected. All the different calculation cases used in the selection of the transmissivity realisations are presented in Table 3-1.

Due to the numerical problems it has not been possible to use large enough variance in the transmissivity field. This has resulted too low volume aperture of the fracture and caused too short transport times. To get a correct transport aperture an additional factor of 11 has been used as the ratio between the transport and flow apertures. This factor was estimated by simulating the PDT-3 tracer test.

Simulation of the PDT-3 test also indicated that the molecular diffusion and the advective flow field do not produce enough dispersion in the breakthrough curve. Therefore, instead of molecular diffusion coefficient of 10^{-9} m^2/s a dispersion coefficient of 10^{-4} m^2/s was applied in the particle tracking simulation. The dispersion coefficient of 10^{-4} m^2/s was calculated by simulating the PDTR3 test.

Table 3-1. Simulation cases in the conditioning of the transmissivity field.

Test	Inj.	ml/min	Vol (l)	Draw-down (m)	Extr.	ml/min	sampling (ml/h)	Draw-down (m)
RC-1	T1R2	0,102	1,560	0,60	T3R2	200,0	2,12	3,1
	T2R2	0,005	1,548	2,20	T3R2	200,0	1,26	3,1
	T4R3	0,118	1,898	0,30	T3R2	200,0	1,42	3,1
	5AR3	0,007	2,285	0,30	T3R2	200,0	1,71	3,1
DP-1	T1R2	10,000	1,560	-4,60	T3R2	102,5	10,20	1,2
DP-2	T2R2	10,000	1,548	-18,00	T1R2	36,0	6,00	40,0
DP-3	T2R2	3,500	1,548	-5,00	T1R2	36,0	6,00	44,5
DP-4	T2R2	10,000	1,548	-15,00	T4R3	38,0	6,00	11,0
RC-2	T1R2	0,120	1,560	0,20	T4R3	102,0	2,80	27,0
DP-5	T4R3	10,000	1,898	-2,00	T3R2	102,0	4,00	1,1
DP-6	T4R3	10,000	1,898	-0,80	T3R2	202,0	8,00	3,2
PDT-1	T1R2	0,280	1,560	0,40	T3R2	101,0	3,90	1,3
	T4R3	0,040	1,898	0,20	T3R2	101,0	3,00	1,3
PDT-2	T1R2	0,500	1,560	0,80	T3R2	201,0	3,90	3,1
	T4R3	0,130	1,898	0,50	T3R2	201,0	3,18	3,1
PDT-3	T4R3		1,898	1,20	T3R2	401,0	3,00	8,2

3.2 Boundary conditions

The hydraulic head values on the boundary were calculated by fitting a linear model into the calculated natural fresh water head values measured for the PDT-3 test (Winberg, 1997) and extrapolating the head values on the boundary of the model.

The boundary condition of the pumping hole were given for the closest node. To ensure a good hydraulic connection between the pumping node the rest of the fracture plane the transmissivities inside circles of 0.1 metres from the boreholes were risen to $5 \cdot 10^{-5}$ m^2/s.

3.3 Tracer data

Sorption parameters and effective diffusion coefficients of the tracers are based on the values reported in the Progress Report HRL-97-07. The selected parameters resulted retardation factors presented in Table 3-2. The radioactive decay was not taken into account.

Table 3-2. Applied sorption parameters.

Tracer	Ka (m)	Kd (m^3/Kg)	De (m^2/s)
Uranine	0	1	10^{-13}

HTO	0	1	10^{-13}
Cs	$8*10^{-3}$	$6*10^{-3}$	10^{-13}
Rb	$5*10^{-4}$	$4*10^{-4}$	10^{-13}
Sr	$8*10^{-6}$	$4.7*10^{-6}$	$4*10^{-14}$
Na	$7*10^{-7}$	$1.4*10^{-6}$	$6.7*10^{-14}$

4 Computer programs used

Three main computer programs were used in this study. The transmissivity field was generated with TFIELD-program. Numerical solution of the flow field and the particle tracking in the solved head field were calculated with computer programs FEFTRA and BTSIMU. Postprocessing of the results to take into account the sorption and matrix diffusion and to convolute the impulse responses with the measured source terms were made with comercial Matlab program package (Matlab, 1997). The numerical programs are presented in this section The matlab programs are based directly on the analytical equations.

4.1 TFIELD

The program TFIELD was made for this study to generate the transmissivities of the elements. The method is based on a fast algorithm developed by Dietrich and Newsam (1993). Currently the program is capable to generate an isotropic and correlated transmissivity field in which the transmissivity distribution is lognormal and correlation function spherical. Limitations of the method are that the points where the transmissivities are generated should be in a regular and rectangular grid and that the random field should be stationary.

The algorithm is based on the discovery that the correlation matrix in a regular grid have a block Toeplitz structure and it can be therefore embedded in a large circulant matrix S. Matrix S can be decomposed using Fast Fourier Transform (FFT) and based on the decomposition it is possible to form a random realisation of the correlated transmissivity field.

A regular grid of points is created over the region of the element mesh. The spacing between the gridpoints is the minimum spacing between the element centres. Using this grid a realisation of the transmissivity field is generated. Then the transmissivities of the elements are interpolated by choosing the transmissivity of the grid point next to element centre. More sophisticated two dimensional interpolation methods could of course be used, but because the generated transmissivity values are calculated with a higher resolution than the element mesh it was considered that the error caused by this very simple method is negligible.

4.2 FEFTRA

FEFTRA, earlier known as FEFLOW, is a numerical computer code package developed in VTT (Taivassalo, Koskinen and Meling, 1994). The code is based upon the finite element method (FEM) and solves the partial differential equations describing either the hydraulic head, pressure,

temperature or concentration of a flow field under consideration. The quantities are solved either separately and independently from each other or coupled together. That applies usually for the pressure, temperature and concentration which may be coupled together.

4.3 BTSIMU

BTSIMU calculates the transport applying a particle tracking method to the solution of the hydraulic head field. The solved head field and the transmissivity field are used to calculate the components of the flow velocity at each node of the element mesh. The advective part of the transport is calculated applying bicubic interpolation to the calculated grid of the flow velocity. Interpolation of the velocities makes the velocity field continuous which helps the convergence of the statistical simulations. Beside the advection also dispersion is taken into account. The dispersion is modelled as a random Brownian motion.

5 RESULTS

The solution of the hydraulic head is based on the element method. The fracture plane is covered with a mesh of about 15 000 square elements. All the elements are same size and shape to ensure a isotropic structure for the transmissivity field. A set of 30 different realisations of the transmissivity field were used.

5.1 Drawdowns

Steady state drawdowns were calculated for the pumping and injection boreholes. In Table 1 are presented the statistics of the calculated drawdowns from the 30 realisations.

Table 1. Predicted drawdowns (m).

Borehole	s(5%)	s(50%)	s(95%)
KXTT3	16	12	10
KXTT4	2.5	2.1	1.6

5.2 Breakthrough curves

The transport of the tracers were calculated using a particle tracking method. A set of 2000 particles were released from the KXTT4. Breakthrough times of the particles represent a response for the pulse input. Possible matrix diffusion was taken into account by applying analytical solution of one dimensional matrix diffusion equation into the simulated breakthrough. For the sorbing tracers the sorption was taken into account in conjunction with the matrix diffusion. The predicted breakthrough times are presented in Table 5-1.

Table 5-1. Breakthrough times in hours.

	t_5 (5%)	t_5 (50%)	t_5 (95%)	t_{50} (5%)	t_{50} (50%)	t_{50} (95%)	t_{95} (5%)	t_{95} (50%)	t_{95} (95%)
UR	2.1	2.7	3.3	4.2	4.8	5.7	5.4	6.3	7.5
HTO	2.1	2.4	3.0	3.9	4.8	5.7	5.4	6.0	7.5
Cs	120.	130.	130.	430.	450.	490.	1200	1300	5600
Rb	6.3.	6.9	7.5	11.	12.	13.	15.	16	18
Sr	2.1	2.7	3.3	4.2.	4.8	6.0	5.4	6.3	7.8
Na	2.1	2.4	3.0	3.9	4.8	5.7	5.1	6.0	7.5

The calculated breakthrough times in Table 5-1 refer to times of t_{100} given in Table 5-2.

Table 5.2. Breakthrough times t_{100} used in the calculation of the breakthrough times in Table 5-1.

Tracer	T_{100} (h)
Uranine	195
HTO	333
Cs	5600
Rb	553
Sr	505
Na	1292

The simulated breakthroughs are presented in Figure 2.

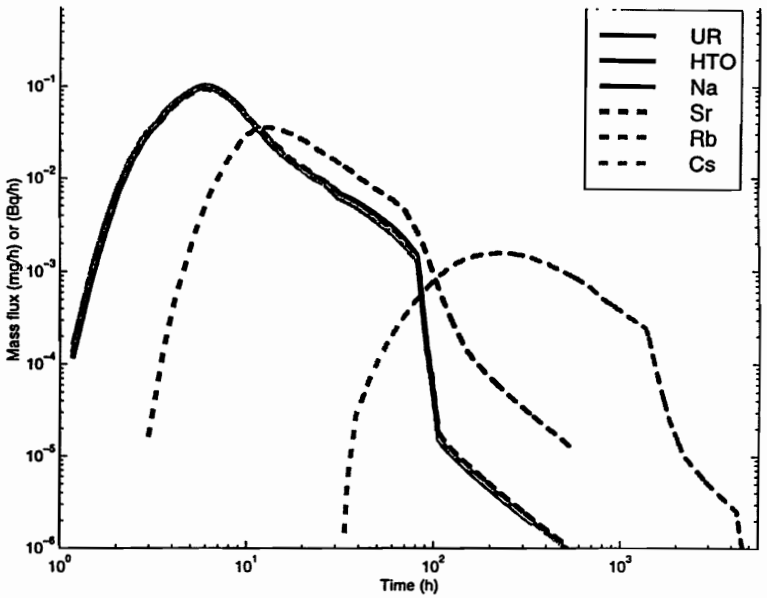

Figure 2. Predicted breakthrough curves.

6 REFERENCES

Dietrich, C.R. and Newsam, G.N., 1993. A Fast and Exact Method for Multidimensional Gaussian Stochastic Simulations. Water Resources Research, Vol. 29, No. 8, Pages 2861-2869. August 1993.

Hautojärvi, A., 1989. Effects of Matrix Diffusion on Transport of Tracers in Rock Fractures. Helsinki, Technical Research Centre of Finland, Nuclear Engineering Laboratory, Technical Report TOKA-4/89. (In Finnish).

Matlab, 1997. Matlab version 5.1. The MathWorks Inc. Natick, MA, USA

Taivassalo, V., Koskinen, L. and Meling, K., 1994. Groundwater Flow Analysis in Preliminary Site Investigations, Modelling Strategy and Computer Codes. Nuclear Waste Commission of Finnish Power Companies. Report YJT-94-04.

Winberg, A. (Editor), 1996. First TRUE Stage. Descriptive structural-hydraulic Models on Block and Detailed Scales. Äspö Task Force, Task 4A. Final Draft.

Winberg, A., 1997. TRUE 1st Stage Tracer Test Programme. Update on the Descriptive Conceptual Model of Feature A, TRUE-1 Site. Technical memorandum prepared for Äspö Task Force Modelling teams. Conterra AB. Gothenburg, Sweden.

Prediction of sorbing tracer tests in the First TRUE Stage. Task 4E:II.

Vladimir Cvetkovic & Hua Cheng (KTH/WRE)

Jan Olof Selroos (SKB)

Prediction of Sorbing Tracer Tests

in the First TRUE Stage

TASK 4E:II

TRUE MODELLING TEAM:
Vladimir Cvetkovic, Water Resources Eng., KTH
Jan-Olof Selroos, SKB
Hua Cheng, Water Resources Eng., KTH

August1998

Description of Simulation Approach and Data

The tools and conceptual models used for the prediction of STT-1b are briefly discussed below prior to the presentation of the results.

Conceptual and Mathematical Models

The transport is assumed to take place in a single fracture with spatially variable aperture. Mass transfer of conservative tracer is represented by one-dimensional (transverse) matrix diffusion into a surrounding, infinite matrix and into stagnant water. The reactive solute may undergo equilibrium sorption on fracture surfaces and kinetic sorption in the gauge material.

The reaction function for diffusion into the rock matrix and stagnant water is

$$\gamma_1(t,\tau;\beta)=\frac{H(t-\tau)\kappa\beta}{2\sqrt{\pi}(t-\tau)^{3/2}}\exp\left[\frac{-\kappa^2\beta^2}{4(t-\tau)}\right]$$

where

$$\kappa\beta=\kappa_1\beta_1+\kappa_2\beta_2$$

$$\tau(l)=\int_0^l\frac{dl'}{v(l')}$$

$$\beta_1(l)=\int_0^l\frac{dl'}{v(l')b(l')}$$

$$\kappa_1=\theta\sqrt{DR_m}$$

$$\beta_2(l)=\int_0^l\frac{dl'}{v(l')w(l')}$$

$$\kappa_2=\sqrt{D_w}$$

$$R_m=1+K_d^m\rho(1-\theta)/\theta$$

The reaction function for equilibrium sorption on fracture surfaces and for kinetic sorption in gauge material are

$$\gamma_2(t,\tau;\beta)=\delta(t-\tau-K_a\beta_1)$$

and

$$\gamma_3(t,\tau;\beta)=e^{\alpha K_d^g\tau}\delta(t-\tau)+\alpha^2K_d^g\tau\exp\{-\alpha\left[K_d^g\tau+(t-\tau)\right]\}\tilde{I}_1\left[\alpha^2K_d^g\tau(t-\tau)\right]$$

and H is the heaviside function, v is the velocity with length coordinate l, b is the half aperture, w is the radius of the borehole, θ is the matrix porosity, D is the matrix diffusion coefficient, Ka is the equilibrium surface sorption coefficient, Kd is the distribution coefficient in gauge material, α is the mass transfer rate, and ρ is the density.

If all processes above (i.e. diffusion into the rock matrix and stagnant water, equilibriumsorption on fracture surfaces and kinetic sorption in the gauge material) are present, the resulting γ is obtained through convolution of the individual γ_1, γ_2, and γ_3 functions above. In the predictions for the reactive tracers, the diffusion is neglected due to its relative small effect.

It is observed that the mass transfer solution thus is dependent on two Lagrangian parameters integrated along the flow paths. Both β and τ are random variables due to the aperture heterogeneity, and pdfs of both parameters are needed in order to estimate the mass transfer affected breakthrough. However, in the present analysis an approximate linear relationship between β and τ is used for calculating β. Then only τ is random. The β and τ relationship is discussed below.

If the pdf of τ is denoted by g and the input function by ϕ, then the resulting mass flux is obtained as $s(t) = \int (\phi * \gamma) g(\tau) d\tau$ [M/T] where $*$ denotes the convolution operator and ϕ has the same units as s. $g(\tau)$ is assumed to have an inverse-Gaussian distribution. The moments of $g(\tau)$ are obtained by fitting the calculated breakthrough with the experimental data from PDT4.

Computational Tools

Numerical simulations of flow and conservative transport in a single fracture with spatially variable aperture are used to obtain the β-τ relationship and the drawdowns in the boreholes.

The same numerical tools as used for the prediction of STT1 have been used in the current study. Transmissivity fields conditional to both measured transmissivities and head values in the five boreholes are as previously obtained through a stochastic inverse method based on an iterative technique that couples geostatistics and optimization (Gómez-Hernández et al., 1997). The flow problem for the prevailing conditions is solved using a standard, commercially available code (MODFLOW, 1994). Conservative transport is modelled using a particle tracking technique where the transit time in each element is calculated after the entrance and exit points of the element have been establisehed (Mosé et al., 1994). The mass transfer calculations are performed using a numerical integration scheme implemented in Fortran 77.

By calculating β_1 and τ in multiple realizations, a correlation between these two variables is obtained. The specific correlation used in the present analysis was obtained along the KXTT4-KXTT3 path of Feature A. β_2 is obtained by $\beta_2 = \tau/w$.

Flow and Non-Reactive Transport Results

The case with pumping in KXTT3 with Q=0.4 l/min and injection of tracer in KXTT1 is simulated.

Head value:

Tracer test Borehole section	$s_{(5\%)}{}^{c}$	$s_{(50\%)}{}^{c}$	$s_{(95\%)}{}^{c}$ (m)
Q=0.4 l/min			
KXTT1	-79.0	-55.1	-48.9
KXTT2	-56.0	-48.6	-47.0
KXTT3	-49.9	-47.1	-46.5
KXTT4	-47.3	-46.6	-46.4
KA3005	-52.4	-48.3	-47.3

Mass recovery pulse input:

Tracer test	$F_{(5\%)}{}^{c}$	$F_{(50\%)}{}^{c}$	$F_{(95\%)}{}^{c}$ (-)
Q=0.4	0.64	1.00	1.00

Breakthrough pulse input:

t_5, t_{50} and t_{95} (h)

TEST	$t_{5(5\%)}$	$t_{5(50\%)}$	$t_{5(95\%)}$	$t_{50(5\%)}$	$t_{50(50\%)}$	$t_{50(95\%)}$	$t_{95(5\%)}$	$t_{95(50\%)}$	$t_{95(95\%)}$
Q=0.4	1.2	6.3	26.7	1.5	8.1	32.2	1.7	11.5	44.7

Sorbing Transport Results

The following tracer data has been used:

Tracer	K_a (m)	K_d^m (m^3/kg)	D (m^2/s)	K_d^g (-)	α (1/h)
HTO	0	0	3.0×10^{-11}	-	-
Na	7×10^{-7}	1.4×10^{-6}	1.6×10^{-11}	0.5	0.3
Sr	8×10^{-6}	4.7×10^{-6}	1.0×10^{-11}	1.0	0.3
K	4×10^{-5}	2×10^{-4}	1.0×10^{-11}	4.5	0.3
Rb	5×10^{-4}	4.0×10^{-4}	2.5×10^{-11}	6	0.24
Co	3.2×10^{-3}	1.6×10^{-2}	2.5×10^{-11}	14	0.03

in conjunction with a matrix porosity of $\theta = 0.004$ and $\rho = 2700\ \mathrm{kg/m^3}$ based on Andersson et al. (1997). The values of K_a, K_d^m and D are obtained from the laboratory. K_d^g and α are fitted values for gauge material; the same values of K_d^g and α are used as in the evaluation of Na, Sr and Rb in STT-1.

The results for travel time and mass recovery are given below:

Travel times (in hours) and mass recovery for a pulse input:

Tracer	t_5 [hr]	t_{50} [hr]	t_{95}[hr]	Recovery
Uranin	3.4	11.0	91.0	0.97
HTO	3.4	11.0	91.0	0.98
Na	3.4	12.5	41.4	1.0
Sr	3.8	16.9	55.7	1.0
K	11.3	47.9	149.1	0.39
Rb	17.7	66.5	203.8	1.0
Co	48.2	168.2	510.6	1.0

The recovery is calculated at the termination time provided by the Task Force Secretariate.

Travel times (in hours) and mass recovery for measured input:

Tracer	t_5 [hr]	t_{50} [hr]	t_{95} [hr]	Recovery
Uranin	5.6	18.0	109.5	1.06
HTO	5.5	16.0	97.0	1.09
Na	6.5	22.2	113.0	1.03
Sr	8.2	31.4	168.8	1.0
K	21.6	64.3	173.0	0.23
Rb	32.5	113.2		0.86
Co	103.0	597.0		0.73

The recovery is calculated at the termination time provided by the Task Force Secretariate.

References

Andersson, P., et al., TRUE 1st stage tracer test programme, Experimental plan for tests with sorbing tracers at the TRUE-1 site, SKB Äspö HRL-97-07, 1997.

Gómez-Hernández, J. J., Sahuquillo, A., and Capilla, J. E., Stochastic simulation of transmissivity fields conditional to both transmissivity and piezometric data. 1. Theory, J. Hydrology, 203 (1-4), 162-174, 1997.

MODFLOW/EM, The USGS Three Dimensional Ground Water Flow Model, Maximal Engineering Software, Inc, 1994.

Mosé, R., Siegel P., and Ackerer P. Application of the mixed hybrid finite element approximation in a groundwater flow model: Luxury or necessity?, Water Resour. Res., 30, 3001-3012, 1994.

Modelling and blind predictions for STT-1b tracer test.

Andreas Jakob & Walter Heer (NAGRA/PSI)

Modelling and blind-predictions for STT1b tracer tests

Andreas Jakob, Walter Heer
Paul Scherrer Institute PSI, Switzerland
January 1998

Table of contents

1. Introduction

This report briefly summarises the modelling approach used by PSI to predict the breakthrough curves o uranine and various radioactive tracers, corresponding to the STT1b tracer tests of Task 4E of th TRUE-1 program.

During the autumn of 1997 blind-predictions for the STT1 tracer tests were made. The fundamentals fo modelling flow and transport are outlined in [1] and values for the nuclide dependent transport parameter are also specified therein. A comprehensive modelling report is in preparation [2].
After the release of the measurement data, these blind-predictions were complemented by a subsequen analysis and inverse modelling in order to improve our understanding of the major geometrical aspects o the flow domain and of the transport mechanisms involved to obtain - finally - information for mode refinement.
With the up-dated model, together with best-fit values for the transport parameters from inverse modelling the STT1 tracer tests, blind-predictions for the STT1b migration experiments were performed.

2. Procedure for the blind-predictions of the STT1 tracer tests and inverse modelling

2.1. Model used for the blind-predictions of the STT1 tracer test

For the sake of completeness a brief overview about our modelling methodology for the STT1 tracer test is presented. Further details can be found in [1] and [2].
Due to the special experimental conditions at the TRUE-1 site at Äspö (an extreme narrow and fast flow field) our model is strongly based on the one applied to successfully model the Grimsel migration experiments.
For the blind-predictions of the STT1 tracer tests the hydrological part of the model is based on a 2D streamline/streamtube formalism with underlying homogeneous and isotropic transmissivity field. In addition, an averaged and uniform natural background flow field is taken into account. Tracer transport is performed in the frame of a dual porosity medium approach with averaged and constant transport parameters. Matrix diffusion occurs in the model into a limited porous zone adjacent to the fracture and sorption processes are described by linear isotherms.
Geometry of flow paths: Structural geological investigations indicated that groundwater is flowing mainly in a network of connected major faults and is not only in contact with fault gouge, characterised by a relative large porosity, but also with altered rock of much lower porosity.

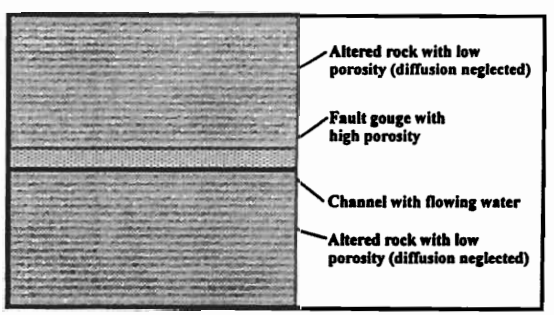

Figure 1: Schematic diagram of the geometrical aspects of the model used as a basis for the blind-predictions of the STT1 tracer tests.

The existence of fault gouge is documented in [3] by colour micrographs of thin sections of borecores. The model simplifies the complex fracture network into a small number of parallel water-conducting channels in contact with a diffusion accessible porosity - the fault gouge - as sketched in Figure 1.

The model was calibrated by fitting one single uranine breakthrough curve (PDT-3) performed in the same flow field as used for the STT1 tracer test. The best-fit yielded a good representation of the measured data and the shape of the trailing edge and indicated a surprisingly large effect of matrix diffusion confirming the assumption that the fault gouge observed by structural analysis in the neighbourhood of Feature A is also present in this fracture network. However, due to the nature of the input pulse (a more or less square pulse injection followed by a long injection tail at lower concentrations) it was not possible to identify any tail-end perturbation at the trailing edge of the breakthrough curve indicative of a limitation of the fault gouge. Hence, a value for the limitation had to be guessed, and the value chosen (1 mm) represents a relatively small (averaged) thickness of the diffusion accessible zone. From the uranine-PDT3 calibration a specific surface area at the flowing water/fault gouge interface of about 21900 m^2/m^3 and a fault gouge porosity of 0.15 was deduced. For the predictions, all the nuclide dependent parameters were based on Swedish laboratory experiments but were re-scaled in an appropriate manner. The values for K_d were related to those of crushed mylonite which is considered to be closest to fault gouge. The values for the surface based sorption coefficients K_a were taken from Andersson et al. [4]. The pore diffusion constant D_p for a given tracer was obtained by the tracer dependent diffusion constant D_w in free water times a tracer independent geometric factor. The latter was simply the ratio of fitted D_p and (theoretical) D_w for uranine of PDT3.
However, a part of the trailing edge of the calibrating PDT3 uranine-breakthrough curve was only approximately reproduced by the model and this was considered to be an indication for an oversimplification of the flow domain.

2.2. Inverse modelling of the STT1 breakthrough curves and consequences for the model

From their sorption behaviour, the tracers applied in the STT1 tracer tests, can be grouped roughly into two classes: The non-sorbing or weakly sorbing tracers uranine, HTO, Na, Sr and Ca; and the moderately sorbing tracers Ba, Rb and Cs. In figures 2 and 3, the blind-predictions of sodium, representing the first tracer class and barium for the second are also given for comparison purposes.
Whereas the differences between blind-predictions and measurements for group 1 tracers are of minor importance, those for the second group show more systematic deviations. For the first group predicted peak position and peak height differ within a factor of two from the measurements and the shape of the breakthrough curves correspond to those measured. However, for the more strongly sorbing tracer group the picture is different. For rubidium and barium the predicted peak-height is the same as measured but is a factor of five too high for caesium. Moreover, all of these tracers show an early breakthrough which was not predicted at all and the time for the peak-maximum in the experiments is always delayed by a factor of five.
As mentioned above, since the injection tailing dominates the later part of the breakthrough curve for uranine, a proper time for the beginning of the tail-end perturbation could not be determined and a value for the thickness of the fault gouge had to be estimated. Subsequent inverse modelling, using all eight tracer breakthrough curves, clearly showed that this value (1mm) was too small and had to be adjusted to 5 mm. However, especially for the stronger sorbing tracers, an early tracer breakthrough could not be obtained by the model even when the values for dispersion were increased dramatically. Only by using a refined model in which a second flow path family was included, could an improved representation of the rising edge be achieved. For the non-sorbing uranine and tritium an insignificant decrease in accuracy was obtained. Further details of the geometrical aspects of the model can be taken from Figure 4.
Applying the refined model to caesium indicates irreversible sorption or sorption with a very slow desorption rate for about half of the tracer. A laboratory check of caesium sorption and desorption on fault gouge would be clarifying additional information.

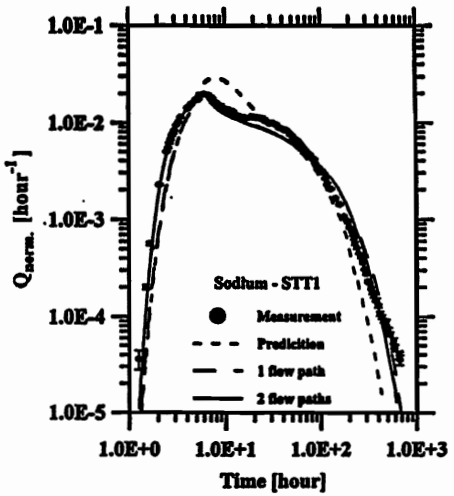

Figure 2: Comparative plot of measurements, blind-prediction and best-fits using either one or two flow path families for sodium in the STT1 tracer test.

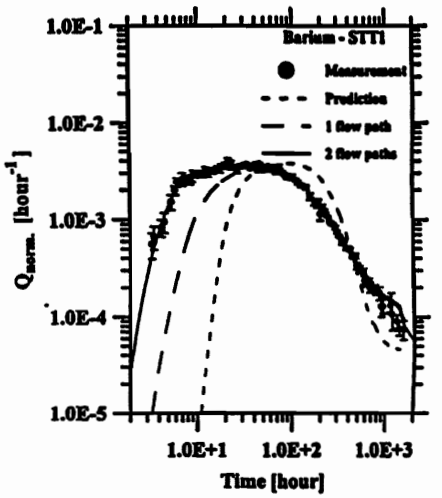

Figure 3: Comparative plot of measurements, blind-prediction and best-fits using either one or two flow path families for barium in the STT1 tracer test.

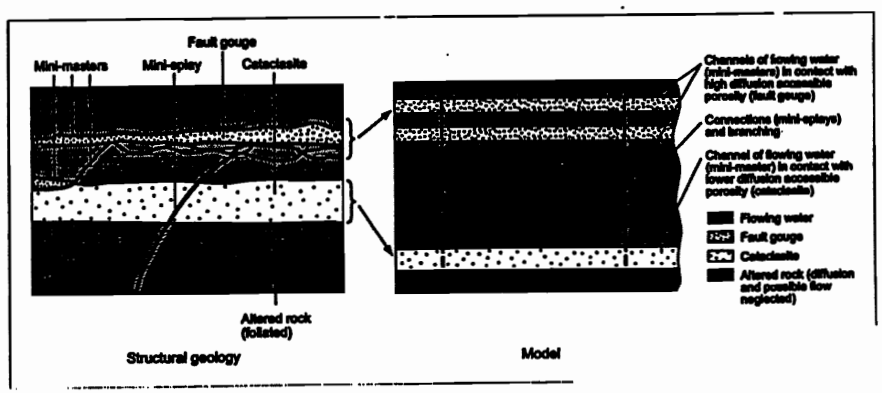

Figure 4: Sketch of the refined geometry for flow and transport after the analysis of the STT1 tracer breakthrough curves. The left sketch illustrates some important aspects of the fracture as they were identified in structural geological investigations [3]. In the right sub-figure the transformations into a relatively simple geometry are shown which was the basis for the subsequent blind-predictions of the STT1b tracer test performed in the frame of the dual porosity medium approach.

3. Blind-predictions for the STT1b tracer tests

3.1. Flow field for the STT1b tracer tests

To guarantee full tracer recovery a rigid flow field was installed with an essentially passive injection and strong pumping at the extraction borehole. From the decaying part of the injection distribution for the uranine test of the STT1b experiment, a constant flow rate Q_i of 0.624 ml/min was determined. Q_i contains a correction factor determined from the injection and breakthrough distributions of uranine from the PDT4 test. In addition, the sampling flow rate of $4.83 \cdot 10^{-2}$ ml/min (2.9 ml/hour) was taken into account. This value for Q_i was used for all seven tracers in STT1b. A fixed pumping rate Q_w of about 400 ml/min was installed as the downstream boundary; hence, the ratio $Q_w / Q_i = 641$ generated a practically monopole-like flow field.

Due to these conditions the flow domain remains very restricted for all tracers. The flow field was discretised using a 2D-streamtube formalism. In addition, the natural background flow was treated as being uniform and time-independent. Its strength and direction were determined from the head distribution in Feature A measured on June 6th 1997 and using kriging. For $|\nabla \Phi|$ we determined a value of about $5.6 \cdot 10^{-2}$ m/m and for its direction an angle of 180° with respect to the line connecting the injection and extraction borehole.

In the figures 5 and 6 we plot the flow field used for the subsequent tracer transport modelling.

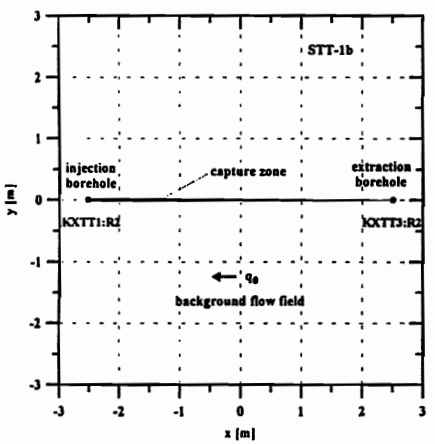

Figure 5: Flow domain for the STT1b tracer tests. The injection borehole is KXTT1:R2, the extraction borehole is KXTT3:R2. Ten 1D-streamlines of the capture zone [1] are shown along which all fluid flow and transport calculations were performed. Due to a weak background flow-field the water flow in the capture zone is slightly weakened. As a consequence of the high pump flow rate at the extraction borehole all the injected tracer migrates within the capture zone ensuring full tracer recovery.

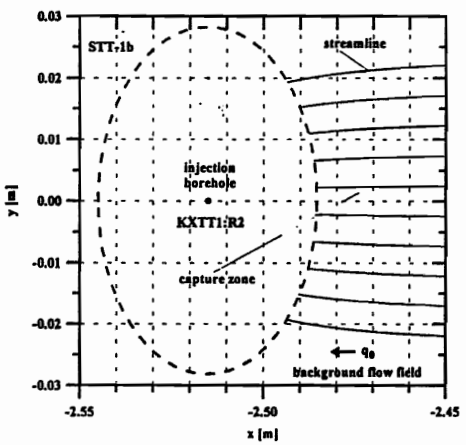

Figure 6: Magnification of a part of the flow domain from Figure 5 close to the injection borehole. Again ten 1D-streamlines are shown which start at the borehole/rock interface. Due to the strong pumping at the downstream boundary and passive injection, the capture zone is very narrow and has a width of only a few centimetres. (Note the different scales in both directions.)

[1] Regions of interflow between a recharge and a pumping well within a flow domain are denoted as the capture zone.

3.2. Fitting the uranine PDT4 breakthrough curve for calibration of the up-dated model

Based on the best-fit parameter values obtained by inverse modelling of all eight tracers of the STT1 tracer tests, the uranine breakthrough of PDT4 was calculated. Compared to the measurements, the peak-arrival time was too early by about three hours which was compensated in subsequent calculations by a larger value for the flow width ($\varepsilon_f B$) resulting in a smaller value for the water-velocity v_f. Consequently, to achieve the same effect of matrix diffusion in the trailing edge of the breakthrough curve, the specific interface area (channel with flowing water/fault gouge and channel with flowing water/cataclasite, respectively), had to be reduced simultaneously. With such a procedure a good representation of the peak-region was achieved; however, the first part of the trailing edge, between 10 and 12 hours, is underestimated in the calculation by a factor of two. This might indicate that the flow field is not well enough defined. Further investigations will be part of the forthcoming analysis of the STT1b tracer test after the release of the experimental data.

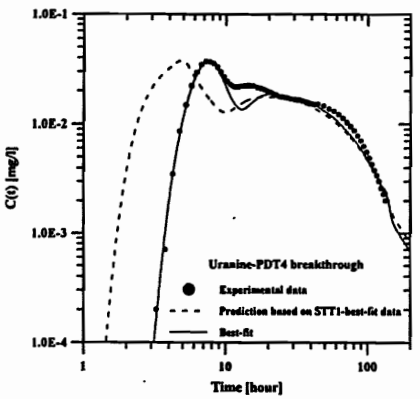

Figure 7: Comparative plot of calculated and measured breakthrough curves for uranine-PDT4 versus time in a log-log representation. The dashed line represents a calculation based on the refined model and using best-fit parameter values obtained from inverse modelling the STT1 tracer tests. The solid line represents a best-fit calculation of uranine-PDT4 break-through in the frame of the up-dated model (see text).

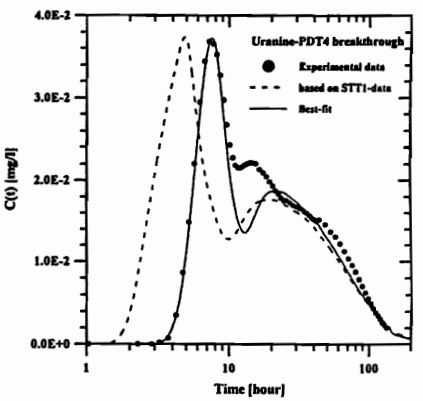

Figure 8: The same as for Figure 7 but in a lin-log representation.

Having fixed the values for the flow-width and the specific interface-area we performed blind-predictions for all seven tracers of STT1b.

3.3. Final values for the transport parameters used for the blind-predictions of STT1b

The fit of the model to the experimental breakthrough data of uranine for PDT4 can be represented by the following three fit-parameters:

$B \cdot \varepsilon_f = 1.33 \cdot 10^{-3}$ m	Total flow width of all the channels (B = aquifer thickness, ε_f = flow porosity),
$a_L = 0.12$ m	longitudinal dispersion length ($Pe = 42.4$),
$1/b = 7000$ m^{-1}	specific interface area.

Additional parameters derived from inverse modelling the STT1 tracer tests and applied without further changes are:

$\varepsilon_p^{(1)} = 0.17$	Porosity of the fault gouge,
$\varepsilon_p^{(2)} = 0.027$	porosity of the cataclasite,
$\varepsilon_f^{(1)} / \varepsilon_f = 0.75$	relative flow porosity of the first fracture family,
$\varepsilon_f^{(2)} / \varepsilon_f = 0.25$	relative flow porosity of the second fracture family,
$\Delta x = 5 \cdot 10^{-3}$ m	thickness of the fault gouge and of the cataclasite,
$D_p = 3.475 \cdot 10^{-11}$ m^2/s	pore diffusion constant for uranine.

Tracer	Fault gouge and cataclasite		Surface
	D_p [m^2/s]	K_d [m^3/kg]	K_a [m]
Uranine	$3.5 \cdot 10^{-11}$	---	---
HTO	$5.7 \cdot 10^{-11}$	---	---
Na	$5.8 \cdot 10^{-11}$	$3.2 \cdot 10^{-5}$	$7.0 \cdot 10^{-6}$
K	$8.4 \cdot 10^{-11}$	$5.0 \cdot 10^{-4}$	0
Sr	$8.8 \cdot 10^{-11}$	$4.5 \cdot 10^{-5}$	$2.5 \cdot 10^{-5}$
Rb	$8.8 \cdot 10^{-11}$	$1.3 \cdot 10^{-3}$	$6.9 \cdot 10^{-5}$
Co	$3.9 \cdot 10^{-11}$	1.0	0

Table 1: Values for the tracer dependent transport parameters. For K and Co the K_d-values were estimated according to the procedure outlined more in detail in the appendix and the values for D_p were extrapolated from those of Rb and Ca, respectively.

3.4. Predictions for the recovery of all seven tracers

In the following table we have compiled the breakthrough times t_5, t_{50}, t_{95} and $t_{99.9}$ for all seven tracers. The breakthrough time t_i is defined as the actual time needed to recover i = 5, 50, 95 or 99.9 % of the total injected and decay-corrected activity or mass. t_{end} is the time of termination of monitoring and Q_c is the calculated mass recovery at t_{end}.

Tracer	t_5 [hour]	t_{50} [hour]	t_{95} [hour]	$t_{99.9}$ [hour]	t_{end} [hour]	$Q_c(t_{end})$ [%]
Uranine	6.2	19.2	178	526	195	95.8
HTO	6.4	20.7	148	384	333	99.8
Na^+	7.0	25.8	208	720	1292	100.0
Sr^{2+}	8.3	37.2	218	669	505	99.7
K^+	11.3	75.3	963	---	39	33.6
Rb^+	23.5	193	2320	---	553	70.7
Co^{2+}	3780	$5.54 \cdot 10^4$	$2.08 \cdot 10^6$	$1.78 \cdot 10^7$	3622	4.7

Table 2: Calculated tracer breakthrough times t_5, t_{50}, t_{95} and $t_{99.9}$ [hour] and the simulated mass recovery $Q_C(t_{end})$ [%] at t_{end}, the time of termination of monitoring, for all seven tracers and for the measured tracer injection distributions.

Tracer	t_5 [hour]	t_{50} [hour]	t_{95} [hour]	$t_{99.9}$ [hour]	t_{end} [hour]	$Q_c(t_{end})$ [%]
Uranine	4.2	8.3	147	497	195	97.0
HTO	4.4	10.1	127	356	333	99.8
Na^+	4.9	13.1	190	630	1292	100.0
Sr^{2+}	5.8	19.2	189	621	505	99.8
K^+	8.7	71.9	960	---	39	35.9
Rb^+	17.4	178	2300	---	553	71.2
Co^{2+}	3500	$5.50 \cdot 10^4$	$2.06 \cdot 10^6$	$1.42 \cdot 10^7$	3622	5.2

Table 3: Calculated tracer breakthrough times t_5, t_{50}, t_{95} and $t_{99.9}$ [hour] and the simulated mass recovery $Q_C(t_{end})$ [%] at t_{end}, the time of termination of monitoring, for all seven tracers and for Dirac delta input.

On the following pages we have plotted our blind-predictions for the flow normalised to the total injected mass, and the tracer recovery versus time for all seven tracers for both the measured injection distribution and a Dirac delta pulse-input.

3.5. Predictions for uranine

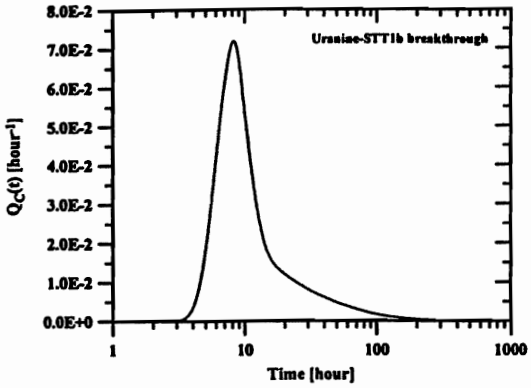

Figure 9: Flow of uranine-STT1b [hour $^{-1}$] versus time [hour].

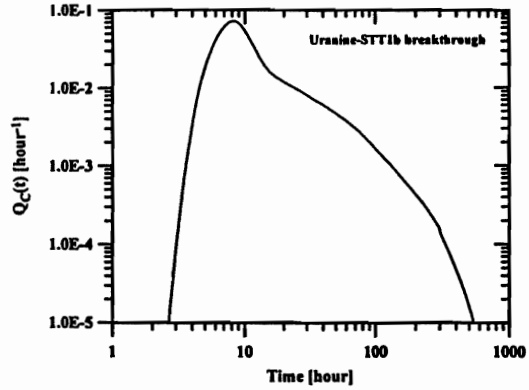

Figure 10: Flow of uranine-STT1b [hour $^{-1}$] versus time [hour].

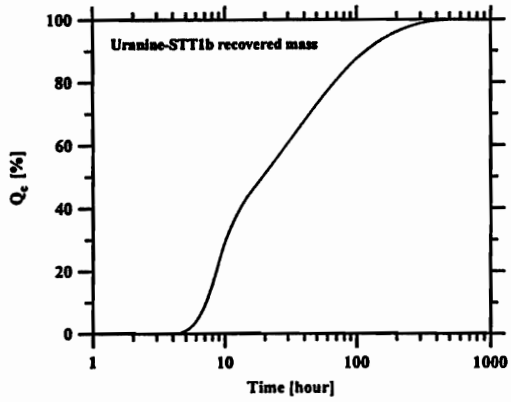

Figure 11: Tracer recovery for uranine-STT1b [%] versus time.

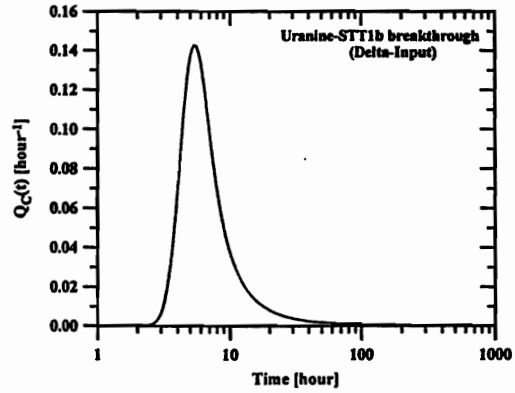

Figure 12: Flow of uranine-STT1b [hour $^{-1}$] versus time [hour] for delta-input.

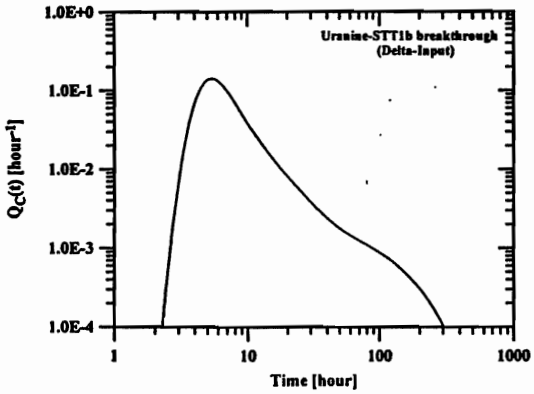

Figure 13: Flow of uranine-STT1b [hour $^{-1}$] versus time [hour] for delta-input.

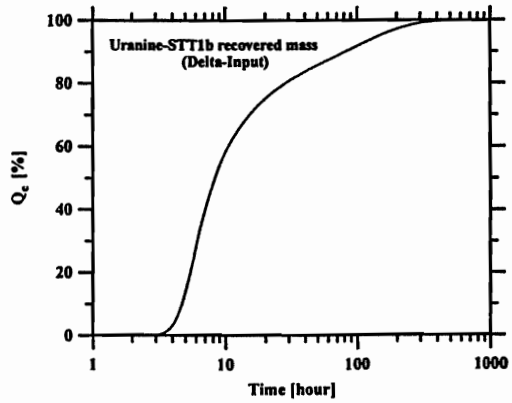

Figure 14: Tracer recovery for uranine-STT1b [%] versus time for delta-input.

3.6. Predictions for tritium (HTO)

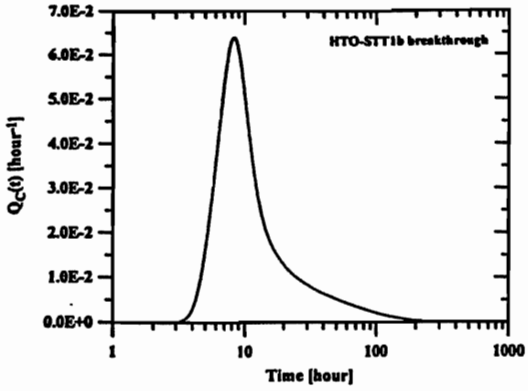

Figure 15: Flow of HTO-STT1b [hour $^{-1}$] versus time [hour].

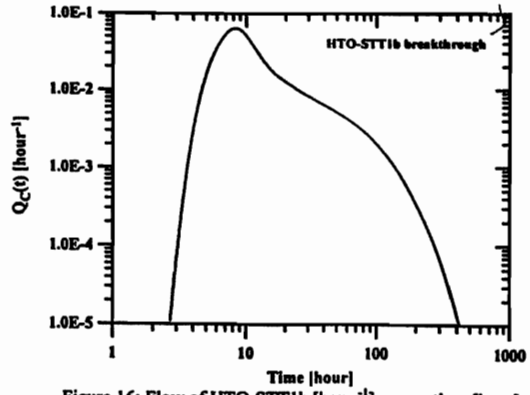

Figure 16: Flow of HTO-STT1b [hour $^{-1}$] versus time [hour].

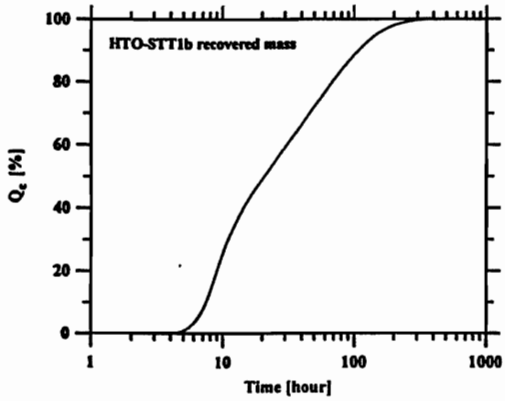

Figure 17: Tracer recovery for HTO-STT1b [%] versus time.

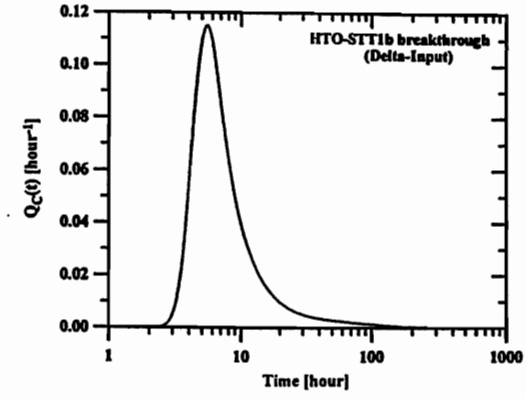

Figure 18: Flow of uranine-STT1b [hour $^{-1}$] versus time [hour] for delta-input.

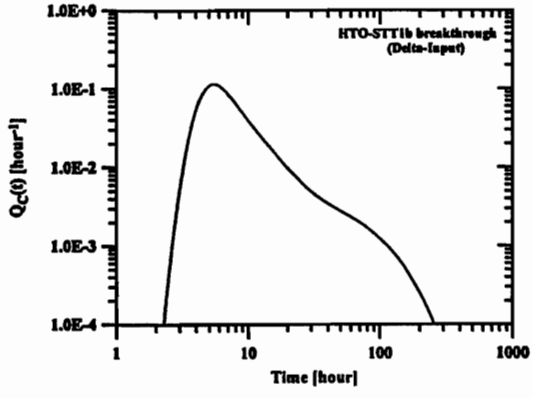

Figure 19: Flow of HTO-STT1b [hour $^{-1}$] versus time [hour] for delta-input.

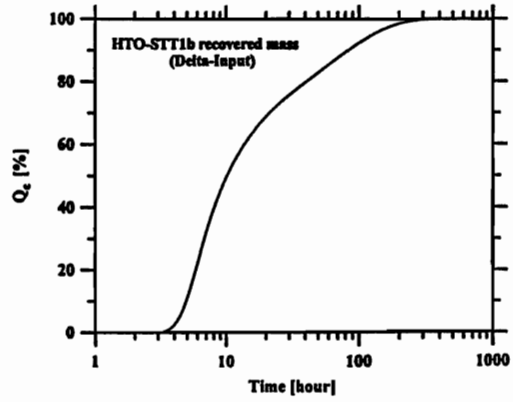

Figure 20: Tracer recovery for uranine-STT1b [%] versus time for delta-input.

3.7. Predictions for sodium

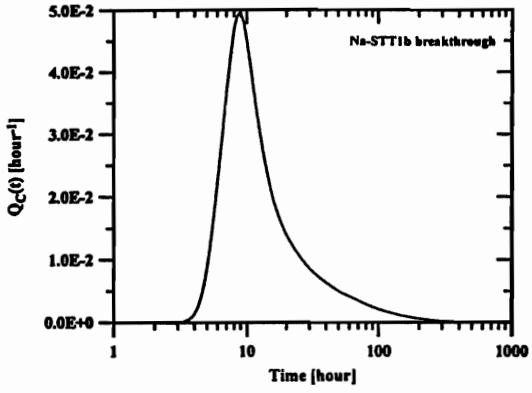

Figure 21: Flow of sodium-STT1b [hour $^{-1}$] versus time [hour].

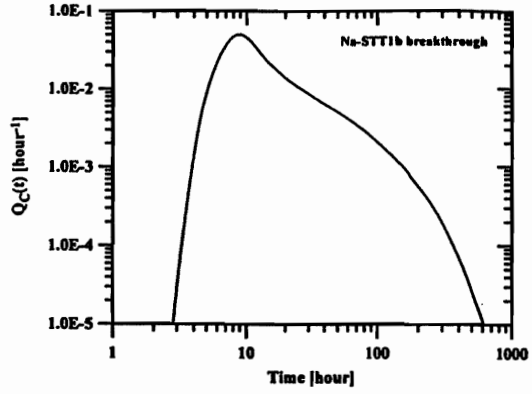

Figure 22: Flow of sodium-STT1b [hour $^{-1}$] versus time [hour].

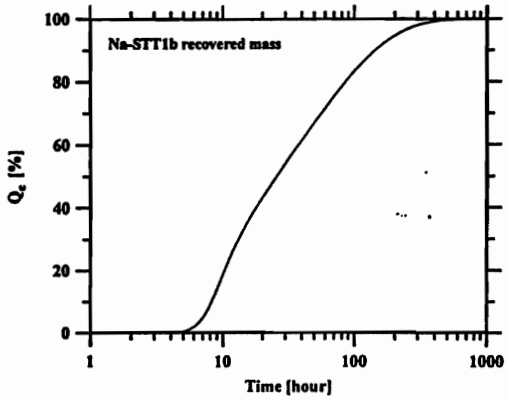

Figure 23: Tracer recovery for sodium-STT1b [%] versus time.

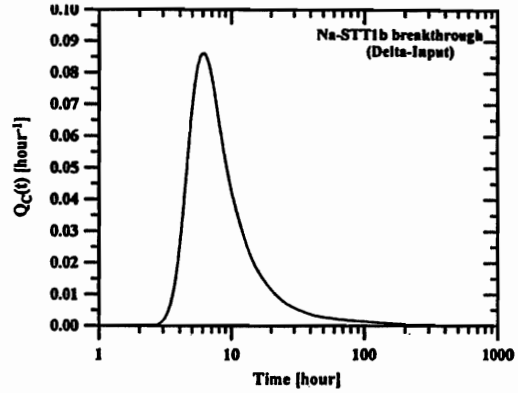

Figure 24: Flow of sodium-STT1b [hour $^{-1}$] versus time [hour] for delta-input.

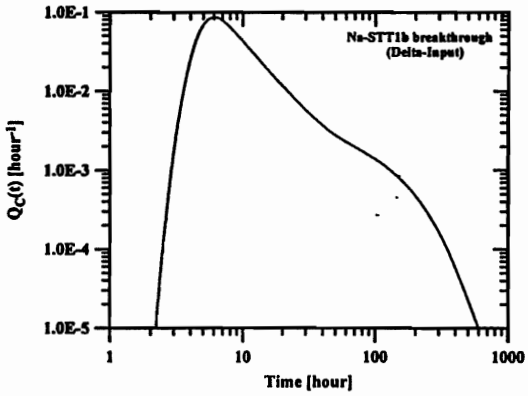

Figure 25: Flow of sodium-STT1b [hour $^{-1}$] versus time [hour] for delta-input.

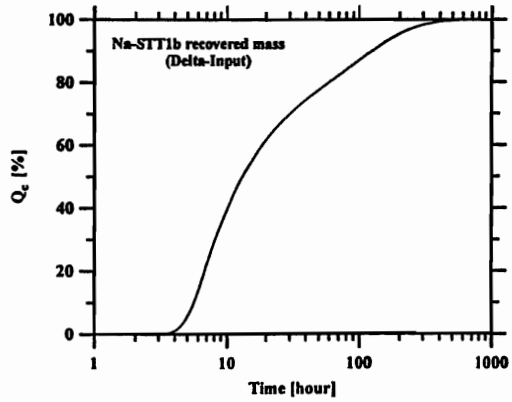

Figure 26: Tracer recovery for sodium-STT1b [%] versus time for delta-input.

3.8. Predictions for strontium

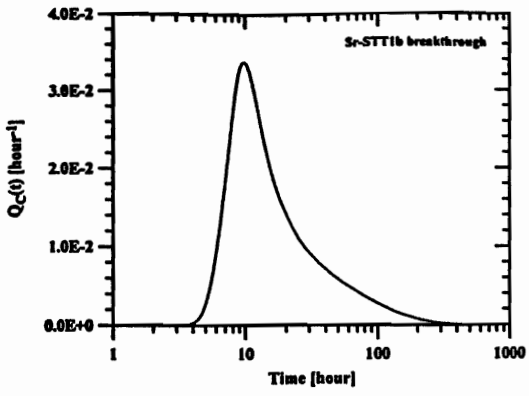

Figure 27: Flow of strontium-STT1b [hour $^{-1}$] versus time [hour].

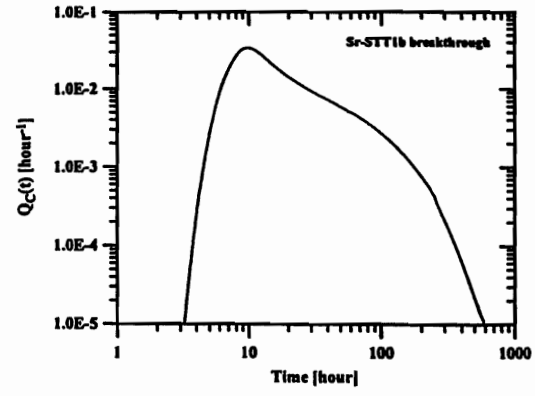

Figure 28: Flow of strontium-STT1b [hour $^{-1}$] versus time [hour].

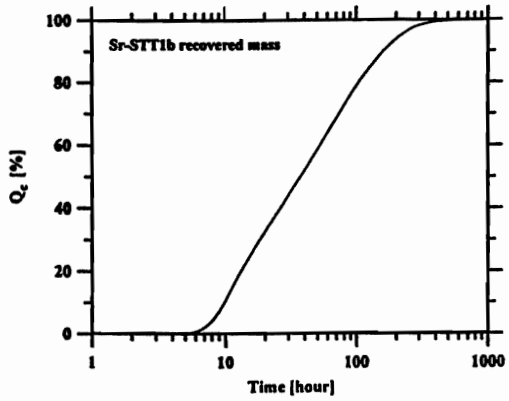

Figure 29: Tracer recovery for strontium-STT1b [%] versus time.

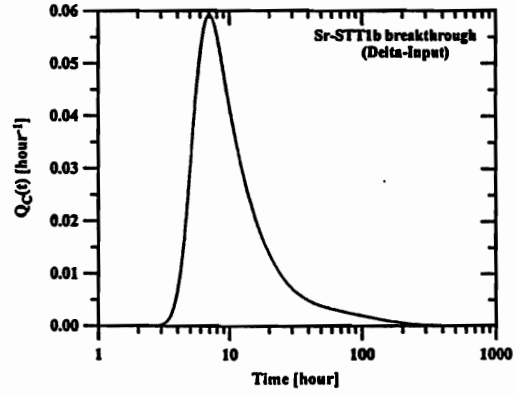

Figure 30: Flow of strontium-STT1b [hour $^{-1}$] versus time [hour] for delta-input.

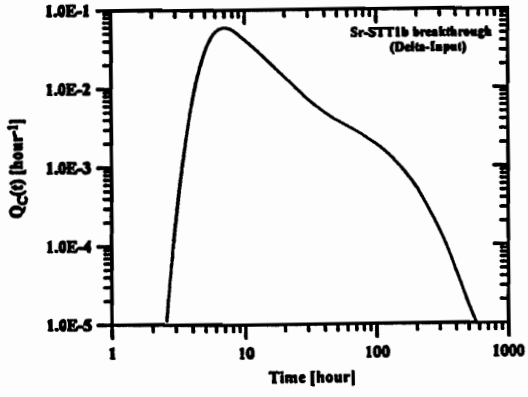

Figure 31: Flow of strontium-STT1b [hour $^{-1}$] versus time [hour] for delta-input.

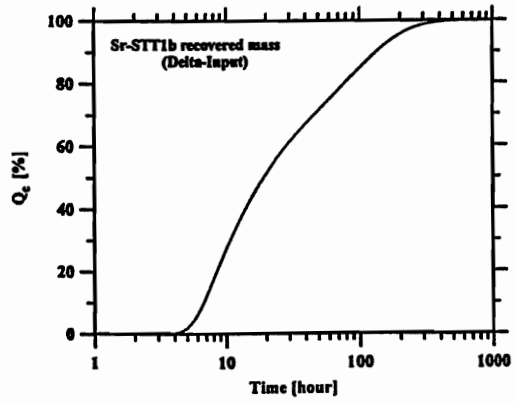

Figure 32: Tracer recovery for strontium-STT1b [%] versus time for delta-input.

3.9. Predictions for potassium

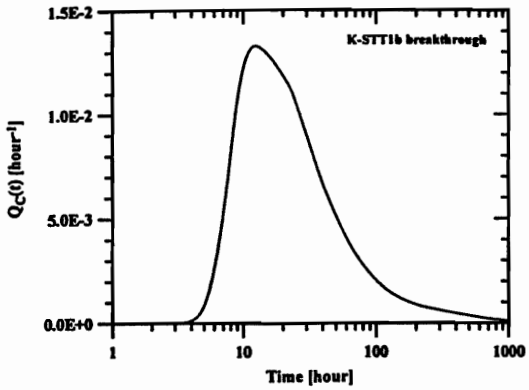

Figure 33: Flow of potassium-STT1b [hour $^{-1}$] versus time [hour].

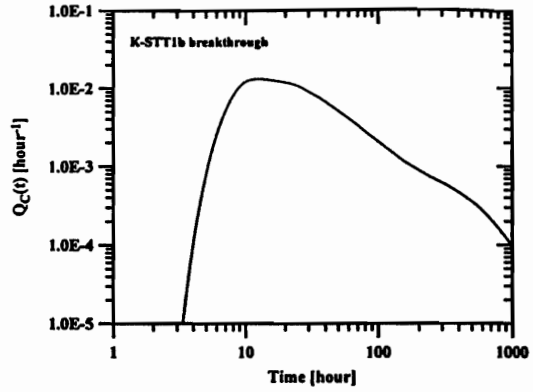

Figure 34: Flow of potassium-STT1b [hour $^{-1}$] versus time [hour].

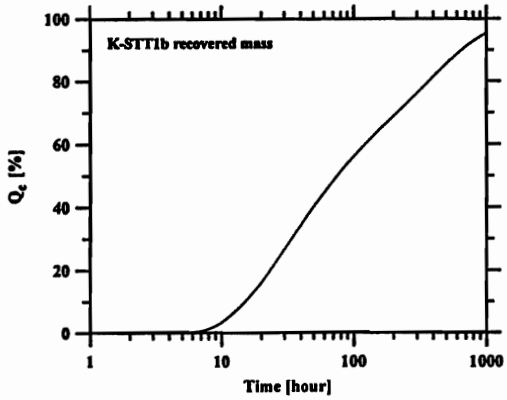

Figure 35: Tracer recovery for potassium-STT1b [%] versus time.

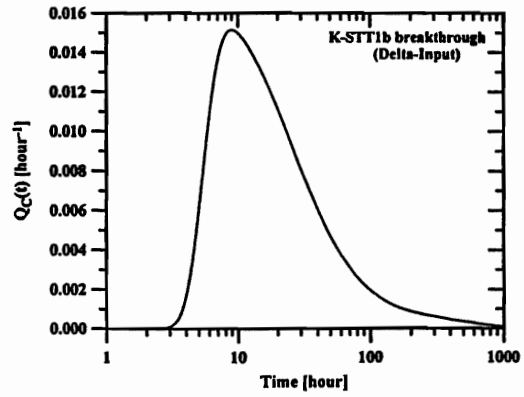

Figure 36: Flow of potassium-STT1b [hour $^{-1}$] versus time [hour] for delta-input.

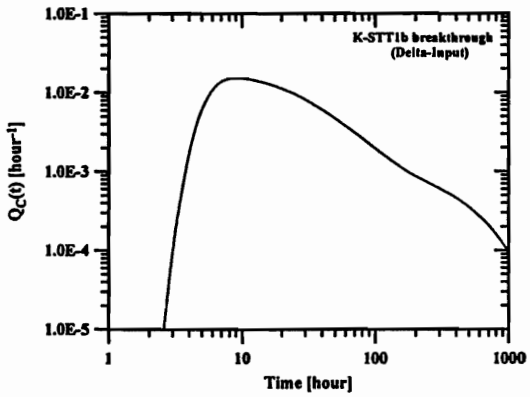

Figure 37: Flow of potassium-STT1b [hour $^{-1}$] versus time [hour] for delta-input.

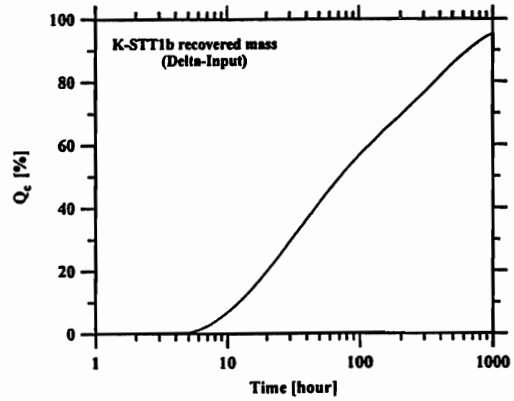

Figure 38: Tracer recovery for potassium-STT1b [%] versus time for delta-input.

3.10. Predictions for rubidium

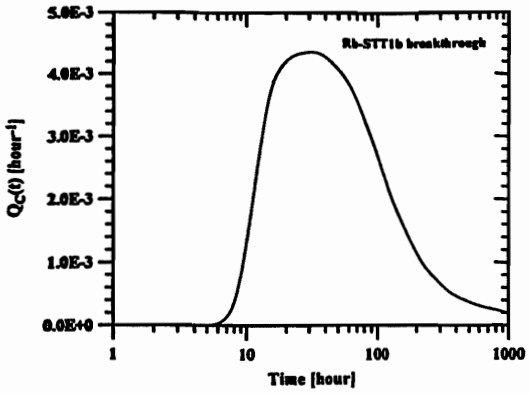

Figure 39: Flow of rubidium-STT1b [hour $^{-1}$] versus time [hour].

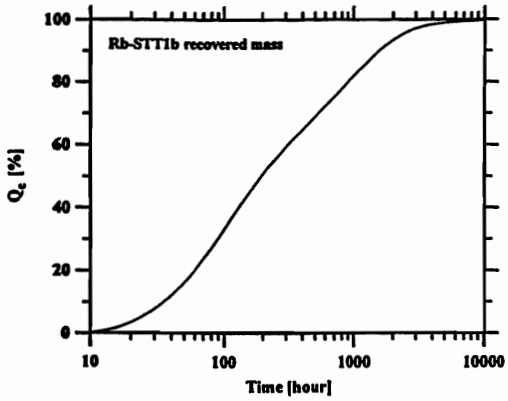

Figure 41: Tracer recovery for rubidium-STT1b [%] versus time.

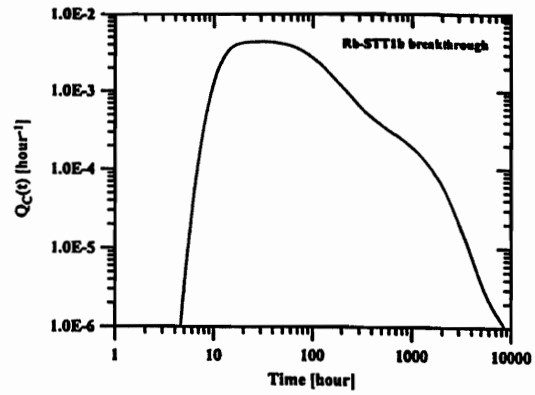

Figure 40: Flow of rubidium-STT1b [hour $^{-1}$] versus time [hour].

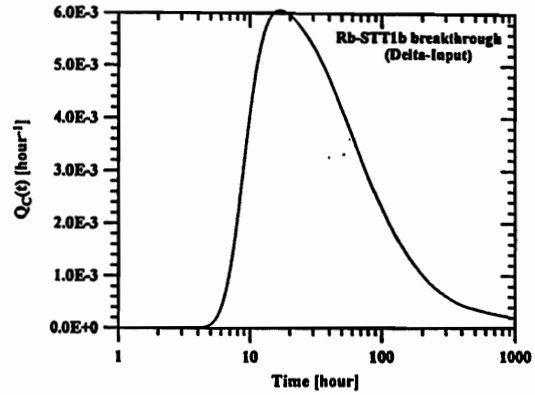

Figure 42: Flow of rubidium-STT1b [hour $^{-1}$] versus time [hour] for delta-input.

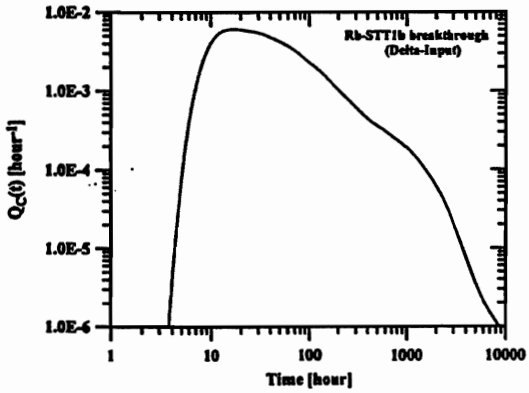

Figure 43: Flow of rubidium-STT1b [hour $^{-1}$] versus time [hour] for delta-input.

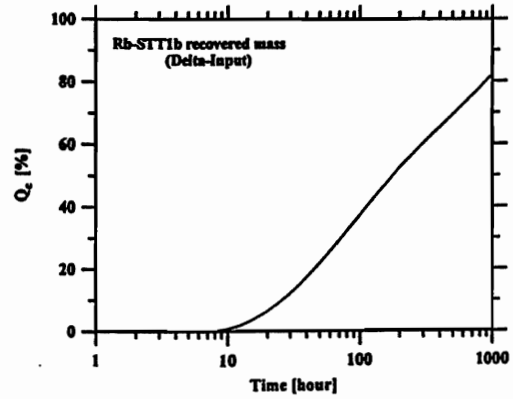

Figure 44: Tracer recovery for rubidium-STT1b [%] versus time for delta-input.

3.11. Predictions for cobalt

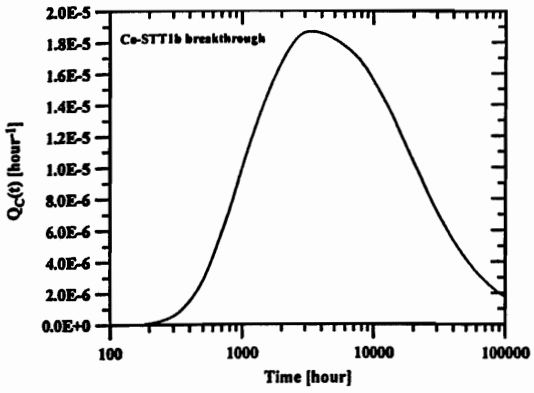

Figure 45: Flow of cobalt-STT1b [hour $^{-1}$] versus time [hour].

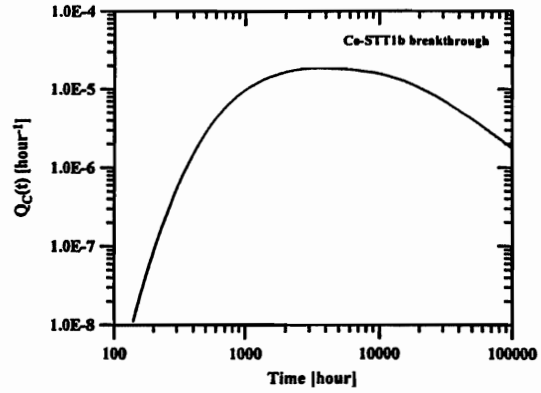

Figure 46: Flow of cobalt-STT1b [hour $^{-1}$] versus time [hour].

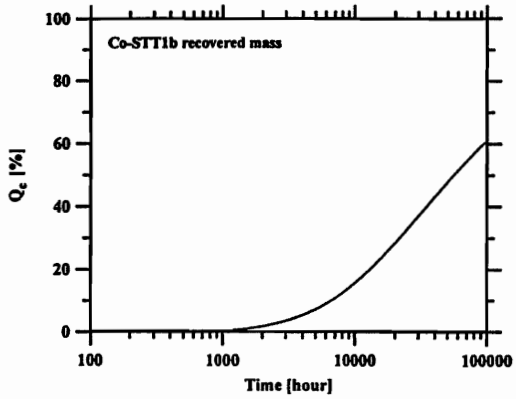

Figure 47: Tracer recovery for cobalt-STT1b [%] versus time.

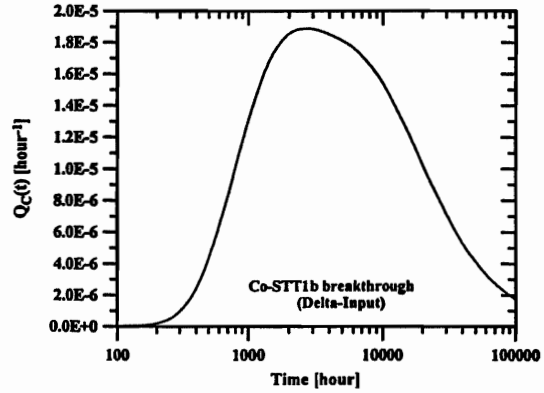

Figure 48: Flow of cobalt-STT1b [hour $^{-1}$] versus time [hour] for delta-input.

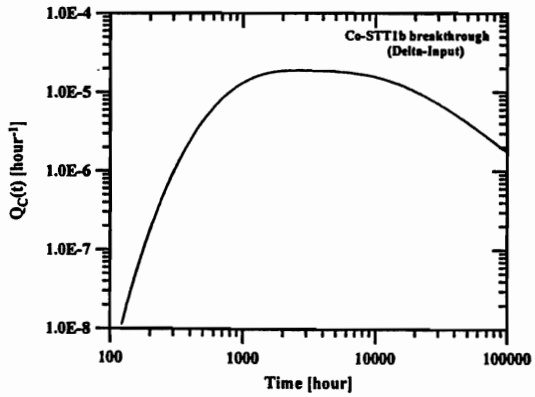

Figure 49: Flow of cobalt-STT1b [hour $^{-1}$] versus time [hour] for delta-input.

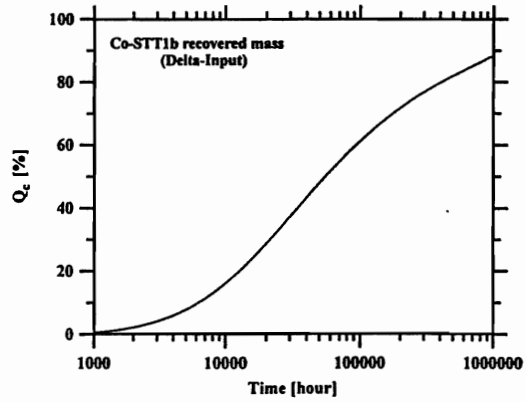

Figure 50: Tracer recovery for cobalt-STT1b [%] versus time for delta-input.

Appendix

Estimates of R_d values for potassium and cobalt for Äspö migration experiments

Bart Baeyens and Mike Bradbury, Paul Scherrer Institute PSI

It should be made clear at the outset that we have no experience of the sorption characteristics of the clay mineral chlorite which we take to be the major material sorbing in the fault gouge, see later. Further, there is so little information available generally that it is impossible to make any rigorous evaluation/prediction of sorption values appropriate to the in situ fault gouge.
Having said this, all that is possible is to "guesstimate" what the required sorption values might be on the basis of reasonable assumptions and our general experience of clay mineral systems.

We assume that

1. Water chemistry data are correct
2. R_d values extracted from breakthrough curves are

representative of distribution ratios for the in-situ fault gouge.

3. The dominant sorption phase is the chlorite fraction (<2 μm) of the fault gouge (~ 8 wt%)

Potassium

We assume that the uptake mechanism for Na, Sr, Ca, Cs, Rb and K is cation exchange on the planar sites of the clay mineral fraction of the fault gauge material, predominantly chlorite. Sorption for these radionuclides would then be expected to be linear.
From the water chemistry it can be seen that the clay minerals are loaded principally with Na and Ca.
Neither the appropriate selectivity coefficients nor the exchange capacity of the clay minerals are known. These parameters are normally required to calculate sorption values in the cation exchange model incorporated in MINSORB (Bradbury and Baeyens, 1995b).
Because of this lack of critical information, the approach adopted was to try to generate selectivity coefficient and site capacity data sets which are compatible with the sorption values supplied and to then use these to predict a sorption value for K.
To a first approximation we assume that the selectivity coefficients governing sorption on the planar sites of different clay minerals of the TOT type such as illite, montmorillonite, chlorite etc. are very similar. In accord with this hypothesis a set of selectivity coefficients for Cs-Na, Rb-Na and K-Na exchange on the planar sites of illite were chosen from the work of Brouwer et al. (1983) and a value for Ca-Na exchange on the planar sites of montmorillonite from Baeyens and Bradbury (1995a). These values are summarised in Table A1.
The cation exchange capacity of chlorite clay minerals (< 2 μm) lies between 100 and 400 meq kg^{-1} (Grim, 1953) which would translate to an estimated 10 to 50 meq kg^{-1} for the Äspö fault gouge.

Ion exchange	Kc	Reference
Ca - Na	4	Baeyens and Bradbury (1995a)
K - Na	8	Brouwer et al. (1983)
Rb - Na	16	Brouwer et al. (1983)
Cs - Na	37	Brouwer et al. (1983)

Table A1: Summary of selectivity coefficients

Note: The selectivity coefficients of Ca-Sr and Ca-Ba exchange are normally close to unity (see for example Brouwer et al. 1983) and the Kc values for Sr-Na and Ba-Na were set equal to that for Ca-Na i.e. Kc = 4

The procedure was then to take the groundwater composition, fix the selectivity coefficients and use the cation exchange site capacity as a variable to find a value giving the best fit to the sorption data for the Na, Rb, Cs, Ca, Sr and Ba obtained from the breakthrough curves. By using a value of 10 meq-kg for the CEC of the :Äspö fault gouge a very good prediction is made for the 2 dominant cations, Na and Ca. (Note that the cation exchange capacity estimated in this way represents an in situ value.) The results of the calculations are given in Table A2.

Nuclide	Concentration in groundwater (M)	R_d from Äspö breakthrough curves (m^3/kg)	R_d estimated (m^3/kg)
Na	7.7 E-2	3.2 E-5	3.3 E-5
Rb	5.0 E-7	1.3 E-3	5.2 E-4
Cs	3.0 E-8	2.6 E-3	1.1 E-3
Ca	3.3 E-2	1.0 E-4	1.2 E-4
Sr	2.4 E-4	4.6 E-5	1.2 E-4
Ba	4.0 E-7	1.2 E-3	1.2 E-4
K	**3.7 E-4**	**—**	**2.6 E-4**

Table A2: R_d values from breakthrough curves and calculated values.

The data for Rb and Cs are under predicted by a factor of about 2. This is not entirely unexpected since the selectivities used were obtained at much higher clay mineral loadings than is the case here and the selectivity coefficients of these two alkali metals tend to increase with decreasing loadings. Also a factor of 2 uncertainty in selectivity coefficients is not unusual, particularly when they have not been determined on the system in question.
It may well be that K also behaves in this manner so an R_d value in the range 3 to $6 \cdot 10^{-4}$ m^3 kg^{-1} might be expected with a preferred value near the top end of the range.

We propose a K sorption value for Äspö fault gouge of $5 \cdot 10^{-4}$ m^3 kg^{-1}.

The reason why there is such a discrepancy between Sr and Ba is unclear based on pure cation exchange concepts. Normally similar values would be expected (see above).
Grütter et al. (1993) have investigated the sorption of Sr and Ba on chlorite (<40 μm) and observed considerably higher sorption values for Ba than for Sr which would be in accord with the general trend in the sorption values extracted from the breakthrough curves. However, the sorption data for Sr measured by Grütter et al. (1993) is compatible with a Sr-Ca selectivity coefficient of unity which was effectively used for the prediction presented in Table A2.

Why the laboratory sorption value for Ba is approximately two orders of magnitude greater than that of Sr under similar experimental conditions is not clear to us.

Cobalt

No reliable sorption data exist for Co on Äspö fault gouge material. Also, it is anticipated that Co will most probably sorb by a surface complexation mechanism at the pH of the Äspö groundwater (~ 7.5). Sorption by surface complexation is much more complicated than cation exchange and it is considerably more difficult to make "guesstimates" of sorption values.

Grütter et al. (1993) have measured sorption of Co (and Ni) on chlorite (< 40 μm). The cation exchange capacity of the material used was ~ 14 meq kg^{-1} i.e. relatively close to the estimated in situ value above. R_d values for Co measured in a synthetic groundwater (pH -7.7, $CaCl_2 \sim 2 \cdot 10^{-3}$ M) varied between 4 m^3 kg^{-1} and 0.3 m^3 kg^{-1} for Co equilibrium concentrations between ~ 10^{-8} and ~ 10^{-5} M respectively. (For Co sorption by surface complexation the composition of the Äspö groundwater is not expected to have any great influence on sorption values taken from Grütter et al., 1993.)

Based on the very sparse information available, we would propose a sorption value for Co of ~ 1 m^3 kg^{-1} provided that the equilibrium concentrations of Co are very low, < 10^{-7} M.

References

BAEYENS, B. and BRADBURY, M. H. (1995a): "A quantitative mechanistic description of Zn, Ca and Ni sorption on Na-montmorillonite. Part II: Sorption measurements", PSI-Bericht Nr. 95-11. Paul Scherrer Institute, Villigen, Switzerland and Nagra Technical Report NTB 95-05, Nagra, Wettingen, Switzerland.

BRADBURY, M. H. and BAEYENS, B. (1995b): "A quantitative mechanistic description of Ni, Zn and Ca sorption on Na-montmorillonite, Part III: Modelling", PSI-Bericht Nr. 95-12. Paul Scherrer Institute, Villigen, Switzerland and Nagra Technical Report NTB 95-06, Nagra, Wettingen, Switzerland.

BROUWER, E., BAEYENS, B., MAES, A. and CREMERS, A. (1983): "Caesium and rubidium ion equilibria in illite clay", J. Phys. Chem. **87**, 1213-1219.

GRIM, R.E. (1953): "Clay Mineralogy", Mc Graw Hill, New York.

GRÜTTER, A., VON GUNTEN, H.R., RÖSSLER, E. AND KEIL, R. (1994): "Sorption of nickel and cobalt on a size-fraction of unconsolidated glaciofluvial deposits and on clay minerals", Radiochimica Acta **65**, 181-187.

References

[1] **Jakob, A., Heer, W.:** "Blind-predictions of the Task 4E tracer migration experiments at the TRUE-1 site", in: SKB Progress Report HRL-98-01, Proceedings of the 10th meeting in Kamaishi, Japan, November 11 - 13, 1997, Stockholm, Sweden, 1998.

[2] **Jakob, A., Heer, W., Mazurek, M.:** "Tracer migration experiments at the Äspö TRUE-1 site – blind-predictions and inverse modelling for the STT-1 tracer test", to be published in Äspö Hard Rock Laboratory International Cooperation Report ICR 98-xx, SKB, Stockholm, Sweden.

[3] **Mazurek, M., Bossart, P., Eliasson, T.:** "Classification and characterisation of water-conducting features at Äspö: Results of investigations on the outcrop scale", Äspö Hard Rock Laboratory International Cooperation Report ICR 97-01, SKB, Stockholm, Sweden, (especially chapters 7, 8.5, 8.6 and Figure 8.8).

[4] **Andersson, P., Byegard, J., Cvetkovic, V., Johansson, H., Nordqvist, R., Selroos, J.-O., Winberg, A.:** "Experimental plan for tests with sorbing tracers at the TRUE-1 site", Äspö Hard Rock Laboratory, Progress Report HRL-97-07, 1997 (especially Table 3-7).

The interaction of sorbing and non-sorbing tracers with different Äspö rock types.

Sorption and diffusion experiments in the laboratory scale.

Johan Byegård, Henrik Johansson, Mats Skålberg (CTH),
Eva Lena Tullborg (Terralogica)

The Interaction of Sorbing and Non-Sorbing Tracers with Different Äspö Rock Types Sorption and Diffusion Experiments in the Laboratory Scale

Johan Byegård, Henrik Johansson and Mats Skålberg
Department of Nuclear Chemistry
Chalmers University of Technology
S-412 96 Göteborg, Sweden

Eva-Lena Tullborg
Terralogica AB
Box 4140
S-44314 Gråbo, Sweden

Final draft: 98.08.27

Abstract

Laboratory experiments studying the sorption and diffusivity of different tracers in Äspö Hard Rock Laboratory (ÄHRL) site specific conditions have been performed. The experiments were conducted by applying both the batch sorption and the through diffusion technique. The investigation was focused on slightly sorbing tracers, i.e., alkaline metals (Na^+, Rb^+ and Cs^+) and alkaline earth metals (Ca^{2+}, Sr^{2+} and Ba^{2+}), but some presumed non-sorbing species have also been included. The dominating generic rock material from ÄHRL, Äspö diorite and Fine-grained granite, were used as well as some altered wall rock and mylonites from the Feature A fracture, the fracture where *in situ* migration studies are presently being performed. Synthetic groundwater was used, similar to the high saline groundwater found at the 350 m level at ÄHRL and at the Feature A site.

The results of batch experiments show that the sorption of the tracers increase in the order $Na^+ < Ca^{2+} \approx Sr^{2+} < Rb^+ \approx Ba^{2+} < Cs^+$ with the sorption coefficient of Na^+ in the order of $(4\text{-}30)\cdot10^{-6}$ m^3/kg and for Cs^+ in the range of $(1\text{-}400)\cdot10^{-3}$ m^3/kg. The variations in sorption coefficients are due to differences in the composition of the geological material, contact time and particle size. Sorption is generally stronger for the Äspö diorite than for the Fine-grained granite which is explained by the much higher concentration of biotite in Äspö diorite than in Fine-grained granite. In the altered material the biotite has been transformed to chlorite and a lower sorptivity is shown for those material compared to the fresh diorite and granite, respectively. Attempts to explain the sorption and desorption results to a surface sorption - diffusion model are presented.

The diffusion results show that the tracers were retarded in the same order as was expected from the measured batch sorption coefficients. Furthermore, the largest size fraction was the most representative when comparing batch sorption coefficients with sorption coefficients evaluated from the diffusion experiments. The observed effective diffusivities and transport porosities decreased with increasing sample lengths. It was also observed that the formation factor obtained for sorbing and non-sorbing tracers in the same sample is approximately equal.

A heteogeneous and mineral specific porosity distribution was found in the Äspö diorite using the ^{14}C-PMMA method, whereas the porosity pattern of Fine-grained Granite was more uniformly distributed. The porous mineral areas were found to be consistent with the sorptive mineral areas in Äspö diorite. A double porosity network of slow and fast migration pathways, with different sorption capabilites, was used to describe the diffusion of Cs and Ba.

The diffusivity and porosity was low in the Feature A sample containing mylonite compared to the generic material.

Appendix C – Task 5 Preliminary modelling

Contents:

The origin and composition of groundwater leaking into the Äspö tunnel.

Urban Svenson (SKB/CFE)

Objectives

- **General : Integrate/compare hydrological and chemical information.**
- **This project:**
  - **Evaluate two methods for transport calculations.**
  - **Estimate the origin and composition of groundwater leaking into the Äspö tunnel.**

Outline

- **Describe the problem studied.**
- **Introduce the methods for transport calculations.**
- **Results, steady state.**
- **Results, transient.**
- **Results, comparisons with chemical data.**
- **Discussion/Conclusions.**

THE ORIGIN AND COMPOSITION OF GROUNDWATER LEAKING INTO THE ÄSPÖ TUNNEL

Urban Svensson
CFE AB

Transport models

Backtracking

- **Reverse the flow field and release particles where the water leaks into the tunnel.**

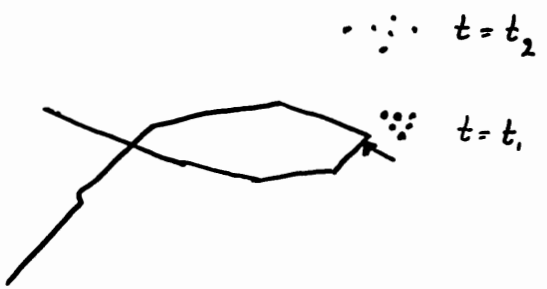

The Fluid Population Method

- **Use Advection/Diffusion equations to track the origin of the water leaking into the tunnel.**

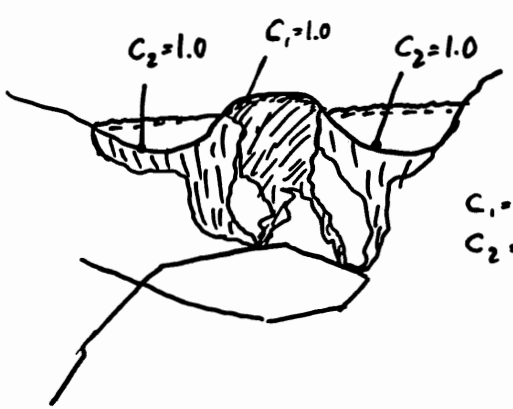

The problem studied

Basic question: **Where does the water leaking into the tunnel come from?**

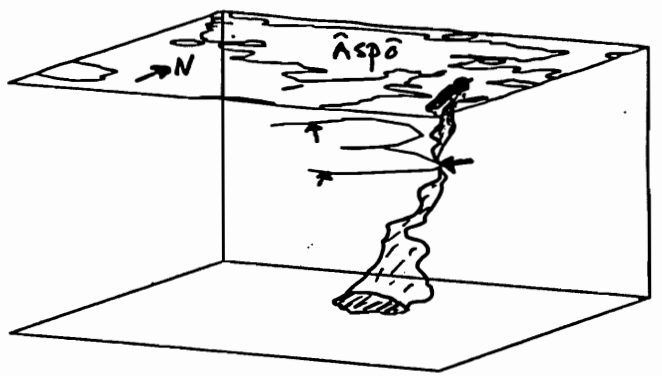

Steady or transient?

- **One can estimate the transport velocity in the fracture zones to 10m/day. This means that water from the domain boundaries may reach the tunnel in a few months time.**

Assumption used in this study

- **The steady-state flow fields (for complete tunnel) from regional (TR 97-09) and site-scale (TR 97-17) models are used in this study.**

Table 1. Comparison of the two transport models. Contributions (in %) from boundary areas in the site-scale model to inflow sections in the tunnel. The two figures in each box are from the Fluid Population Method (top) and the particle tracking.

Tunnel section (m)	Selected zone(s) for withdrawal	PA	BS	PM	BO	SH	SL	NH	NL	WH	WL	EH	EL
0-850	NE4	0.0	30.7	9.2	0.0	59.3	0.2	0.0	0.0	0.0	0.0	0.6	0.0
		0.0	30.5	9.2	0.0	59.4	0.2	0.0	0.0	0.0	0.0	0.7	0.0
850-1030	NE3	0.0	18.5	9.8	0.0	47.0	5.7	0.0	0.0	0.1	0.1	18.2	0.5
		0.0	19.2	9.3	0.0	46.9	5.4	0.0	0.0	0.0	0.0	18.5	0.6
1030-1160	NNW3	0.1	23.4	5.3	0.1	40.5	6.3	0.0	0.0	0.2	0.2	23.5	0.5
		0.1	23.4	5.2	0.0	40.0	6.5	0.0	0.0	0.2	0.2	23.8	0.5
1160-1310	NE1	3.7	65.1	3.1	0.2	3.2	2.2	0.0	0.0	14.7	2.6	4.8	0.4
		3.5	65.6	3.0	0.2	3.2	2.1	0.0	0.0	14.6	2.6	4.9	0.3
1310-1460	EW3	11.6	65.6	3.8	0.3	0.5	1.6	0.0	0.0	7.1	3.9	5.1	0.5
		11.2	65.9	4.2	0.2	0.6	1.3	0.0	0.0	6.9	4.1	5.2	0.5
1460-1584	NE2	20.0	55.1	0.1	9.3	0.1	1.2	0.1	0.0	5.3	8.4	0.2	0.1
		20.5	54.8	0.1	8.9	0.1	1.2	0.1	0.0	5.4	8.6	0.3	0.1
1584-1745	NNW7	47.3	27.4	0.0	2.3	0.0	0.1	10.9	1.4	9.0	1.6	0.1	0.0
		47.7	26.6	0.0	2.3	0.0	0.1	10.6	1.4	9.6	1.7	0.1	0.0
1745-1883	NNW1	78.2	10.1	0.0	0.0	0.0	0.0	11.3	0.2	0.0	0.0	0.2	0.0
		78.5	9.3	0.0	0.0	0.0	0.0	11.9	0.1	0.0	0.0	0.2	0.0
1745-1883	NNW2	68.3	27.9	0.0	0.0	0.0	0.0	3.6	0.0	0.0	0.0	0.1	0.0
		68.0	28.0	0.0	0.0	0.0	0.0	3.8	0.0	0.0	0.0	0.1	0.0
1883-2028	NNW4	16.7	78.8	4.5	0.0	0.0	0.0	0.0	0.0	0.0	0.0	0.0	0.0
		16.0	79.9	4.2	0.0	0.0	0.0	0.0	0.0	0.0	0.0	0.0	0.0
2028-2178	NNW4	5.3	84.6	0.0	0.0	0.0	0.0	0.0	0.0	0.0	0.0	1.8	0.0
		5.5	84.6	0.2	0.0	0.0	0.0	0.0	0.0	0.0	0.0	1.6	0.0
2178-2357	NNW1	22.7	23.3	1.4	6.4	0.4	6.5	2.1	0.4	2.7	23.7	8.4	1.9
		23.0	23.4	1.6	5.9	0.4	6.6	2.2	0.4	3.0	23.5	8.3	1.8
2178-2357	NNW2	1.7	74.5	17.9	0.0	0.0	0.0	0.0	0.0	0.0	0.0	5.8	0.0
		1.7	74.7	17.8	0.0	0.0	0.0	0.0	0.0	0.0	0.0	5.7	0.0
2357-2496	NE2	0.1	1.3	0.1	10.9	0.6	4.0	0.0	0.0	21.1	61.3	0.4	0.2
		0.1	1.3	0.0	10.8	0.6	4.0	0.0	0.0	20.3	62.2	0.5	0.1
2496-2699	NNW7	4.2	7.1	0.0	54.4	0.0	0.6	5.3	5.0	13.9	9.3	0.1	0.0
		4.4	6.3	0.0	53.5	0.0	0.6	5.6	5.0	14.7	9.7	0.0	0.1
2699-2875	NNW1	0.7	1.0	0.0	32.6	0.0	0.0	30.8	32.5	0.1	0.4	1.7	0.1
		0.6	0.8	0.0	33.1	0.0	0.0	30.5	32.7	0.1	0.5	1.6	0.1
2699-2875	NNW2	11.7	13.7	0.0	22.1	0.0	0.0	30.3	15.1	0.0	0.0	6.5	0.6
		11.4	13.3	0.0	22.4	0.0	0.0	30.2	15.2	0.0	0.0	6.9	0.6
2875-2994	NNW4	19.7	16.6	0.4	20.1	0.0	0.0	10.7	6.0	0.0	0.0	17.5	9.0
		20.1	16.4	0.4	20.2	0.0	0.0	10.5	6.2	0.0	0.0	17.5	8.6
2994-3179	NNW4	4.8	39.9	16.8	15.6	0.0	0.8	0.2	0.3	0.0	0.4	17.3	3.9
		5.1	39.5	17.0	15.3	0.0	0.5	0.2	0.3	0.0	0.4	17.5	4.1
3179-3426	NNW1	0.0	0.3	0.1	71.8	0.1	5.9	0.1	0.5	0.6	17.5	1.9	1.1
		0.0	0.4	0.1	73.0	0.1	5.0	0.1	0.6	0.7	16.7	2.2	1.0
3179-3426	NNW2	2.2	26.8	7.2	35.3	0.1	4.6	0.6	0.8	0.4	5.5	14.1	2.3
		2.3	27.6	7.1	34.5	0.1	4.1	0.7	1.0	0.4	5.1	14.7	2.4
3426-3600	NNW5	7.2	8.9	0.0	16.1	0.1	0.5	0.0	0.0	32.6	34.5	0.0	0.0
		7.8	8.8	0.0	15.9	0.2	0.5	0.0	0.0	32.5	34.3	0.0	0.0
Shaft	NNW7	70.9	16.6	0.1	4.5	0.0	0.9	0.4	0.0	0.3	5.6	0.5	0.1
		70.6	16.6	0.1	4.5	0.0	0.9	0.5	0.0	0.4	5.8	0.5	0.1

Results, steady-state

- **In the steady-state limit all water leaking into the tunnel must origin from the domain boundaries.**

- **Use the two transport models to determine the contributions from the boundaries.**

Site-scale model

Domain boundaries are identified as follows:

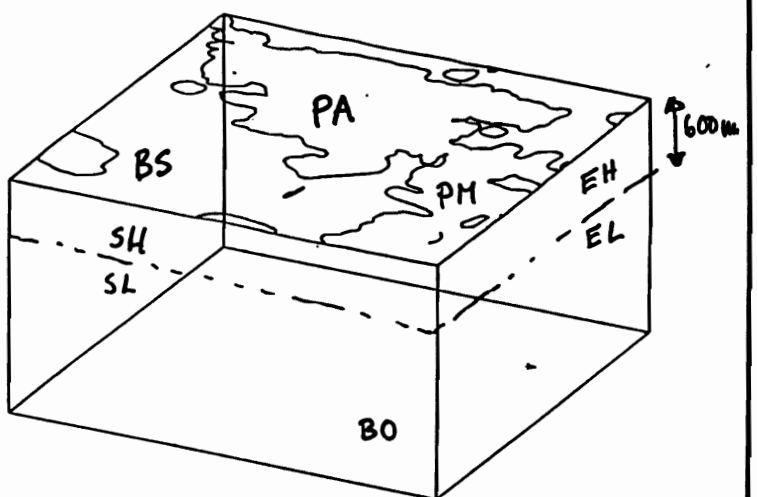

PA = Precipitation Äspö
PM = -"- Mjälen
BS = Baltic Sea
EH = East High
EL = East Low
BO = Bottom bound.

Regional scale

Domain boundaries are identified as follows:

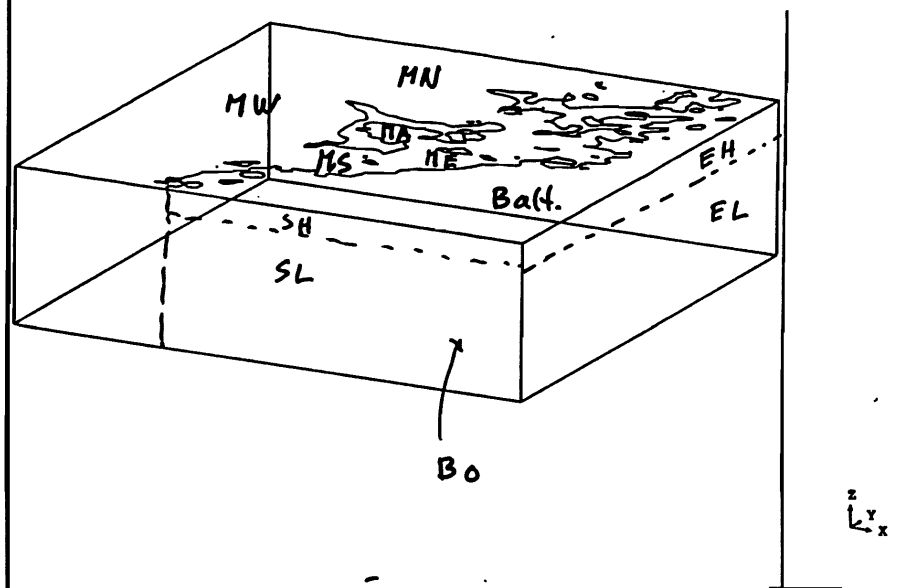

MA = Meteoric Åspö

ME = -"- East of Åspö

Balt = Baltic sea

Bo = Bottom boundary, brine

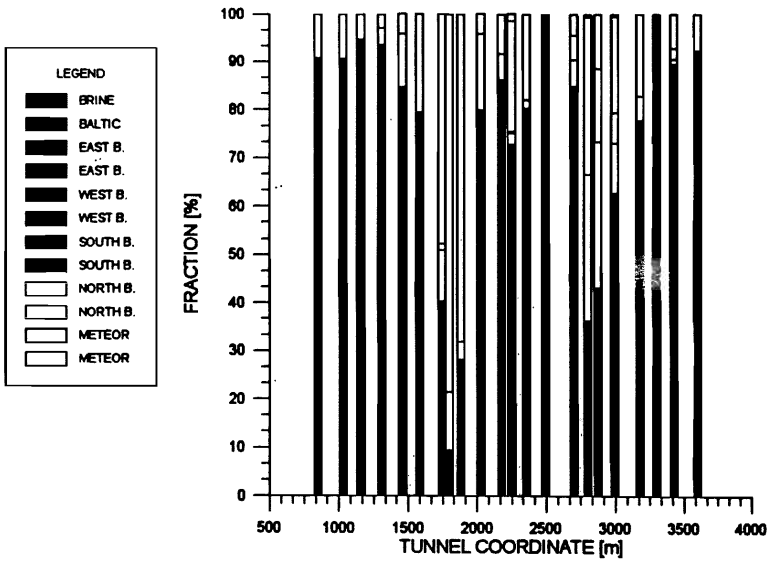

Figure 1. Water composition along the tunnel, based on the site-scale model.

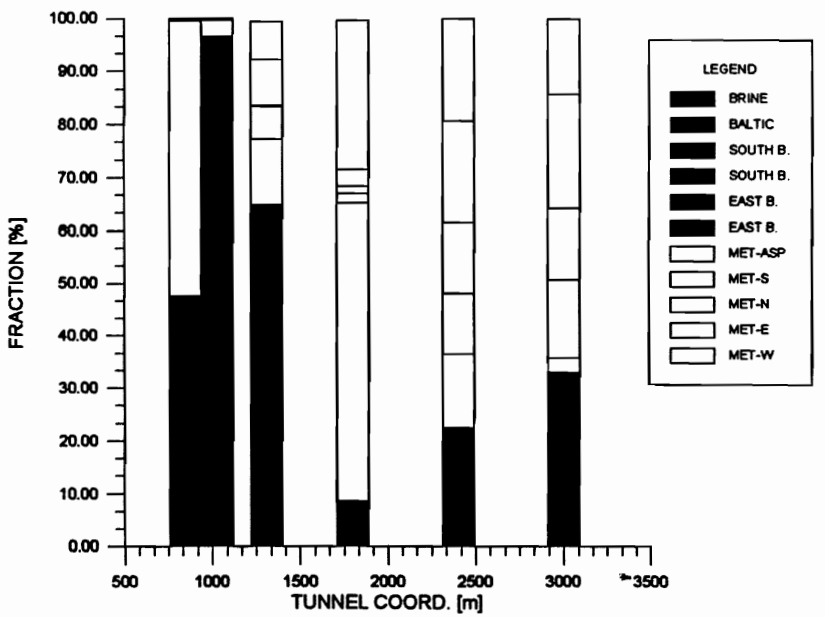

Figure 2. Water composition along the tunnel, based on the regional-scale model.

Table 2. Comparison of the two transport models. Contributions (in %) from boundary areas in the regional-scale model to inflow sections in the tunnel. The two figures in each box are from the Fluid Population Method (top) and the particle tracking.

Tunnel section (m)	Selected zone(s) for withdrawal	MA	MS	MN	ME	MW	Balt.	Brine	SH	SL	EH	EL
0-850	NE4	0.0 0.0	46.7 46.5	0.1 0.2	0.3 0.3	51.9 52.0	0.0 0.0	0.0 0.0	0.8 0.0	0.1 0.0	0.0 0.0	0.0 0.0
850-1 030	NE3	0.0 0.0	96.6 96.6	0.4 0.4	0.1 0.0	3.0 3.0	0.0 0.0	0.0 0.0	0.0 0.0	0.0 0.0	0.0 0.0	0.0 0.0
1 030-1 310	NE1	12.3 12.5	64.4 64.8	7.2 7.3	8.6 8.3	6.2 6.1	0.1 0.0	0.0 0.0	0.4 0.0	0.2 0.0	0.0 0.0	0.0 0.0
≈ 1 800	NNW*	56.7 56.9	8.5 8.7	28.1 28.3	3.2 3.1	1.7 1.8	1.4 1.2	0.0 0.0	0.0 0.0	0.0 0.0	0.1 0.0	0.0 0.0
≈ 2 400	NNW*	13.8 14.3	12.3 12.5	19.1 18.5	19.2 19.3	11.6 11.5	13.6 13.4	1.4 1.1	1.3 1.2	2.0 1.6	2.8 2.9	2.8 2.6
≈ 3 000	NNW*	2.7 2.8	10.1 10.1	14.2 14.0	21.6 21.6	14.9 14.8	13.6 13.6	3.4 3.4	2.5 2.4	5.3 5.3	5.3 5.3	6.4 6.2

The columns are mixed up!

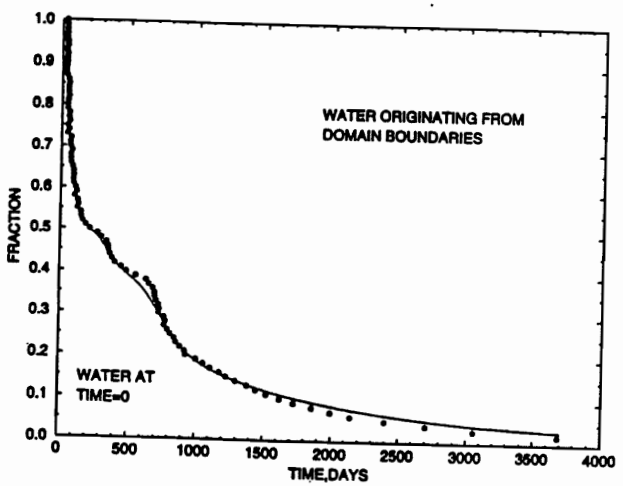

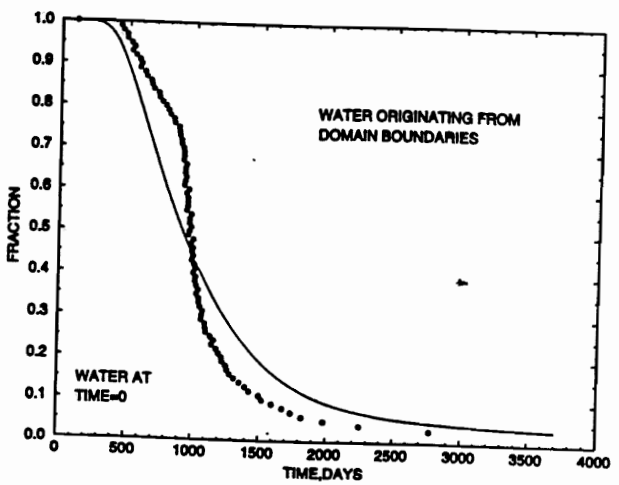

Figure 3. Transient response to the tunnel. Replacement of water in NE1 (top) and NNW1 (coord. 1745 - 1883 m).
—— Fluid Population Method
• Particle tracking

Results, transient

Questioned addressed: **How long time does it take to replace the water in a box (1.2 x 1.2, 1.0 km^3), centred around the tunnel, with water from outside the boundaries?**

Backtracking

Keep track of how many particles have reached the boundary of the box.

Fluid Population Method

Specify a variable which has the initial value 1.0 everywhere in the domain and has the value 0.0 on all boundaries.

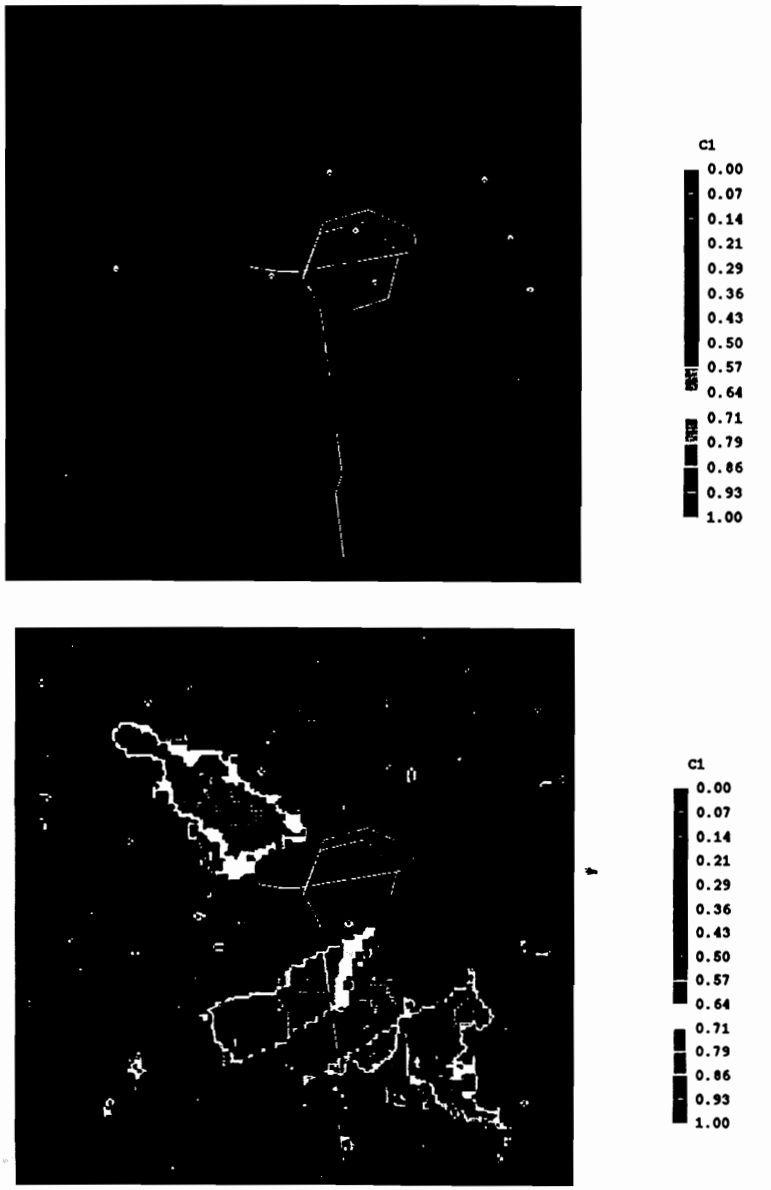

Figure 5. Distribution of water marked at $t = 0$ after 10 years of integration. Top, 450 m depth; bottom 700 m depth.

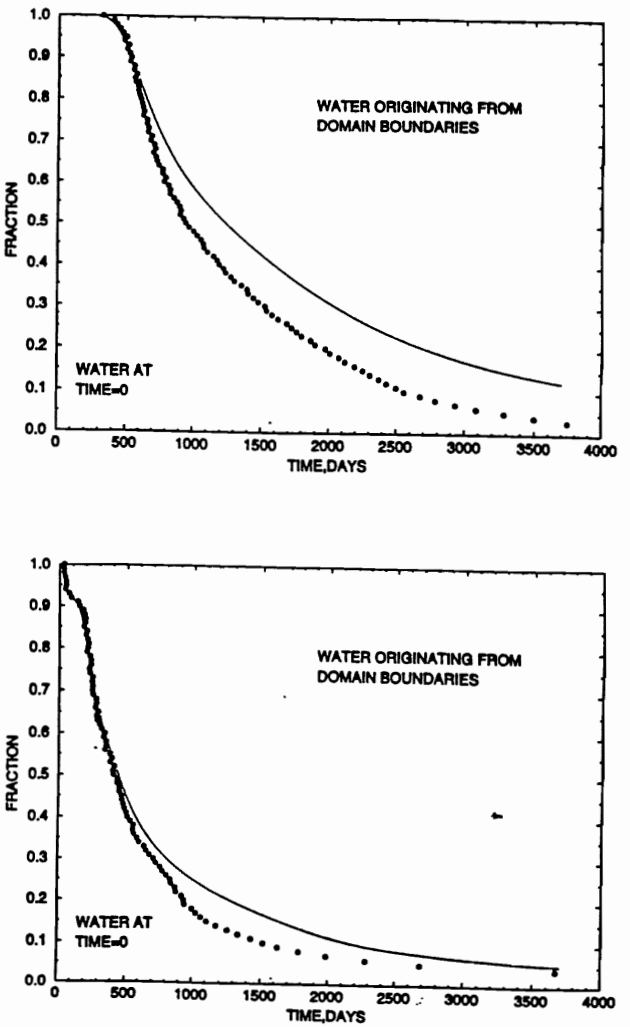

Figure 4. Transient response to the tunnel. Replacement of water in NNW1 (coord. 2699 - 2875 m) and NNW4 (coord. 2994 - 3179 m).

—— Fluid Population Method

• Particle tracking

Comparison with chemical data

Approach: The boundary areas identified earlier can be used to classify the origin of various water types, with known chemical character.

Example:

BO (Bottom) ↔ Brine

BS (Baltic Seawater) ↔ Modern Baltic Water

PA, PM (Precipitation Äspö, Mjälen) ↔ Meteoric

NH (North High) ↔ Old Marine Water etc

We are thus close to the point where a first comparison between "hydrological and chemical" estimates can be done.

Example:

Fracture		Meteoric	Baltic Sea	Glacial	Brine	Others
NE1	chemical	16	76	6	2	0
	hydrol	7	65	1	0	27

However, it is still unclear how waters entering through the vertical boundaries should be classified.

Concluding remarks

- **The two transport models evaluated are found to be in close agreement.**
- **The composition and origin of the water leaking into the Äspö tunnel have been determined.**
- **We are close to the point where a first comparison with chemical data can be made.**

Large scale integrated hydrologic and Geochemical Model of the Äspö site

William Dershowitz (Golder) & Masahiro Uchida (PNC)

PAWorks Pathways Analysis in Support of Task 5

Large Scale Integrated Hydrologic and Geochemical Model of the Äspö Site

Äspö Modeling Task Force Meeting
Äspö, Sweden
1 September, 1998

Bill Dershowitz/Golder
Masahiro Uchida/PNC

Task 5 FracMan/PAWorks Study

- **Geochemical Prediction of End Member Breakthrough to Äspö Tunnels**
  - **Integration of Geochemistry and Hydrogeology with DFN Approach**
  - **Improve Understanding of Transport Pathways**

923 1089.824/67929

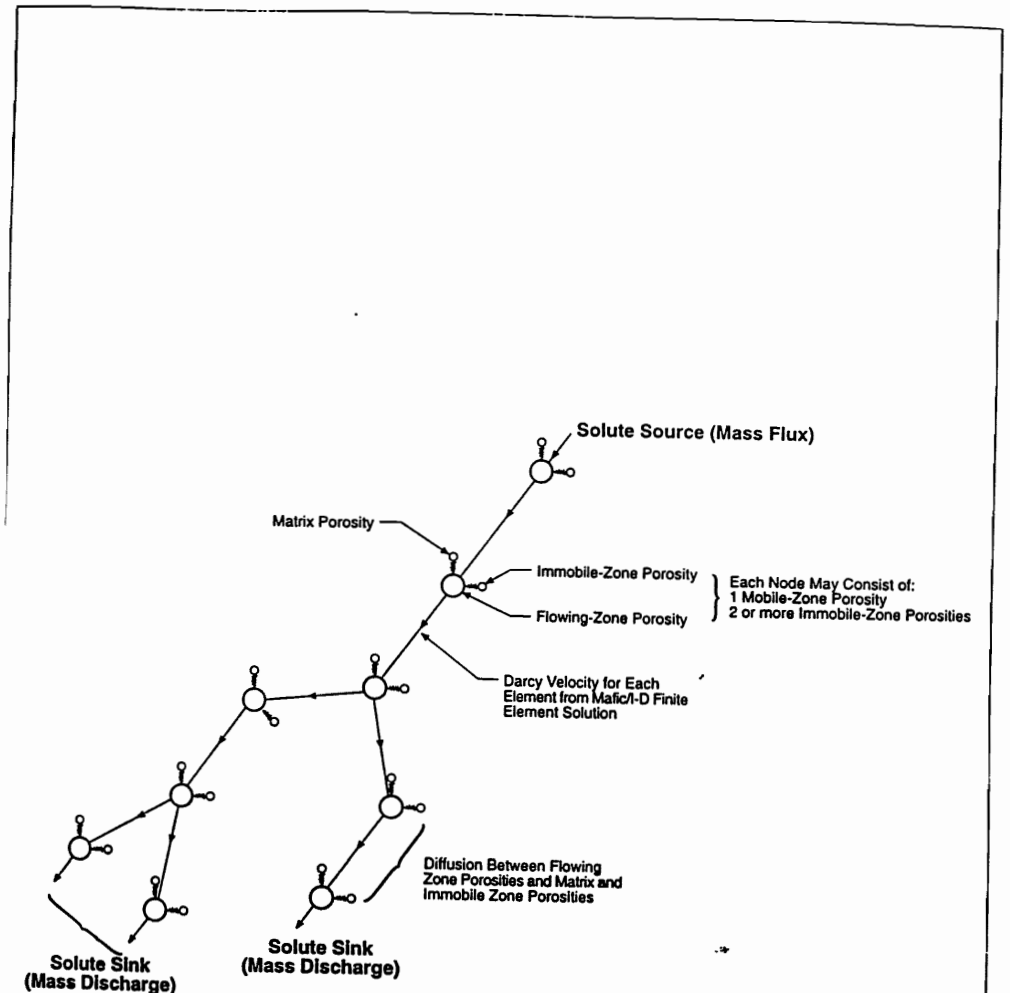

FIGURE **1-5**
PAWorks/LTG SOLUTE TRANSPORT
PNC/PAWORKS/JAPAN

PROJECT NO. 923 1089.911 DRAWING NO. 79136 DATE 7/22/96 DRAWN BY EA

Golder Associates

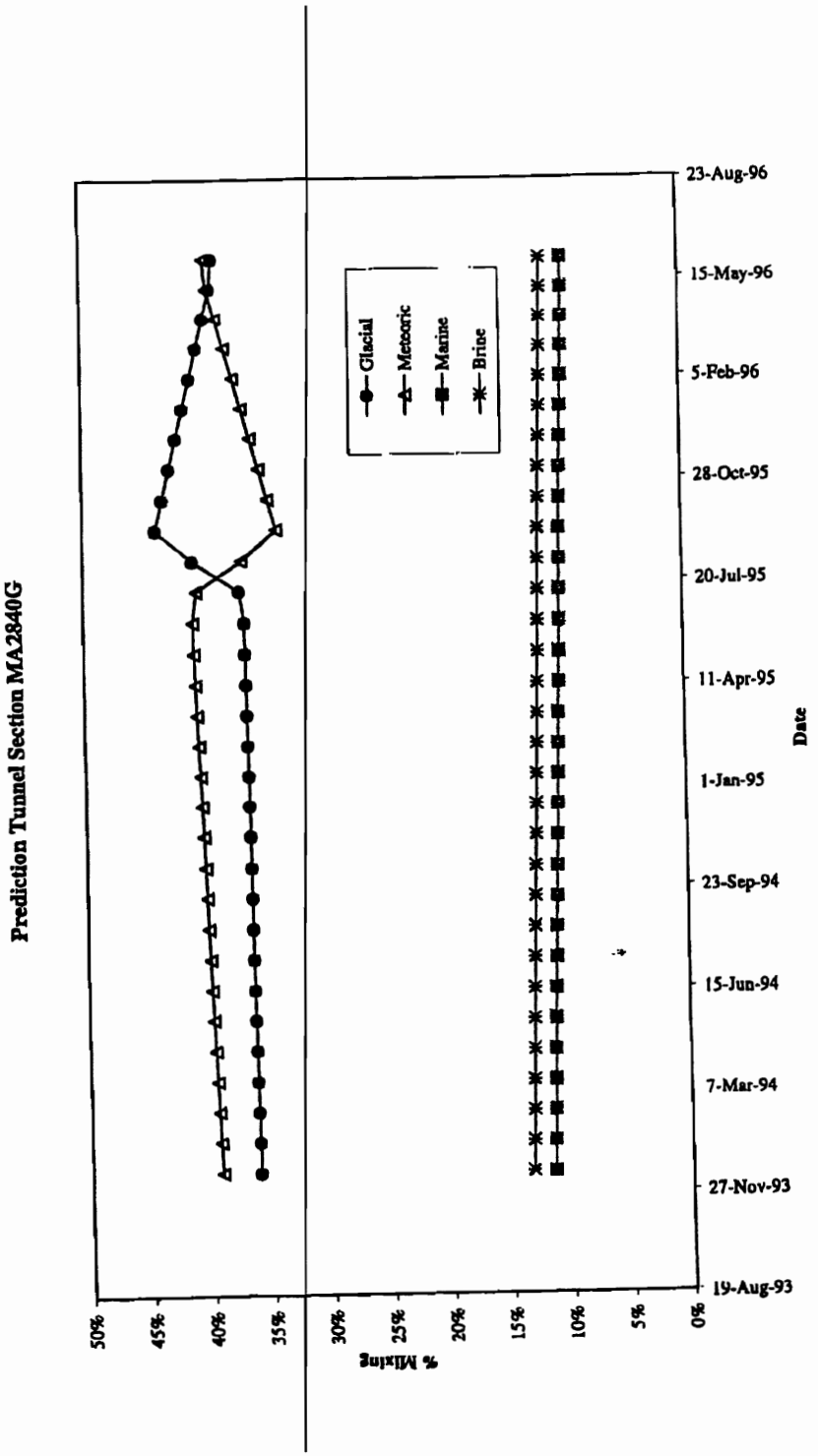

Task 5 FracMan/PAWorks Study

- **Initial "Task 3" DFN Hydrogeological Model**
  - **SKB Äspö Structural Model**
  - **Background Fracturing Based on Tunnel Maps**
  - **Weir Flux Boundary Condition**
  - **Forward Model Matched Measured Borehole Pressure Response Time Histories**
- **Geochemical Calibration of Hydrogeologically Based DFN Model**
  - ~~**"Task 3 Hydrogeological Model" with Weir Flux BC**~~
  - **Comparison of Measured and Predicted End Member Breakthrough at Control Points**

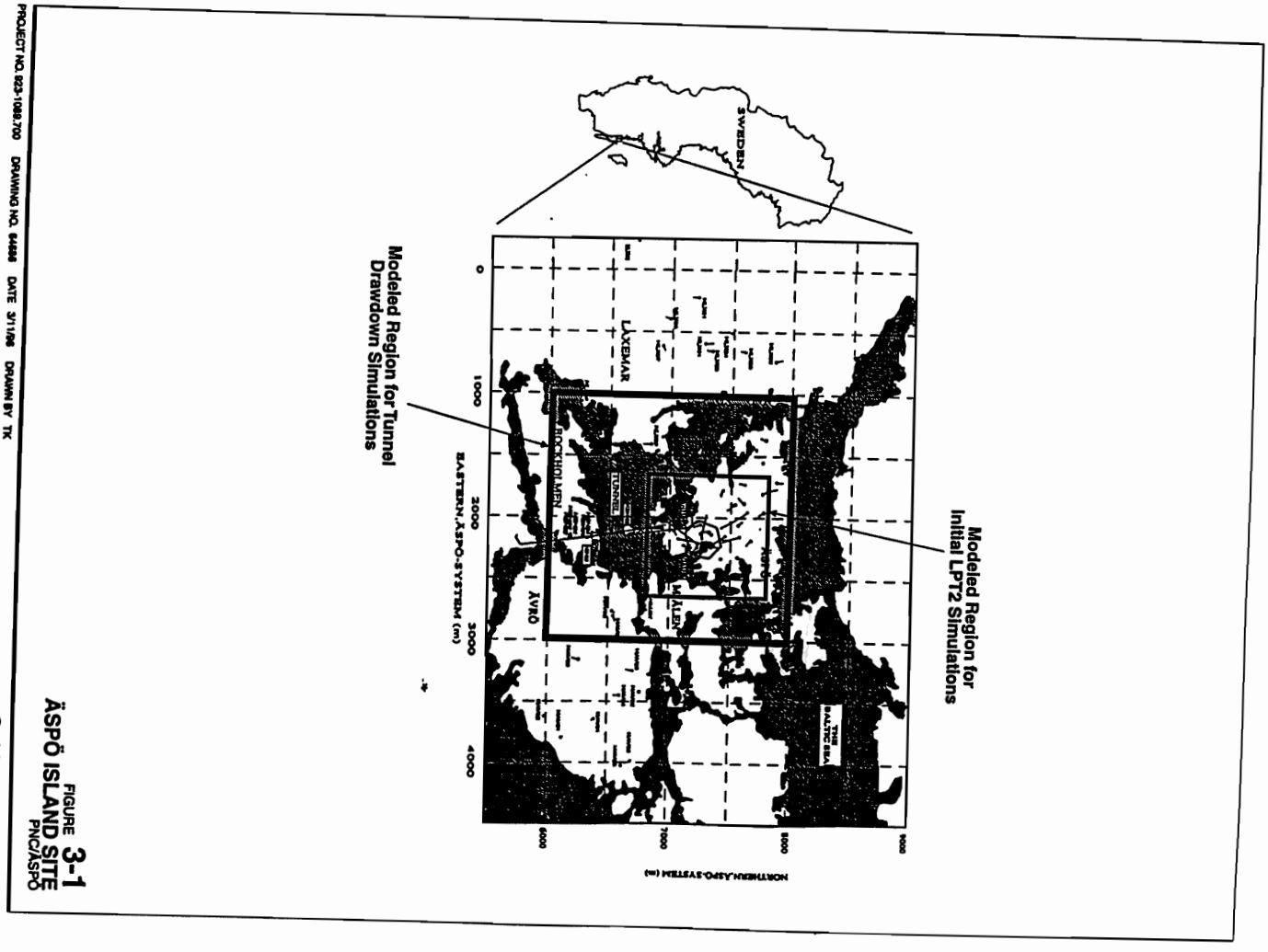

PROJECT NO. 923-1089.700 DRAWING NO. 64888 DATE 3/11/98 DRAWN BY TK

FIGURE 3-1
ÄSPÖ ISLAND SITE
PNC/ÄSPÖ

Golder Associates

Boundary Conditions

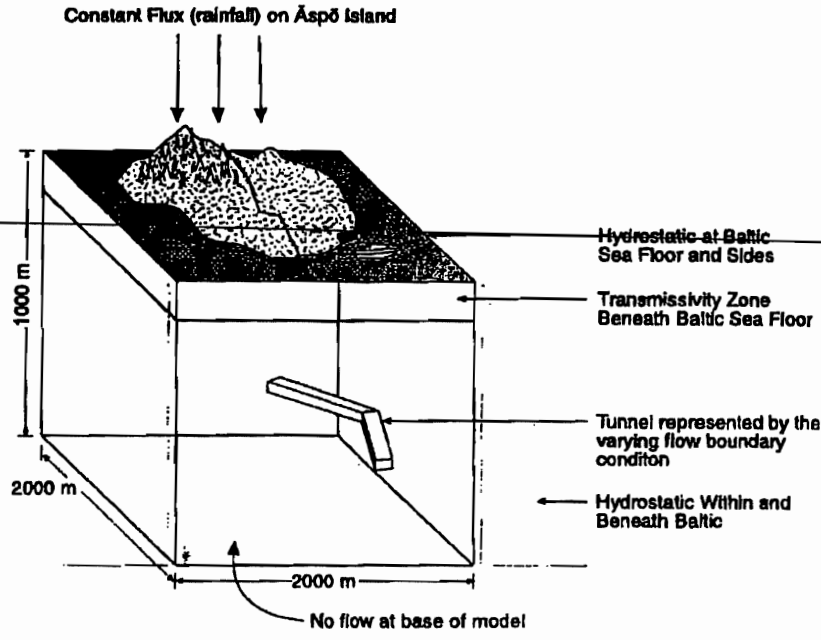

Schematic- Not to scale

Golder Associates

Task 5 DFN Model

Fracture Model Parameters (Geometry, Flow)

Fracture Set	Deterministic Fracture Zones	Background Fracture Properties
Name	Fracture Zone Fractures	Background fractures
Location	22 Planar Homogeneous Zones	Baecher/Bart Model
Size	Surface Traces Mean = 1420m	LogNormal (μ = 13.7m, σ = 12.7 m)
Orientation	3 Point Solution	Bootstrap SKB, 1994 Fractures Mapped in Tunnels
Transmissivity (m^2/s)	TR-91-22 & Olsson, 1995a	LogNormal ($\mu = 9 \times 10^{-7}$ m^2/s, $\sigma = 5 \times 10^{-6}$ m^2/s)
Storativity	0.001 $T^{1/2}$	0.001 $T^{1/2}$
Intensity (m/m^2)	Surface traces $P_{21} = 7.83 \times 10^{-3}$	P_{32} = 0.020214

Weir Flux Time History Boundary Condition

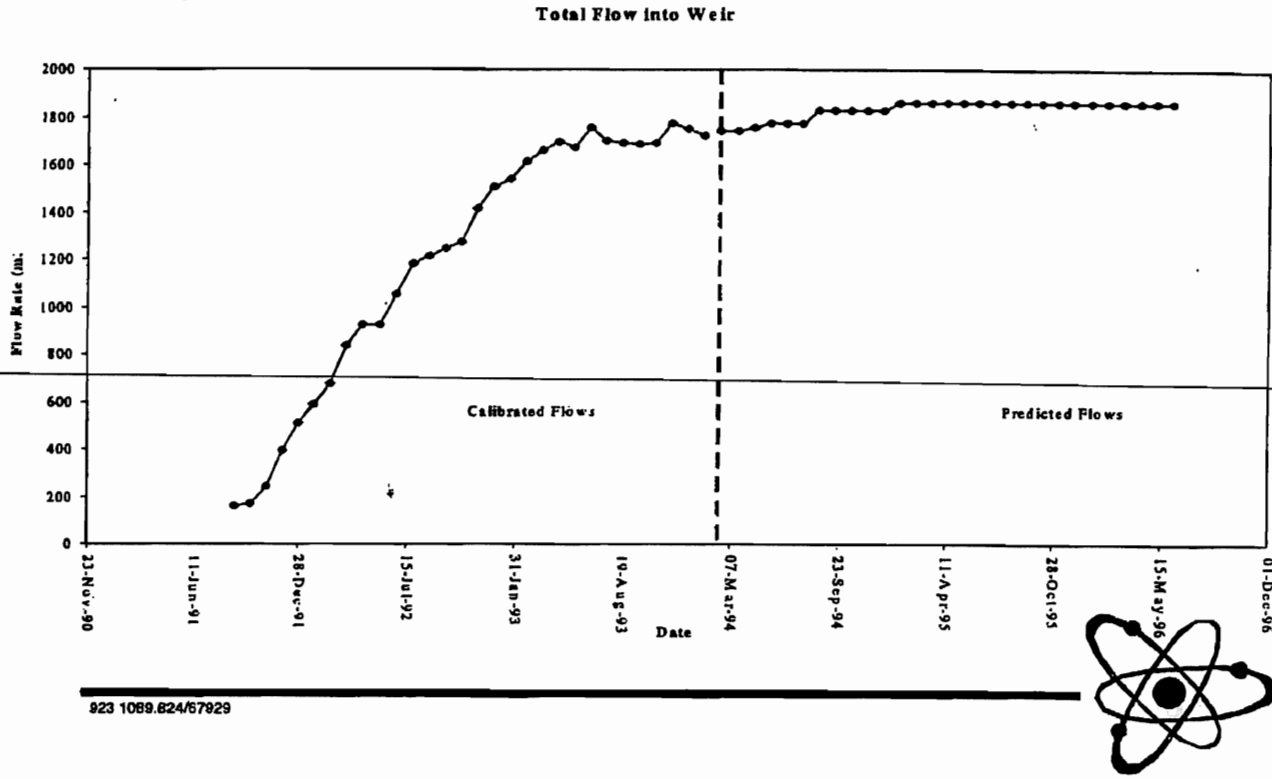

Task 5 Calculation Sequence

- **Calculate Head Field for 61 Time Steps to 60 Months (Tunnel Weir Flux Boundary Condition)**
- **Identify Transport Pathways to Tunnel Under Changing Head Field (PAWorks Pathways Analysis)**
- **Calculate Pathway Travel Times Including Rock Mass Storage Effects (500x pathway storage)**
- **PAWorks Identifies the Original Locations of Waters Arriving to Tunnel by Month**
- **Calculate End Member Mixing Based on Assumed Initial Conditions**

PAWorks Pathways

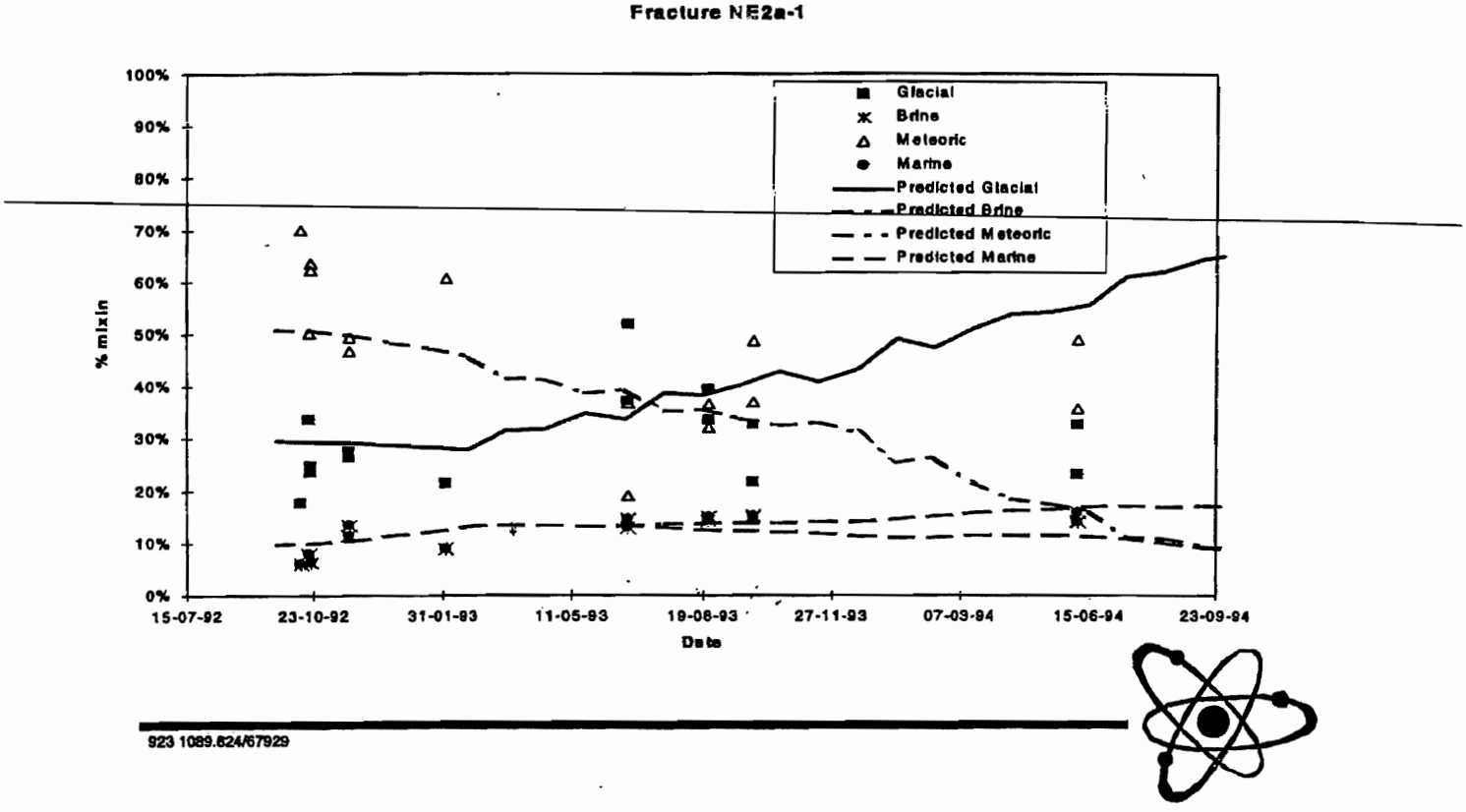

NE-2a-2

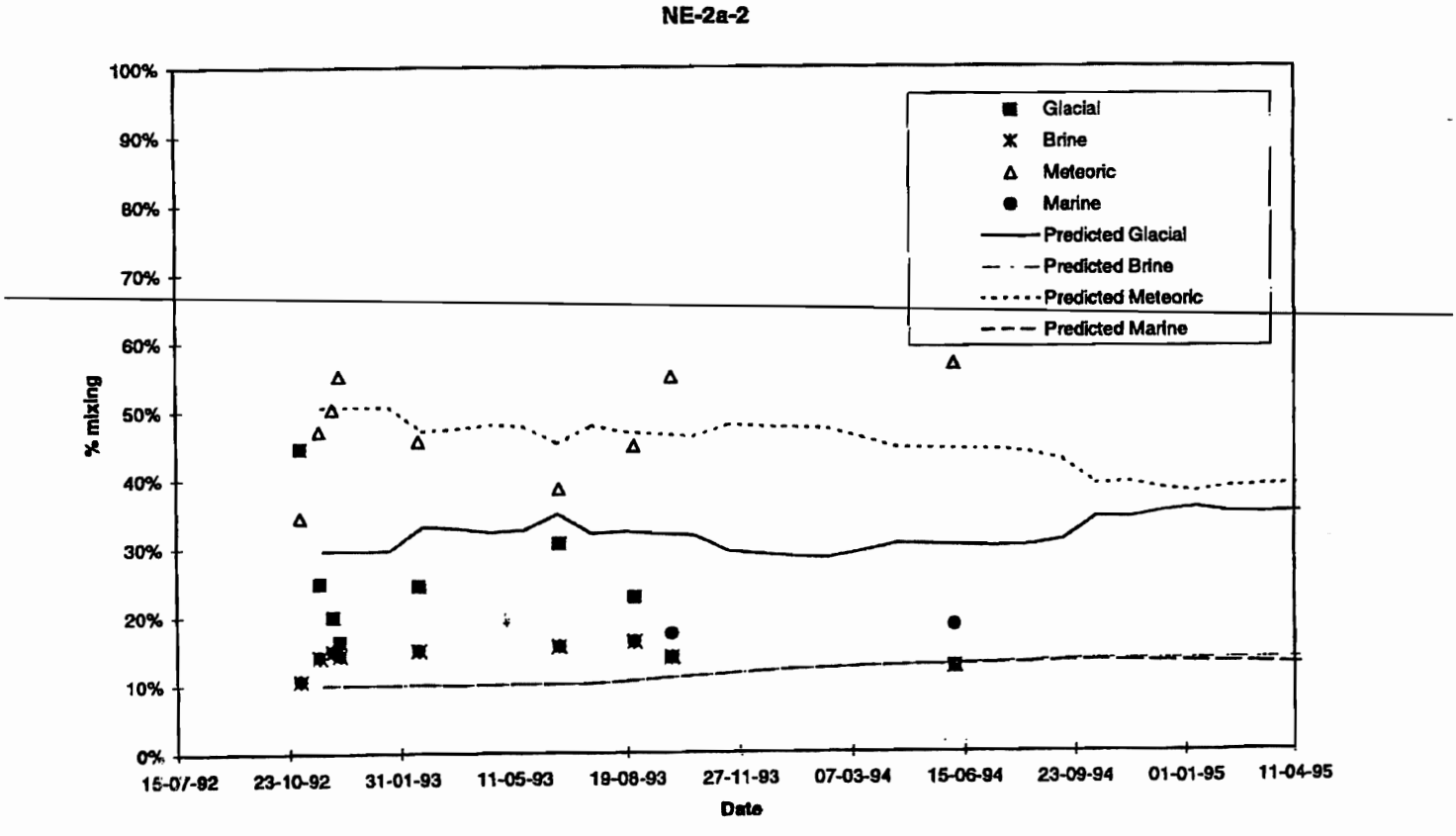

Task 5 Technical Issues

- **Transient Flow Due to Ongoing Excavation**
  - **Pressure Transient Modeled Using MAFIC with Time Varying Weir Flux Boundary Condition**
  - **Rock Mass Storativity Addressed by Calibration to End-Member Breakthrough at Control Points**
- **Density Effects on Flow**
  - **Environmental Head: Appropriate where Flow is Vertical**
  - **Freshwater Head: Appropriate where Flow is Horizontal**
  - **Task 5 Approximation: Assumes pressures from constant density simulation are correct, heads are then corrected based on density and flow direction**

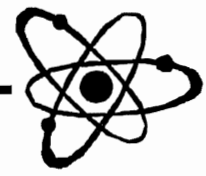

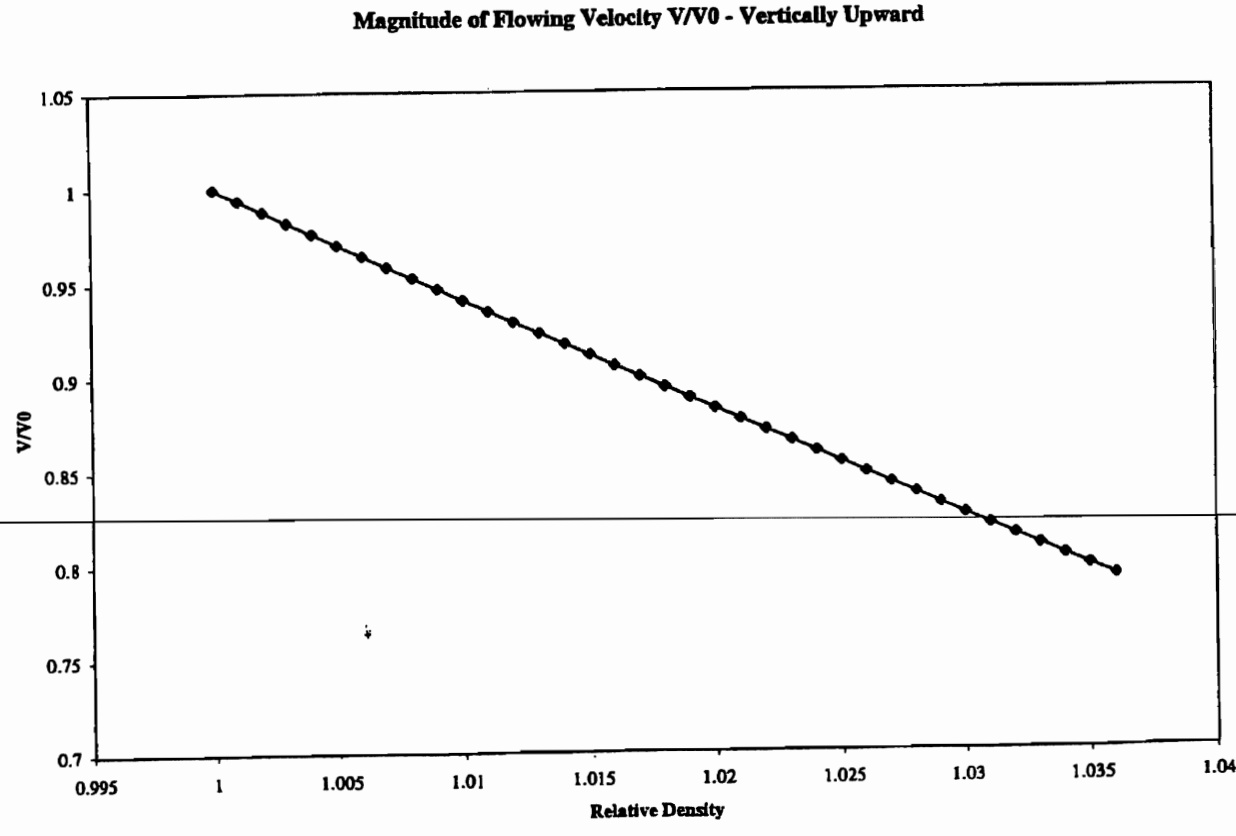

Magnitude of Flowing Velocity V/V0 - Vertically Downward

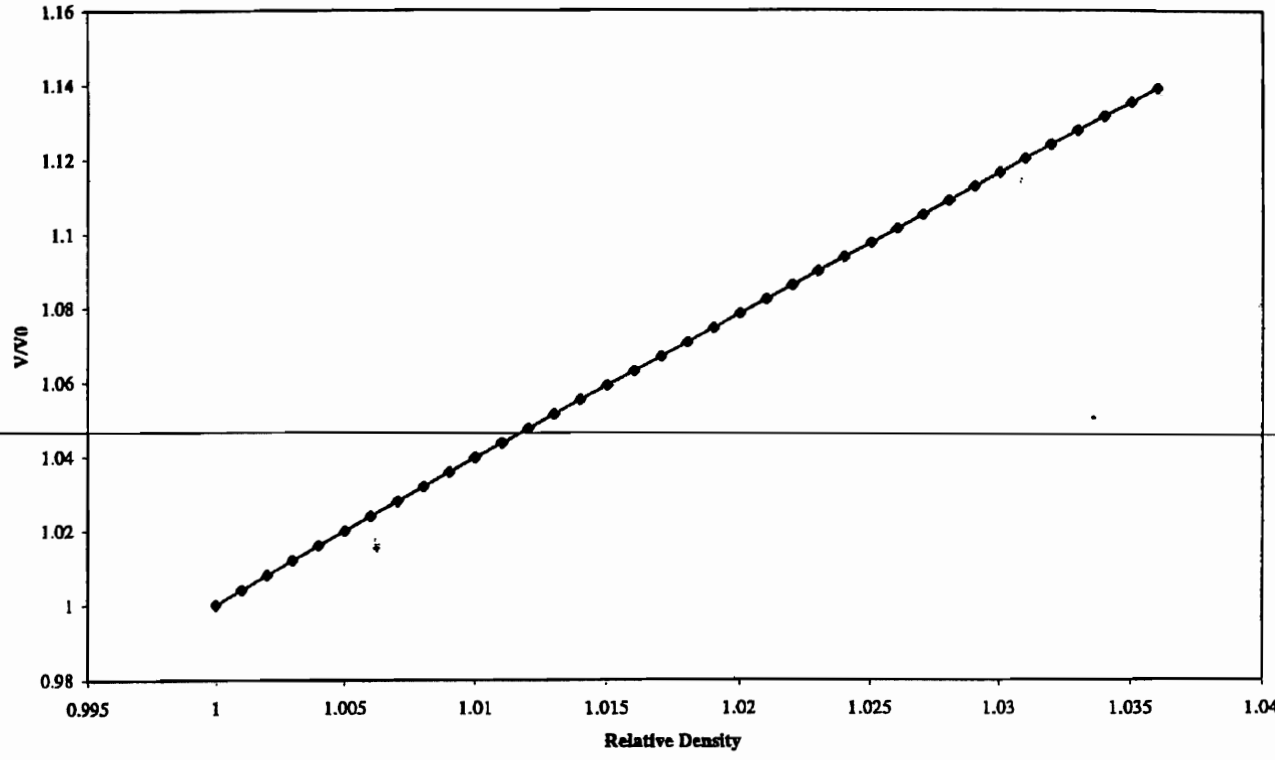

Chart2

Velocity versus Angle Theta (In 10 degree increments)

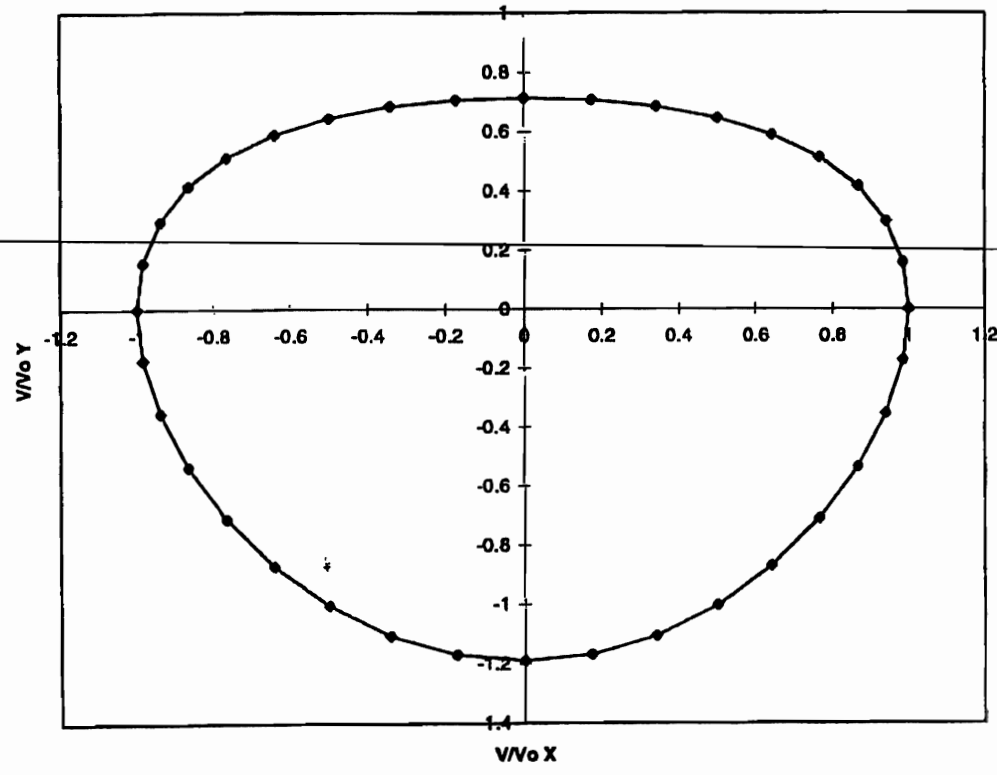

End Member Geochemistry Calibration

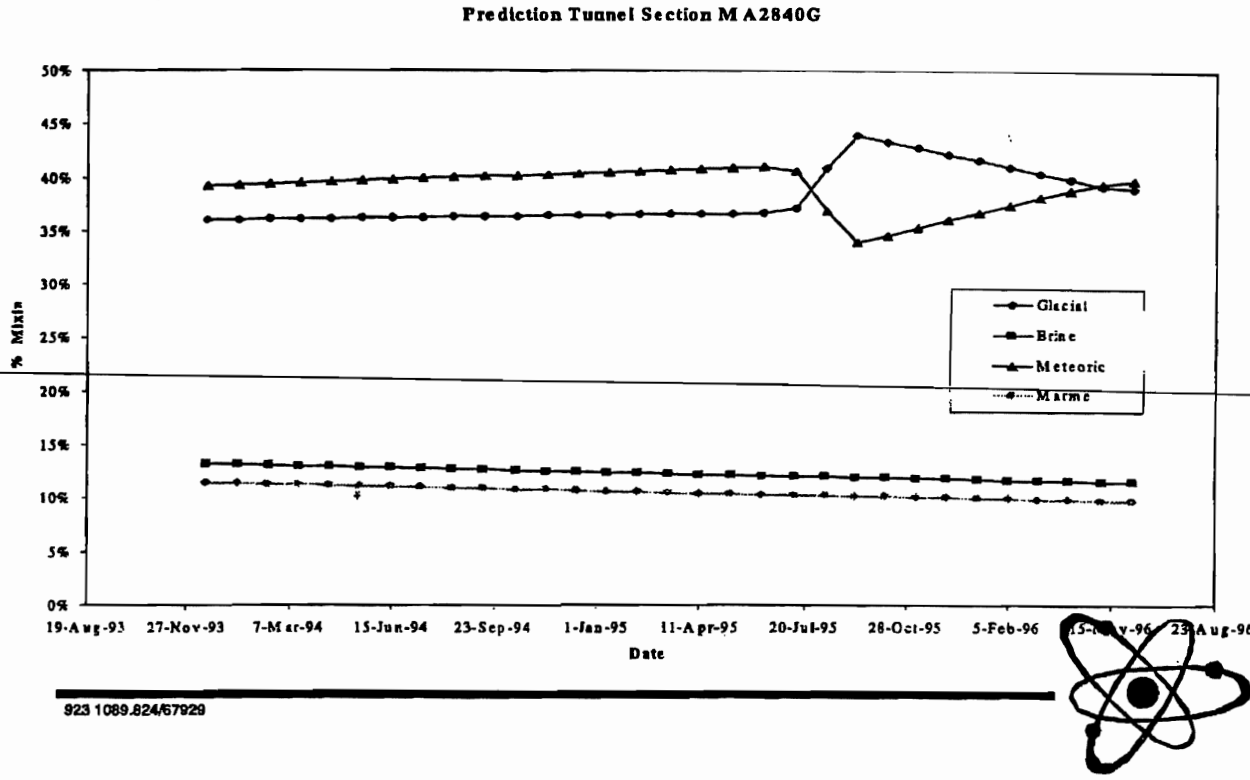

923 1089.824/67929

End Member Geochemistry Calibration

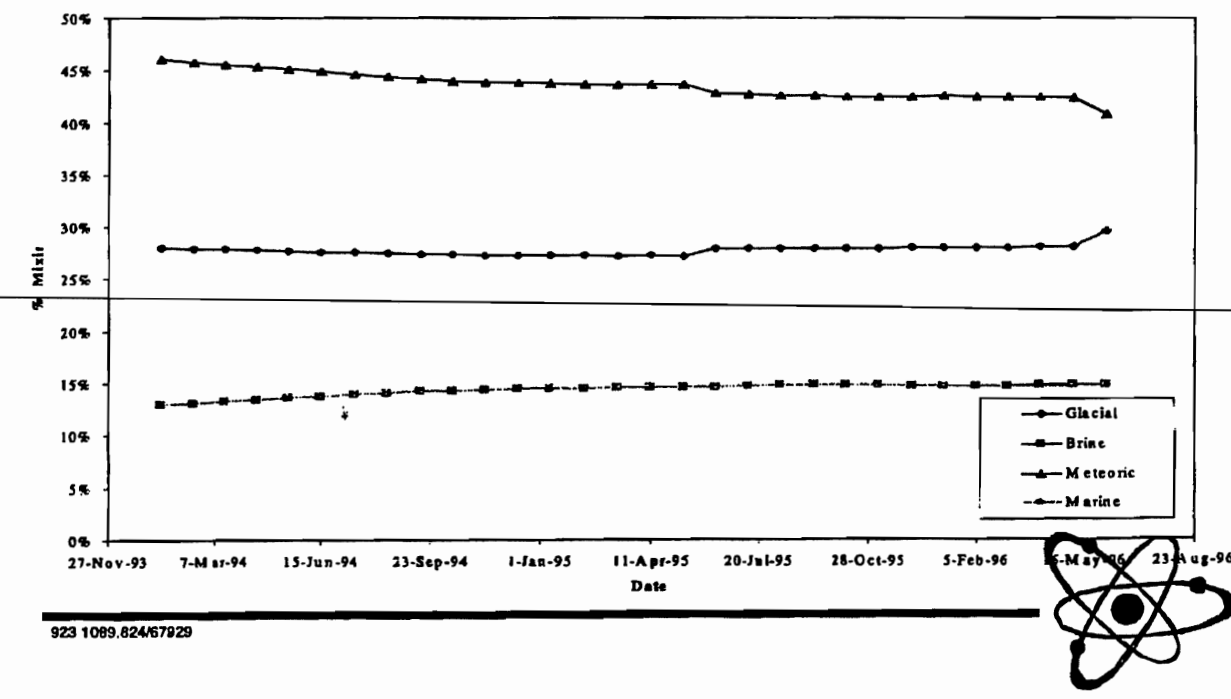

923 1089.824/67929

Prediction Tunnel Section MA3179G

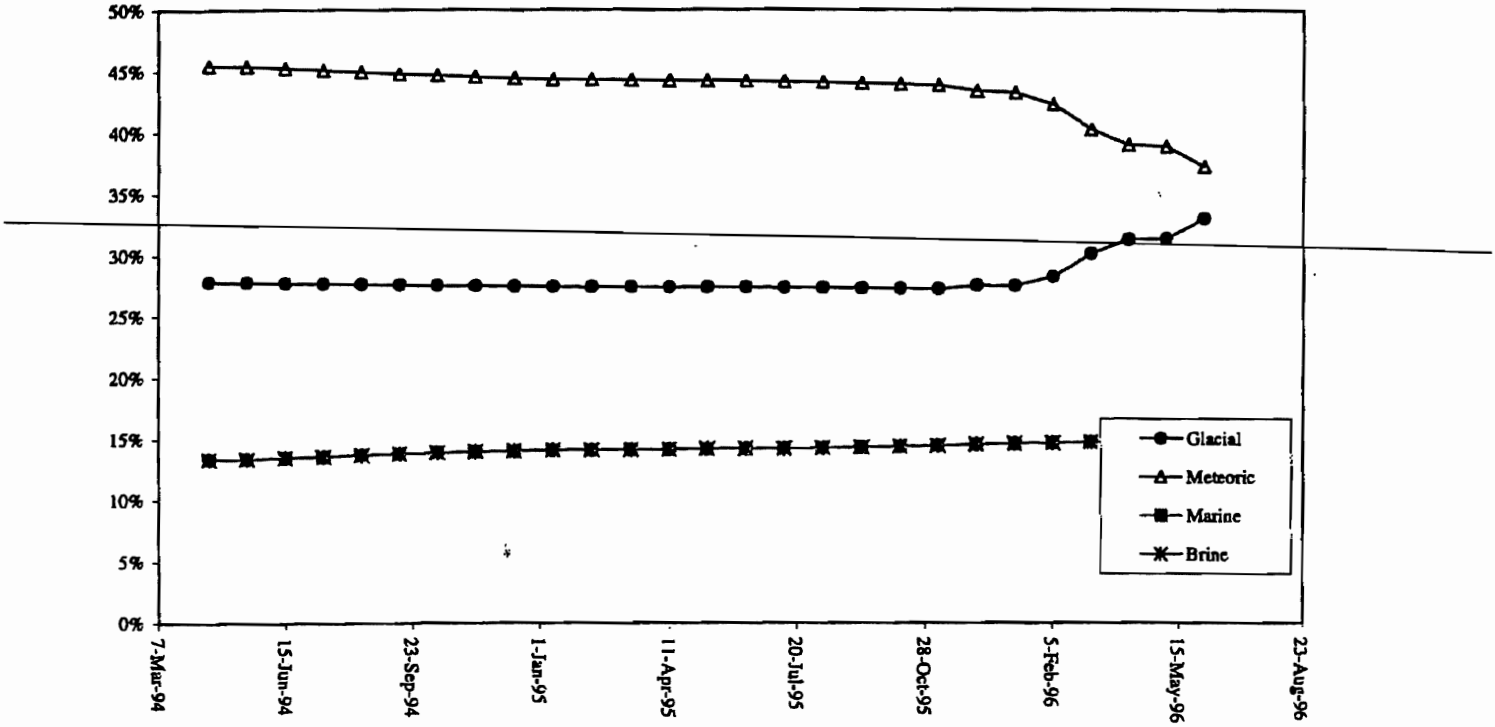

Prediction Tunnel Section MA2994G

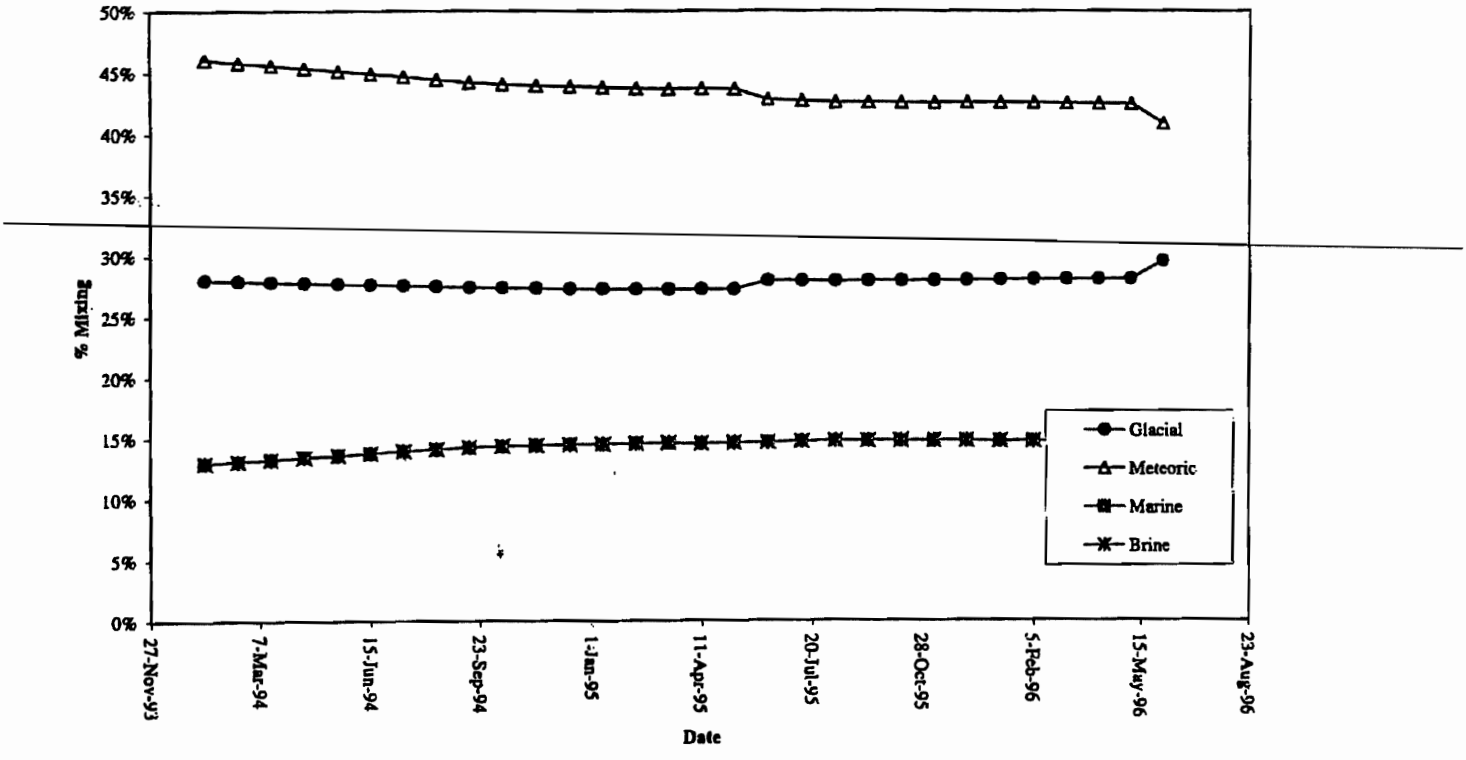

Conclusions

- **Demonstration of the FracMan/PAWorks DFN/Pathways Approach**
- **Successful Transport Pathway Calibration based on Geochemical End Members**
- **Large Scale (>1000 m) Transport Pathway Prediction under Transient Pressure Conditions**

- **Future Refinements: Possible to Address**
  - **Density Effects**
  - **Mixing Processes**
  - **Storage Capacity**
  - **Geochemical Basis for Initial End Member Pattern (Paleo-Geochemistry)**

Modelling of the hydraulic regime in and around the Äspö HRL considering the results of hydrochamical measurements.

Lutz Liedtke, Hua Shao (BMBF/BGR)

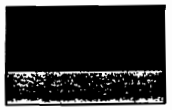

BMBF **SKB**

BGR

ÄSPÖ HRL Task Force on
Modelling of Groundwater Flow and Transport of Solutes

Modelling of the Hydraulic Regime in and around the Äspö Hard Rock Laboratory considering the Results of Hydro-chemical Measurements

31 August 1998

Federal Institute for Geosciences and Natural Resources, Hannover

ÄSPÖ Hard Rock Laboratory, Sweden

Dr. Lutz Liedtke
Dr. Dirk Schäfer

DRAFT V02

Table of Content

DRAFT V02

⇒ some results

BGR Modelling of the hydraulic regime in and around the Äspö HRL considering the results of hydrochemical measurements
The 11th meeting of the Task Force on modelling of Groundwater Flow and Transport of Solutes – Task 5
September 1-3, 1998

DRAFT V02

List of Figures

2 SITE DESCRIPTION

4 MODEL CONCEPTS AND FORMULATION

6 CALIBRATION

6.4 MAIN RESULTS

DRAFT V02

DRAFT V02

1 INTRODUCTION

1.1 BACKGROUND

The pre-investigations for the Äspö Hard Rock Laboratory started in 1986 and a large number of investigation boreholes have been drilled on Äspö and adjacent areas since then. The borehole lengths vary from 22 to 1700 m and usually they are equipped with borehole packers that separates the borehole into sections representing different hydraulic units. On Äspö 13 cored, deep boreholes, have instrumentation with a total of 70 packed-off sections and 22 of these are equipped for chemical sampling as well as for flow measurements.

The construction works of the Äspö Hard Rock Laboratory have proceeded during 4 years, October 1990 to October 1994. The maximum depth of the laboratory is 460 m and the tunnel has a total length of 3.16 km. The tunnel excavation affected the flow and the chemical composition of the groundwaters in the rock fractures, which is reflected in the borehole sections where the measurements are performed.

At Äspö Hard Rock Laboratory (HRL) the groundwater chemical composition, flow and piezometric levels in borehole sections, straddling hydraulic conductive fracture zones, have been monitored from undisturbed conditions before the excavation of the HRL access tunnel and then at successive intervals as the tunnel approaches the HRL target area deep down under Äspö island. The change in chemical composition indicates groundwater flow and transport of solutes. In this report borehole sections connected to specific major fracture zones have been studied and the change in the chemical composition has been related to the tunnel face position during the construction phase.

1.2 Objectives

The aim of Task #5 is to compare and ultimately integrate hydrochemistry and hydrogeology. The general method is to compare the outcome of the hydrochemical models with the groundwater flow models. The Task #5 modelling will also be useful for a future assessment of the stability of the hydrodynamic and hydrochemical conditions at ÄSPÖ. This modelling approach could, if successful, then be used for any future repository site investigation and evaluation, especially in a crystalline bedrock environment.

The specific objectives are:

- To assess the consistency of groundwater flow models and hydrochemical mixing-reaction models through integration and comparison of hydraulic and chemical data obtained before, during and after tunnel construction

- To develop procedure for integration of hydrological and hydrochemical information which could be used for assessment of potential disposal sites

1.3 PERFORMANCE

The following procedure have been used during the performance of this working draft :

1. Evaluating of groundwater flow and chemical composition in one fracture zone at the target area of ÄSPÖ HRL.
   - during undisturbed (natural) conditions June 1990
   - during the construction of the tunnel, i.e. tunnel influence April 1994
2. compare and interpret the undisturbed and influenced conditions with the prediction made

4 NUMERICAL METHODS

The *DURST/Rockflow* software used to simulate flow (SM2 - flow model) and solute transport (TM2 - transport model) in the modelling of Tasks #5 are based on the assumption of a double porosity continuum for the fractured rock. This software was developed jointly by BGR and the University of Hannover.

4.1 BASIC ASSUMPTION

In particular, the finite element method is used for the numerical simulation of flow and transport in subsurface system. Time derivatives were evaluated by using different schemes of various order of accuracy. The stability of numerical solutions will depend on the reference point in time of difference formula. In general, we distinguish between explicit and implicit schemes. We examine a number of approximate schemes with respect to stability and consistency. The stability criterion by von Neumann states that the eigenvalues of the amplifiction matrix of the discretized equation must be lower or equal to unity. Important stability criteria are stated in terms of the Courant number *Cr*, the grid Peclet number *Pg*, and the Neumann number *Fo*. For the non-linear problems, where no

exact discretization criteria exist, the consideration of physical conservativity and the grid convergence test may be appropriate proofs of solution stability. Spatial and temporal discretizations can introduce spurious dispersion effects where the amount of the (physical) hydrodynamic dispersion is enlarged by a numerical one. To estimate the actually resulting dispersion effective in the numerical approach, truncation errors must be determined.

4.2 GOVERNING EQUATIONS

The transient saturated groundwater flow is described by

$$S_0 \frac{\partial h}{\partial t} + \nabla v = q \,, \qquad (4\text{-}1)$$

where h is the piezometric head,
S_0 the specific storativity,
v the average fluid velocity vector, and
q the fluid sink/source.

The velocity is given by the three-dimensional, linear Darcy law:

$$v = -K \cdot \nabla h \,, \qquad (4\text{-}2.a)$$

where K is the hydraulic conductivity tensor, or by the general form of various non-linear laws for fracture or tube flow:

$$v = -K^* \cdot (\nabla h)^\alpha \,, \qquad (4\text{-}2.b)$$

where K^* is the hydraulic conductivity as a function of the piezometric head or its gradient and
α a coefficient for different non-linear flow laws.

If v is substituted into the mass balance equation (4-1), the equation may be rewritten as

$$S_0 \frac{\partial h}{\partial t} + \nabla (K \cdot \nabla h) = q \,, \qquad (4\text{-}3)$$

which is the governing equation for the flow model.

The differential equation for solute transport is

$$\frac{\partial}{\partial t}(nc) + v \cdot \nabla c - \nabla(nD \cdot \nabla c) + n\lambda c + q(c - c^*) = 0, \qquad (4\text{-}4)$$

where c is the mass fraction of solute per fluid mass,
n the volumetric porosity,
D the diffusion/dispersion tensor,
λ the radioactive decay constant of the injected radioelement, and
c^* the concentration of solute in the source fluid.

This formulation includes dispersion effects according to Fick's first law. The three-dimensional diffusion/dispersion tensor in a ξ, η, ζ-coordinate system oriented according to the flow path is written as

$$D_s = \begin{bmatrix} \alpha_L|v| + d_0 & 0 & 0 \\ 0 & \alpha_T|v| + d_0 & 0 \\ 0 & 0 & \alpha_T|v| + d_0 \end{bmatrix}, \qquad (4\text{-}5)$$

where α_L, α_T are the longitudinal and transverse coefficients of mechanical dispersion and
d_0 is the diffusion coefficient.

This is identical to the Scheidegger approach after transformation of D_s into a global x, y, z-coordinate system.

The term $n\lambda c$ describes the non-conservative behavior of the solute and can be interpreted as a decay term for radioactive solutes, with λ for the decay constant in the decay law.

The last term of equation (4-4) is the source term for fluid sources within the modelled domain.

NUMERICAL REALIZATION

Equations (4-3) and (4-4) are both solved numerically using a finite-element method. An implicit Crank-Nicolson finite difference scheme is employed to approximate the time-dependent terms, while in space a Bubnow-Gelerkin technique is used. In this case, the test and shape functions are the same.

The modelling system consists of one-, two- and three-dimensional isoparametric elements with linear shape functions. The position of nodes and elements in the domain to be modelled can be arbitrary, with the restriction that each quadrangular element must be in a plane (Fig. 4-1).

BGR Modelling of the hydraulic regime in and around the Äspö HRL considering the results of hydrochemical measurements
The 11th meeting of the Task Force on modelling of Groundwater Flow and Transport of Solutes – Task 5
September 1-3, 1998

DRAFT V02

Time-dependent piezometric heads at the boundaries and time-dependent fluxes at arbitrary nodes act as boundary conditions of the flow model. The velocities are used as input data for the transport model. Time-dependent concentrations at the inflow boundary are to be given, as well as the initial concentration distribution.

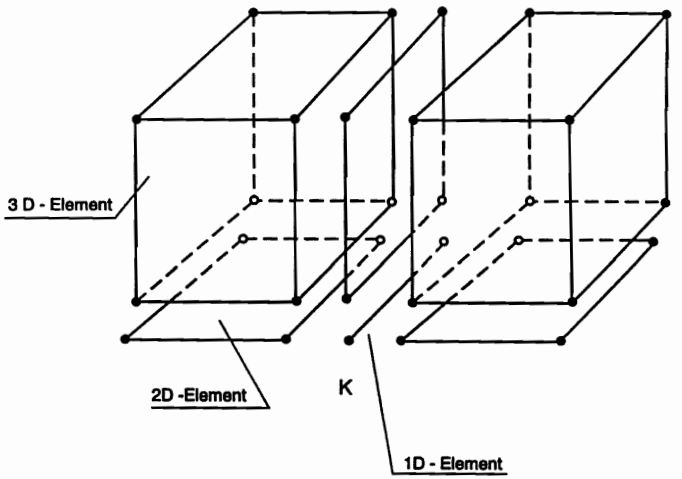

Figure 4-1: Arbitrary combination of elements of different dimensions

The time-step increments for transport simulations can be controlled in different ways. They can be taken directly from the flow model or described independently. In the latter case, the velocities are linearly interpolated if the time steps for the transport model are different from the flow-field calculation.

Solute transport in the fracture is advection-dominated. A Taylor series expansion describing artificial diffusion was used to modify the numerical formulation in order to reduce the instability of the modelling.

6 CALIBRATION

6.1 INTRODUCTION

Selected fracture: NE-1 A and NNW4

⇒ fracture with highest transmissivity in investigated area
⇒ important for the whole area
⇒ influence of other fractures NNW-4 on flow and transport in NE-1 A
⇒ fracture intersected by several boreholes, pressure and chemical measurements available

Concept:

1. Calculate stationary flow and pressure
   Calibrate transmissivities using head measurements
   a) without tunnel
   b) with tunnel

2. Calculate transport of a conservative tracer (chloride)
   Calibrate transport properties using measured tracer concentrations
   a) without tunnel as start values
   b) with tunnel

3. Calculate chemical reactions coupled to transport
   Equilibrium chemistry given by equilibrium constants
   a) without tunnel as start values
   b) with tunnel

6.2 CALIBRATION CRITERIA

Chemical Reactions in Äspö HRL

- Most important ions in Äspö groundwater:

Na^+	Cl^-
Ca^{2+}	HCO_3^-
Mg^{2+}	SO_4^{2-}

- Reactions to be taken into account
  - dissolution / precipitation of carbonate: $CaCO_3 \Leftrightarrow Ca^{2+} + CO_3^{2-}$
  - dissolution / precipitation of gypsum: $CaSO_4 \Leftrightarrow Ca^{2+} + SO_4^{2-}$
  - dissolution / precipitation of $Mn(OH)_2$: $Mn(OH)_2 \Leftrightarrow Mn^{2+} + 2OH^-$
  - carbonate chemistry: $H_2CO_3 \Leftrightarrow H^+ + HCO_3^-$
    $HCO_3^- \Leftrightarrow H^+ + CO_3^{2-}$
  - sulfate chemistry: $H_2SO_4 \Leftrightarrow 2\,H^+ + SO_4^{2-}$
  - dissociation of water: $H_2O \Leftrightarrow H^+ + OH^-$

- Reactions, which may be neglected
  - dissolution / precipitation of salt: $NaCl \Leftrightarrow Na^+ + Cl^-$
    (undersaturated in simulated area)
  - dissolution / precipitation of (iron)-sulfides ?
    (low concentrations of iron and sulfide)
  - dissolution / precipitation of fluorides
    (low concentration of fluoride)
  - dissolution / precipitation of Ba - salts
    (barium not measured)

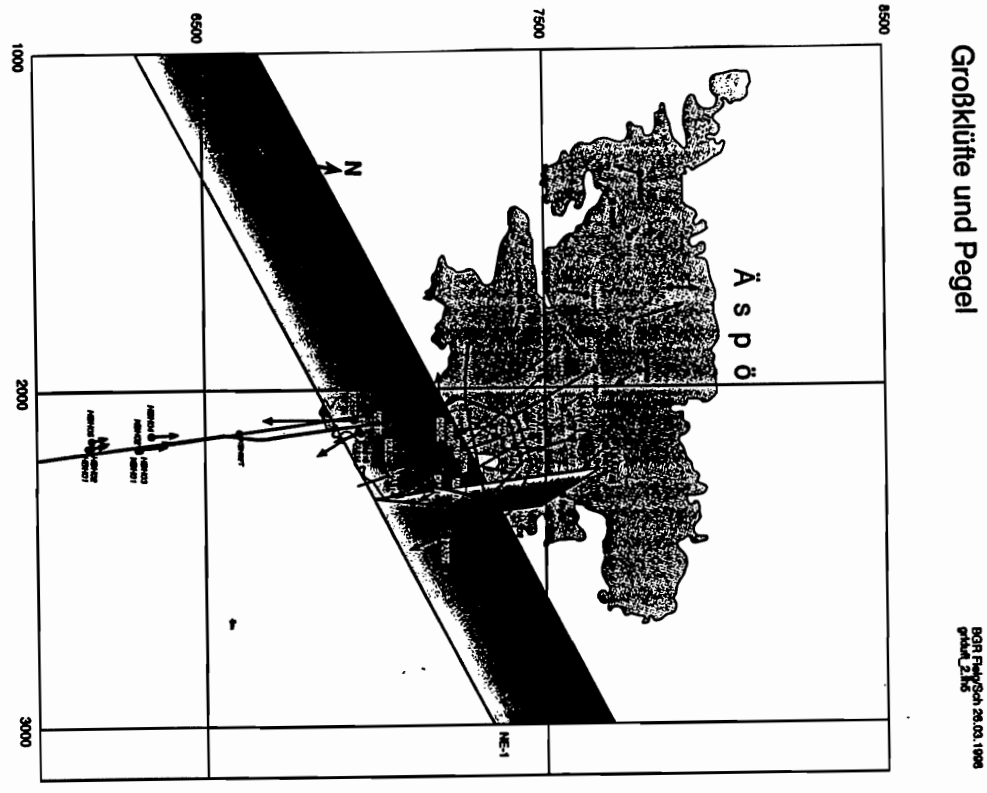

Großklüfte und Pegel

Standrohrspiegelhöhen im Kluftsystem NE-1 über die Zeit

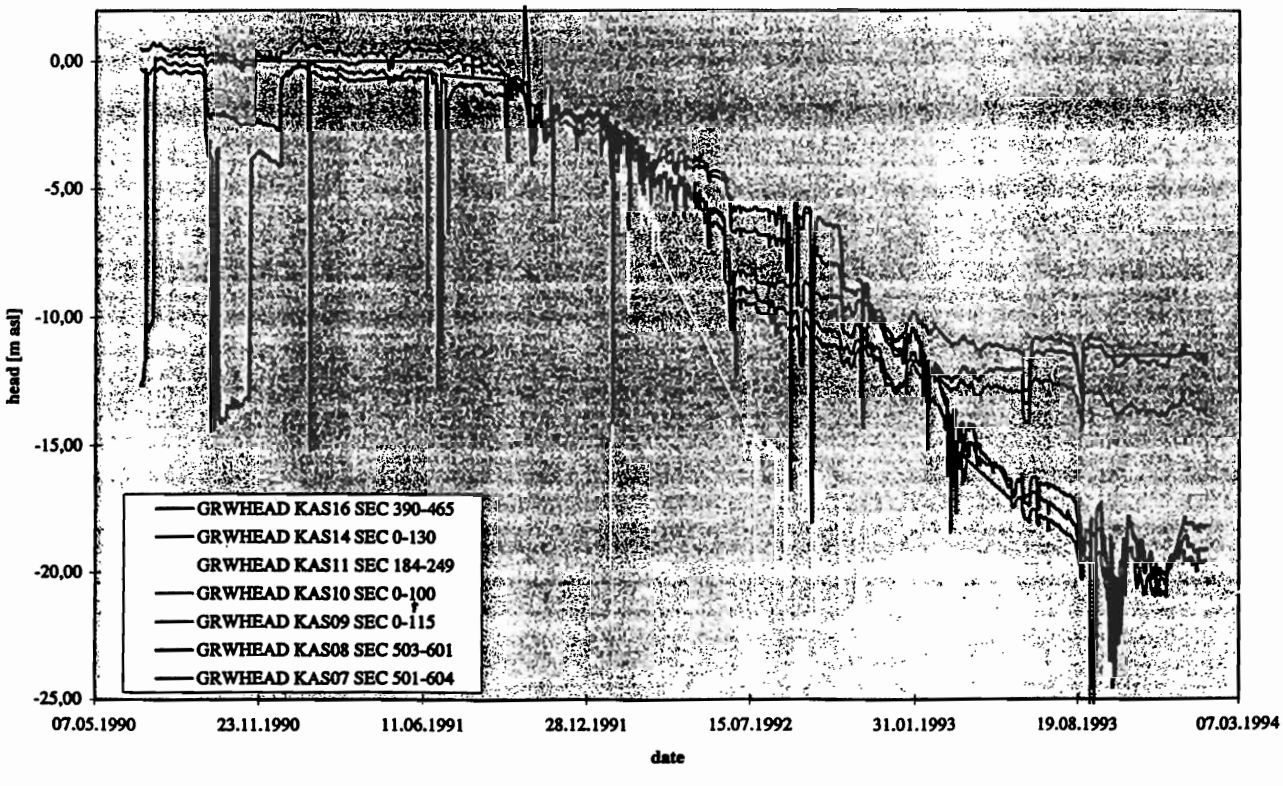

Chloridkonzentrationen in Kluft NE 1

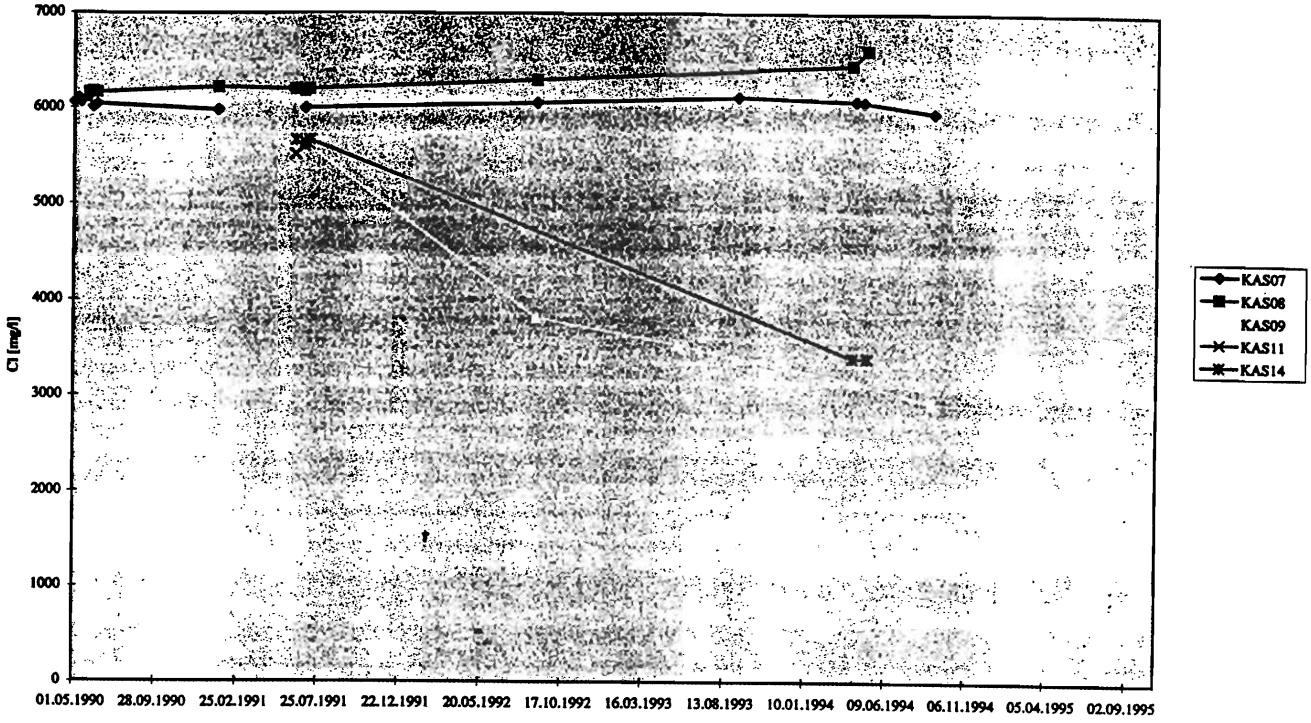

Natriumkonzentrationen in Kluft NE 1

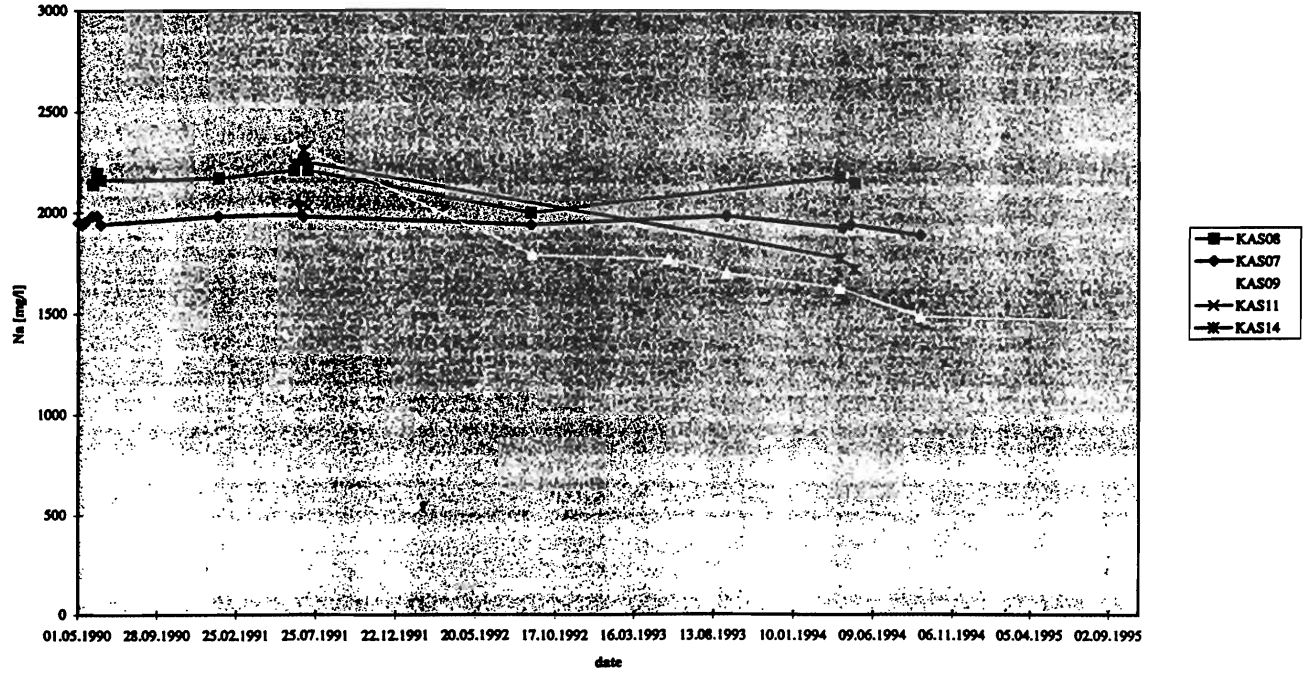

Calciumkonzentrationen in Kluft NE1

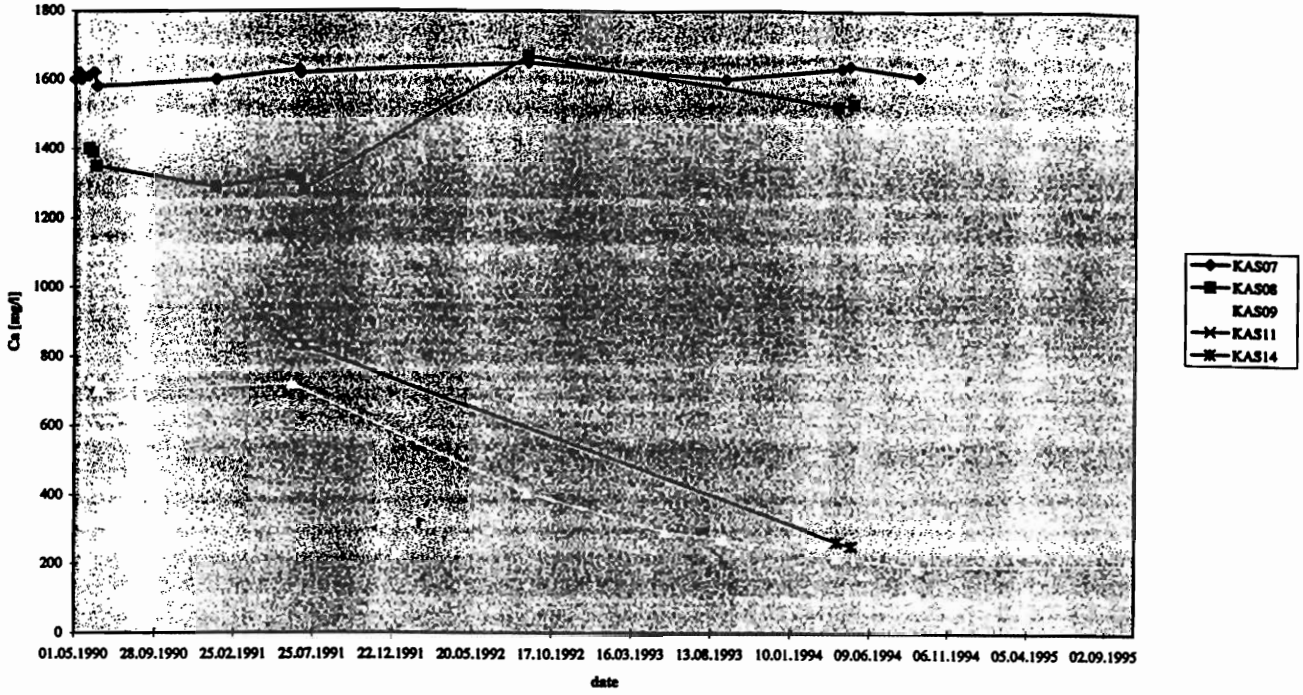

Hydrogencarbonatkonzentrationen in Kluft NE1

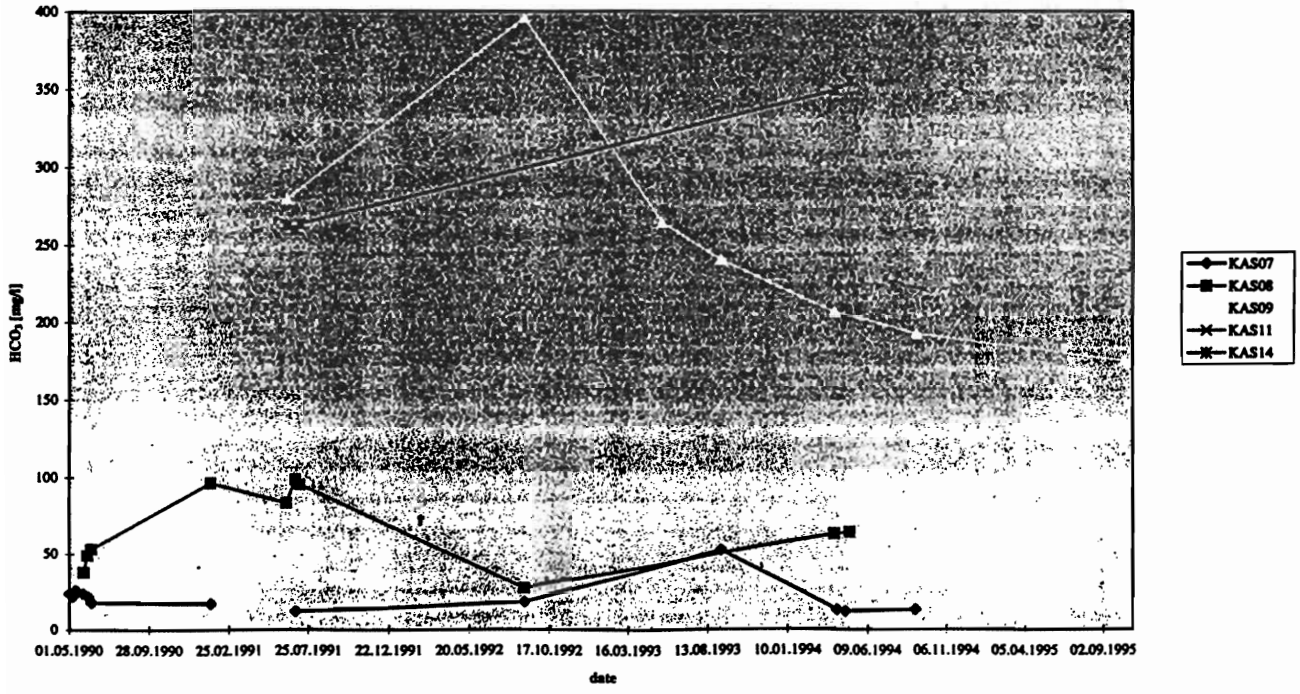

Sulfatkonzentrationen in Kluft NE1

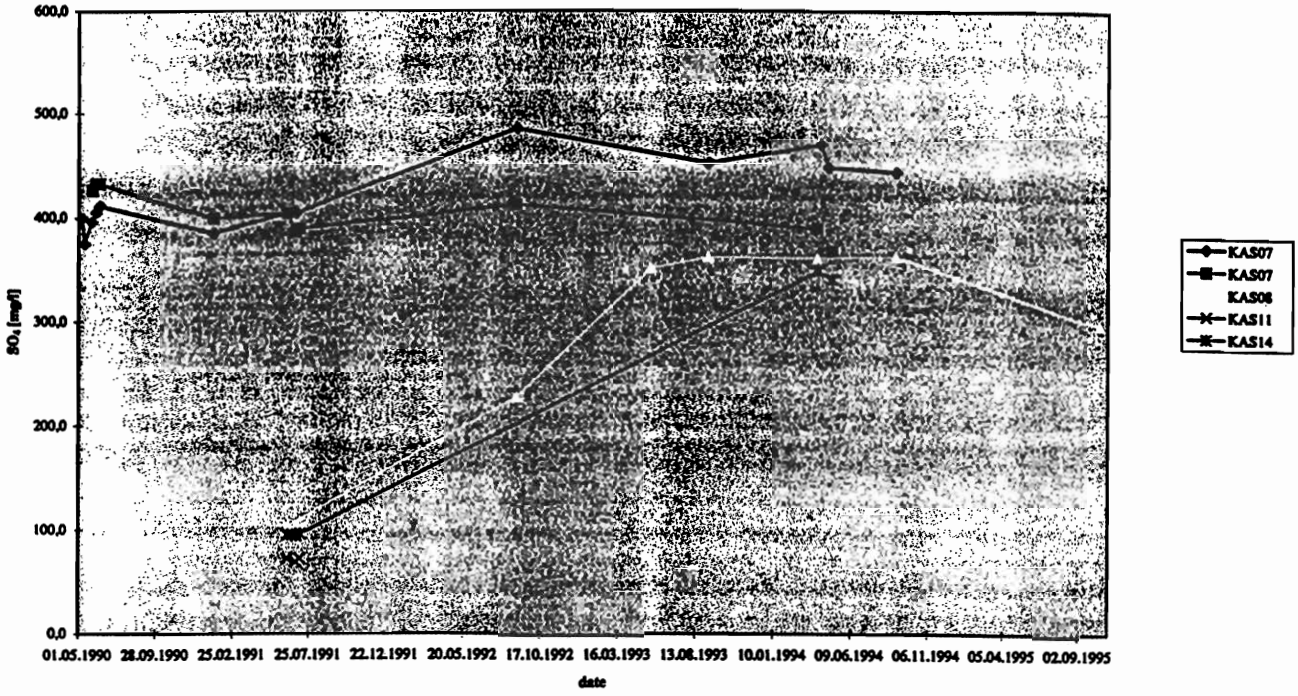

Kaliumkonzentrationen in Kluft NE1

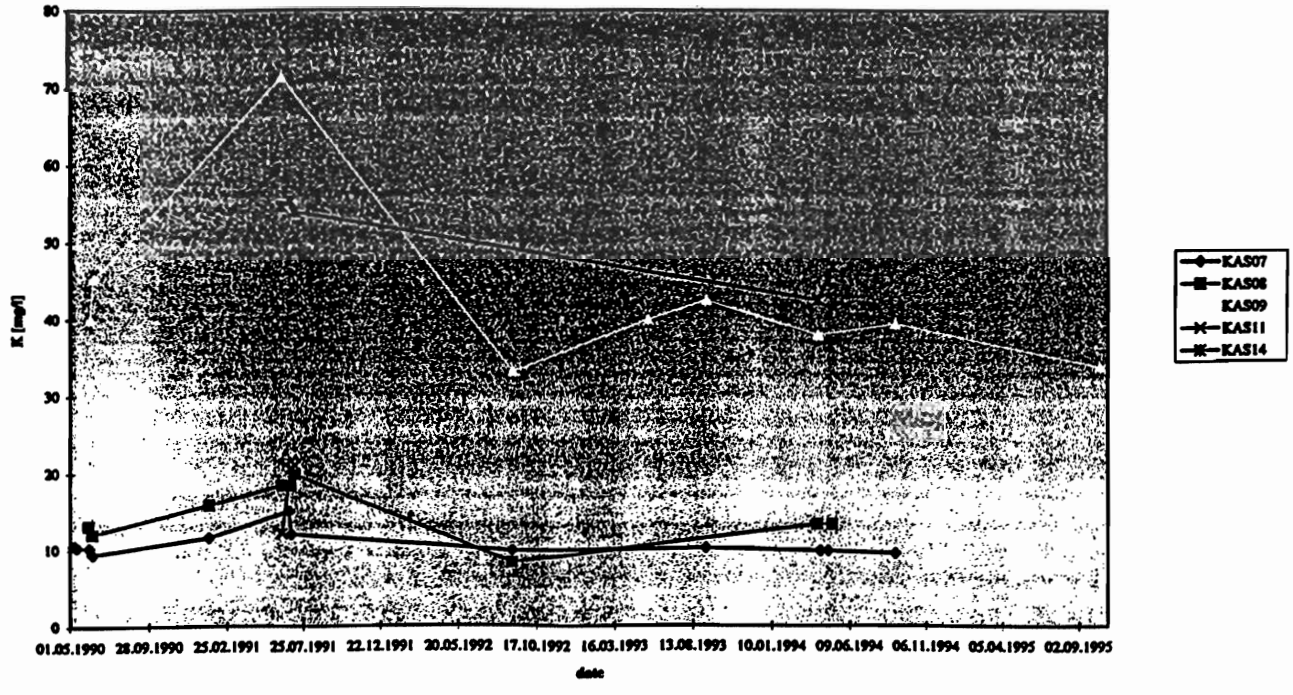

Magnesiumkonzentrationen in Kluft NE1

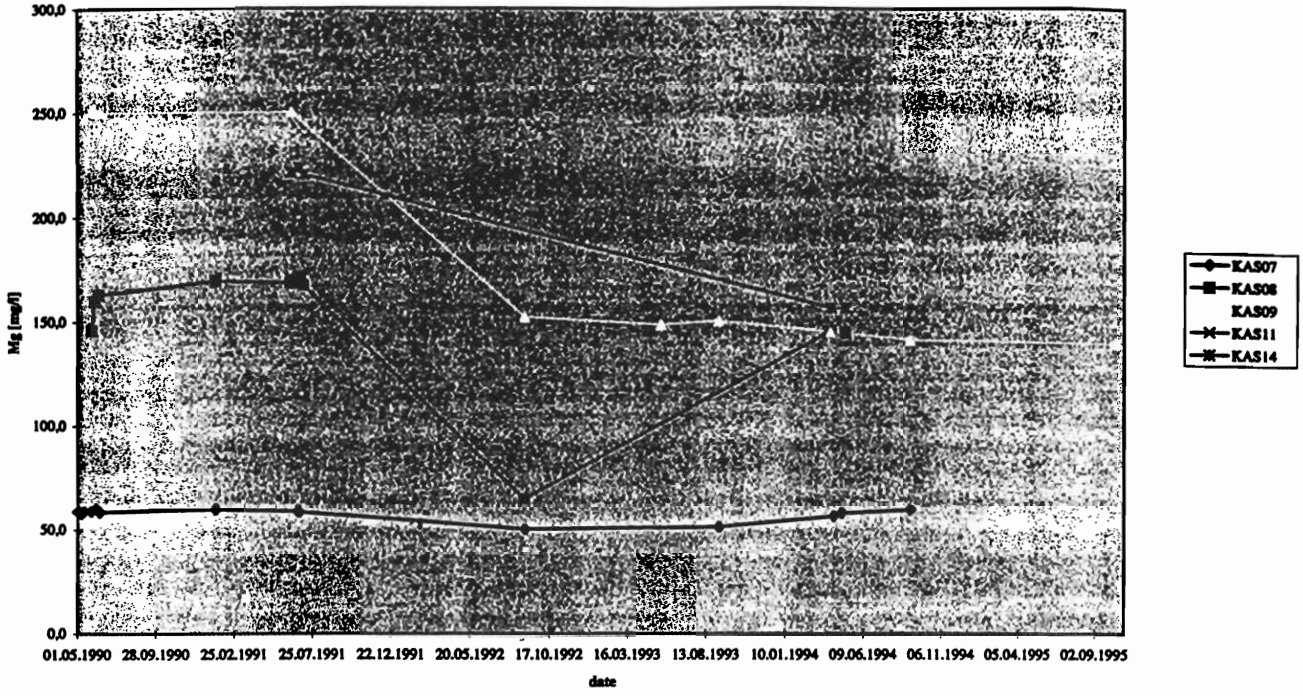

pH-Wert in Kluft NE1

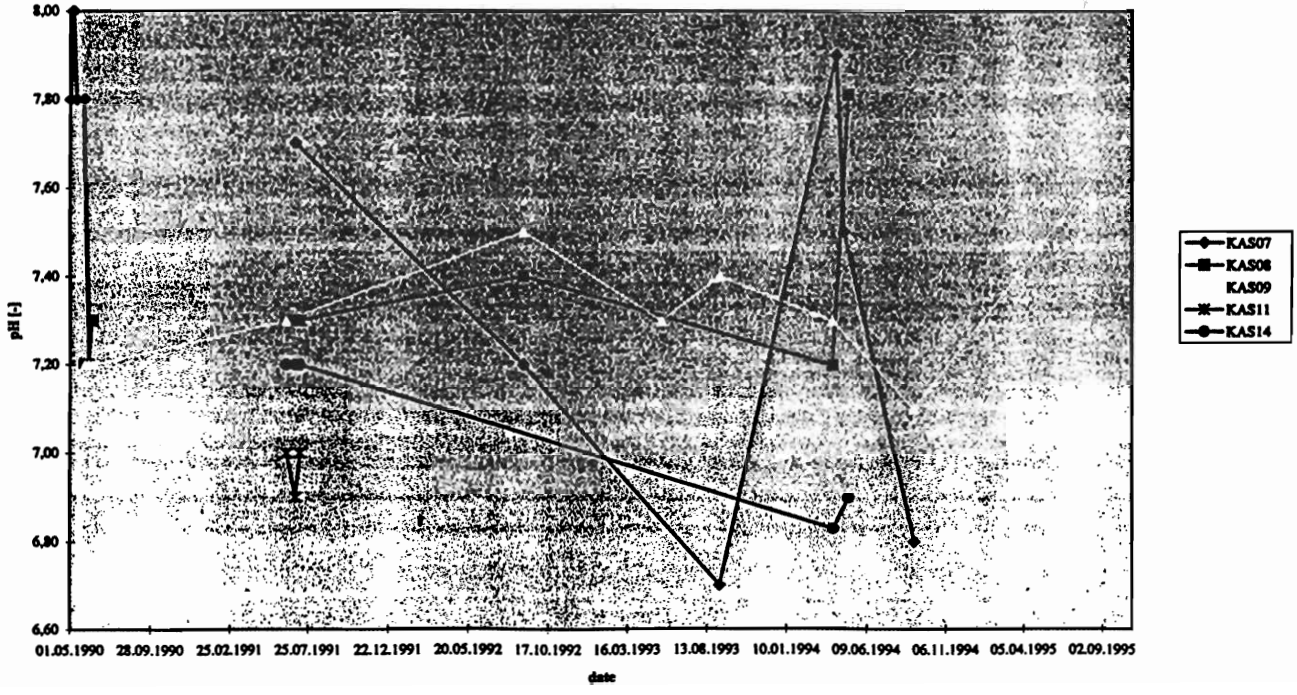

Leitfähigkeit in Kluft NE 1

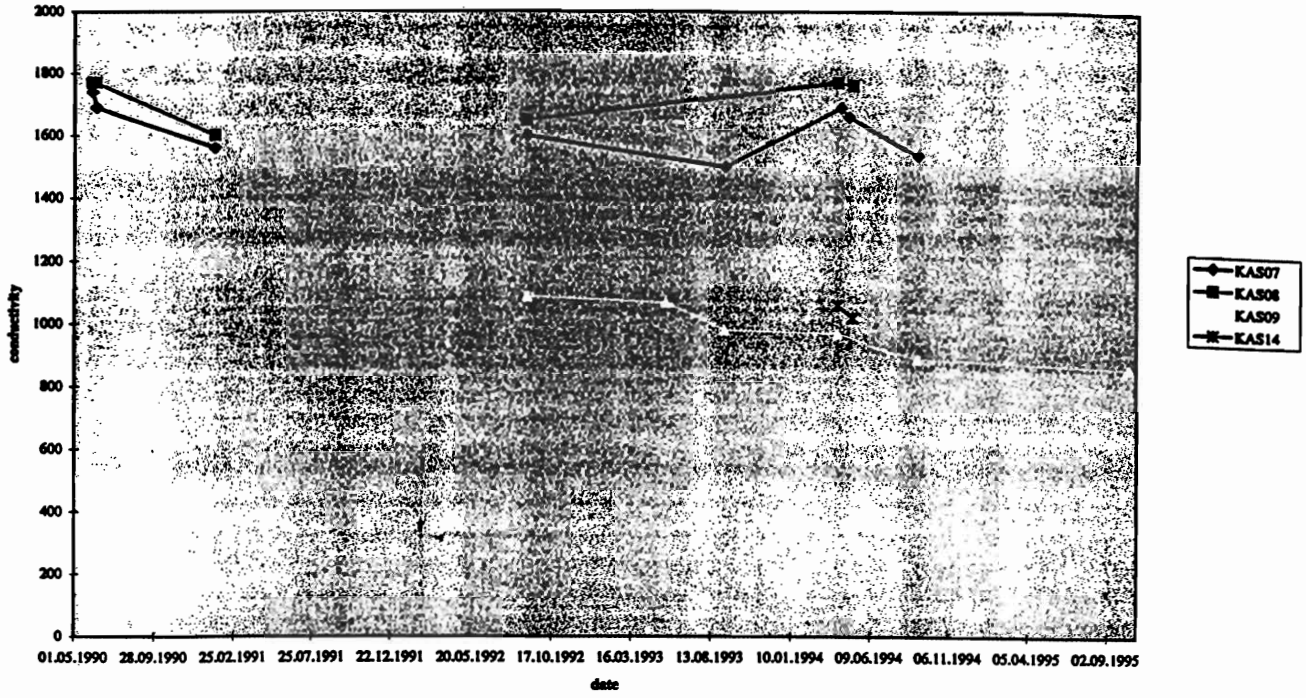

^{18}O-Konzentrationen in Kluft NE 1

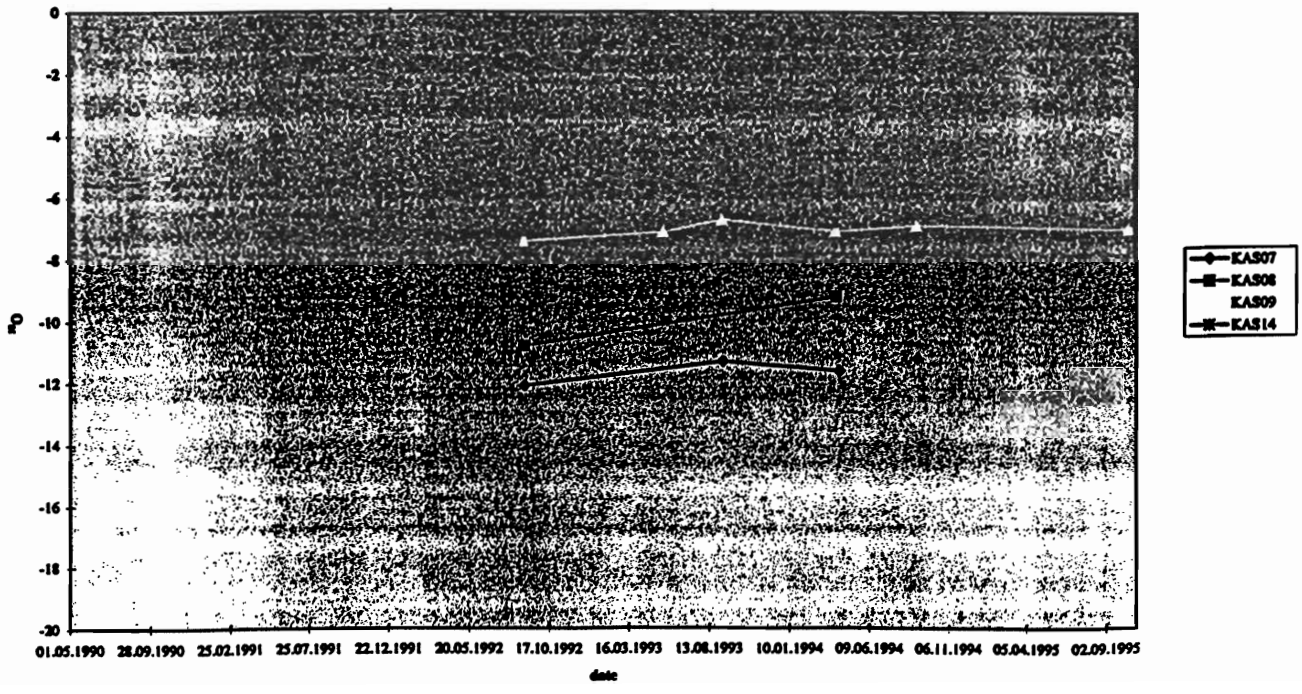

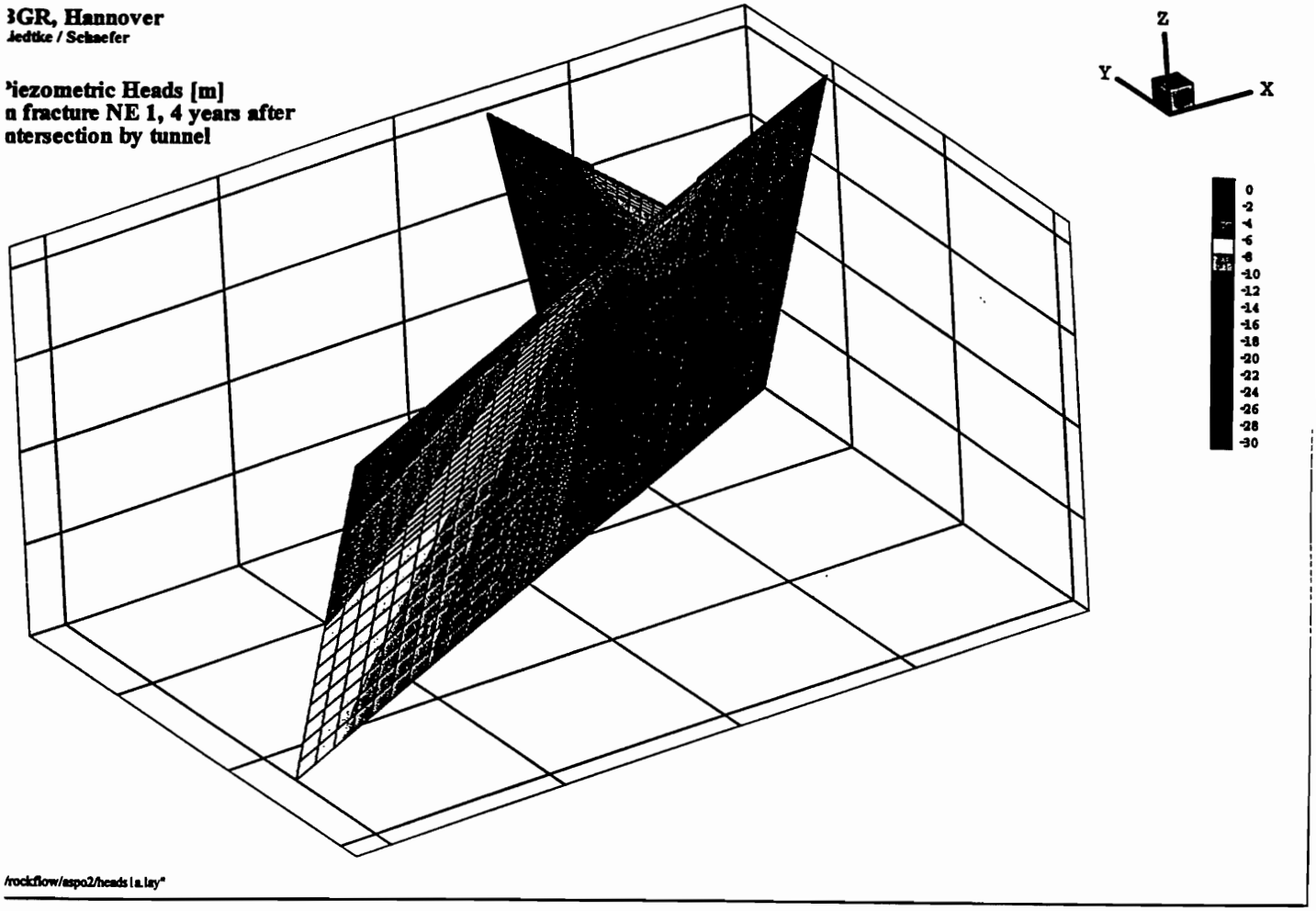
BGR, Hannover
Liedtke / Schaefer
Piezometric Heads [m]
in fracture NE 1, 4 years after
intersection by tunnel
Z
Y
X
0
-2
-4
-6
-8
-10
-12
-14
-16
-18
-20
-22
-24
-26
-28
-30
/rockflow/aspo2/heads1a.lay"

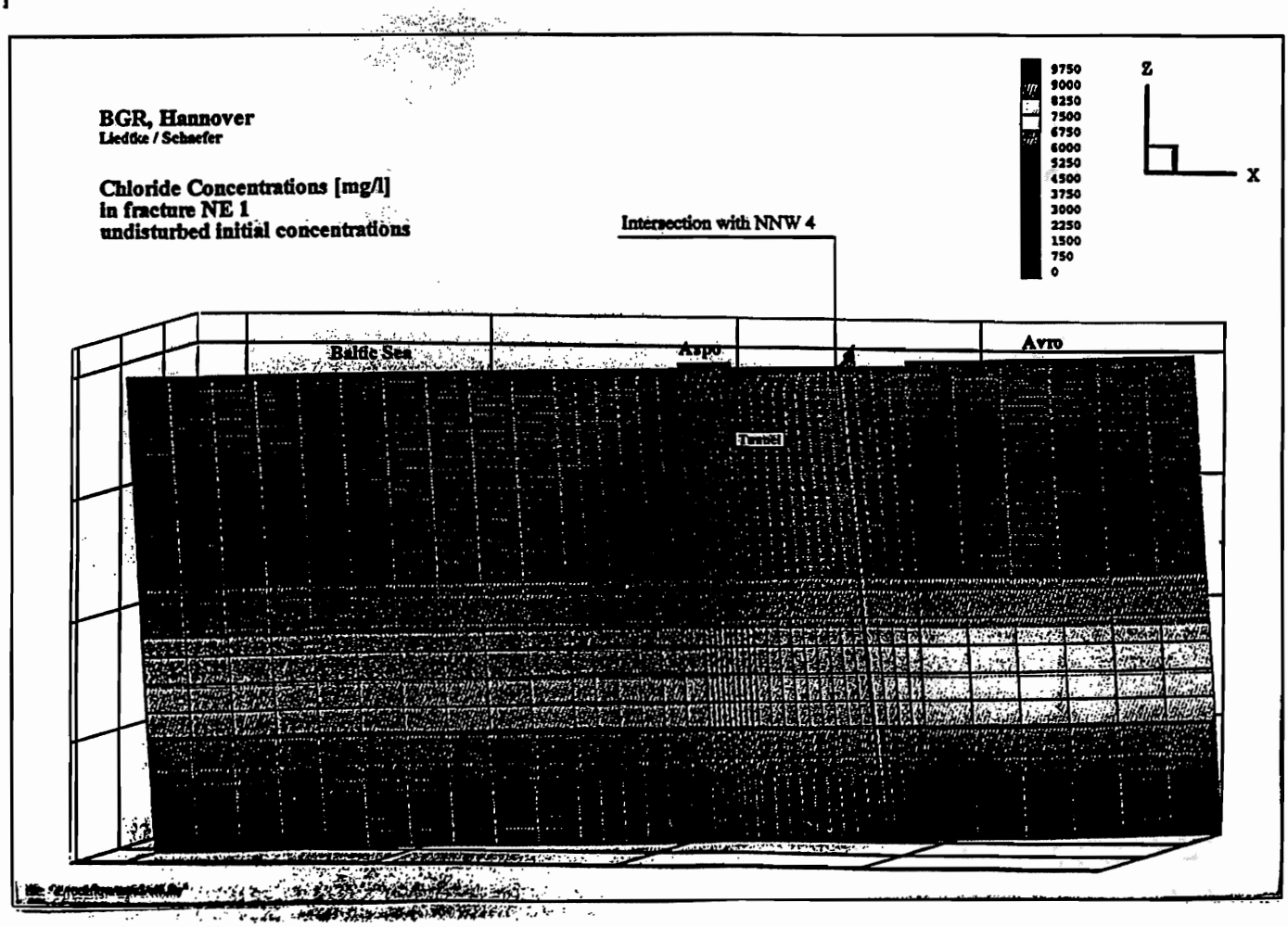
BGR, Hannover
Liedtke / Schaefer
Chloride Concentrations [mg/l]
in fracture NE 1
undisturbed initial concentrations
9750
9000
8250
7500
6750
6000
5250
4500
3750
3000
2250
1500
750
0
Z
X
Intersection with NNW 4
Baltic Sea
Aspo
Avro
Tunnel

BGR, Hannover
Liedtke / Schaefer

Piezometric Heads [m]
in fracture NE 1
undisturbed initial conditions

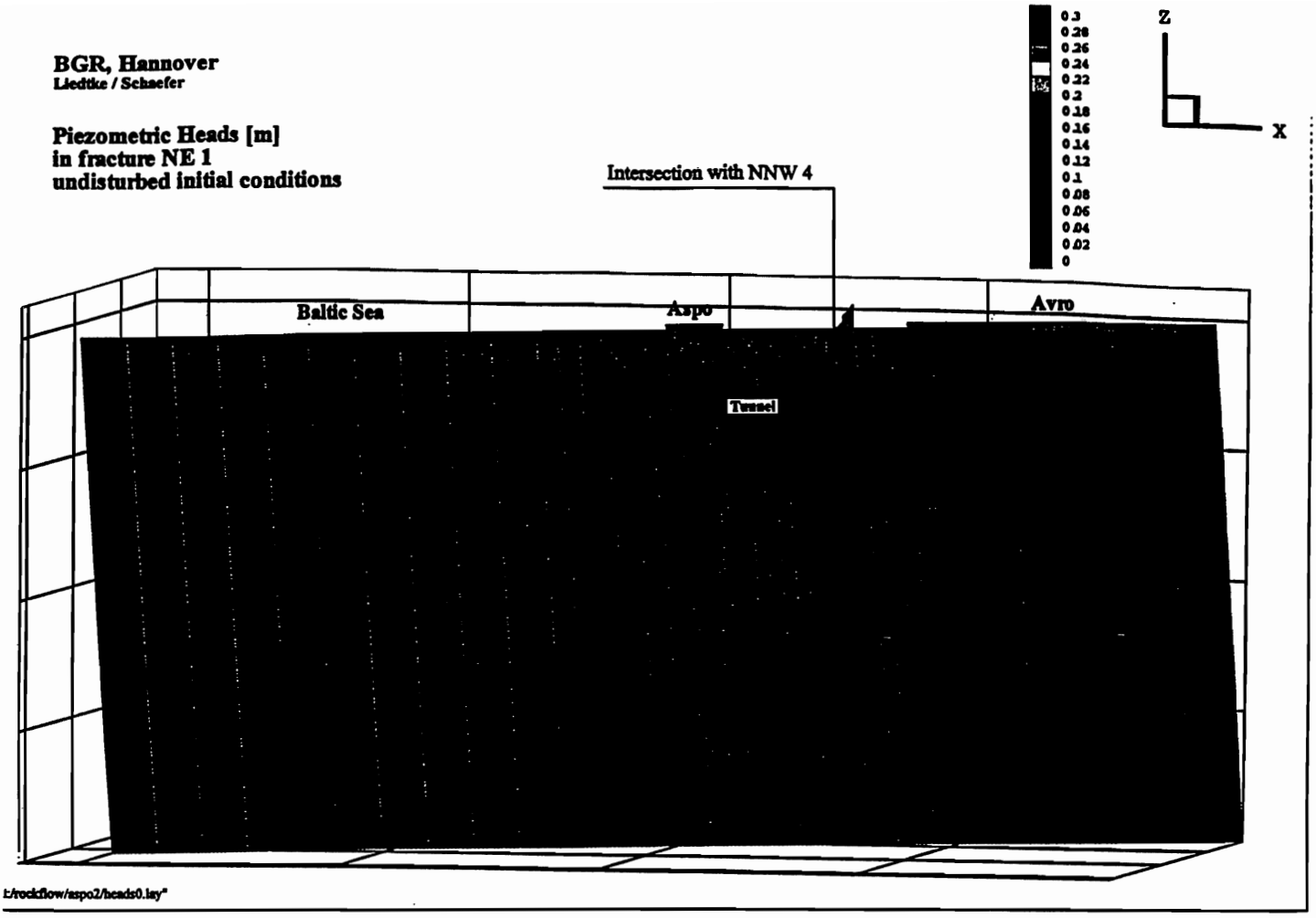

BGR, Hannover
Liedtke / Schaefer

Piezometric Heads [m]
in fracture NE 1
4 years after intersection by tunnel

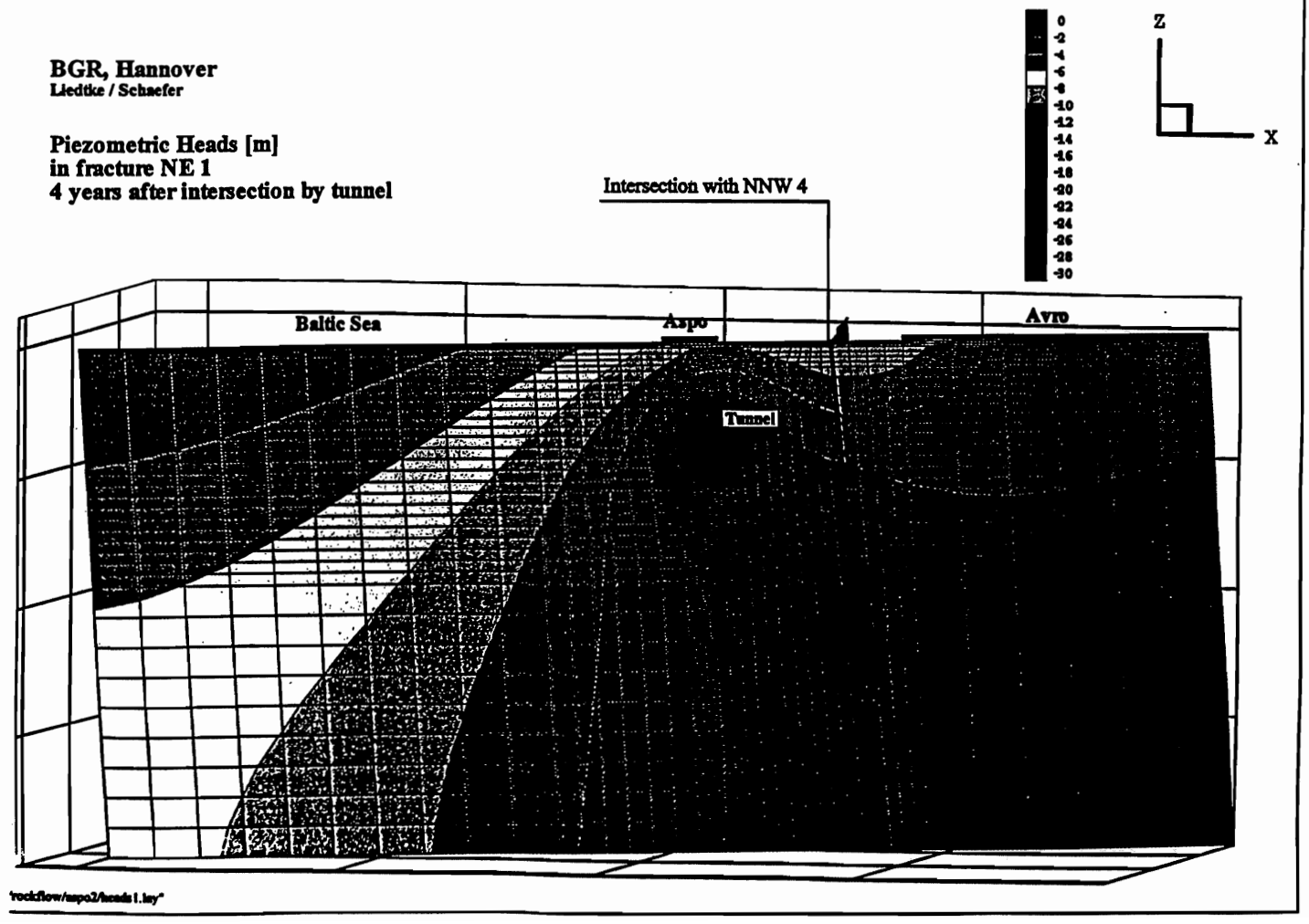

BGR, Hannover
Liedtke / Schaefer

Chloride Concentrations [mg/l]
in fracture NE 1
4 years after intersection by tunnel

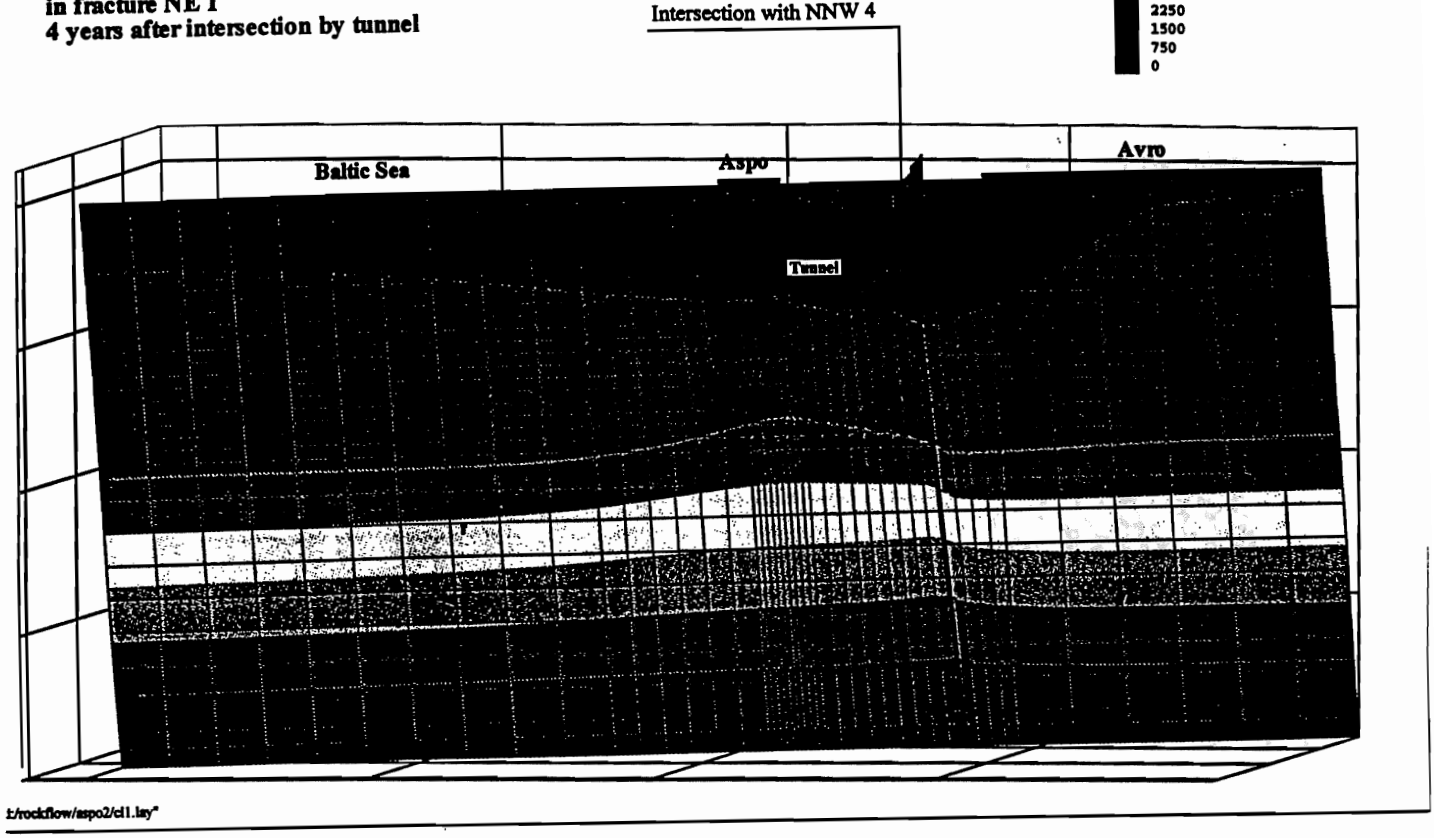

t:/rockflow/aspo2/cl1.lay"

BGR, Hannover
Liedtke / Schaefer

Sodium Concentrations [mg/l]
in fracture NE 1
undisturbed initial concentrations

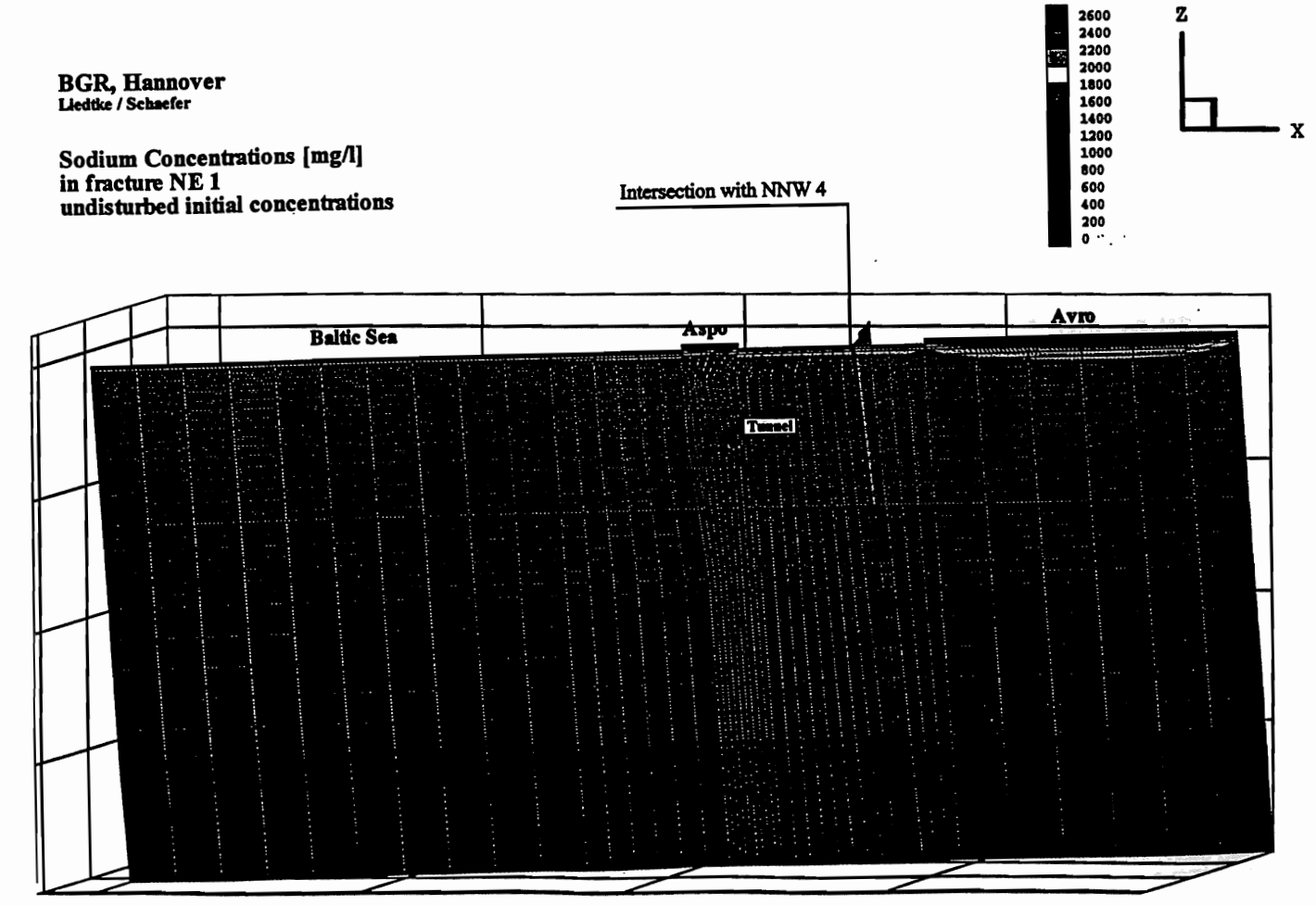

/rockflow/aspo2/na0.lay"

BGR, Hannover
Liedtke / Schaefer

Sodium Concentrations [mg/l]
in fracture NE 1
4 years after intersection by tunnel

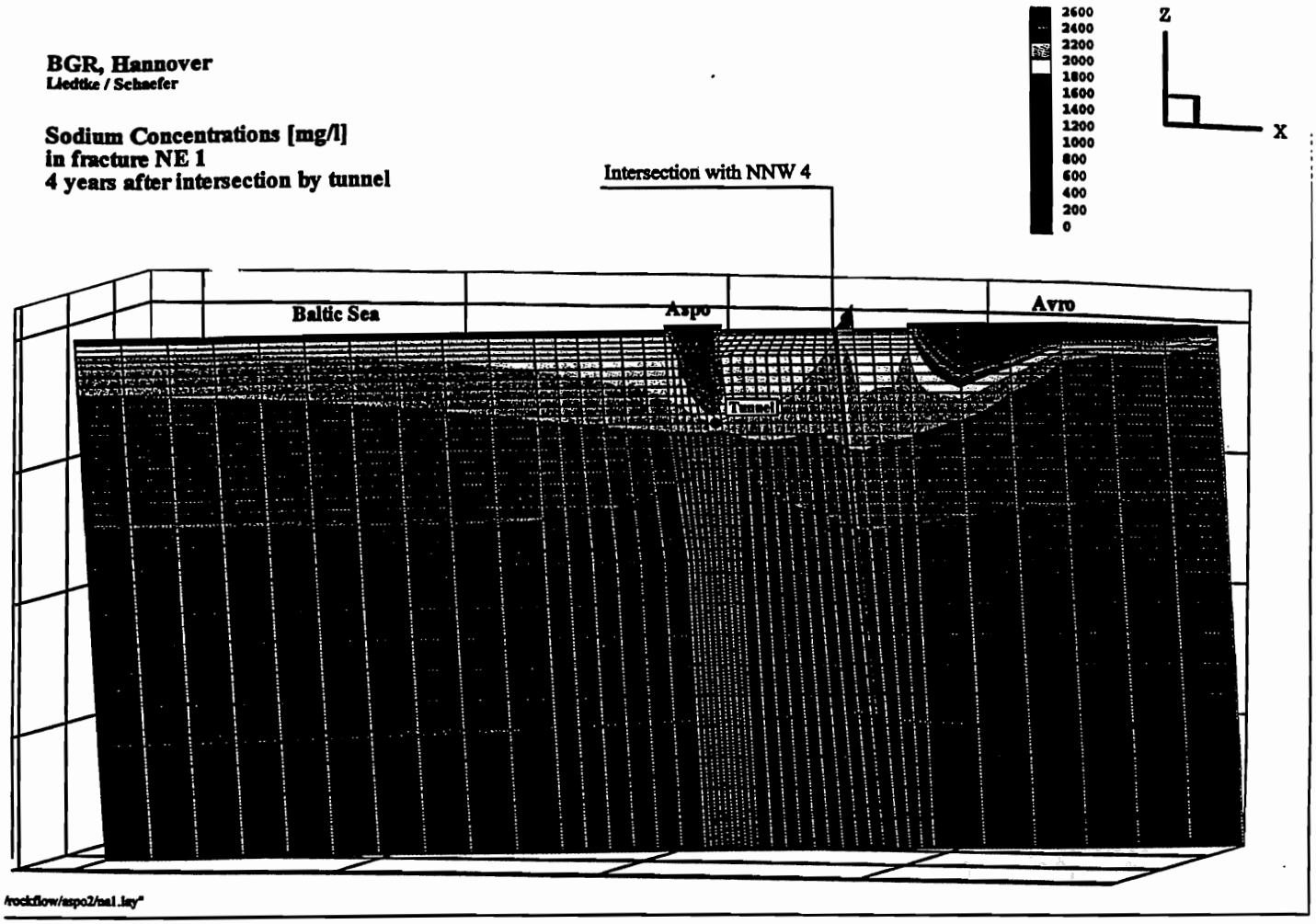

/rockflow/aspo2/na1.key"

BGR, Hannover
Liedtke / Schaefer

Calcium Concentrations [mg/l]
in fracture NE 1
undisturbed initial concentrations

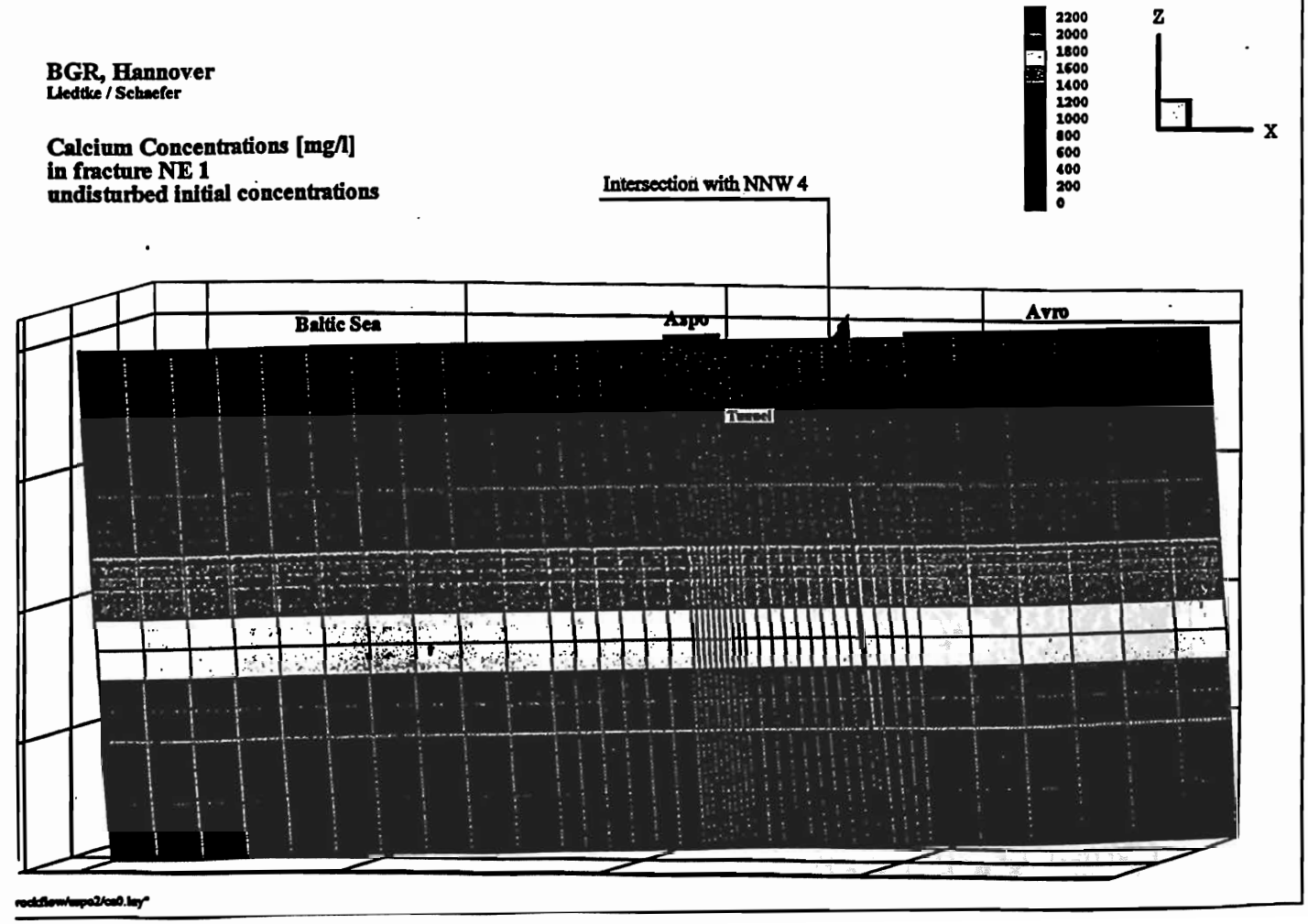

rockflow/aspo2/ca0.key"

Sodium Concentrations in Fracture Zone NE 1

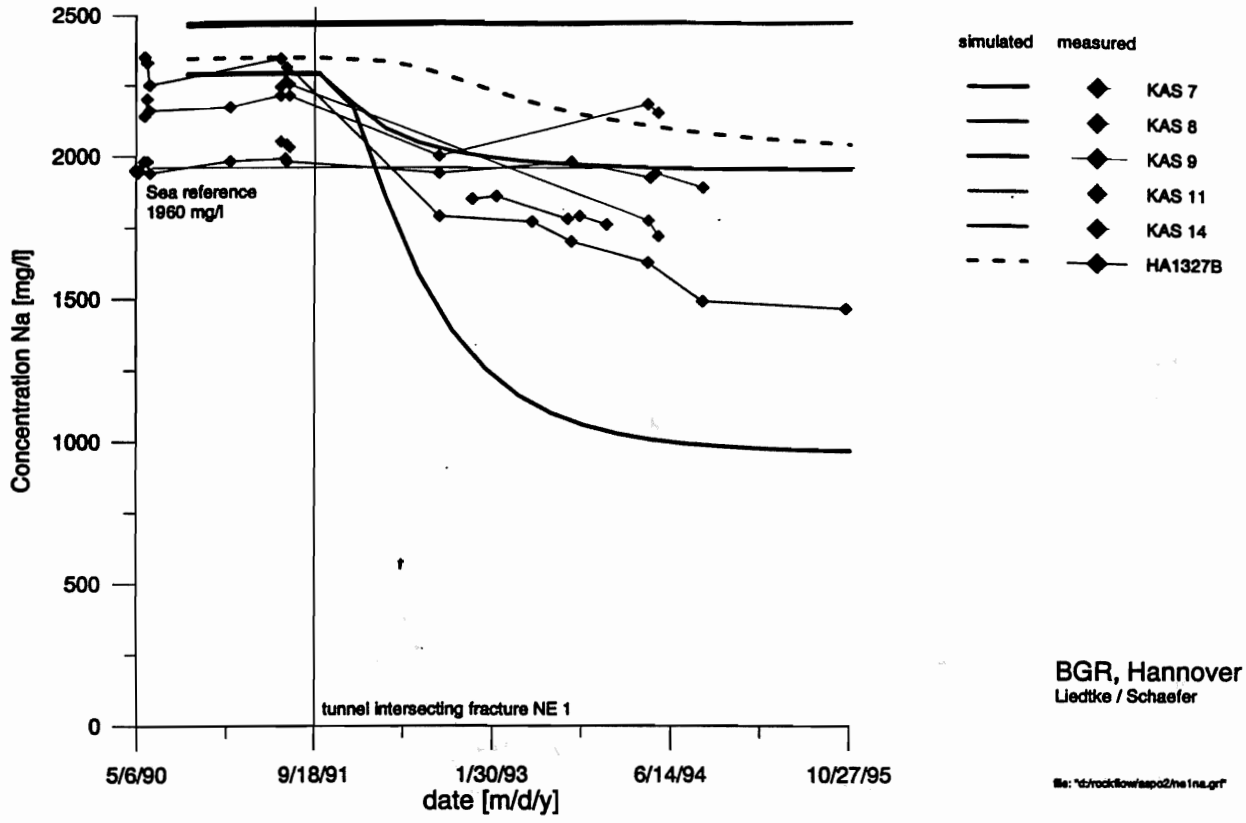

BGR, Hannover
Liedtke / Schaefer

file: "d:/rockflow/aspo2/ne1na.grf"

Calcium Concentrations in Fracture Zone NE 1

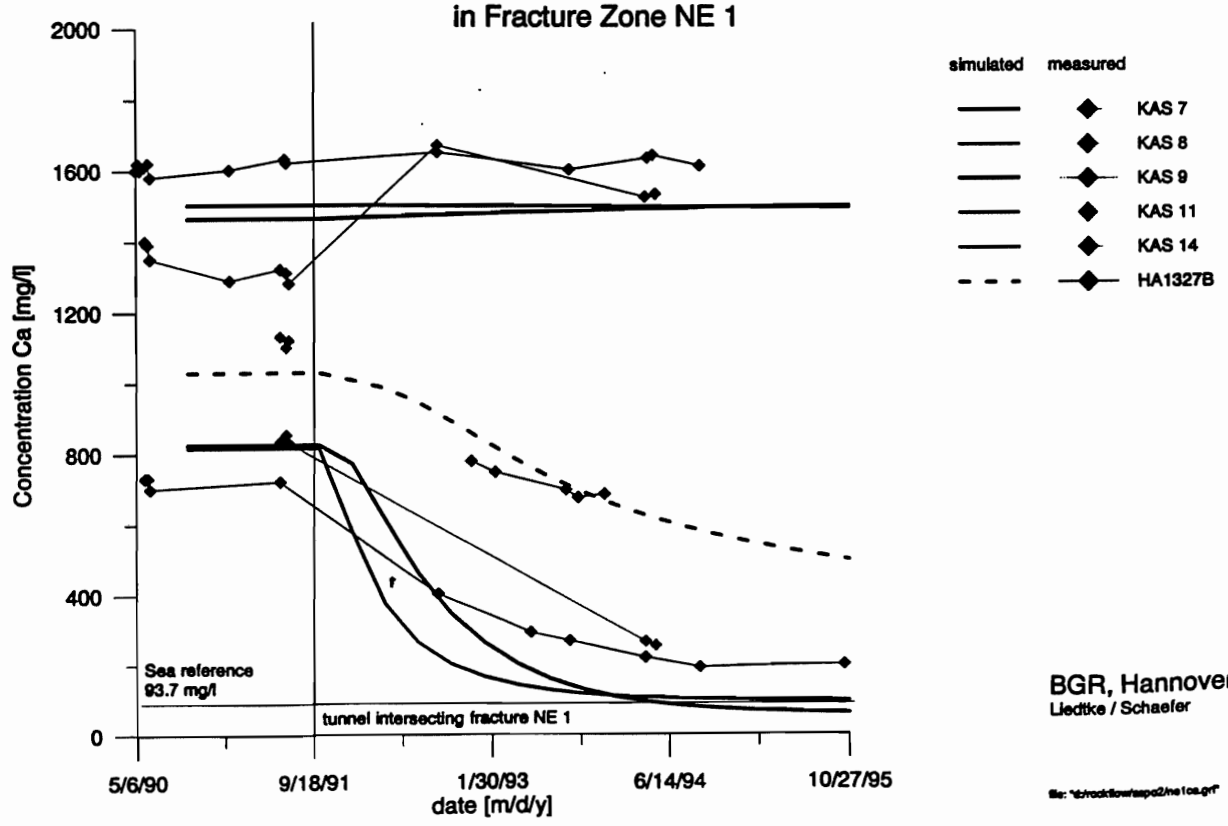

BGR, Hannover
Liedtke / Schaefer

file: "d:/rockflow/aspo2/ne1ca.grf"

BGR, Hannover
Liedtke / Schaefer

Calcium Concentrations [mg/l]
in fracture NE 1
4 years after intersection by tunnel

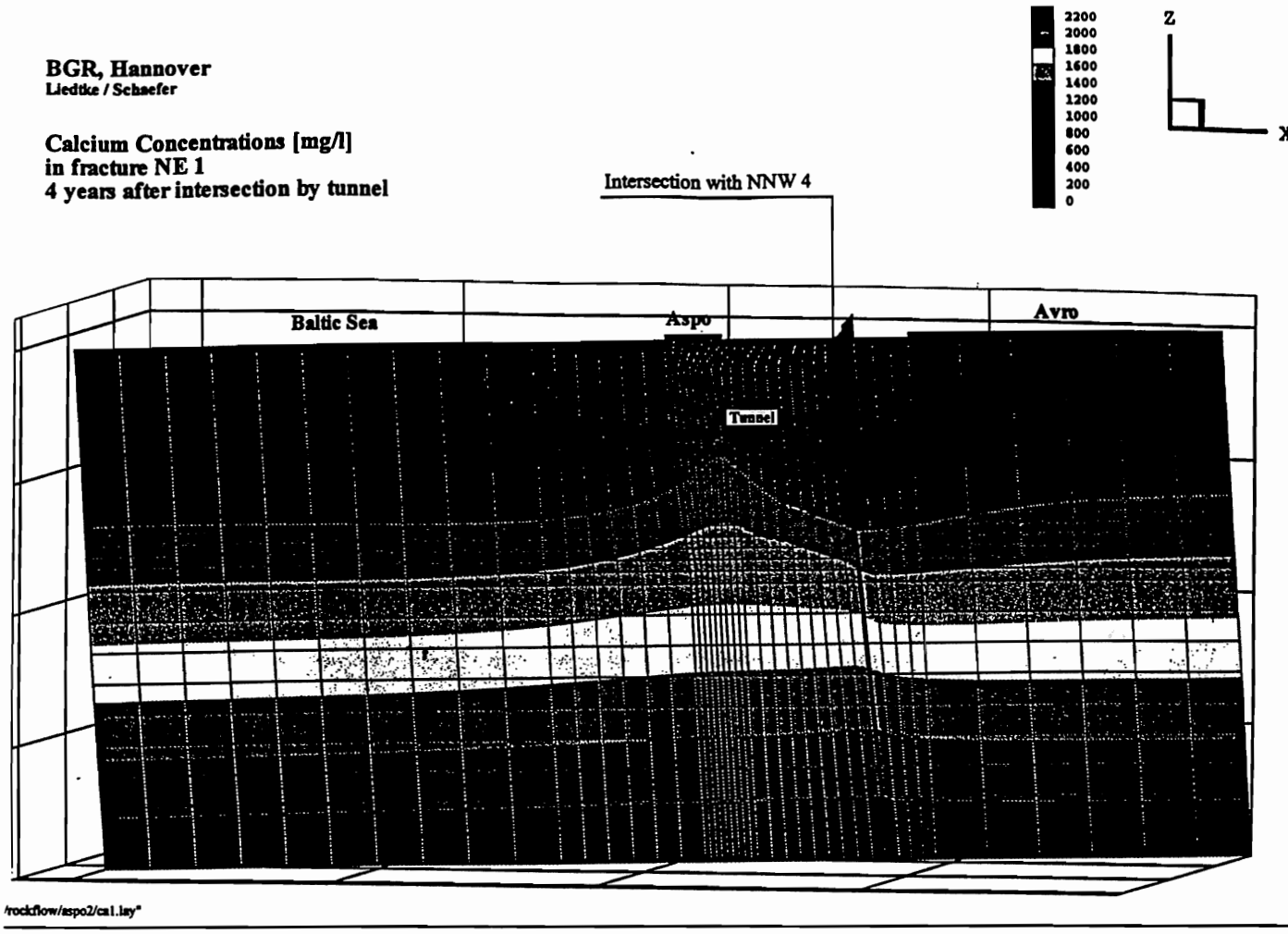

/rockflow/aspo2/ca1.lay*

Chloride Concentrations in Fracture Zone NE 1

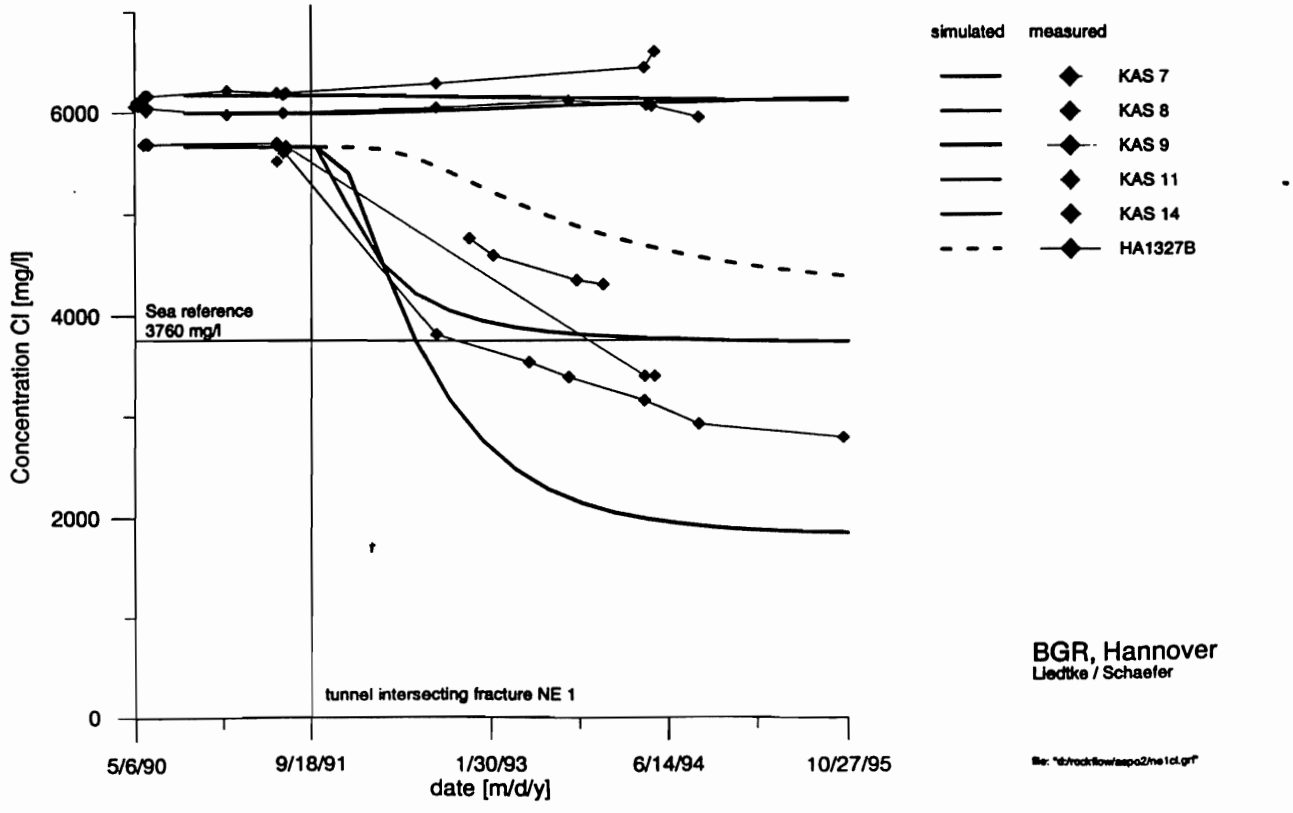

BGR, Hannover
Liedtke / Schaefer

file: *d:/rockflow/aspo2/ne1cl.grf*

Preliminary groundwater flow modelling results of Task5.

Eero Kattilakoski (POSIVA)

STATUS REPORT

Preliminary Groundwater Flow Modelling Results of Task 5

Eero Kattilakoski
VTT Energy

August 1998

TABLE OF CONTENTS

1 INTRODUCTION

1.1 Background

Task 5 (Impact of the tunnel construction on the groundwater system at Äspö, a hydrological-hydrochemical model assessment exercise) aims for the comparison and ultimate integration of hydrochemistry and hydrogeology. The consistency of groundwater flow models and hydrochemical mixing-reaction models is assessed through the integration and comparison of hydraulic and chemical data obtained before and during the tunnel construction. The modelling task will be useful for a stability assessment of the hydrodynamic and hydrochemical conditions at Äspö. A specific objective is the development of a procedure for the integration of hydrological and hydrochemical information which could be used for disposal site assessments — especially in a crystalline bedrock environment. (Wikberg, 1998)

1.2 Objectives

This work concerns with the groundwater flow modelling part of Task 5. No groundwater reactions have been modelled, only mixing. The simulation time steps cover the period from the natural conditions until the completed tunnel and shafts.

The flow model was constructed by including the hydrologic connections recognised during the tunnel construction. The observed properties of water and bedrock were included in the simulation model. The initial salinity boundary condition was fixed in accordance with the observations of the groundwater composition. The salinity and hydraulic data gained from boreholes was utilised to confirm the boundary conditions.

The FEFTRA code (formerly known as FEFLOW) was used to solve both the coupled equations of pressure and concentration and the transport equations of the different water types. The dual porosity transport model was applied to the equations of the different groundwater types, which were solved using the previously simulated pressure and salinity fields. The calculated mixing ratios were compared with those from a chemistry model.

2 MODEL CONCEPTS AND FORMULATION

2.1 Governing equations

The mathematical formulation of the equivalent continuum approach and the dual porosity approach is explained in detail by Löfman and Taivassalo (1995) and Löfman (1996).

The flow equation is expressed in terms of the residual pressure p — the actual pressure minus the hydrostatic component of freshwater (e.g. Bear, 1979; de Marsily, 1986):

$$\nabla \cdot (\frac{\rho \mathbf{k}}{\mu} \nabla (p + (\rho - \rho_0) g z)) = S_S \frac{\partial p}{\partial t}, \qquad (2.1)$$

where
- p is the residual pressure (Pa),
- ρ is the density of water (kgm^{-3}),
- ρ_0 is the freshwater density (kgm^{-3}),
- μ is the viscosity of water ($kgm^{-1}s^{-1}$),
- k is the permeability tensor of the medium (m^2),
- g is the gravitational acceleration (ms^{-2}) and
- S_S is the specific storage of the medium (m^{-1}).

The permeability tensor $\boldsymbol{k}$ in Eq. (2.1) can be expressed in terms of the hydraulic conductivity $\boldsymbol{K}$ (m/s):

$$\mathbf{k} = \frac{\mathbf{K}\mu}{\rho g}. \qquad (2.2)$$

The transport equation in the equivalent continuum model is written for the concentration of a solute as follows (e.g., Huyakorn and Pinder, 1983):

$$\nabla \cdot (\mathbf{D} \nabla c) - \nabla \cdot (\mathbf{q} c) + Q_{in} c_{in} - Q_{out} c = \frac{\partial (\phi_f c)}{\partial t}, \qquad (2.3)$$

where
- c is the concentration of the solute (g/l),
- $\boldsymbol{D}$ is the hydrodynamic dispersion tensor (m^2s^{-1}),
- q is the Darcy velocity (ms^{-1}),
- Q_{in} is the term for sources (s^{-1}),
- c_{in} is the concentration in the inflowing water (kgm^{-3}),
- Q_{out} is the term for sinks (s^{-1}) and
- ϕ_f is the flow porosity (-).

The components of the hydrodynamic dispersion tensor in Eq. (2.3) are

$$D_{ij} = \varepsilon_T |\mathbf{q}| \delta_{ij} + (\varepsilon_L - \varepsilon_T) \frac{q_i q_j}{|\mathbf{q}|}, \qquad (2.4)$$

where ε_L is the longitudinal dispersion length (m),
ε_T is the transversal dispersion length (m) and
δ_{ij} is the Kronecker delta function (-).

The Darcy velocity q in Eq. (2.3) in terms of the residual pressure p is

$$\mathbf{q} = -\frac{\mathbf{k}}{\mu}\nabla(p + (\rho - \rho_0)gz). \qquad (2.5)$$

In *the dual porosity approach* the equation describing mass transport in the water-bearing fractures is as follows (Huyakorn et al., 1983):

$$\nabla\cdot(\mathbf{D}\nabla c) - \nabla\cdot(\mathbf{q}c) + Q_{in}c_{in} - Q_{out}c + (1-\phi_f)\Gamma = \phi_f\frac{\partial c}{\partial t}, \qquad (2.6)$$

where c is the concentration of the solute (g/l),
D is the hydrodynamic dispersion coefficient, which includes dispersion and diffusion (m^2s^{-1}),
q is the Darcy velocity (ms^{-1}),
Q_{in} is the term for sources (s^{-1}),
c_{in} is the concentration in the inflowing water (kgm^{-3}),
Q_{out} is the term for sinks (s^{-1}),
ϕ_f is the flow (fracture) porosity (-) and
Γ is the rate of solute transfer from the matrix block to the fracture ($kgm^{-3}s^{-1}$).

The molecular diffusion, which dominates the mass transport in the matrix blocks, can be described with a one-dimensional diffusion equation

$$\frac{\partial}{\partial z'}(D_e'\frac{\partial c'}{\partial z'}) = \phi'\frac{\partial c'}{\partial t}, \qquad (2.7)$$

where c' is the concentration of the solute (g/l),
D_e' is the effective diffusion coefficient (m^2s^{-1}) and
ϕ' is the porosity in the matrix blocks (-).

In accordance with Archie's law (Valkiainen, 1992), the connection between the effective diffusion coefficient and the porosity can be stated

$$D_e' = 0{,}71\cdot D_0\phi'^{1.58}, \qquad (2.8)$$

where D_0 (m^2s^{-1}) is the molecular diffusion coefficient in water.

Equations (2.6) and (2.7) are coupled by the continuity of the diffusive mass flux at the interface of the fracture and the matrix block. For a rectangular matrix block unit the rate of solute transfer from the matrix block to the fracture is

$$\Gamma = -\frac{1}{a}(D_e'\frac{\partial c'}{\partial z'}\Big|_{z'=a}), \qquad (2.9)$$

where a (m) is half the fracture spacing, i.e., half the matrix block.

2.2 Numerical tool (Löfman, 1996)

The flow equation (2.1) and the transport equation (2.3) or (2.6) are coupled by the density ρ and the Darcy velocity **q** (Eq. (2.5)). This results in a system of two non-linear partial differential equations that can rarely be solved analytically. The finite element code FEFTRA was used in this work for the numerical solution.

The finite element method with linear elements was employed. The conventional Galerkin technique was applied to the flow equation. In order to avoid the numerical problems related to highly convective cases the transport equation was solved using the streamline-upwind/Petrov-Galerkin (SUPG) method (Brooks and Hughes, 1992; implemented in FEFTRA by Laitinen, 1995).

The dual porosity approach utilised the SUPG method with linear elements, too, when solving the transport equation (2.6) in the fractures. The conventional Galerkin method was applied to the diffusion equation (2.7) in the matrix blocks.

Non-linearities were treated by the Picard iteration scheme (Huyakorn and Pinder, 1983), which applies the finite element procedure for both the flow and the transport equation sequentially. At the end of each iteration sweep the pressure and concentration values are updated using an underrelaxation scheme. This way the oscillations of concentration changes from iteration to iteration are reduced. No iteration was needed in the mixing calculations of a single water type, which utilised the previously simulated pressure and salinity fields.

An initial estimate for the nodal values of the pressure and the concentration at the beginning of the first iteration sweep of each time step was obtained by using a linear time extrapolation formula.

The mass matrices resulting from the finite element formulation were formed by a diagonalization procedure known as "lumping" (Huyakorn and Pinder, 1983). In practical problems this leads to a more stable solution than with a "consistent" matrix.

The Gauss-Seidel method (Laitinen, 1994) was used to solve the matrix equation (2.6) in the mixing calculations. In the coupled calculations the conjugate gradient method was used to solve the finite element formulation of equation (2.1) for pressure and the Gauss-Seidel method to solve the finite element formulation of equations (2.3) and (2.6).

3 SIMULATION MODEL

3.1 Geometric framework

All the certain, probable and possible structures proposed by Rhén et al. (1997) were included in the model.

The regional zones SFZ05 and SFZ12 have dip angles of about 70 degrees. The other regional zones are vertical. All the regional zones extend to the depth of 1500 m.

The local zones were defined as quadrangles with corner points as proposed by the three points given by Rhén et al. (1997). The vertical zones were extended to the depth of 1500 m (except NNW-8, which extends to the depth of 700 m).

The hydraulic connections were established as given by Rhén et al. (1997, Fig. 6-31 and Table A2-6).

The definitions of the zones SFZ07 and EW-1N were combined: thus, the zone EW-1N has a regional extension in the model. The geometry of the zone NE-1 was combined with the geometry of SFZ12. The directions of the zones NE-3 and NE-4 were approximated with the average values of X, Y and Z given. In addition, NE-3 was connected with SFZ11 and EW-7.

The zone EW-1S was given an extension as far as SFZ07 and SFZ03. The assumed hydraulic connection of EW-1S with the zones NNW-1, NNW-2 and NNW-4 was formed. EW-3 stops at SFZ14 and SFZ12. The zone EW-7 was continued as far as SFZ12 and SFZ10.

The zones NE-2 and EW-1S were connected. The conductor NW-1 is assumed to terminate to the south at EW-1N. The conductor NNW-4 intersects with EW-1S and SFZ12. In the southern end, NNW-5 was connected with NE-4 and NNW-6 with EW-7. NNW-7 forms a connection with EW-3 and EW-1S. In addition, it was extended to the depth of 191 m.

The coordinates of the fracture zones included in the flow model are shown in Appendix A.

3.2 Finite element mesh

The finite elements for the rock blocks are linear hexahedrals and wedges. The base mesh formed by these elements is the same as in the study by Mészáros (1996). Triangles and quadrangles are used for the fracture zones. Furthermore, one-dimensional elements are needed to model the tunnel and shaft sections. The mesh contains 58308 three-dimensional elements, 13443 two-dimensional elements and 87 one-dimensional elements.

The element mesh extends from the sea level to the depth of 1500 m (as in Mészáros, 1996).

3.3 Material properties (Rhén et al., 1997)

The properties of water employed in the simulations are shown in Table 3.1.

Table 3.1. The properties of water.

Symbol	Parameter	Value	Reference
μ	Viscosity	1,0e-3 $kgm^{-1}s^{-1}$	Lide (1990)
ρ_0	Freshwater density	998,585 kgm^{-3}	
D_0	Molecular diffusion coefficient [1)]	1,0e-9 m^2s^{-1}	Löfman and Taivassalo (1995)
a_C	Density dependence on salinity	0,741	Rhén et al. (1997) s. 183
ε_L	Longitudinal dispersion length	100 m	Löfman and Taivassalo (1995), de Marsily (1986)
ε_T	Transversal dispersion length	10 m	Löfman and Taivassalo (1995), de Marsily (1986)
ϕ	Diffusion porosity [1)]	3,5e-3	Rhén et al. (1997) s. 22, s. 403
C_{vh}	Coefficient for dependence between the volume and hydraulic apertures	10	Vieno et al. (1992)

[1)] employed only with the dual porosity model

The properties of the fracture zones are shown in Table 3.2. The transmissivities T (m^2/s), the widths of the zones, storage coefficients S (-), the fracture spacings $2a$ (m), the fracture apertures $2b$ (m) and the flow porosities ϕ_f (-) are shown.

Rhén et al. (1997) give the linear relationship between $\log_{10}T$ and $\log_{10}S$. They notice that the relation seems to give unrealistic low S values for very low T values. For that reason, for S the value max(1,0e-6; S) is used in this work. There are also few points for the regression which makes the relation mentioned above uncertain. However, the variability in S values is probably relatively large.

The fracture aperture $2b$ (m) is given as a function of the fracture spacing $2a$ (m) and the hydraulic conductivity K as follows (Taivassalo and Saarenheimo, 1991)

$$2b = C_{vh}\left(\frac{12\mu}{\rho_0 g} K 2a\right)^{1/3}, \qquad (3.1)$$

where C_{vh} (Vieno et al., 1992) is the coefficient for the dependence between the volume and the hydraulic fracture aperture, μ the viscosity of water (Lide, 1990), ρ_0 the freshwater density and g the gravitational acceleration (9,81 m/s^2).

The flow porosity ϕ_f (-) is given as follows (as in Löfman, 1996)

$$\phi_f = \frac{b}{a+b}. \qquad (3.2)$$

The transmissivity of the zone EW-3 has a depth dependence (Rhén et al., 1997 A2:14)

$$T = T_0 \cdot 10^{cd}, \qquad (3.3)$$

where T_0 is the transmissivity at the ground surface given in Table 3.2, c is the coefficient for the depth dependence (-3,9e-3 m^{-1}) and d is the depth (m). The ratio S/T is kept constant (S/T_0).

Table 3.2. The properties of the fracture zones.

zone	T (m^2/s)	width of zone (m) Rhén et al., 1997	a	b	$S=aT^b$ (-) Rhén et al., 1997 s. 214-215	max (1,0E-6; S)	$2a$ (m) Rhén et al., 1997 s. 117	$2b$ (m)	ϕ_f (-)
SFZ01	3,0E-06	2,0E+01	9,2E-03	7,9E-01	4,3E-07	1,0E-06	5,0E-02	8,3E-05	1,7E-03
SFZ02	1,0E-04	2,0E+01	9,2E-03	7,9E-01	6,7E-06	6,7E-06	5,0E-02	8,3E-05	1,7E-03
SFZ03	3,0E-06	2,0E+01	9,2E-03	7,9E-01	4,3E-07	1,0E-06	5,0E-02	8,3E-05	1,7E-03
SFZ04	3,0E-06	2,0E+01	9,2E-03	7,9E-01	4,3E-07	1,0E-06	5,0E-02	8,3E-05	1,7E-03
SFZ05	1,0E-04	2,0E+01	9,2E-03	7,9E-01	6,7E-06	6,7E-06	5,0E-02	8,3E-05	1,7E-03
SFZ06	3,0E-06	2,0E+01	9,2E-03	7,9E-01	4,3E-07	1,0E-06	5,0E-02	8,3E-05	1,7E-03
SFZ08	3,0E-06	2,0E+01	9,2E-03	7,9E-01	4,3E-07	1,0E-06	5,0E-02	8,3E-05	1,7E-03
SFZ09	3,0E-06	2,0E+01	9,2E-03	7,9E-01	4,3E-07	1,0E-06	5,0E-02	8,3E-05	1,7E-03
SFZ10	1,0E-04	2,0E+01	9,2E-03	7,9E-01	6,7E-06	6,7E-06	5,0E-02	8,3E-05	1,7E-03
SFZ11	3,0E-06	2,0E+01	9,2E-03	7,9E-01	4,3E-07	1,0E-06	5,0E-02	8,3E-05	1,7E-03
SFZ12	3,0E-04	2,0E+01	9,2E-03	7,9E-01	1,6E-05	1,6E-05	5,0E-02	8,3E-05	1,7E-03
SFZ13	3,0E-06	2,0E+01	9,2E-03	7,9E-01	4,3E-07	1,0E-06	5,0E-02	8,3E-05	1,7E-03
SFZ14	3,0E-06	2,0E+01	9,2E-03	7,9E-01	4,3E-07	1,0E-06	5,0E-02	8,3E-05	1,7E-03
SFZ15	1,0E-04	2,0E+01	9,2E-03	7,9E-01	6,7E-06	6,7E-06	5,0E-02	8,3E-05	1,7E-03
EW-1N	5,2E-07	3,0E+01	9,2E-03	7,9E-01	1,1E-07	1,0E-06	5,0E-02	8,3E-05	1,7E-03
EW-1S	1,2E-05	3,0E+01	9,2E-03	7,9E-01	1,3E-06	1,3E-06	5,0E-02	8,3E-05	1,7E-03

Table 3.2. (cont.) The properties of the fracture zones.

zone	T (m^2/s)	width of zone (m) Rhén et al., 1997	a	b	$S=aT^b$ (-) Rhén et al., 1997 s. 214-215	max (1,0E-6; S)	$2a$ (m) Rhén et al., 1997 s. 117	$2b$ (m)	ϕ_f (-)
EW-3	1,2E-05 (T_0)	1,5E+01	9,2E-03	7,9E-01	1,3E-06	1,3E-06	5,0E-02	8,3E-05	1,7E-03
EW-7	1,5E-05	1,0E+01	9,2E-03	7,9E-01	1,5E-06	1,5E-06	5,0E-02	8,3E-05	1,7E-03
NE-2	8,0E-06	5,0E+00	9,2E-03	7,9E-01	9,2E-07	1,0E-06	5,0E-02	8,3E-05	1,7E-03
NE-3	3,2E-04	5,0E+01	9,2E-03	7,9E-01	1,7E-05	1,7E-05	5,0E-02	8,3E-05	1,7E-03
NE-4	3,1E-05	4,0E+01	9,2E-03	7,9E-01	2,7E-06	2,7E-06	5,0E-02	8,3E-05	1,7E-03
NW-1	4,1E-07	1,0E+01	9,2E-03	7,9E-01	8,9E-08	1,0E-06	5,0E-02	8,3E-05	1,7E-03
NNW-1	3,0E-05	2,0E+01	9,2E-03	7,9E-01	2,6E-06	2,6E-06	5,0E-02	8,3E-05	1,7E-03
NNW-2	1,0E-05	2,0E+01	9,2E-03	7,9E-01	1,1E-06	1,1E-06	5,0E-02	8,3E-05	1,7E-03
NNW-3	2,0E-05	2,0E+01	9,2E-03	7,9E-01	1,9E-06	1,9E-06	5,0E-02	8,3E-05	1,7E-03
NNW-4	6,5E-05	1,0E+01	9,2E-03	7,9E-01	4,8E-06	4,8E-06	5,0E-02	8,3E-05	1,7E-03
NNW-5	4,0E-06	2,0E+01	9,2E-03	7,9E-01	5,3E-07	1,0E-06	5,0E-02	8,3E-05	1,7E-03
NNW-6	1,4E-05	2,0E+01	9,2E-03	7,9E-01	1,4E-06	1,4E-06	5,0E-02	8,3E-05	1,7E-03
NNW-7	8,0E-05	2,0E+01	9,2E-03	7,9E-01	5,6E-06	5,6E-06	5,0E-02	8,3E-05	1,7E-03
NNW-8	1,0E-06	2,0E+01	9,2E-03	7,9E-01	1,8E-07	1,0E-06	5,0E-02	8,3E-05	1,7E-03

The properties of the rock are shown in Table 3.3. The specific storage S_S (m^{-1}) is derived from a linear relationship between $\log_{10}K$ and $\log_{10}S_S$ given by Rhén et al. (1997).

Table 3.3. The properties of the rock.

rock	K (m/s) Rhén et al., 1997 s. 365, 219	a	b	S_S $=aK^b$ (m^{-1}) Rhén et al., 1997 s. 241-242	$2a$ (m) Rhén et al., 1997 s. 131	$2b$ (m)	ϕ_f (-)
	9,3E-09	6,0E-05	2,3E-01	8,4E-07	4,5E-01	1,7E-04	3,8E-04

The properties of the tunnel and the shafts are shown in Table 3.4. The value K_{ID} is the hydraulic conductivity of the feature times the area of a cross-section. S_{ID} is the product of the specific storage and the cross area of the feature. The values K_{ID} and S_{ID} are given by Mészáros (1996).

Table 3.4. The properties of the tunnel and the shafts.

	K_{1D} (m³/s)	S_{1D} (m)	$2a$ (m) Rhén et al., 1997 s. 131	$2b$ (m)	ϕ_f (-)
tunnel 1D	3,5E-02	1,0E-07	2,0	2,8E-04	1,4E-04
tunnel 1D (seals)	3,5E-15	1,0E-10	2,0	2,8E-04	1,4E-04
shafts 1D	3,5E-02	1,0E-10	3,33	3,4E-04	1,0E-04

3.4 Boundary conditions

Twelve time steps were chosen. They cover the period from the natural conditions until the completed tunnel and shafts (Table 3.5).

Table 3.5. The modelling period with comments on the tunnel and shaft updating.

Time step	Date	Days after 19.10.1990	Comments on modelling
0	0,5 years before 19.10.1990	-	Start of modelling period
1	19.10.1990	0	
2	21.05.1991	214	First tunnel updating, release of groundwater table over the land
3	10.02.1992	479	
4	03.08.1992	654	
5	10.11.1992	753	First updating of shafts
6	24.02.1993	859	
7	03.06.1993	958	
8	03.11.1993	1111	No updating of tunnel
9	24.01.1994	1193	Second updating of shafts
10	16.06.1994	1336	
11	16.09.1994	1428	
12	24.01.1995	1558	Last updating of shafts

The tunnel advance is modelled by giving a zero residual pressure to the nodes describing the tunnel and shafts in each time step. Thus, the linear one-dimensional elements used to describe the tunnel and shafts are all along in the model, because for the time being the element mesh cannot be modified during the solver part of the simulation. In fact, the modification of the element mesh would not be necessary — the changing of the hydraulic conductivities attached to the tunnel and shaft elements would be adequate.

3.4.1 Solving of pressure and salinity fields

The fixing of the initial salinity boundary condition is described in detail in Section 4.

The density of saline water (kg/m³) is given by the following equation (Rhén et al., 1997)

$$\rho = \rho_0 + a_C S, \tag{3.4}$$

where ρ_0 is the freshwater density (998,585 kg/m³), a_C is the coefficient of the density dependence on the salinity (0,741) and S is the salinity (g/l).

Thus, the hydraulic pressure (Pa) can be expressed as

$$p = p_{fresh}(d) + a_C g \int_0^d S(d_z)\, dd_z, \tag{3.5}$$

where p_{fresh} is the freshwater pressure, g is the gravitational acceleration (9,81 m/s²) and d is the depth (m).

The residual pressure (Pa) is

$$p_{res} = a_C g \int_0^d S(d_z)\, dd_z. \tag{3.6}$$

The initial (t=0) pressure boundary condition for each node of the element mesh under the sea level is calculated with Eq. (3.6), after the initial salinity distribution has been determined (Section 4.2). Zero residual pressure is applied at the sea level, while groundwater table is specified over the land.

In the first time step the pressure and salinity boundary conditions given in the interior nodes of the element mesh are released. The pressure boundary condition in the bottom nodes is also released.

In the second time step the progress of the tunnel is taken into account for the first time. The groundwater table boundary condition at the surface of the model is released (see Table 3.5).

3.4.2 Transport of water types or tracers

Table 3.6 shows the concentrations of the main constituents in the 100 % mixing ratios of the different water types. The main constituents used in this work are Na, K, Ca, Mg, HCO_3, Cl and SO_4.

Table 3.6. The concentrations of the main constituents (mg/l) in the different groundwater types identified in Äspö.

Main constituents (mg/l)								Water type			
Na	K	Ca	Mg	HCO3	Cl	SO4	Σ	Brine %	Glacial %	Meteoric %	Marine %
8500	45,5	19300	2,12	14,1	47200	906	75967,7	100,0	0,0	0,0	0,0
0,17	0,4	0,18	0,1	0,12	0,5	0,5	1,97	0,0	100,0	0,0	0,0
3180	154	152	380	146	6100	527	10638,8	0,0	0,0	0,0	100,0
0,4	0,29	0,24	0,1	12,2	0,23	1,4	14,86	0,0	0,0	100,0	0,0

The initial boundary conditions for the different water types are given in the basis of the chemical modelling done by Gurban et al. (1998). They give calculated mixing ratios in a grid covering from west to east Laxemar, Äspö, Ävrö and Mjälen. The concentrations of each water type identified by those given ratios are then interpolated to the nodes of the element mesh used in this work. For example, in the point (Easting, Northing, elevation) = (2200,4; 5880,1; -1500,0) Gurban et al. (1998) give the following mixing ratios: brine 96,7 %, glacial 4,3 %, meteoric 0 % and marine 1,6 %. Thus, according to the summed up contents of the main constituents given in Table 3.6, the concentrations used in the interpolation are approximately the following: brine 73,5 g/l, glacial 0,08 mg/l, meteoric 0 g/l and marine 0,17 g/l.

The boundary condition given in an interior node is then released in the first time step.

4 CALIBRATION

4.1 Introduction

The calibration was made in order to give the model an initial boundary condition consistently with the natural conditions which prevailed before the tunnel construction.

4.2 First calibration case

The model was calibrated in accordance with the salinity data available from boreholes KAS02-KAS09, KAS11-KAS14, KAS16 and KBH02. The data measured before the start of the tunnel excavation (19.10.1990) was used.

The inspection of the salinity measurements resulted in the following linear salinity distribution (Table 4.1) used throughout the modelled volume. Over the land zero salinity was used. The salinity at the sea level was 5 g/l.

Table 4.1. Initial salinity in the first calibration case.

Depth (m)	Salinity (g/l)
0	3
200	5
450	10
725	11,6
950	18
1500	18

In order to compare the freshwater hydraulic heads gained from boreholes with the calculated residual pressures, the corresponding residual pressures were calculated from the freshwater hydraulic heads, as follows:

$$p_{res}(z) = \rho_0 g h_0(z), \qquad (4.1)$$

where ρ_0 is the freshwater density (998,585 kg/m^3), g is the gravitational acceleration (9,81 m/s^2) and $h_0(z)$ is the freshwater hydraulic head (m) given in the basis of borehole measurements.

The calibration results of the first calibration case are shown in Figures 4.1 and 4.2. Calculated and measured salinities in boreholes are shown in Figure 4.1, while the residual pressures are shown in Figure 4.2.

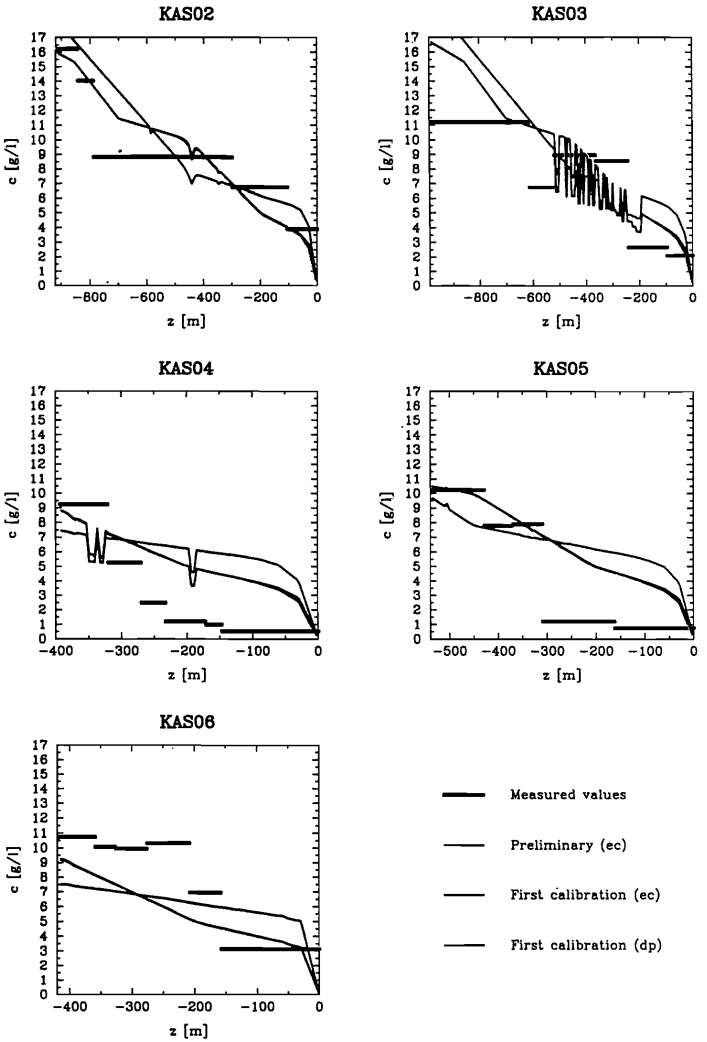

Figure 4.1. Calculated and measured salinities in boreholes KAS02-KAS06 in the first calibration case. Results are shown both from the equivalent continuum model (ec) and the dual porosity model (dp).

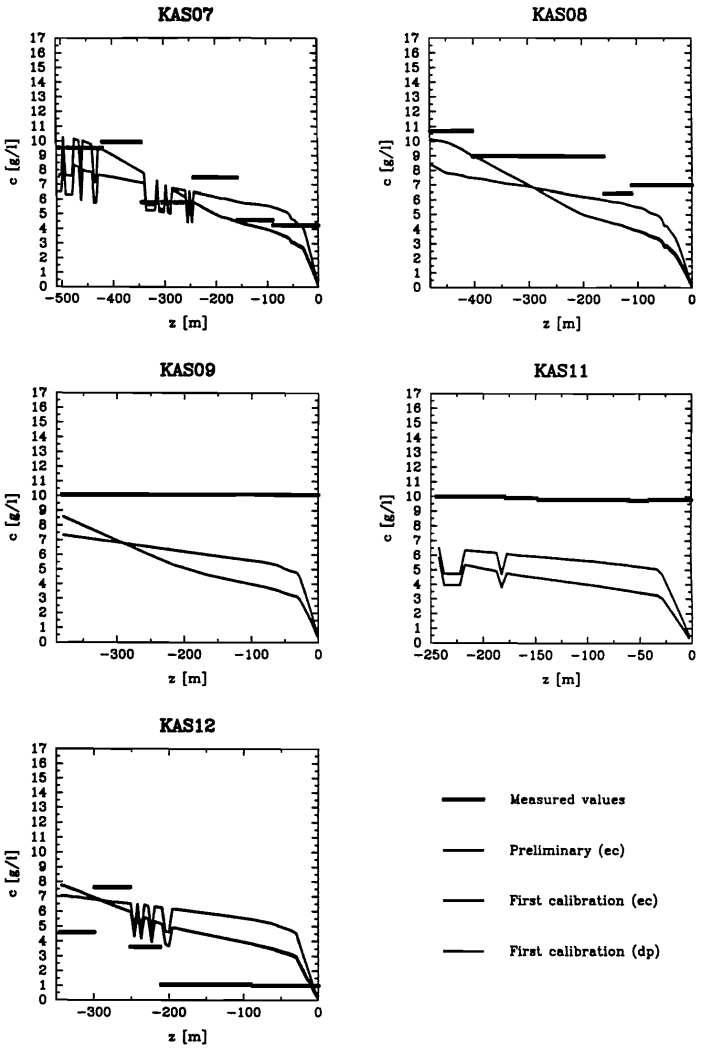

Figure 4.1. (cont.) Calculated and measured salinities in boreholes KAS07-KAS09, KAS11 and KAS12 in the first calibration case. Results are shown both from the equivalent continuum model (ec) and the dual porosity model (dp).

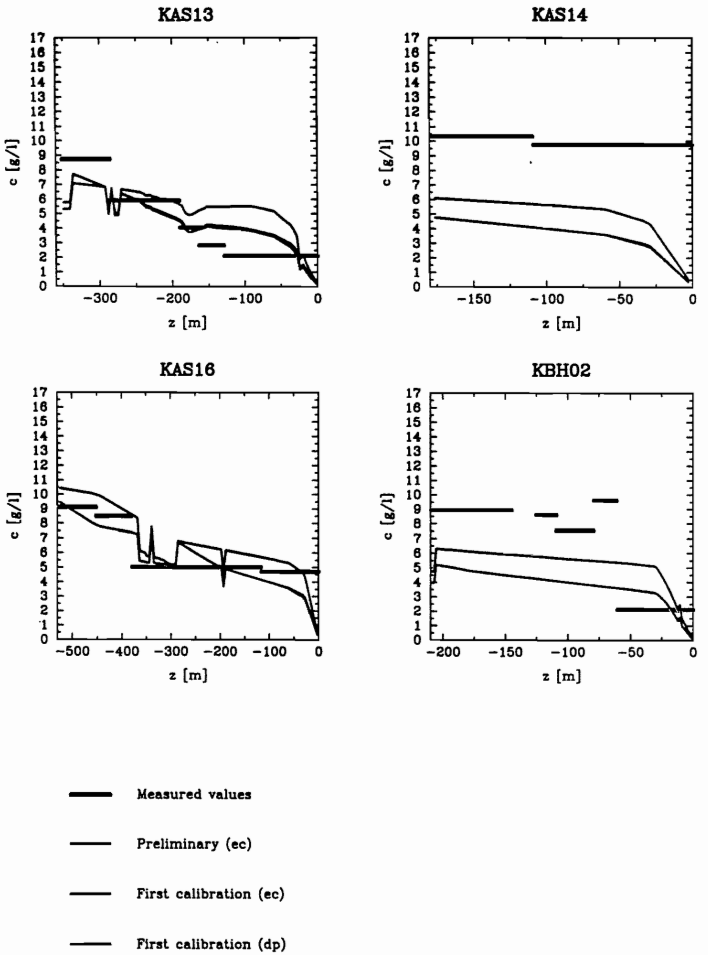

Figure 4.1. (cont.) Calculated and measured salinities in boreholes KAS13, KAS14, KAS16 and KBH02 in the first calibration case. Results are shown both from the equivalent continuum model (ec) and the dual porosity model (dp).

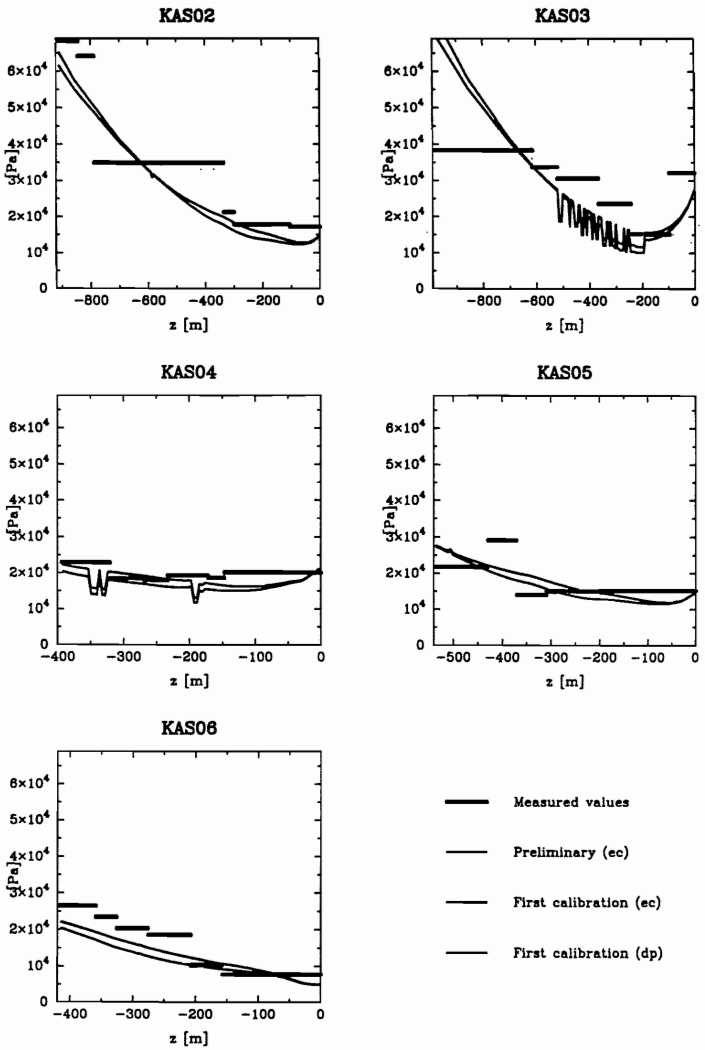

Figure 4.2. Residual pressures in boreholes KAS02-KAS06 in the first calibration case. Results are shown both from the equivalent continuum model (ec) and the dual porosity model (dp).

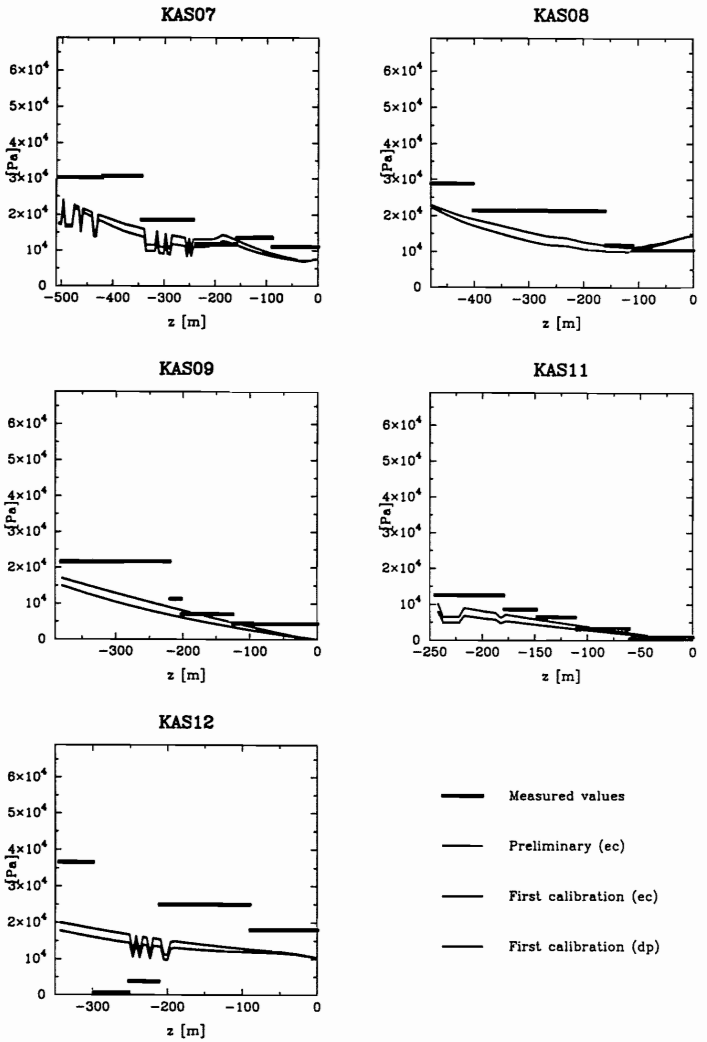

Figure 4.2. (cont.) Residual pressures in boreholes KAS07-KAS09, KAS11 and KAS12 in the first calibration case. Results are shown both from the equivalent continuum model (ec) and the dual porosity model (dp).

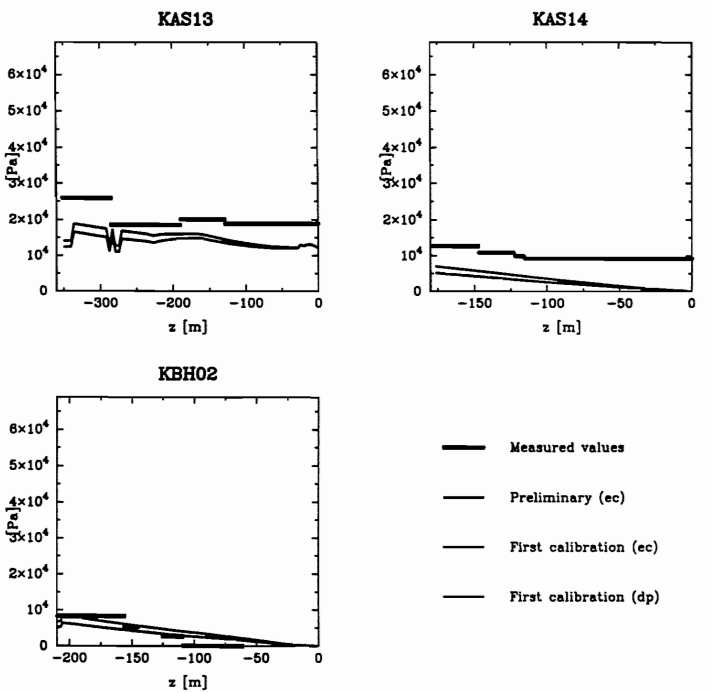

Figure 4.2. (cont.) Residual pressures in boreholes KAS13, KAS14 and KBH02 in the first calibration case. Results are shown both from the equivalent continuum model (ec) and the dual porosity model (dp).

4.3 Second calibration case

In the second calibration case the initial salinity boundary condition was defined in accordance with the chemical modelling by Gurban et al. (1998). They present the concentrations of the main constituents Na, Ca, HCO_3, Cl and SO_4 extracted from an interpolation grid prior to the tunnel construction. The interpolation was based on the measured data. Their model domain covers an area with the surface coordinates as following: (-300,0; 5600,0), (-300,0; 8121,0), (3450,44; 5600,0), (3450,44; 8121,0). The depth of the box is 1500 m.

Initially each node inside, in the vertical sides and in the bottom of the mesh used in this work was assigned with the summed up concentration value of the main constituents (g/l) from the nearest point in the model by Gurban et al. (1998). In the first time step, the interior boundary condition was released, however. Zero salinity was used over the land due to the freshwater

flow into the groundwater system. This is caused by the hydraulic gradient of the water table of the Äspö island. The salinity used at the sea level was 3 g/l.

The pressure boundary condition used was the same as in the first calibration case; thus, the pressure and concentration boundary conditions were not consistent. Nonetheless, there were no problems with the convergence in the first time step during the actual result calculation.

The calibration results of the second calibration case are shown in Figures 4.3 and 4.4. Calculated and measured salinities in boreholes are shown in Figure 4.3, while the residual pressures are shown in Figure 4.4.

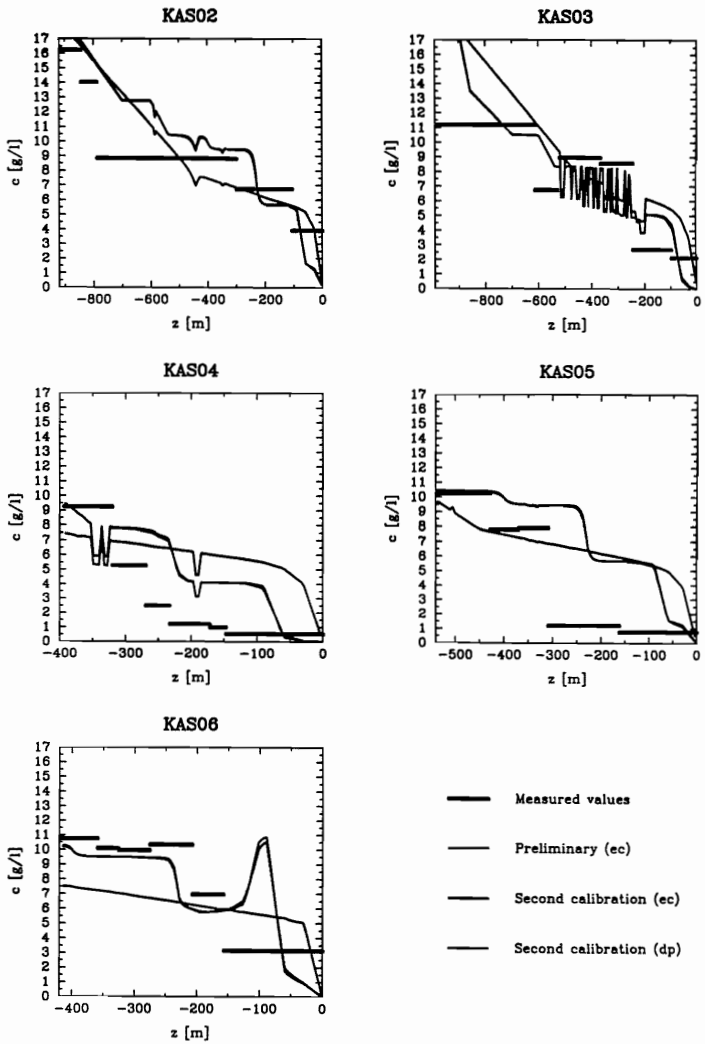

Figure 4.3. Calculated and measured salinities in boreholes KAS02-KAS06 in the second calibration case. Results are shown both from the equivalent continuum model (ec) and the dual porosity model (dp).

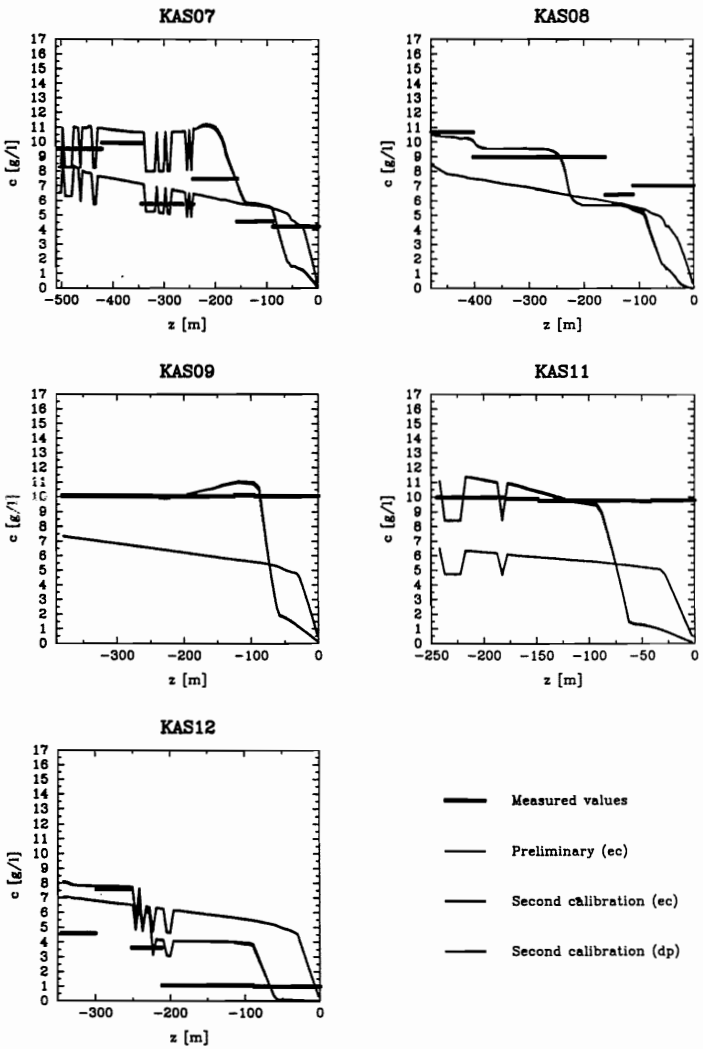

Figure 4.3. (cont.) Calculated and measured salinities in boreholes KAS07-KAS09, KAS11 and KAS12 in the second calibration case. Results are shown both from the equivalent continuum model (ec) and the dual porosity model (dp).

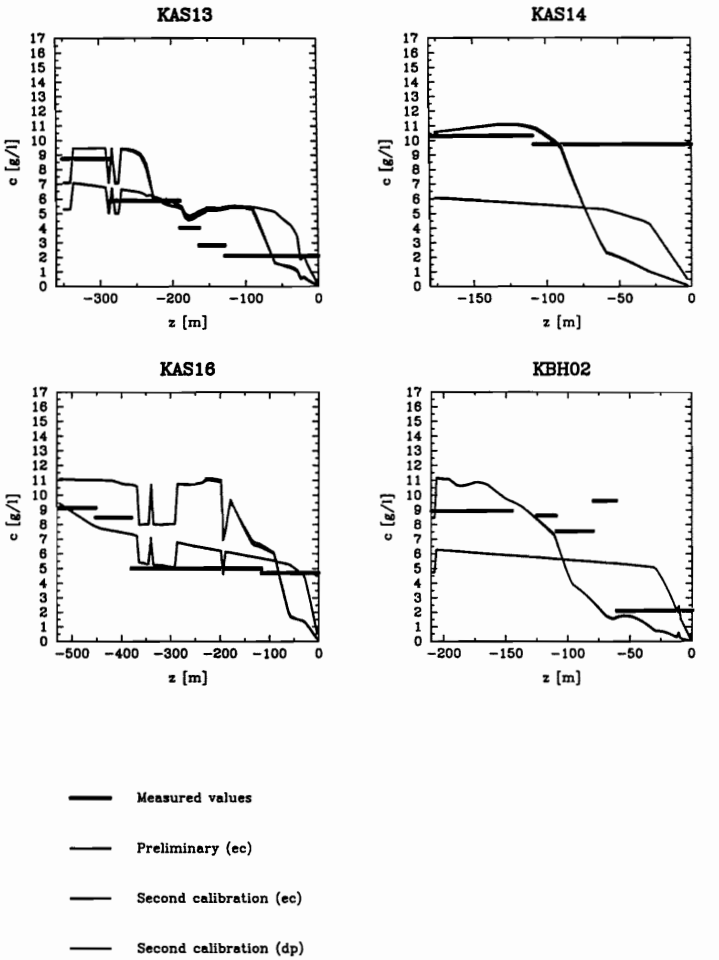

Figure 4.3. (cont.) Calculated and measured salinities in boreholes KAS13, KAS14, KAS16 and KBH02 in the second calibration case. Results are shown both from the equivalent continuum model (ec) and the dual porosity model (dp).

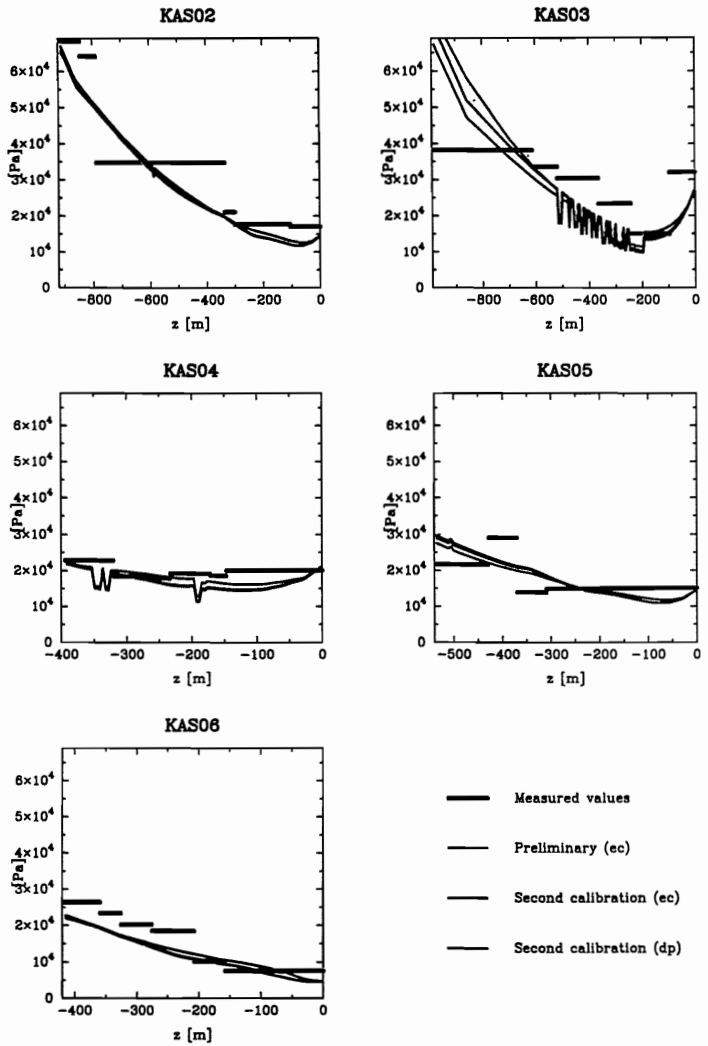

Figure 4.4. Residual pressures in boreholes KAS02-KAS06 in the second calibration case. Results are shown both from the equivalent continuum model (ec) and the dual porosity model (dp).

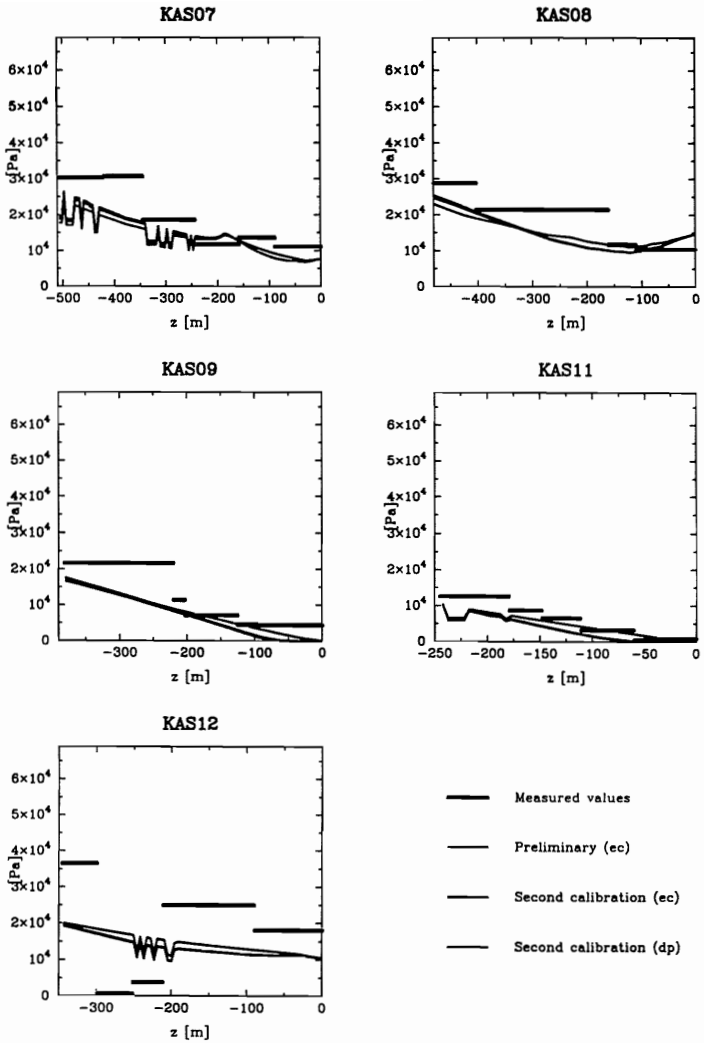

Figure 4.4. (cont.) Residual pressures in boreholes KAS07-KAS09, KAS11 and KAS12 in the second calibration case. Results are shown both from the equivalent continuum model (ec) and the dual porosity model (dp).

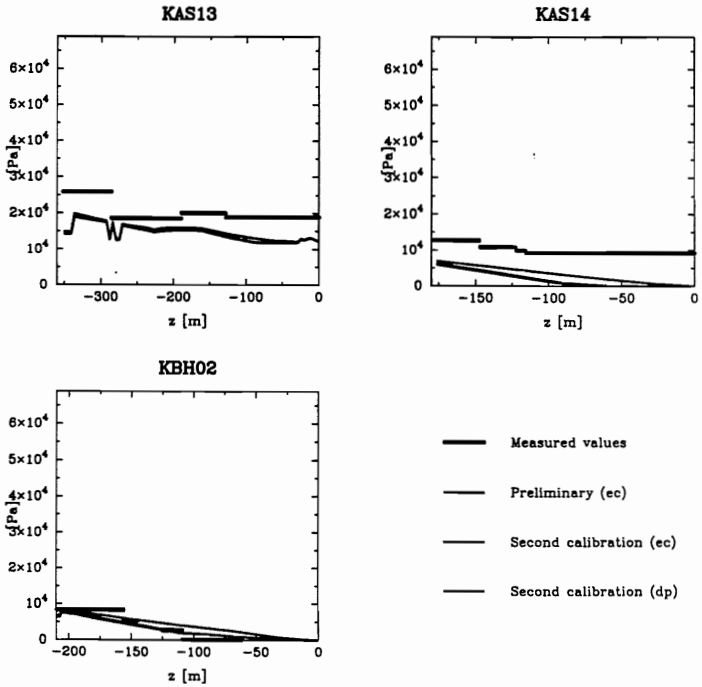

Figure 4.4. (cont.) Residual pressures in boreholes KAS13, KAS14 and KBH02 in the second calibration case. Results are shown both from the equivalent continuum model (ec) and the dual porosity model (dp).

5 MAIN RESULTS

5.1 Introduction

In the first calibration case the coupled calculation of the pressure and the salinity fields was performed with the equivalent continuum model and in the second case with the dual porosity model. The mixing calculations of the different water types were then performed using these previously simulated pressure and salinity fields. The mixing results which are presented in this section were calculated with the dual porosity model.

Gurban et al. (1998) list overall 65 control points in Äspö HRL tunnel, where measurement data concerning the concentrations is available. The mixing results available from the chemical modelling by Gurban et al. (1998) are compared here with the results from the two calibration cases (Section 4).

5.2 Natural conditions

In this work, the flow equation is expressed in terms of the residual pressure. The flow direction can not generally be determined from the residual pressure contours, except in a freshwater zone. The "driving" pressure is defined as a sum of the residual pressure p and the buoyancy term as follows

$$p_d = p + (\rho - \rho_0) g z \,. \tag{5.1}$$

The flow direction is determined by the gradient of the "driving" pressure. Thus, the flow direction is perpendicular to the equipotential lines of the "driving" pressure. Taking into account that water flows from the area of higher pressure to the area of a lower value, the direction can be deduced from the contours. However, only the main flow directions can be determined from the contours. (Löfman, 1996)

Figure 5.1 presents the "driving" pressure (kPa) on a NS trending cutplane before and after the tunnel construction in the first calibration case. Figure 5.2 presents the salinity (g/l) on the same cutplane. The "driving" pressure and the salinity on a EW trending cutplane are presented in Figures 5.3 and 5.4, respectively.

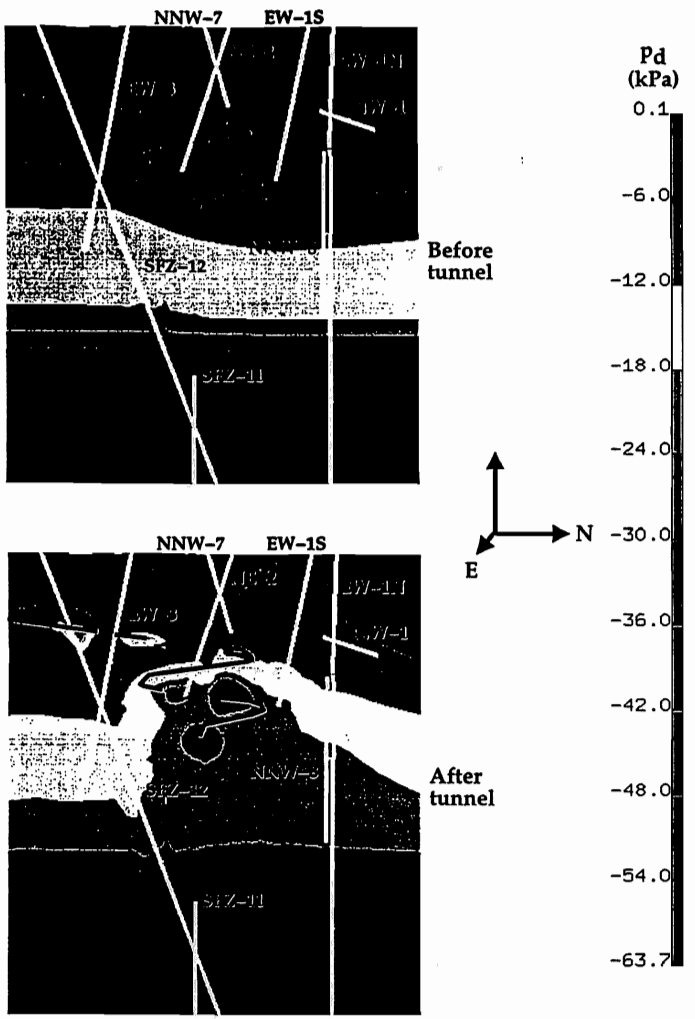

Figure 5.1. The "driving" pressure (kPa) on a NS trending cutplane before and after the tunnel construction in the first calibration case.

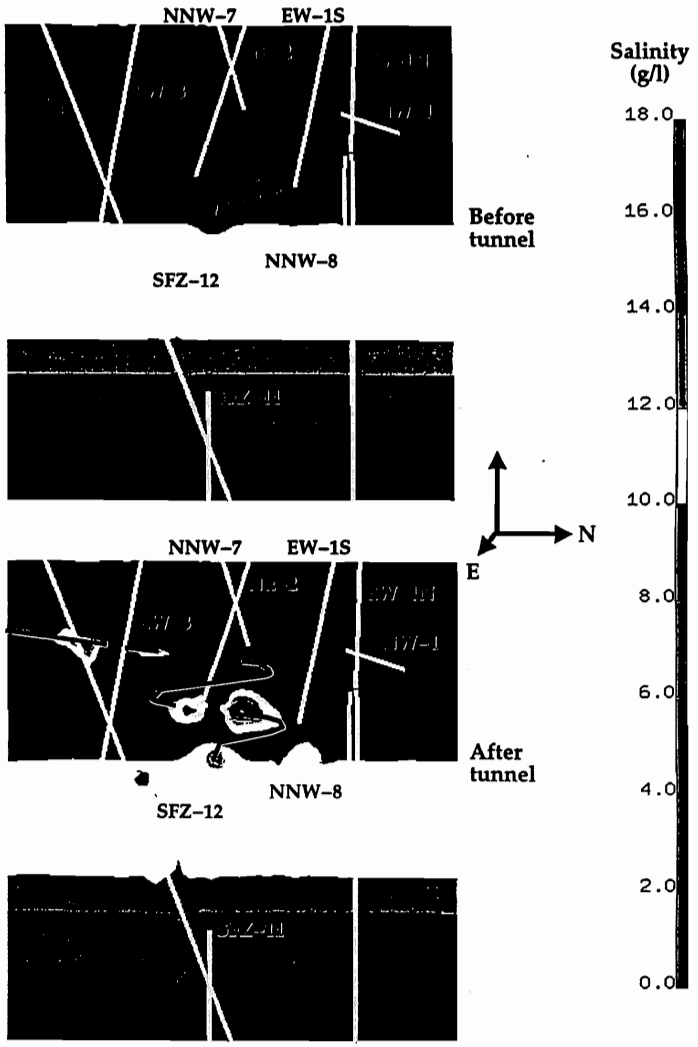

Figure 5.2. The salinity (g/l) on a NS trending cutplane before and after the tunnel construction in the first calibration case.

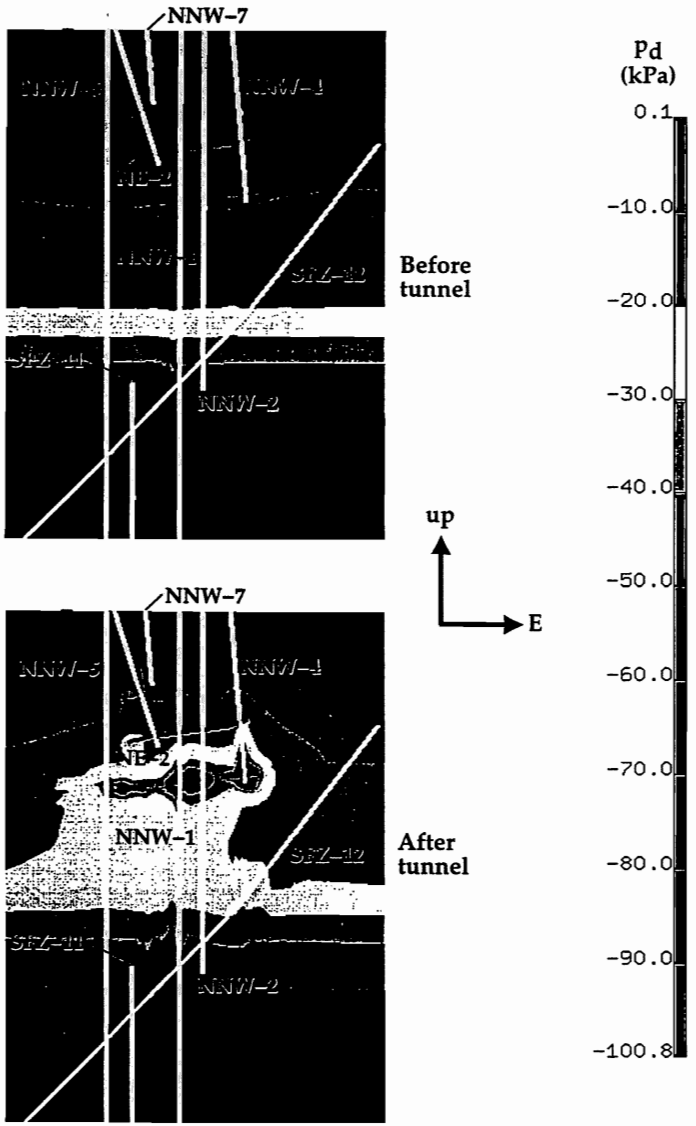

Figure 5.3. The "driving" pressure (kPa) on a EW trending cutplane before and after the tunnel construction in the first calibration case.

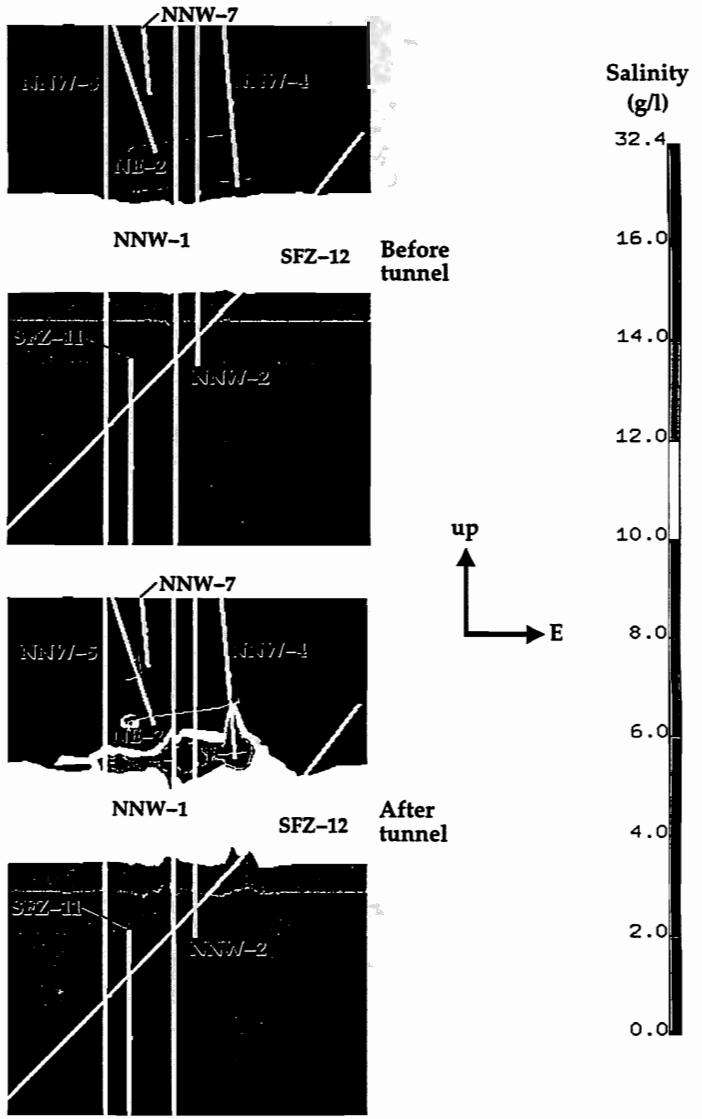

Figure 5.4. The salinity (g/l) on a EW trending cutplane before and after the tunnel construction in the first calibration case.

5.3 Completed tunnel

Table 5.1 shows the calculated mixing ratios of brine and glacial waters in one of the control points in Äspö HRL tunnel, SA1009B. From the same control point the mixing ratios of meteoric and marine waters are shown in Figure 5.5.

The Figures 5.6 and 5.7 illustrate the mixing ratios in the control points SA1730A and SA2783A, respectively.

The deviations of the calculated mixing proportions from the values given by Gurban et al. (1998) do not show very clear depth dependence. Deeper in the model the deviations of the mixing ratios of brine and glacial waters in percentage units increase a little. In most of the samples below the depth level of about 120 m the maximum deviation follows either the meteoric or the marine component of groundwater. The deviation of the marine component is especially large in the depth of about 350 m. As far as the depth of about 120 m the maximum deviation follows the marine component. The smallest deviations are reached in the depth interval 250-300 m.

Table 5.1. Mixing ratios of brine and glacial water in SA1009B.

SA1009B	Chemistry modelling (Gurban et al., 1998)		Calibration case 1		Calibration case 2	
Days after 19.10.1990	Brine	Glacial	Brine	Glacial	Brine	Glacial
983	1,4	1,4	0	0,1	0,1	0,4
1041	3,9	3,9	0	0,1	0,1	0,4
1075	13	13	0	0,1	0,1	0,4
1328	5,5	5,5	0	0,2	0,1	0,5
1417	5	5	0	0,2	0,1	0,5
1671	3,5	3,5	0	0,2	0,1	0,5

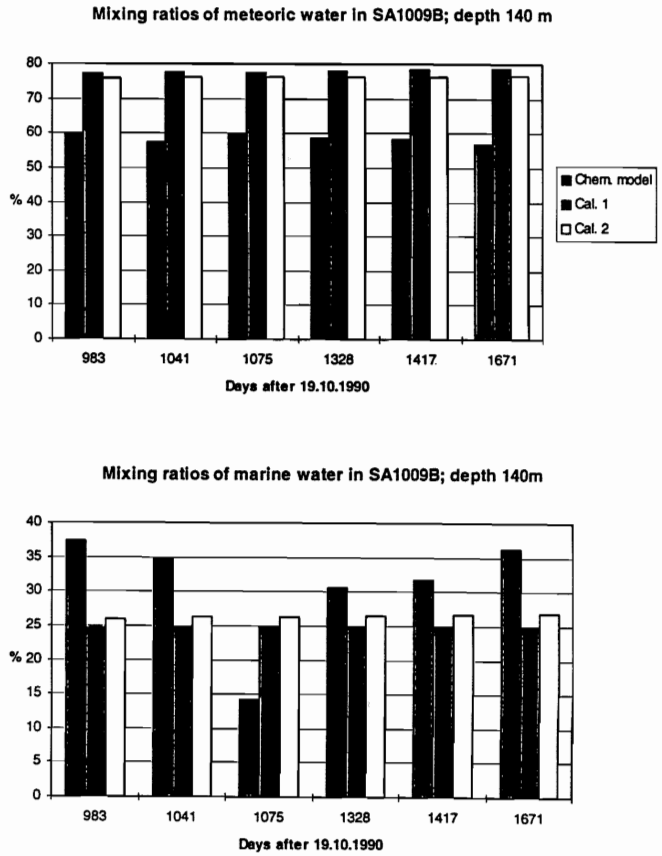

Figure 5.5. Mixing ratios of meteoric and marine water in SA1009B. The results from the chemistry modelling are given by Gurban et al. (1998).

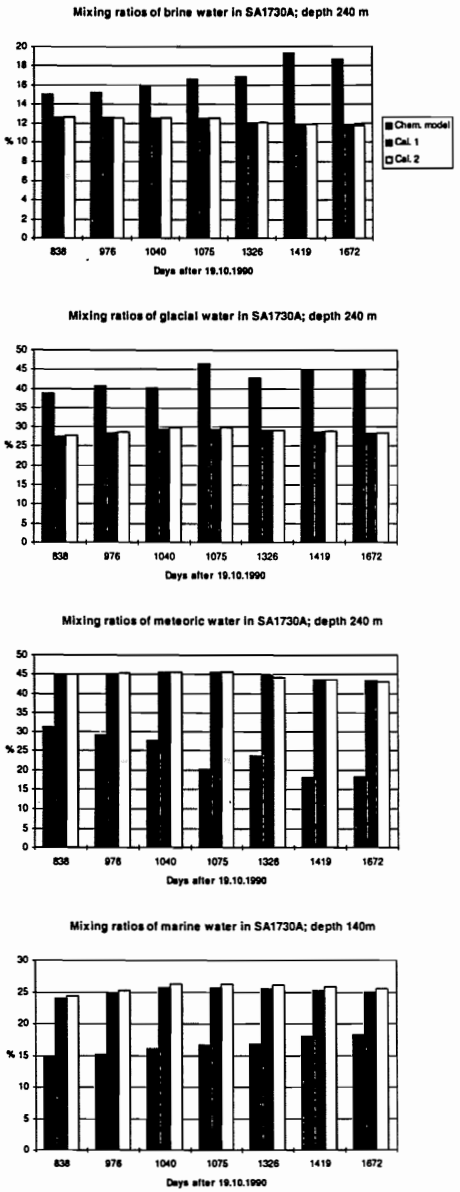

Figure 5.6. Mixing ratios of water types in SA1730A. The results from the chemistry modelling are given by Gurban et al. (1998).

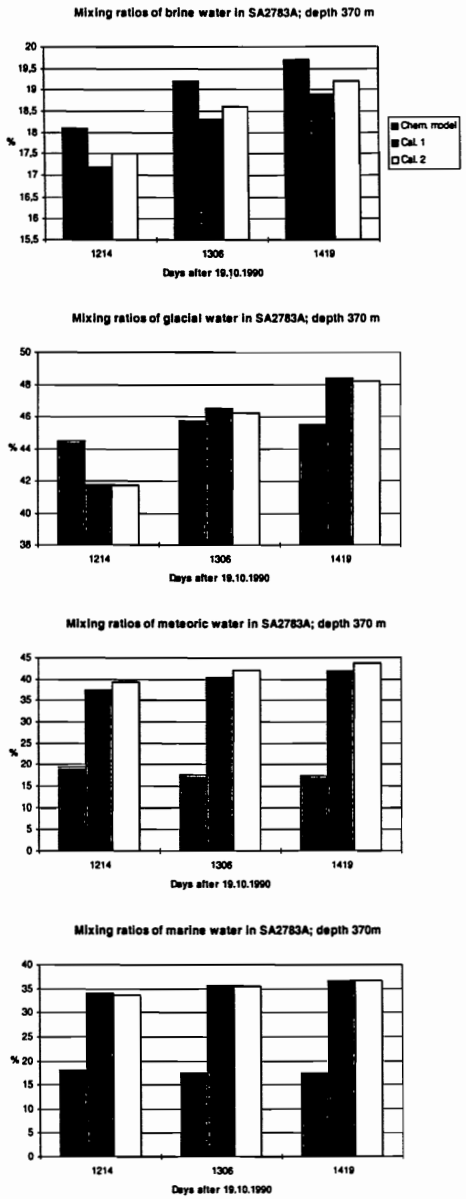

Figure 5.7. Mixing ratios of water types in SA2783A. The results from the chemistry modelling are given by Gurban et al. (1998).

6 COMPARISON AND CONSISTENCY CHECK

The equivalent continuum model and the dual porosity model give nearly the same results in boreholes both in the first and in the second calibration case (Section 4). In this sense the equivalent continuum model and the dual porosity model are consistent.

The pressure and salinity fields in the calibration cases are calculated in two different ways. The measurement data is used in two different ways to derive the initial salinity boundary condition. In the first case, the measured salinities in boreholes are compared with the calculated salinities in order to define the initial salinity boundary condition. After the modification the consistency of the residual pressures is also checked. This could be called a purely hydrologic approach.

The second approach utilises the interpolated measurement data initially used in the chemistry modelling by Gurban et al. (1998). Of course, the pressure and salinity fields gained from the two calibration cases differ (see figures in Section 4), although certain similarity can be assumed: both the cases are based on the measurements. However, the mixing ratios calculated are very similar (see Table 5.1 and Figs. 5.5-5.7).

In the mixing calculations, the initial concentration of each water type has been striven to give in accordance with the chemistry modelling by Gurban et al. (1998). Despite that the mixing ratios calculated here and the mixing ratios delivered from the chemistry modelling do differ. For that many reasons can be found:

- No reactions have been modelled, only mixing. This is true for both the salinity field and the mixing calculations of a single water type.
- The deuterium, tritium and ^{18}O distributions have not been modelled.
- The inaccuracy of the interpolation from the 3D volume used in the chemistry modelling (Gurban et al., 1998) may be high especially in the north-eastern part of the model.
- The inaccuracy of the boundary condition on the vertical sides and at the bottom used in later time steps.
- The material properties provide with variation possibilities. Especially, there is uncertainty in the hydraulic conductivity of the rock K, the fracture spacing $2a$ and the conductivity assigned to the one-dimensional elements representing the tunnel and the shafts.

- The depth extensions of some of the regional fracture zones and most of the local fracture zones are uncertain.
- Numerical inaccuracy.

7 REFERENCES

J Bear, 1979. Hydraulics of Groundwater. McGraw-Hill, Israel.

A N Brooks and T J R Hughes, 1992. Streamline Upwind/Petrov-Galerkin Formulations for Convection Dominated Flows with Particular Emphasis on the Incompressible Navier-Stokes Equations. Computer Methods in Applied Mechanics and Engineering, 32, pp. 199-259.

I Gurban, M Laaksoharju and C Andersson, 1998. Influences of the Tunnel Construction on the Groundwater Chemistry at Äspö. INTERA KB, Stockholm. June 1998.

P S Huyakorn, B H Lester and J W Mercer, 1983. An Efficient Finite Element Technique for Modelling Transport in Fractured Porous Media, 1, Single Species Transport. Water Resources Research, vol. 19, no. 3, pp. 841-854.

P S Huyakorn and G F Pinder, 1983. Computational Methods in Subsurface Flow. Academic Press INC, Orlando.

M Laitinen, 1994. Developing an Iterative Solver for the FEFLOW Package. Technical Report, VTT Energy, POHJA-2/94, Espoo (in Finnish).

M Laitinen, 1995. Modelling Convection Dominated Transport Problems with Improved Galerkin Finite Element Formulations. Technical Research Center of Finland, Espoo. VTT Julkaisuja - Publikationer 804. (in Finnish)

D R Lide (ed.), 1990. CRC Handbook of Chemistry and Physics. 71st edition 1990-1991. CRC Press Inc., Boston.

J Löfman, 1996. Groundwater Flow Modelling at the Olkiluoto Site. Flow under Natural Conditions. Posiva Oy, Helsinki. Work report PATU-96-76e.

J Löfman and V Taivassalo, 1995. Simulations of Pressure and Salinity Fields at Äspö. SKB ICR 95-01.

G de Marsily, 1986. Quantitative Hydrogeology — Groundwater Hydrology for Engineers. Academic Press INC, Orlando.

F Mészáros, 1996. Simulation of the Transient Hydraulic Effect of the Access Tunnel at Äspö. Äspö International Cooperation Report ICR 96-06.

I Rhén (ed.), G Gustafson, R Stanfors and P Wikberg, 1997. ÄSPÖ HRL — Geoscientific Evaluation 1997/5. Models Based on Site Characterization 1986 - 1995. SKB TR 97-06.

V Taivassalo and A Saarenheimo, 1991. Groundwater Flow Analysis for the VLJ Repository. Nuclear Waste Commission of Finnish Power Companies, Helsinki. YJT-91-10.

M Valkiainen, 1992. Diffusion in the Rock Matrix — A Review of Laboratory Tests and Field Studies. Nuclear Waste Commission of Finnish Power Companies, Report YJT-92-04, Helsinki.

T Vieno, A Hautojärvi, L Koskinen, H Nordman, 1992. TVO-92 Safety Analysis of Spent Fuel Disposal. Nuclear Waste Commission of Finnish Power Companies, Helsinki. YJT-92-33E.

P Wikberg, 1998. Äspö Task Force on Modelling of Groundwater Flow and Transport of Solutes. Plan for Modelling Task # 5: Impact of the Tunnel Construction on the Groundwater System at Äspö, a Hydrological-Hydrochemical Model Assessment Exercise. Äspö Hard Rock Laboratory Progress Report HRL-98-07.

2785.0	2190.0	0.0
2810.0	2525.0	0.0
2810.0	2525.0	-1600.0
2785.0	2190.0	-1600.0
2810.0	2525.0	0.0
3550.0	7000.0	0.0
3550.0	7000.0	-1600.0
2810.0	2525.0	-1600.0
3550.0	7000.0	0.0
3710.0	8020.0	0.0
3710.0	8020.0	-1600.0
3550.0	7000.0	-1600.0
3710.0	8020.0	0.0
4285.0	9740.0	0.0
4285.0	9740.0	-1600.0
3710.0	8020.0	-1600.0
4285.0	9740.0	0.0
4760.0	11620.0	0.0
4760.0	11620.0	-1600.0
4285.0	9740.0	-1600.0
4760.0	11620.0	0.0
5050.0	13000.0	0.0
5050.0	13000.0	-1600.0
4760.0	11620.0	-1600.0

SFZ11

2512.7	7182.4	0.0
3550.0	7000.0	0.0
3550.0	7000.0	-1600.0
1665.9	7331.3	-1600.0
3550.0	7000.0	0.0
3810.0	6975.0	0.0
3810.0	6975.0	-1600.0
3550.0	7000.0	-1600.0
3810.0	6975.0	0.0
7570.0	6165.0	0.0
7570.0	6165.0	-1600.0
3810.0	6975.0	-1600.0

SFZ12

3899.5	8448.2	-1503.5
3760.2	8080.1	0.0
3367.2	8446.5	-1503.5
3899.5	8448.2	-1503.5
2420.0	7070.0	0.0
2212.8	7576.5	-1503.5
3367.2	8446.5	-1503.5
3760.2	8080.1	0.0
2212.8	7576.5	-1503.5
2420.0	7070.0	0.0
-706.0	5145.9	0.0
-992.9	5611.9	-1503.5

SFZ13

-50.0	9140.0	0.0
1230.0	8500.0	0.0
1230.0	8500.0	-1600.0
-50.0	9140.0	-1600.0
1230.0	8500.0	0.0
1120.0	8070.0	0.0
1120.0	8070.0	-1600.0
1230.0	8500.0	-1600.0

SFZ14

905.0	6525.0	0.0
1095.0	7860.0	0.0
1095.0	7860.0	-1600.0
905.0	6525.0	-1600.0
1095.0	7860.0	0.0
2670.0	8070.0	0.0
2670.0	8070.0	-1600.0
1095.0	7860.0	-1600.0
2670.0	8070.0	0.0
1230.0	8500.0	0.0
1230.0	8500.0	-1600.0
2670.0	8070.0	-1600.0

SFZ15

2285.0	9450.0	0.0
2620.0	12000.0	0.0
2620.0	12000.0	-1600.0
2285.0	9450.0	-1600.0
2620.0	12000.0	0.0
2810.0	13430.0	0.0
2810.0	13430.0	-1600.0
2620.0	12000.0	-1600.0

5200.0	7900.0	0.0
5800.0	7930.0	0.0
5800.0	7930.0	-1600.0
5200.0	7900.0	-1600.0
5800.0	7930.0	0.0
8330.0	8000.0	0.0
8330.0	8000.0	-1600.0
5800.0	7930.0	-1600.0

SFZ04

-5240.0	3520.0	0.0
-3740.0	4690.0	0.0
-3740.0	4690.0	-1600.0
-5240.0	3520.0	-1600.0
-3740.0	4690.0	0.0
-3050.0	5285.0	0.0
-3050.0	5285.0	-1600.0
-3740.0	4690.0	-1600.0
-3050.0	5285.0	0.0
-2570.0	5570.0	0.0
-2570.0	5570.0	-1600.0
-3050.0	5285.0	-1600.0
-2570.0	5570.0	0.0
-590.0	6670.0	0.0
-590.0	6670.0	-1600.0
-2570.0	5570.0	-1600.0
-590.0	6670.0	0.0
200.0	7160.0	0.0
200.0	7160.0	-1600.0
-590.0	6670.0	-1600.0
200.0	7160.0	0.0
1095.0	7860.0	0.0
1095.0	7860.0	-1600.0
200.0	7160.0	-1600.0

SFZ05

-5310.0	2880.0	0.0
-1000.0	5140.0	0.0
-754.1	4651.1	-1503.5
-5048.5	2399.3	-1503.5
-1000.0	5140.0	0.0
-754.1	4651.1	-1503.5
2316.6	5474.2	-1503.5
2165.0	6000.0	0.0
2165.0	6000.0	0.0
2316.6	5474.2	-1503.5
3800.8	6340.3	-1503.5
3520.0	6810.0	0.0
3520.0	6810.0	0.0
3800.8	6340.3	-1503.5
7133.0	7974.4	-1503.5
5800.0	7930.0	0.0

SFZ06

-1950.0	8210.0	0.0
-760.0	8830.0	0.0
-760.0	8830.0	-1600.0
-1950.0	8210.0	-1600.0
-760.0	8830.0	0.0
-50.0	9140.0	0.0
-50.0	9140.0	-1600.0
-760.0	8830.0	-1600.0
-50.0	9140.0	0.0
715.0	9360.0	0.0
715.0	9360.0	-1600.0
-50.0	9140.0	-1600.0
715.0	9360.0	0.0
2285.0	9450.0	0.0
2285.0	9450.0	-1600.0
715.0	9360.0	-1600.0
2285.0	9450.0	0.0
4285.0	9740.0	0.0
4285.0	9740.0	-1600.0
2285.0	9450.0	-1600.0
4285.0	9740.0	0.0
5595.0	9920.0	0.0
5595.0	9920.0	-1600.0
4285.0	9740.0	-1600.0
5595.0	9920.0	0.0
8330.0	10230.0	0.0
8330.0	10230.0	-1600.0
5595.0	9920.0	-1600.0

SFZ08

-70.0	3095.0	0.0
2380.0	2260.0	0.0
2380.0	2260.0	-1600.0
-70.0	3095.0	-1600.0
2380.0	2260.0	0.0
2785.0	2190.0	0.0
2785.0	2190.0	-1600.0
2380.0	2260.0	-1600.0
2785.0	2190.0	0.0
6545.0	1240.0	0.0
6545.0	1240.0	-1600.0
2785.0	2190.0	-1600.0

SFZ09

1165.0	1570.0	0.0
2380.0	2260.0	0.0
2380.0	2260.0	-1600.0
1165.0	1570.0	-1600.0
2380.0	2260.0	0.0
2810.0	2525.0	0.0
2810.0	2525.0	-1600.0
2380.0	2260.0	-1600.0
2810.0	2525.0	0.0
7240.0	4640.0	0.0
7240.0	4640.0	-1600.0
2810.0	2525.0	-1600.0

SFZ10

2670.0	1260.0	0.0
2785.0	2190.0	0.0
2785.0	2190.0	-1600.0
2670.0	1260.0	-1600.0

NNW-7

1988.5	7486.7	-191.2
1957.1	7515.0	0.0
2146.8	7105.3	0.0
2180.4	7072.3	-191.5

NNW-8

1540.0	8060.0	-300.0
2030.0	7570.0	-300.0
2030.0	7570.0	-700.0
1540.0	8060.0	-700.0

SFZ01

-3190.0	13380.0	0.0
-1475.0	12910.0	0.0
-1475.0	12910.0	-1600.0
-3190.0	13380.0	-1600.0
-1475.0	12910.0	0.0
760.0	12380.0	0.0
760.0	12380.0	-1600.0
-1475.0	12910.0	-1600.0
760.0	12380.0	0.0
2620.0	12000.0	0.0
2620.0	12000.0	-1600.0
760.0	12380.0	-1600.0
2620.0	12000.0	0.0
4760.0	11620.0	0.0
4760.0	11620.0	-1600.0
2620.0	12000.0	-1600.0
4760.0	11620.0	0.0
8550.0	10950.0	0.0
8550.0	10950.0	-1600.0
4760.0	11620.0	-1600.0

SFZ02

-1095.0	14250.0	0.0
-1475.0	12910.0	0.0
-1475.0	12910.0	-1600.0
-1095.0	14250.0	-1600.0
-1475.0	12910.0	0.0
-1830.0	11760.0	0.0
-1830.0	11760.0	-1600.0
-1475.0	12910.0	-1600.0
-1830.0	11760.0	0.0
-2050.0	10640.0	0.0
-2050.0	10640.0	-1600.0
-1830.0	11760.0	-1600.0
-2050.0	10640.0	0.0
-2190.0	9760.0	0.0
-2190.0	9760.0	-1600.0
-2050.0	10640.0	-1600.0
-2190.0	9760.0	0.0
-2380.0	8905.0	0.0
-2380.0	8905.0	-1600.0
-2190.0	9760.0	-1600.0
-2380.0	8905.0	0.0
-2570.0	8310.0	0.0
-2570.0	8310.0	-1600.0
-2380.0	8905.0	-1600.0
-2570.0	8310.0	0.0
-3025.0	7285.0	0.0
-3025.0	7285.0	-1600.0
-2570.0	8310.0	-1600.0
-3025.0	7285.0	0.0
-3571.0	5335.0	0.0
-3571.0	5335.0	-1600.0
-3025.0	7285.0	-1600.0
-3571.0	5335.0	0.0
-3740.0	4690.0	0.0
-3740.0	4690.0	-1600.0
-3571.0	5335.0	-1600.0
-3740.0	4690.0	0.0
-3950.0	3620.0	0.0
-3950.0	3620.0	-1600.0
-3740.0	4690.0	-1600.0
-3950.0	3620.0	0.0
-4140.0	2640.0	0.0
-4140.0	2640.0	-1600.0
-3950.0	3620.0	-1600.0

SFZ03

-4140.0	8785.0	0.0
-2570.0	8310.0	0.0
-2570.0	8310.0	-1600.0
-4140.0	8785.0	-1600.0
-2570.0	8310.0	0.0
-1950.0	8210.0	0.0
-1950.0	8210.0	-1600.0
-2570.0	8310.0	-1600.0
-1950.0	8210.0	0.0
-1330.0	8120.0	0.0
-1330.0	8120.0	-1600.0
-1950.0	8210.0	-1600.0
-1330.0	8120.0	0.0
1120.0	8070.0	0.0
1120.0	8070.0	-1600.0
-1330.0	8120.0	-1600.0
1120.0	8070.0	0.0
1120.0	8070.0	-1600.0
2690.0	8080.0	-1600.0
2690.0	8080.0	0.0
2690.0	8080.0	0.0
3000.0	8085.0	0.0
3000.0	8085.0	-1600.0
2690.0	8080.0	-1600.0
3000.0	8085.0	0.0
3710.0	8020.0	0.0
3710.0	8020.0	-1600.0
3000.0	8085.0	-1600.0
3710.0	8020.0	0.0
5200.0	7900.0	0.0
5200.0	7900.0	-1600.0
3710.0	8020.0	-1600.0

EW-1N

-3570.0	2545.0	0.0
-480.0	5285.0	0.0
-480.0	5285.0	-1600.0
-3570.0	2545.0	-1600.0
-480.0	5285.0	0.0
905.0	6525.0	0.0
905.0	6525.0	-1600.0
-480.0	5285.0	-1600.0
905.0	6525.0	0.0
1215.0	6950.0	0.0
1215.0	6950.0	-1600.0
905.0	6525.0	-1600.0
1215.0	6950.0	0.0
1614.4	7359.1	-327.4
1614.4	7359.1	-1600.0
1215.0	6950.0	-1600.0
1215.0	6950.0	0.0
1614.4	7359.1	-327.4
1811.5	7482.0	0.0
1215.0	6950.0	0.0
1811.5	7482.0	0.0
2197.1	7698.3	0.0
2000.0	7575.4	-327.4
1614.4	7359.1	-327.4
1614.4	7359.1	-327.4
2000.0	7575.4	-327.4
2000.0	7575.4	-1600.0
1614.4	7359.1	-1600.0
2000.0	7575.4	-1600.0
2000.0	7575.4	-327.4
2690.0	8080.0	0.0
2690.0	8080.0	-1600.0
2690.0	8080.0	0.0
2197.1	7698.3	0.0
2000.0	7575.4	-327.4
2690.0	8080.0	0.0

EW-1S

1453.1	7217.4	0.0
3006.0	8088.1	0.0
3138.2	8076.0	-369.5
1339.7	7067.6	-369.5

EW-3

2703.6	7229.1	0.0
938.8	6863.0	0.0
920.1	6751.4	-542.2
2166.5	7010.0	-542.2

EW-7

743.3	6075.7	0.0
279.4	5913.4	-231.8
3571.8	6795.9	-231.8
3590.5	6838.9	0.0

NE-2

1829.9	7038.5	0.0
2325.1	7720.0	0.0
2389.6	7671.5	-349.4
1718.4	6747.8	-349.4

NE-3

1621.3	6288.3	0.0
1290.7	6171.2	-227.6
2939.8	7123.4	-227.6
3040.3	7107.6	0.0

NE-4

1818.6	6349.8	0.0
3267.3	7064.3	0.0
3368.7	7044.4	-228.3
1905.5	6322.8	-228.3

NW-1

1257.6	7882.0	0.0
1725.7	7373.8	0.0
2091.3	7607.4	-246.6
1447.6	8306.2	-246.6

NNW-1

2033.4	7551.8	0.0
2240.6	7104.5	0.0
2374.7	6814.7	-1600.0
2161.3	7275.6	-1600.0

NNW-2

2091.2	7583.1	0.0
2300.2	7106.1	0.0
2300.2	7106.1	-319.2
2184.3	7370.7	-1144.1

NNW-3

2143.6	7025.4	0.0
2136.9	6812.9	0.0
2136.9	6812.9	-1600.0
2143.6	7025.4	-1600.0

NNW-4

2240.2	7668.4	0.0
2286.2	7609.0	-436.7
2340.9	7178.9	-436.7
2328.3	6975.0	0.0

NNW-5

1962.8	7394.1	0.0
2025.1	6348.5	0.0
2025.1	6348.5	-1600.0
1962.8	7394.1	-1600.0

NNW-6

2298.7	7058.1	0.0
2382.9	6464.0	0.0
2382.9	6464.0	-1600.0
2298.7	7058.1	-1600.0

Preliminary application of smeared fracture model to Task No 5.

Takuma Hasegawa (CRIEPI)

Status Report

Preliminary application of smeared fracture model to Task #5.

Modeling Task #5:

Impact of the tunnel construction on the groundwater system at Äspö,

hydrological – hydrochemical model assessment exercise

11th Meeting of the Task Force

Äspö HRL, 1-3 Sep., 1998

By

Takuma HASEGAWA, Yasuharu TANAKA, Motoi KAWANISHI, Toshifumi IGARASHI

CRIEPI

1.Introduction

This document summarizes modeling approach and results performed by CRIEPI for Task 5. Task 5 focus on evaluating the effect of the tunnel construction on groundwater system, the changing of the groundwater flow and geochemical distribution. Particularly it is one of the import problems for us to evaluate salinity distribution, because salinity affects the performance of the buffer material and the Japanese Island is surrounded by the sea.

Therefore, we applied FEGM/FERM to evaluate undisturbed and disturbed salinity distribution by tunnel construction in order to prove FEGM/FERM effective. And we also performed numerical analyses for LPT2 to evaluate the updated properties of Fracture zone model and Rock mass model.

2.Modeling description

The object of this study is to predict the changing of the salinity distribution at around Äspö during tunnel construction.

(1)Boundary conditions

The Äspö HRL is located at east coasts of Sweden and surrounded by the Baltic Sea. The schematic model of the boundary and modeling area is shown in Fig.1. It is assumed that the boundary conditions are shown in Table 2. The side boundary is prescribed by constant head and constant concentration that depends on depth, as following equation,

$C_{salinity}=6+0.016Z$ (1)

Where $C_{salinity}$ is the salinity concentration(g/liter) and Z is the depth form sea level(m).

Table 1 Boundary conditions.

Boundary	Groundwater flow	Salinity concentration
Upper		
Island area	Constant flux	Fresh water:0%
Sea area	Constant head: Sea level	Sea water:0.6%
Lower	No flux	No flux
Side	Constant head: Hydrostatic	Interpolated from sampled data in Äspö borehole

(2)Material property

It is assumed that the material properties are divided into two categories, rock mass zone and fracture zone. These properties were characterized by Ingvar Rhen and shown in table 2. Three rock mass model and three Fracture zone models are used in numerical calculation. The specific storage capacity is 1.0e-61/m in all modeling area, and the longitudinal and transverse dispersion lengths are 20m and 2m, respectively. The effective porosity rate is calculated as follows,

$$n_e = 34.87K^{0.753} \quad (2)$$

Where n_e is the effective porosity and K is water conductivity (m/sec).

Table 2 Input parameters for Fracture zone and Rock Mass zone.

Fracture Zone Model	Rock Mass Zone Model
・Model96(Mean) ・Model96(Median) ・Model94(Task 3 update model) (see TR96-06)	Isotropy model ・1.5e-9m/sec ・6.0e-9m/sec Anisotropy model ・Kx,Ky,Kz:5.3e-8,3.0e-9,3.3e-9m/s (Rotating 130 degrees from North to East)

(3)Finite element mesh

Figure 2 shouws the finite element mesh used In numerical analysis. The rock matrix Is modeled as 168,184 hexahedral element. The tunnel and shaft are modeld as 98 and 45 truss elements, respectively.

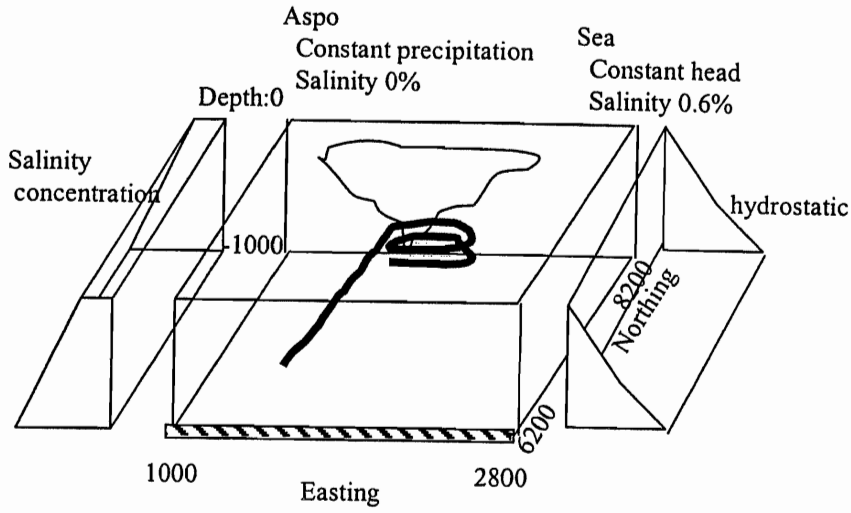

Fig.1 Conceptual model of Äspö.

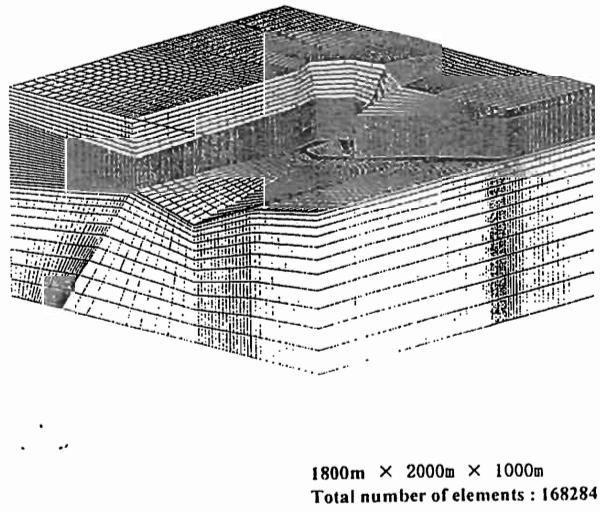

Fig.2 Finite element mesh used In numerical analysis

3.Numerical model description

3.1 Numerical model

The ground water flow and solute transport code called FEGM/FERM have been applied to evaluate salinity distribution. These codes solve the continuity equation of groundwater flow/solute transport by using Galerkin method. To consider the density of salinity, FEGM and FERM were coupled with each other, and the density effect of the motion equation is expressed by Bossinessq approximation.

The governing equations are expressed, as follows,

Groundwater flow: FEGM

$$F\frac{\partial h}{\partial t} = \nabla \cdot (K \nabla H) + Q \qquad (3)$$

$$F = \theta\beta' + \frac{d\theta}{dh} + \frac{\theta}{n}\alpha' \qquad (4)$$

Where F is the generalized specific storage coefficient, h is the pressure head, t is the time, K is the hydraulic conductivity tensor, H is the total head, Q is sink/source term, θ is volumetric water content, β' is compressibility of water, n is porosity rate, and α' is compressibility of media.

Solute transport: FERM

$$R\frac{\partial c}{\partial t} = \nabla \cdot (D \nabla c - vc) - \lambda R c + Q \qquad (5)$$

Where R is the retardation factor, c is the concentration, t is the time, D is the dispersion coefficient, v is the velocity, λ is the decay constant, and Q is the sink/source term.

3.2 Smeared Fracture model

In order to treat fractures easy, FEGM/FERM have the smeared fracture model which incorporates the property of the fracture to finite element by volume weighted method. When the fracture intersects several finite elements as shown in Fig.3, the parameter of shadowed finite element change to volume weighted value.

In this study, this smeared fracture model was used to consider the fracture zone.

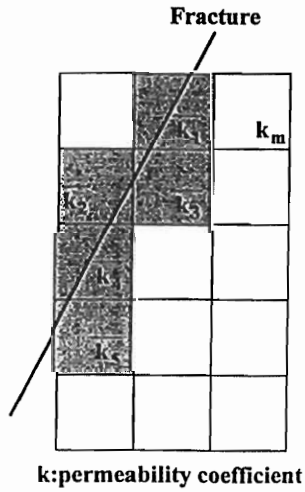

Fig.3 concept of smeared fracture model

4.Modeling Process

To evaluate changing the salinity concentration, we performed the following calculation,

(1) LPT2

(2) Undisturbed condition analysis (Initial condition analysis)

(3) Undisturbed condition analysis (Tunnel Excavation Effect)

(1) LPT2 Experiment

Äspö model has been updated (ex, Fracture zone), so we perform the analyses for LPT2 to evaluate the consistency of update Äspö model. The salinity effect is not taken into account this kind of analyses.

Process

1) Selection of material property (Fracture model and Rock model, Fracture transitivity)

2) Sensitive analysis of infiltration rate (steady state)

Checking the consistency of Initial condition (see TR97-06, pp.201)

3) LPT2 analysis

Checking the consistency of drawdown

(2) Undisturbed condition analysis

To provide the Initial distribution of salinity, steady state analyses ware carried out by using time marching method. After these analyses, the consistency checks by using sampled data before tunnel construction.

Process

1) Selection of material property (Fracture model and Rock model, Fracture transitivity)

2) Steady state analysis (time marching method)

Checking the consistency of initial condition. (See TR97-06, pp.184)

(3) Disturbed condition analysis

To evaluate salinity distribution change during tunnel construction, we performed the unsteady state calculations that prescribe the tunnel excavation to the boundary condition.

Process

1) Selection of material property (Fracture model and Rock model, Fracture transitivity)

2) Steady state analysis (time marching method)

Checking the consistency of initial condition. (See TR97-06, pp.184)

3) Unsteady state analysis (Tunnel excavation effect on salinity distribution)

Checking the consistency of salinity distribution change

5.Simulation results

(1)LPT2

1) Sensitive analysis of Infiletration rate

To estimate Infiltration rate on natural condition, sensitive analyses were carried out. One result is shown in Fig.4. These result were compared with measured pressure head (see TR97-06, pp.201) to decide appropriate infiltration rate. Table 5 shows estimated Infiltration rate for each rock mass model.

Table 3 Estimated infiltration rate

Rock Mass Model	Isotropy 1.5e-9m/s	Isotropy 6.0e-9m/s	Anisotropy
Precipitation rate (mm/year)	2.6	11.0	25.6

2) LPT2 experiment

We performed five numerical calculations for LPT2. Fig 5 shows the normal probability plot of error for drawdown, and Table 4and 5 summarize the results of Fig.5. The relationships between drawdown and distance from ponping area are shown in Fig.6.

Table4 Sensitive analysis for Rock Mass Model

Fracture Model	Model 96 (Mean)		
Rock Mass Model	Isotropy 1.5e-9m/s	Isotropy 6.0e-9m/s	Anisotropy
Average(m)	0.169406	0.369604	0.845347
Standard derivation	2.257223	2.172349	2.26681

Table 5 Sensitive analysis for Fracture Zone Model

Fracture Model	Model96 (mean)	Model96 (median)	Task3
Rock Mass Model	Isotropy 1.5e-9m/s		
Average	0.169406	0.872079	1.682574
Standard derivation	2.257223	2.279059	2.358411

(2)Undisturbed condition analysis

We performed six numerical calculations for undisturbed condition. The measured undisturbed salinity distribution is shown in Fig.7, and the calculated undisturbed conditions are shown in Fig.8 and Fig.9. Fig.8 shows the sensitivity for the boundary condition and dispersion coefficient. The used dispersion length is 10 times as high as other model. Fig.9 shows the sensitivity of the salinity distribution for rock mass model and fracture model, and Fig.10 shows the salinity distribution of these models at northing 7500m.

(3) Disturbed condition analysis

Disturbed condition analyses have been performed, but we have not got the convergence result. The cause of the divergent is the concerted flow to the tunnel. The convergent of this kind of simulation depend on the time step size, but we have not got the suitable time step size.

Fig.11 shows the drawdown of the disturbed condition analysis during tunnel excavation without salinity effect. This analysis does not consider the grouting effect, so the results are not agreement with measured on some borehole.

Concerning with LPT2 analyses, the sensitivity of rock mass is smaller than Fracture model's, so the groundwater flow is governed by fracture. Simulation result by using Model 96 (mean) and Isotoropic (1.5e-9m/sec) is good agreement with LPT2. Otherwise the change of the rock mass model is sensitive for undisturbed salinity distribution. Therefore, simulating concentration distribution is more sensitive than groundwater flow. We performed numerical analysis during tunnel construction taken into account of grouting effect, but we have not got reasonable result during tunnel construction. So we have to do more calibration for grouting effect.

Reference

Rhen I. et al, 1997, Aspo HRL- Geoscientific evaluation 1997/5, Models based on site characterization, 1986-1995 TR97-06.

Igarashi T. et al., 1994. Application of three-dimensional smeared fracture model to the groundwater flow and solute migration of LPT2 experiment, ICR94-08.

Tanaka Y. et al., 1996, Application of three-dimensional smeared fracture model to the hydraulic Impact of Aspo tunnel, ICR96-07.

Svensson U., 1997, A site scale analysis of groundwater flow and salinity distribution in the Aspo area, TR97-17.

Stille H et al., 1992, Passage of water bearing fracture zone. Experiencee from the grouting of the section 1-1400m of the tunnel., PR25-92-19.

Stille H. et al., 1994, Experiencees from the grouting of the section 1340-2565m of the tunnel, PR25-94-13.

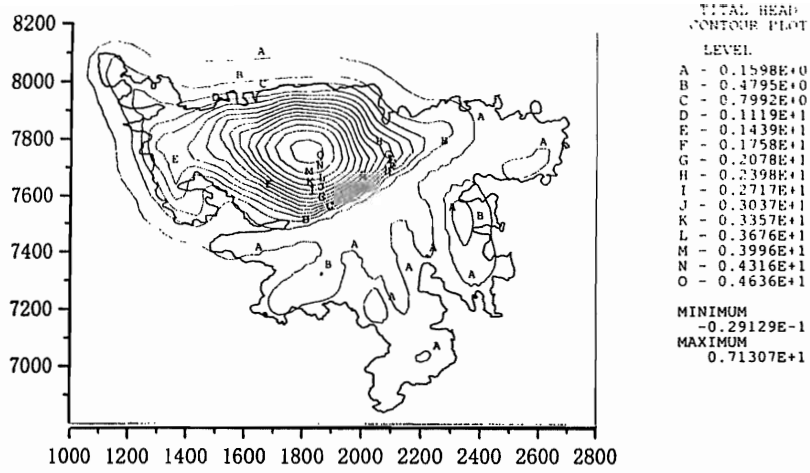

Fig.4 Total pressure head contour at -50m depth on rainfall sensitive analysis

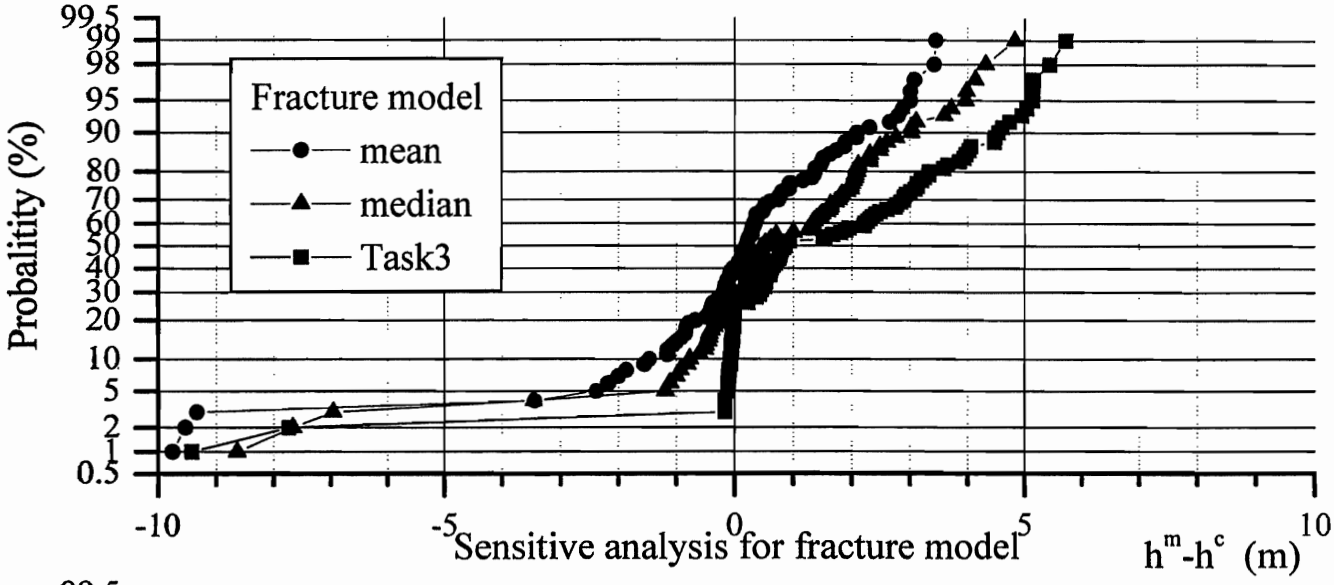

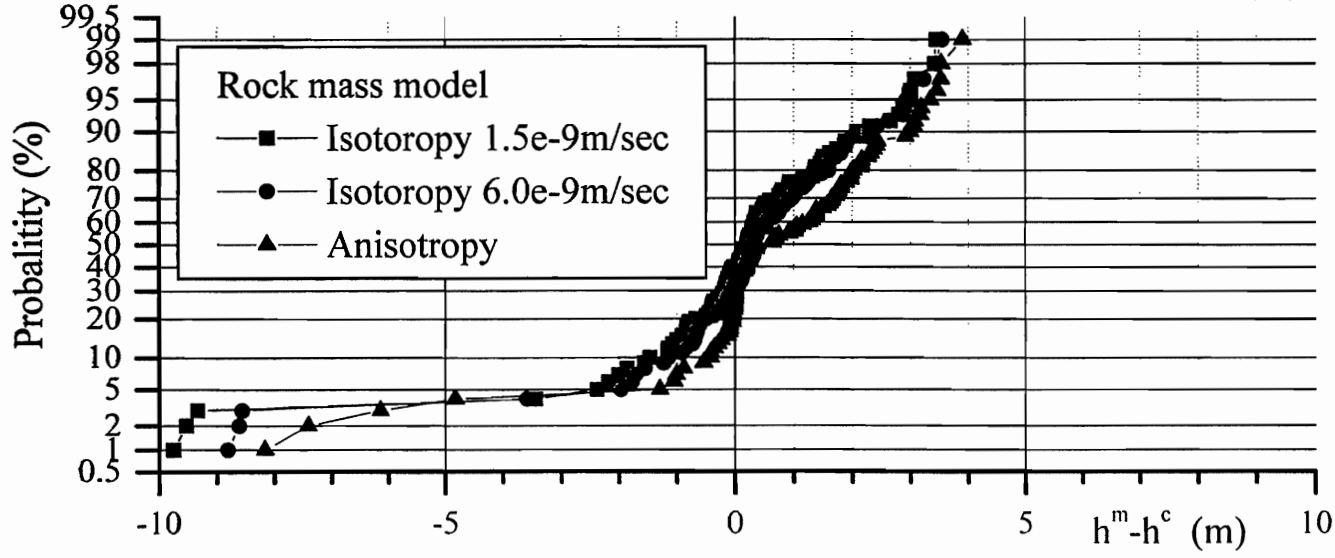

Sensitive analysis for Rock mass model

Fig.5 Sensitive analysis for LPT2(normal probability plot of errors for LPT2)

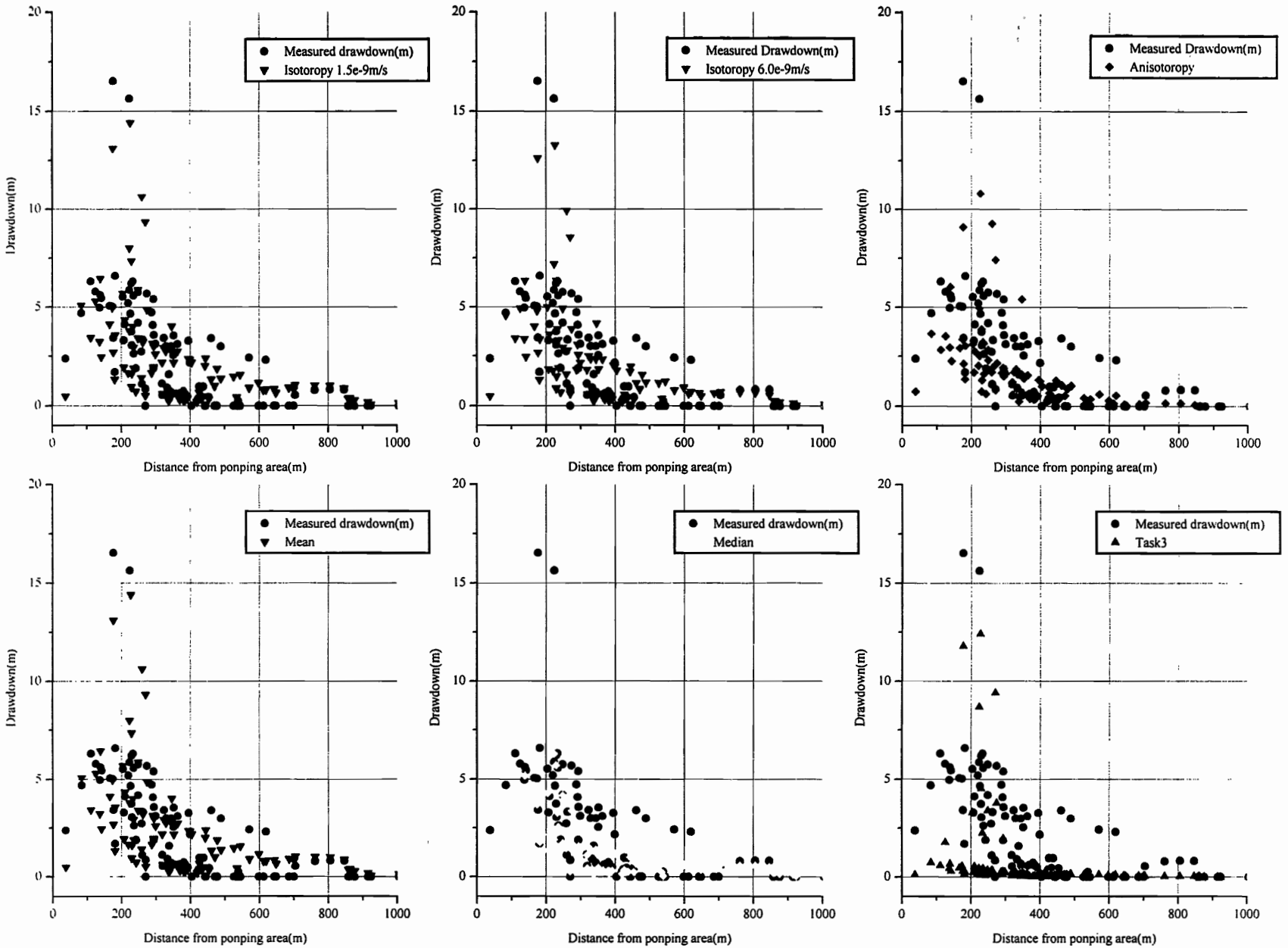

Fig. 6 Sensitive analysis of Rock mass model nad Fracture zone model for LPT2

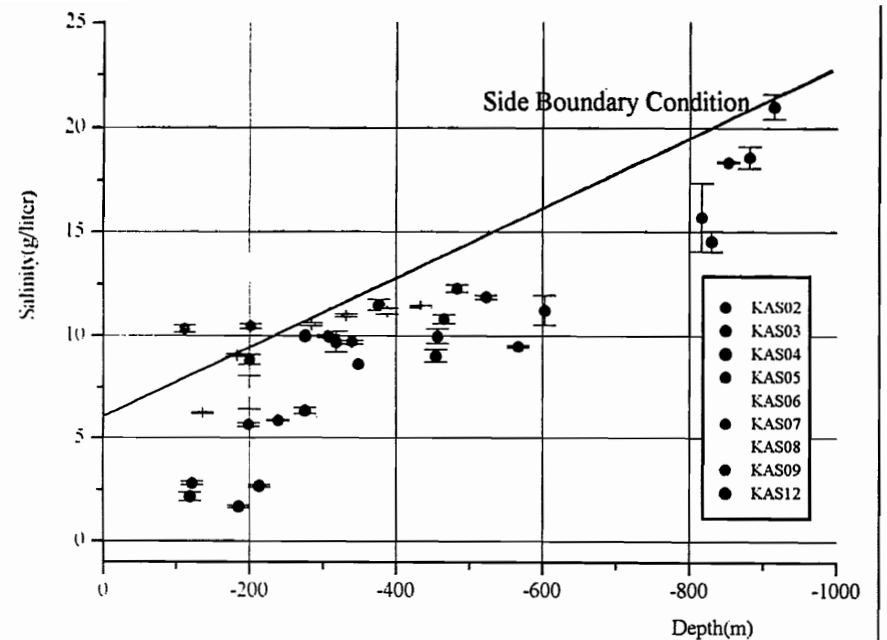

Fig.7 Measured undisturbed salinity distribution.

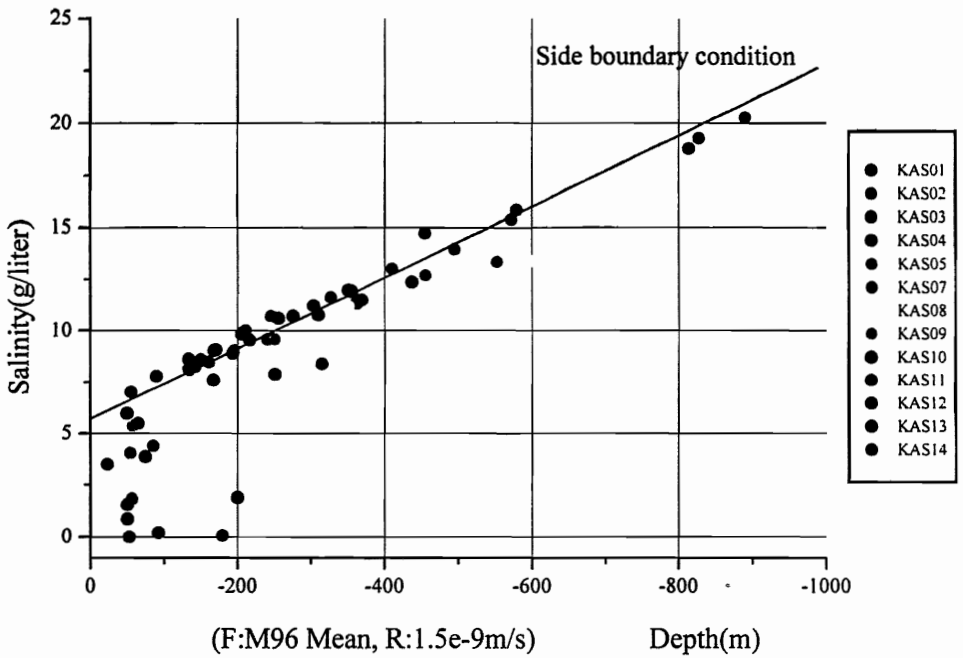

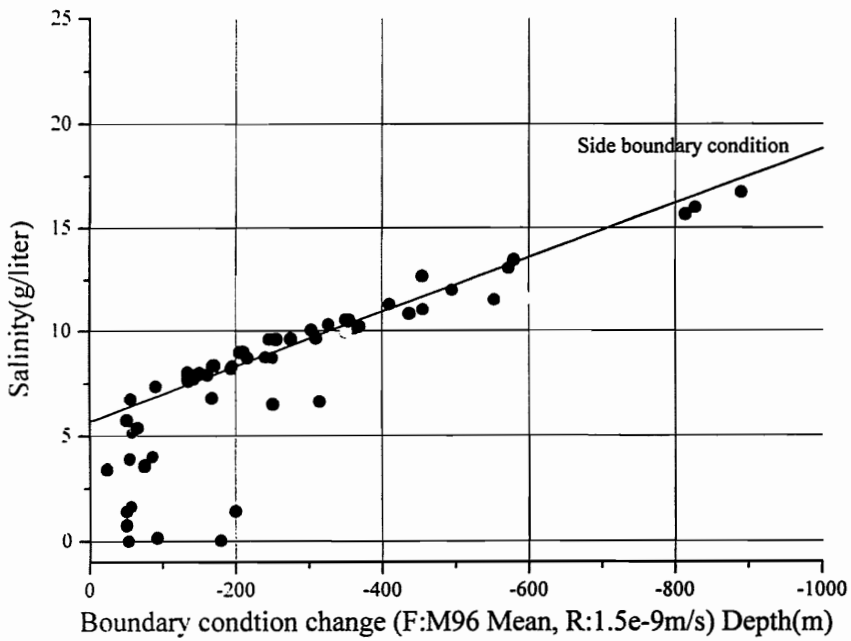

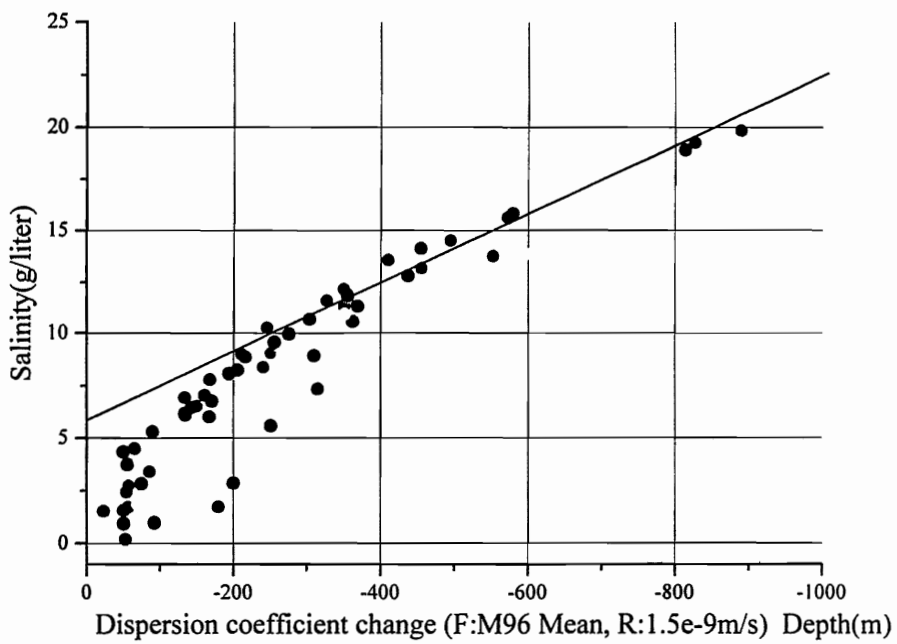

Fig.8 Sensitive analyes of boundary and dispesion parameter for undisturbed salinity distribution

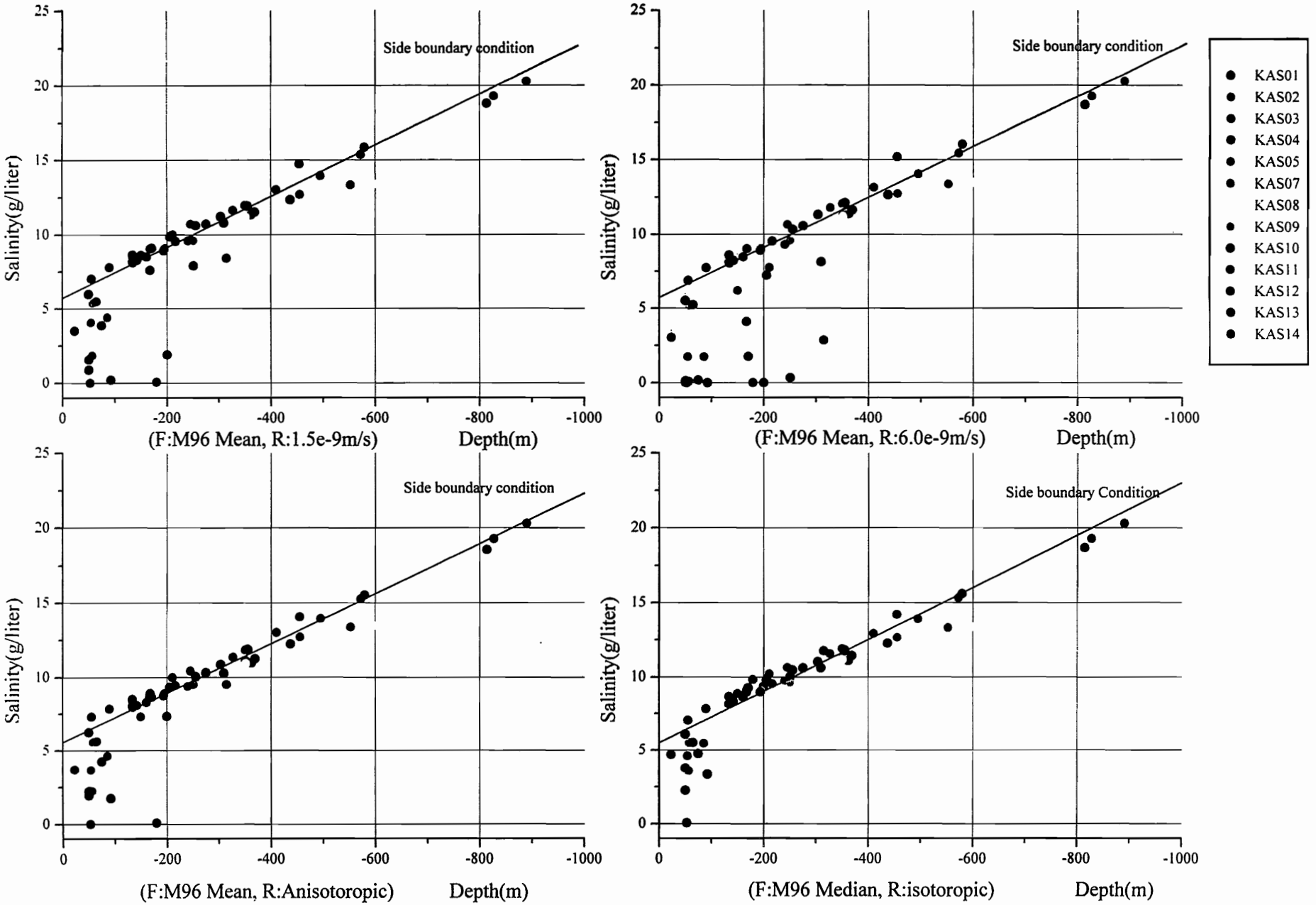

Fig. 9 Sensitive analyes of Rock mass model and Fracture model for undisturbed salinity distribution

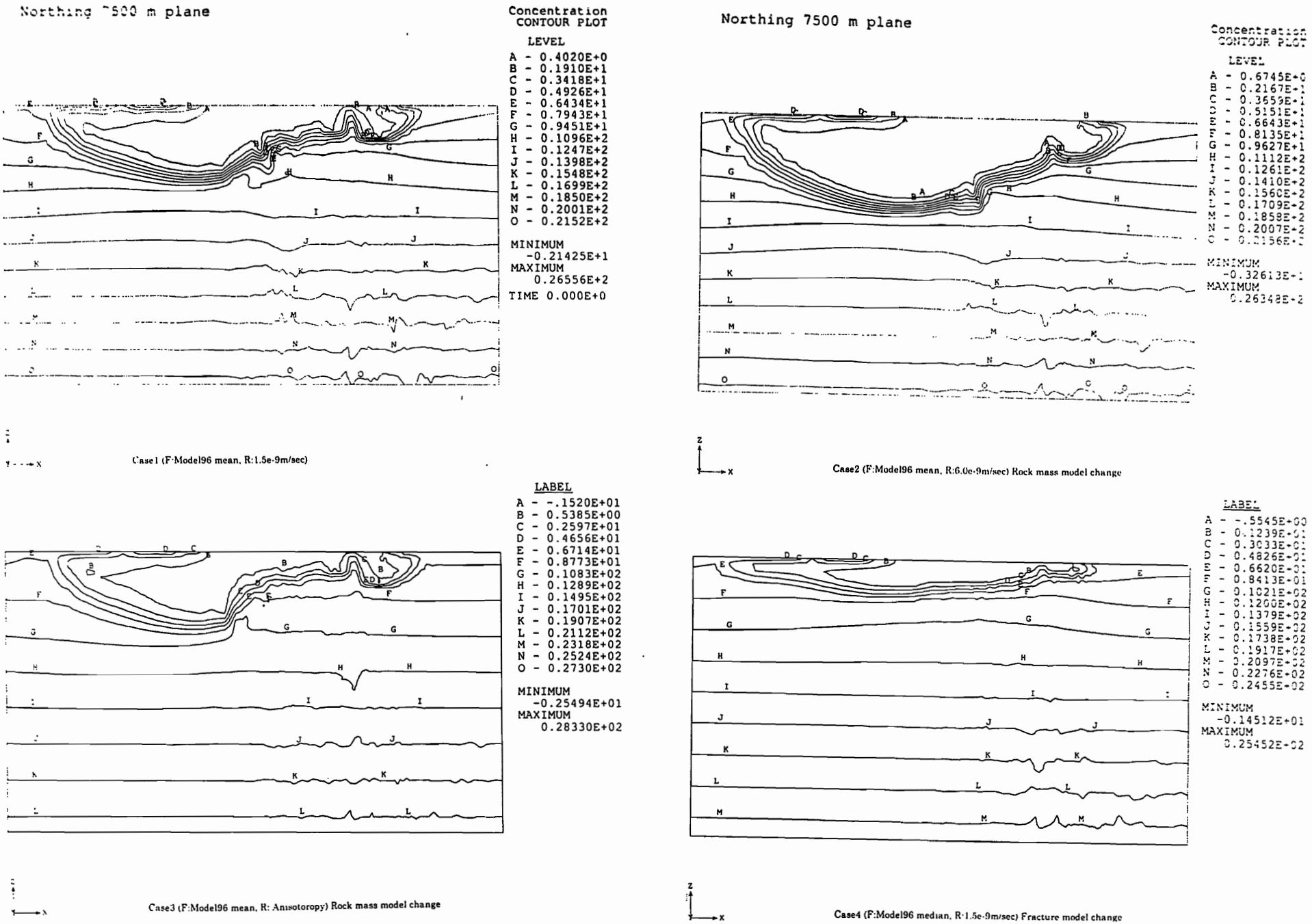

Fig.10 Salinity distribution at northing 7500 vertical cross section

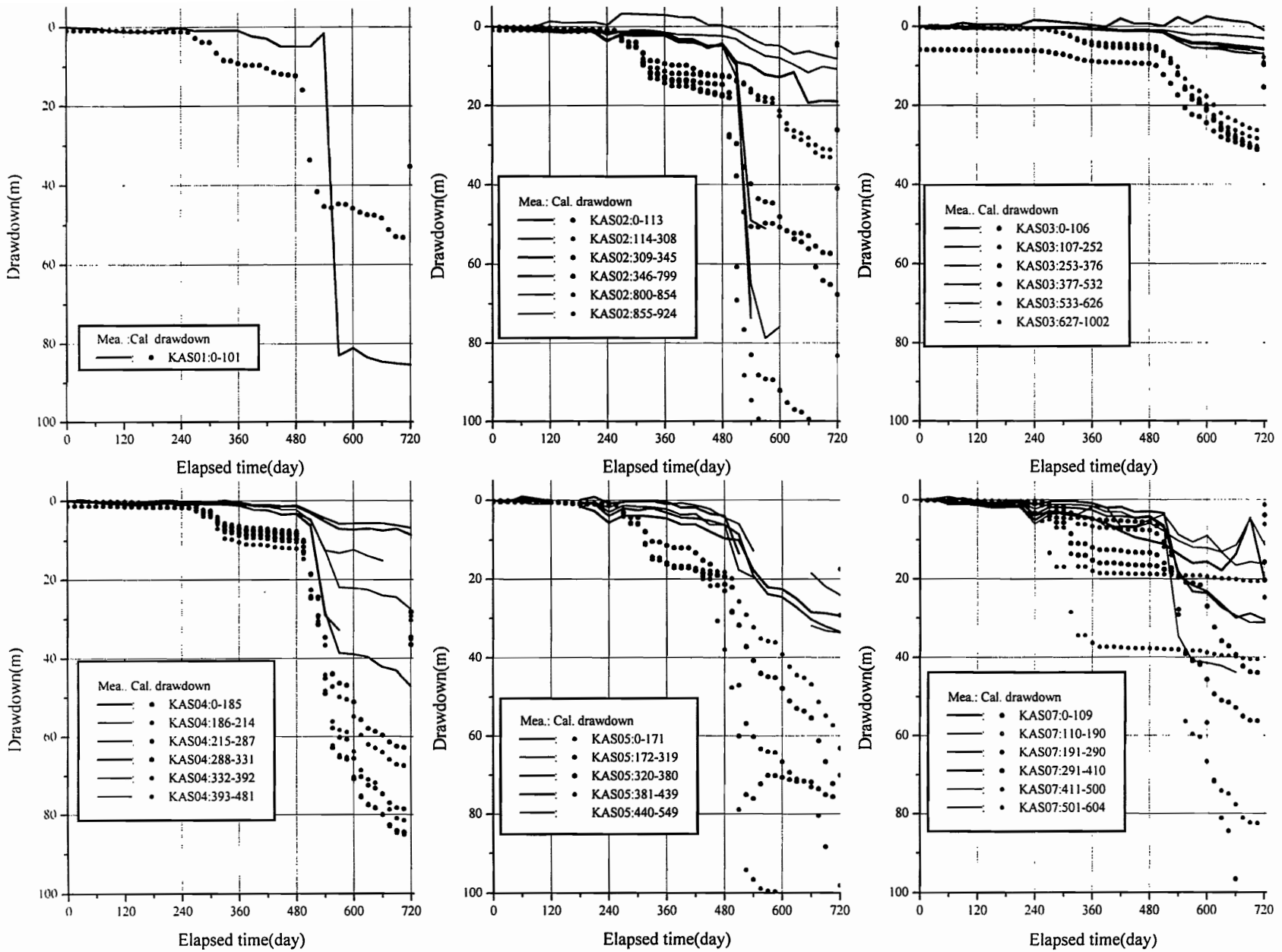

Fig. II-1 Groundwater flow analysis during tunnel construction(KAS01-07)

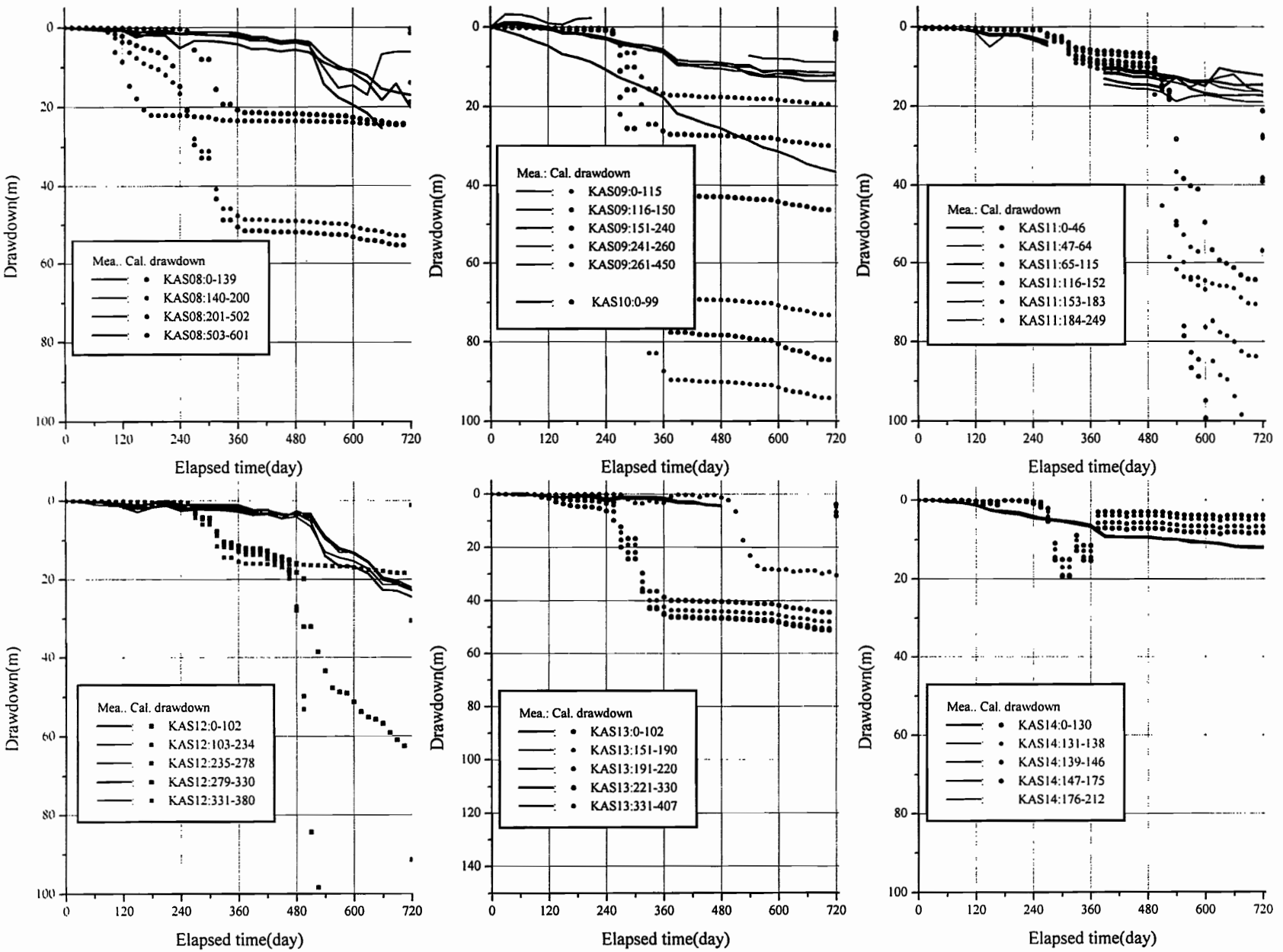

Fig. 11-2 Groundwater flow analysis during tunnel construction(KAS01-07)

Appendix Condensed description of modeling by CRIEPI

CRIEPI's Groundwater flow and solute transport model of the Äspö site Porous media model with smeared fractures		
Process description Continuity description(Mass rate) Equation of motion(Darcy's law with Bousenessq approximation)		
Concept	**Data**	
Generic frame works and parameters		
3D box divided into 168,141Element Nineteen fracture zone	Size1.8 x 2.0 x 1.0km^3	
Material properties		
Fracture zone Hydraulic conductivity Storage capacity Dispersion coefficient	Data from Rhen(1997) Data from Rhen(1997) Assumed Assumed	
Spatial assignment method		
Deterministic Property of Element crossed by fracture calculated as volume-weighted value Reduction of transitivity by grouting	Date from Stille(1992,1994)	
Boundary conditions		
	Groundwater flow	**Solute transport**
Upper Island area Sea area Lower Side	Constant flux Constant head: Sea level No flux Constant head : Hydrostatic	Fresh water:0% Sea water:0.6% No flux Interpolated from sampled data in Äspö borehole
Numerical tool FEGM/FERM		
Output parameter Pressure head, total head, flowrate, salinity		